UNIVERSIDAD NACIONAL DE INGENIERÍA

FACULTAD DE CIENCIAS

TESIS

" HYBRID HIGH ORDER METHODS FOR ELLIPTIC PROBLEMS "

PARA OBTENER EL GRADO DE DOCTOR EN
CIENCIAS CON MENCIÓN EN MATEMÁTICA

ELABORADO POR
Munguia La Cotera, Jonathan Alfredo

ASESOR
DR. ELADIO TEÓFILO OCAÑA ANAYA
ASESOR EXTERNO
DR. ROMMEL ANDRÉS BUSTINZA PARIONA

LIMA–PERÚ

2021

Dedication

This dissertation is lovingly dedicated to my parents, Isabel De Lurdes La Cotera Briones y Alfredo Jaime Munguia Alcantara for their support and encouragement.

Acknowledgements

I would like to thank my advisors, Dr. Rommel Andrés Bustinza Pariona and Dr. Eladio Ocaña Anaya, for sharing with me their knowledge, their advises, encouragement and dedication to complete this work. In these years, I have been able to grow personally and professionally. Thank you so much.

Also, I want to thank

- Dr. Alexandre Ern, who introduced me to the Hybrid High Order (HHO) methods,
- Dr. Tomás Barrios, who kindly provided me with access to his workstation, to perform many of the numerical results in this thesis,
- Dr. Karol Cascavita, for her help to understand some programming issues on HHO methods.

I acknowledge also CONCYTEC-Perú through FONDECYT project "Programas de Doctorado en Universidades Peruanas" CG-176-2015, to Instituto de Matemática y Ciencias Afines (IMCA), to Universidad Nacional de Ingeniería (UNI), to Centro de Investigación en Ingeniería Matemática (CI^2MA), and Departamento de Ingeniería Matemática, Universidad de Concepción (Chile), for the kind hospitality and facilities that was offered to me during my visits to these academic places.

Table of Contents

List of Tables

List of Figures

Abstract

The objective of this thesis is to analyze, develop and implement primal and mixed schemes for certain elliptic problems, based on the philosophy of Hybrid High-Order (HHO) methods.

We make use of known results, such as Lax-Milgram's Lemma for primal formulations, and Babuška-Brezzi's theory for mixed schemes, in order to establish the unique solvability of linear and nonlinear problems that arise in the context of physical problems, for example: fluid mechanics.

We prove the well-posedness of continuous and discrete problems, related to the Neumann problem, a certain class of nonlinear elliptic problems, and an interior transmission problems. We include their corresponding a priori error analysis.

In addition, in each of the next chapters, several numerical experiments are included, which illustrate the good performance of the proposed schemes, and confirm the theoretical convergence results, as established in the corresponding analysis.

Resumen

El objetivo de esta tesis es analizar, desarrollar e implementar esquemas primales y mixtos para ciertos problemas elípticos, basados en la filosofía de los métodos híbridos de alto orden (HHO).

Hacemos uso de resultados conocidos, como el Lema de Lax-Milgram, para formulaciones primales, y la teoría de Babuška-Brezzi, para esquemas mixtos, con el propósito de establecer existencia y unicidad de problemas lineales y no lineales que surgen en el contexto de problemas físicos, como por ejemplo en la mecánica de fluidos.

Establecemos la solubilidad única de los problemas continuo y discreto, con su estimación de error a priori correspondiente, para el problema de Neumann, una cierta clase de problemas elípticos no lineales y para problemas de transmisión interior.

En cada uno de los capítulos desarrollados, se incluye varios experimentos numéricos, que ilustran el buen desempeño de los esquemas propuestos, y confirman los resultados teóricos de convergencia, obtenidos en el análisis correspondiente.

INTRODUCTION

In the last decades, a great variety of engineering problems have been solved, such as the construction of noise maps [128], acoustics [136], aeronautics [55], fluid dynamics [132], etc. Many of these problems in general cannot be solved analytically, and therefore addressed by numerical methods, such as finite differences (FD), finite volumes (FV), finite elements (FE), among others. In this thesis, we choose to use the finite element method, due to its geometric flexibility and high precision with high-order polynomials. For a discussion of its advantages and disadvantages with respect to finite differences and finite volumes, we refer to the introduction in [89].

Engineers frequently face problems that can be described/modeled in most cases by Partial Differential Equations (PDE). Mathematicians and engineers have been developing increasingly sophisticated and robust numerical schemes, to approximate better and faster certain variables such as pressure, speed, deformation and concentration on the discretization of complex domains. One reason for the success of numerical analysis is the wide availability of high-performance computing resources and the increase in the predictive capabilities of the numerical models translated into such schemes. The main objective of the numerical analysis is to describe the relationship between the exact solution of the original equation and the approximate one obtained from its discretized version (numerical scheme). There are two types: a priori and a posteriori error analyses. The a priori error analysis is responsible for establishing the convergence of the method, and deriving the optimal order of convergence, if it is possible. In contrast, the a posteriori error analysis devises a strategy to improve the quality of the approximation without having to perform uniform refinement (which is usual in a priori error analysis and increases the degrees

of freedom very fast). This leads to deduce an a posteriori error estimator, which can be computed in terms of the approximate solution and the data of the problem. This estimator is then implemented in an adaptive mesh refinement algorithm. In this thesis, we will focus only in the a priori error analysis.

In [142] a description of evolution of the finite element method (FEM) is provided. An application of the FEM in 2D, focused on the aerospace industry, is found in the pioneering article by Clough et al. [143]. Unlike the finite difference method, that computes an approximation of the solution at a finite number of points in a grid, the finite element method looks for a solution in a finite-dimensional space, based on the discretization of the variational formulation. This methodology was extended to a wide range of engineering applications during the 1950s and 1960s. For instance, [151] is the first book that deals with the finite element method in the area of structural engineering, while [55] deals with other applications. The finite element method developed in these early years has been commonly known as the standard continuous Galerkin (CG) method, because it uses piecewise polynomial continuous functions and the Ritz-Galerkin principle. Furthermore, it is said to be conforming in the sense that the discrete space is a subspace of the continuous space. To learn more about its beginnings, we refer to [113, 54, 150].

The challenge of approximating the discontinuous solutions of the hyperbolic equations has been involved in different fields such as gas dynamics, geophysics, simulation of oil recovery, granular flows, etc. These discontinuities tend to cause spurious oscillations, which have been addressed by the finite volumes method by incorporating properly defined numerical fluxes and slope limiters. The first work that has allowed the flux to be discontinuous across element interfaces, in the context of transport equation, has been proposed by Reed and Hill in 1973 [138]. This method is called discontinuous Galerkin (DG) and was first formulated and analized by Lesaint and Raviart in 1974 [124]. Besides, Cockburn and Shu in 1998 [61] introduced a slope limiter operator to ensure stability of the Runge-Kutta DG methods (RKDG) for nonlinear hyperbolic problems. RKDG method is an

explicit DG method that satisfies the nonlinear hyperbolic conservation law locally, with the high-resolution of Runge-Kutta time-discretization and a local projection which enforces the global stability of the scheme. For more details, we refer to [56]. Thus, DG methods as well as FV methods can work with nonlinear hyperbolic conservation laws without presenting spurious oscillations. Later, a more general version of Nitsche's method extended the application of DG methods to second order nonlinear parabolic boundary value problems, called symmetric interior penalty (SIP) method, which was proposed and analized by Arnold in 1982 [9]. We refer also the works of Wheeler in 1978 [147] for second-order elliptic problems and Baker in 1977 [13] for fourth-order elliptic problems. Another member of DG methods is the local discontinuous Galerkin (LDG) method, introduced by Cockburn and Shu in 1998 [62] as an extension of the RKDG methods for purely hyperbolic systems to convection-diffusion systems. LDG can been seen as a generalization of the method of Bassi and Rebay [18], proposed for the compressible Navier-Stokes equations. Years later, LDG approach has been applied to elliptic problems in [46, 60]. LDG method requires the use of the so-called numerical fluxes, which are defined in terms of the unknowns and the data of the problem. This makes it possible to impose, in a weak way, the continuity inter elements that is not required in the approximation spaces. Indeed, the numerical flux of the potential does not depend on the discrete flux variable, which allows us to locally eliminate the flux variable and solve the problem only in terms of the potential. The DGs are consistent and unlike the standard CG are nonconforming, locally conservative, and parallelizable methods. For a general description, we refer to [10, 8, 69].

The main disadvantage between CG and DG approaches/techniques is that the latter considerably increases the number of degrees of freedom of the algebraic system obtained after discretization. For this reason, DG methods that can be hybridized, have been studied, in the sense that the potential trace can be introduced as a new unknown, playing as a Lagrange multiplier. In this way, it is obtained, after a static condensation, a system on the mesh skeleton. These methods are called hybridizable discontinuous Galerkin (HDG) methods, and have

been introduced in [58, 59]. The other unknowns are recovered once the Lagrange multiplier is obtained. For a general description applied to fluid mechanics, we refer to [134]. Also, a detailed and understandable exposition, can be found in [84].

This thesis addresses linear and nonlinear elliptic problems, using the well-known Hybrid High Order (HHO) method, introduced by Ern et al. [70, 75] in 2014. This method, like the HDG method, is locally conservative [71], and allows the treatment of polytopal meshes with possibly hanging nodes. This has been very studied in recent years, motivated for example by applications in geoscience, hexagonal geometries in the design of nuclear reactors and oil reservoirs (with geological faults). This method, like HDG, allows obtaining discontinuous solutions. The HHO method belongs to the family of nonconforming schemes, since the approximation space is not contained in the space where the exact solution lives. The term "hybrid" is due to the fact that the method uses in addition to the information in the cells the information on the faces of the skeleton. Furthermore, since polynomials of arbitrary order $k \geq 0$ are used locally in the construction of the discrete space, the term "high order" is adopted.

HHO methods take ideas from the SIP method, such as the design of local reconstruction operators and stabilization by a local penalty term, with the difference that HHO weakly imposes the correspondence between local degrees of freedom (DOFs) based on elements and faces, and not directly between faces. Also, it is not necessary to include some penalty parameter to ensure discrete coercivity. The discrete problem is assembled cell by cell, and the cell-based unknowns can be removed locally using static condensation (Schur's decomposition in the mathematical context), that is, simply solving the unknowns in the faces to recover (at a low computational cost) the unknowns in the cells. This is a characteristic of the HHO, which is also share by other nonconforming finite element schemes, as the HDG schemes. HHO methods, unlike HDG, are not consistent, so it is necessary to bound the consistency error. In [57] and [66, Section 5.1.6], numerical traces are given for the HHO methods, obtaining a mixed formulation equivalent to the primal

HHO. This allows us to establish a link with a new class of HDG methods. Thus, HDG methods can be seen as a generalization of HHO methods. A mixed version of the HHO method is found in [73], whose relation to its discrete primal version [75], is discussed in [3].

Another method of high order that supports polytopal meshes is the so-called virtual element (VE) method, introduced in its conforming form in [20] and as nonconforming approach in [11]. For an unified version of both types, see [43]. The VE method is a generalization of the classic finite element method, which contains, apart from the usual family of polynomials, another class of functions not necessarily polynomial (solutions of particular partial differential equations). These functions allow us to introduce high order regularity conditions, and are not computed explicitly. Then, they are not computationally implemented, reducing the degrees of freedom only on the polynomial part (vertices of the mesh). A link between the HHO and the nonconforming VE methods can be found in [57, Section 2.4], while a unified analysis of VE and HHO methods is described in [125].

To address phenomena involving composite materials and porous media, that appears in elliptic problems with fast oscillation coefficients, monoscale methods are unaffordable, so multiscale methods are used, for example in the context of standard finite element [120], HDG [85], and in the so-called multiscale hybrid-mixed (MHM) method [7]. Thus, the HHO method also addresses these types of problems, see [52, 53]. This is based on solving local problems of the exact equation with Neumann conditions imposed by Lagrange multipliers. These local problems are solved with the monoscale HHO on an initial partition of the heterogeneous domain (scaling the domain).

Although HHO methods are intended to use high order polynomials, it is possible to find connections with low order methods ($k = 0$). For example, they can be linked with hybrid finite volume (HFV) methods in [75]. In addition, HHO approach is related to Hybrid Mixed Mimetic (HMM) methods in [67]. Here, HMM methods,

proposed in [21, 83], can be seen as the unified formulation of HFV methods [88], Mixed Finite Volume (MFV) methods [82], and mimetic finite difference (MFD) methods [22]. It is interesting to mention that our HHO methodology can be directly compared with the classical standard finite element method in the context of diffusion problems [77].

HHO method has addressed a wide variety of models, allowing a robust treatment of the physical parameters involved in such models, such as, for example, heterogeneous/anisotropic diffusion [72, 39], quasi-incompressible linear elasticity [70], transport with dominant advection [67, 4], problems of nonlinear elasticity in the small deformation regime [27], nonlinear problems of Leray–Lions [64, 65], Stokes problem [3], incomprehensible Navier-Stokes equations [26], finite deformations of hyperelastic materials [1], viscoplastic Bingham fluids in pipes [44], among others. For a review of several of these works and a detailed analysis of them, consult the book dedicated to the method [66].

This thesis seeks to complement what has already been studied for HHO. For example, addressing pure Neumann conditions, internal transmission problems and a class of nonlinear elliptic problems, so the interest of this work would be:

- Study well-posed models of engineering problems that come from continuum mechanics.
- Develop appropriate variational formulations to establish existence and uniqueness of the continuous solution of the problem.
- Establish numerical schemes based on the HHO philosophy, for which we define appropriate spaces and discrete operators.
- Analyze the solvability of the HHO scheme and establish the corresponding stability and convergence results of the method.
- Validate the theoretical results obtained through illustrative numerical tests and simulations.

This thesis is organized as follows:

In Chapter 1, we present the main definitions related to meshes and their geometries, as well as some well-known technical results of functional analysis for the treatment of variational formulations (primal and/or mixed ones) [69]. In addition, a description of the HHO method for the Poisson problem with mixed boundary conditions and some numerical examples are included. Part of this discussion is found in the publication:

- Bustinza, R., Munguia, J.: *Revisión del método Híbrido de Alto Orden para un problema de difusión variable*. REVCIUNI 21(1), 6–14 (2018).

As a result, we establish that the HHO method can also be applied to problems with Neumann boundary condition, is stable and converges optimally, under similar regularity assumptions of the exact solution, as considered for Dirichlet problem.

In Chapter 2, the variable diffusion problem with pure Neumann boundary conditions is discussed. This same problem has been already analyzed with Dirichlet boundary condition in [72], and with mixed boundary conditions in [76], but it had not been fully analyzed for the Neumann case. The convergence of the HHO method with the pure Neumann boundary condition is demonstrated. In addition, it is explained how to make the discretization and computational implementation of this problem, under the HHO philosophy. The results of this chapter have led to the publications:

- Bustinza, R., Munguia, J.: *Revisión del método Híbrido de Alto Orden para un problema de difusión variable*. REVCIUNI 21(1), 6–14 (2018).
- Bustinza, R., Munguia-La-Cotera, J.: *A hybrid high-order formulation for a Neumann problem on polytopal meshes*. Numerical Methods for Partial Differential Equations 36, 3 (2020), 524–551. DOI 10.1002/num.22439

In Chapter 3, an extension of the HHO method for nonlinear elliptic problems is proposed. Although the case of homogeneous Dirichlet boundary conditions is considered, the methodology can be adapted, without major difficulties, for

nonhomogeneous, mixed and even pure Neumann boundary conditions. The contribution of this analysis is the deduction of an estimate of the potential error in L^2-norm, which, up to the author's knowledge, have not been established before. Numerical examples are included, validating our theoretical results. This chapter is contained in the pre-print:

- Bustinza, R. and Munguia, J.: *An a priori error analysis for a class of nonlinear elliptic problems applying the hybrid high-order method.* Centro de Investigación en Ingeniería Matemática, Universidad de Concepción, Chile (2020). Pre-print 2020-08

In Chapter 4, we introduce an HHO scheme to analyze transmission problems between two subdomains that can represent porous, gaseous or liquid media depending on the type of physics being analyzed. In [31] the authors present an HHO analysis for internal transmission problems, where the transmission boundary can be curved. However, numerical examples are not included. For this reason, we aim to dedicate this chapter to linear transmission, with a different analysis. The existence and uniqueness of the HHO scheme is established, and it is possible to obtain the expected a priori error estimates. The results of this chapter can be found in the pre-print:

- Bustinza, R. and Munguia, J.: *A mixed Hybrid High-Order formulation for linear interior transmission elliptic problems.* Centro de Investigación en Ingeniería Matemática, Universidad de Concepción, Chile (2020). Pre-print 2020-10

Finally, an accounting of the works we have developed is made, emphasizing their contributions. Also, some problems or theoretical aspects to be considered as future works are included.

INTRODUCCIÓN

En las últimas décadas se han resuelto una gran variedad de problemas de ingeniería como por ejemplo, construcción de mapas de ruidos [128], problemas de acústica [136], aeronáutica [55], dinámica de fluidos [132], etc. Estos modelos, en general, no pueden ser resueltos de manera analítica, y por lo tanto son tratados por métodos numéricos, como Diferencias Finitas (DF), Volúmenes Finitos (VF), Elementos Finitos (EF), entre otros. En este trabajo de tesis optamos por usar el método de elementos finitos, debido a su flexibilidad geométrica y a su alta precisión con polinomios de alto orden. Para una discusión de sus ventajas y desventajas con respecto a diferencias finitas y volúmenes finitos, consultar la introducción en [89].

Los ingenieros se enfrentan frecuentemente a problemas que pueden ser descritos/modelados en la mayoría de los casos por Ecuaciones Diferenciales Parciales (EDP). Matemáticos e ingenieros han ido desarrollando esquemas numéricos cada vez más sofisticados y robustos, para aproximar mejor y más rápido ciertas variables como la presión, velocidad, deformación y concentración, sobre la discretización de dominios complejos. Una razón del éxito del análisis numérico es la amplia disponibilidad de recursos computacionales de alto rendimiento y el aumento de las capacidades predictivas de los modelos numéricos traducidos en dichos esquemas. El objetivo principal del análisis numérico es describir la relación entre la solución exacta de la ecuación original y la aproximada obtenida de su versión discretizada (esquema numérico). Existen dos tipos: análisis de error a priori y a posteriori. El análisis de error a priori se encarga de establecer la convergencia del método empleado, estableciendo los órdenes de convergencia optimales de ser posible. En cambio, el análisis de error a posteriori busca diseñar una estrategia que permita

mejorar la calidad de aproximación sin tener que hacer refinamiento uniforme (lo usual en el análisis de error a priori). Esto conlleva a deducir algún estimador de error, que pueda calcularse en términos de la solución aproximada y de los datos del problema, el cual luego se implementa en un algoritmo de refinamiento adaptativo. En este manuscrito nos enfocaremos al análisis de error a priori.

Una reseña histórica del método de elementos finitos (MEF) se encuentra en [142]. Una aplicación del MEF en 2D, enfocada a la industria aeroespacial, se encuentra en el artículo pionero de Clough et al. [143]. A diferencia del método de diferencias finitas, que calcula una aproximación de la solución en un número finito de puntos de una cuadrícula, el método de elementos finitos busca una solución en un espacio de dimesión finita, basado en la discretización de la formulación débil de la EDP. Esta metodología se extendió a una amplia gama de aplicaciones en ingeniería durante los años 50 y 60. Por ejemplo, [151] es el primer libro que trata el método de elementos finitos en el área de ingeniería estructural, mientras que en [55] se tratan otras aplicaciones. El método de de elementos finitos desarrollado en estos trabajos iniciales se conoce comúnmente como método de Galerkin continuo estándar (continuous Galerkin (CG)), debido a que utiliza funciones continuas polinomiales a trozos y el principio de Ritz-Galerkin. Además se dice que es conforme, en el sentido que el espacio discreto es un subespacio del espacio continuo. Para conocer más detalles sobre sus inicios, referimos al lector a [113, 54, 150].

El desafío fue entonces (quizás aún lo sigue siendo) aproximar las soluciones discontinuas de las ecuaciones hiperbólicas involucradas en diferentes campos como dinámica de gases, geofísica, simulación de recuperación de petróleo, flujos granulares, etc. Estas discontinuidades tienden a provocar oscilaciones espurias, las cuales han sido abordadas por el método de volúmenes finitos al incorporar flujos numéricos y limitadores de pendiente adecuadamente definidos. El primer trabajo que permitió que el flujo fuera discontinuo a través de interfaces de elementos fue en el contexto de la ecuación de transporte, propuesto por Reed y Hill en 1973 [138]. Este método es llamado Galerkin discontinuo (discontinuous Galerkin (DG)) y fue

formulado y analizado por Lesaint and Raviart in 1974 [124]. Además, Cockburn y Shu en 1998 [61] introducen un operador llamado "limitador de pendiente" para asegurar la estabilidad del método DG de Runge-Kutta para problemas hiperbólicos no lineales. El método RKDG es un método DG explícito que satisface la ley de conservación hiperbólica no lineal localmente, con la discretización de tiempo de alta resolución de Runge-Kutta y una proyección local que asegura la estabilidad global del esquema. Para obtener más detalles, consulte [56]. Por tanto, los métodos DG al igual que los métodos FV pueden aproximar las leyes de conservación hiperbólicas no lineales sin presentar oscilaciones espurias. Posteriormente, una generalización del método de Nitsche permitió extender los métodos de DG a problemas de valores de frontera parabólicos no lineales de segundo orden, llamado método de penalización interior simétrico (SIP), que fue propuesto y analizado por Arnold en 1982 [9]. Referimos también los trabajos de Wheeler en 1978 [147] para problemas elípticos de segundo orden y Baker en 1977 [13] para problemas elípticos de cuarto orden. Otro método DG es el llamado método de Galerkin discontinuo local (local discontinuous Galerkin (LDG)) introducido por Cockburn and Shu en 1998 [62] como una extensión de los métodos RKDG de sistemas puramente hiperbólicos a sistemas de convección-difusión. Los métodos LDG pueden ser vistos como una generalización del método de Bassi and Rebay [18] para las ecuaciones de Navier-Stokes de flujos compresibles. Los métodos LDG requieren el uso de los llamados flujos numéricos, los cuales se definen en términos de las incógnitas y de los datos del problema. Esto permite imponer de manera débil la continuidad entre elementos que no se requiere en los espacios de aproximación. Además, el flujo numérico del potencial no depende de la incógnita flujo discreta, lo cual permite eliminar localmente esta incógnita (flujo), y resolver el problema solo en términos del potencial. Los esquemas DG son en general consistentes, y a diferencia del CG estándar, son métodos no conformes, localmente conservativos y paralelizables. Para un enfoque más general, referimos a [10, 8, 69].

La desventaja primordial entre CG y DG es que este último incrementa considerablemente el número de grados de libertad del sistema algebraico obtenido

después de la discretización. Por tal motivo, se introdujeron métodos DG que pueden ser hibridizados, en el sentido que se puede introducir la traza del potencial como una nueva incógnita, actuando como un multiplicador de Lagrange. Después de ejecutar una condensación estática, se obtiene un sistema sobre el esqueleto del mallado. Estos métodos son conocidos como métodos Galerkin discontinuo hibridizable (hybridizable discontinuous Galerkin (HDG)), y fueron introducidos en [58, 59]. Las demás incógnitas (de volumen), son reconstruidas después de calcular el multiplicador de Lagrange. Para una descripción general aplicado a mecánica de fluidos, referimos a [134]. También recomendamos revisar el libro [84], para una exposición más detallada y comprensible.

Esta tesis aborda problemas elípticos lineales y no lineales, usando el ya conocido método híbrido de alto orden (Hybrid High Order (HHO)), introducido en 2014 por Ern et al. [70, 75]. Esta técnica, al igual que el método HDG, es localmente conservativo [71], y permite el tratamiento de mallas politopales incluyendo posiblemente nodos colgantes, muy estudiadas en los últimos años, motivado por ejemplo por aplicaciones en geociencia, geometrías hexagonales en el diseño de reactores nucleares y reservorios de petróleo (con fallas geológicas). Cabe señalar que el tratamiento de mallas politopales puede extenderse naturalmente a HDG, el cual se desarrolló principalmente para mallas simpliciales. El método HHO pertenece a la familia de esquemas no conformes, pues el espacio de aproximación no está contenido en el espacio donde vive la solución exacta. El término "híbrido" (hybrid) se debe a que el método utiliza además de la información sobre las celdas la información de las caras del esqueleto. Además, como se utiliza localmente polinomios de orden $k \geq 0$ arbitrario en la construcción del espacio discreto, es que se adopta el término de "alto orden" (high order).

Los métodos HHO toman ideas del método SIP, como el diseño de operadores locales de reconstrucción y estabilización por un término de penalización local, con la diferencia que impone débilmente la correspondencia entre los grados de libertad local (degrees of freedom (DOFs)), basados en elementos y en caras y

no directamente entre las caras. Además, no tiene la necesidad de incluir algún parámetro de penalización para asegurar coercividad discreta. El problema discreto se ensambla celda a celda, y las incógnitas basadas en las celdas pueden eliminarse localmente mediante condensación estática (descomposición de Schur en el contexto matemático), es decir basta con resolver las incógnitas en las caras para recuperar (a un bajo costo computacional) las incógnitas en las celdas. Esta es una característica propia de los HHO, que también la tienen otros esquemas no conformes de elementos finitos, como se vio en el caso de los esquemas HDG. Los métodos HHO a diferencia de los HDG, no son consistentes por lo que se necesitará acotar el llamado término de consistencia. En [57] y [66, Section 5.1.6], se definen trazas numéricas para los métodos HHO, pudiéndose obtener una formulación mixta equivalente al esquema HHO primal. Esto permite hacer el vínculo con una nueva clase de métodos HDG. Así, los métodos HDG pueden verse como una generalización de los métodos HHO. Una versión mixta del método HHO es encontrada en [73], cuya relación con su versión primal discreta [75], es analizado en [3].

Otro método de alto orden y que soporta mallas politopales es el llamado método de elementos virtuales (virtual element (VE)), introducido en sus formas conforme en [20] y no conforme en [11]. Para ver una versión unificada de ambos tipos, el lector puede consultar [43]. El método VE es una generalización del clásico método de elementos finitos, el cual contiene, además de la usual familia de polinomios, otra clase de funciones no necesariamente polinomiales (soluciones de ecuaciones diferenciales parciales particulares). Tales funciones permiten introducir condiciones de regularidad de alto orden, no se hallan explícitamente y no se implementan, pudiendo reducir los grados de libertad solo sobre la parte polinomial (vértices de la malla). Se puede encontrar una relación con la versión no conforme en [57, Section 2.4] y una versión unificada (enfocado al caso conforme) en [125], donde se transcribe el método VE en el marco algebraico HHO.

Para abordar fenómenos que involucran materiales compuestos y medios porosos que aparecen en problemas elípticos con coeficientes de oscilación rápida, los métodos

monoescala no son recomendables, por lo que se utilizan los métodos multiescala. Algunos estudios al respecto, en el contexto de elementos finitos estándar, se encuentran en [120], para HDG en [85], y en los llamados métodos híbridos mixtos multiescala (multiscale hybrid-mixed (MHM)) en [7]. Es así que el método HHO también aborda este tipo de problemas (véase [52, 53]). Éste se basa en resolver problemas locales de la ecuación exacta con condiciones Neumann impuestas por multiplicadores de Lagrange. Estos problemas locales se resuelven con el HHO monoescala sobre una partición inicial del dominio heterogéneo (escalando el dominio).

Aunque los métodos HHO están pensados para usar polinomios de alto orden, es posible encontrar conecciones con métodos de bajo orden ($k = 0$). Por ejemplo, se pueden vincular con los métodos de volumen finito híbrido (hybrid finite volume (HFV)) en [75]. Además, el método HHO está relacionado con los métodos mimético mixto híbrido (Hybrid Mixed Mimetic (HMM)) en [67]. Aquí, los métodos HMM, propuestos en [21, 83], pueden verse como la formulación unificada de los métodos HFV [88], los métodos de volumen finito mixto (Mixed Finite Volume (MFV)) [82] y el método de diferencia finita mimética (mimetic finite difference (MFD)) [22]. Es interesante mencionar que nuestra metodología HHO puede compararse directamente con el método clásico de elementos finitos estándar, en el contexto de problemas de difusión ([77]).

El método HHO ha abordado una gran variedad de modelos, permitiendo un tratamiento robusto de los parámetros físicos involucrados en dichos modelos, como por ejemplo, difusión heterogénea/anisotrópica [72, 39], elasticidad lineal cuasi-incompresible [70], transporte con advección dominante [67, 4], problemas de elasticidad no lineal en el régimen de deformación pequeñas [27], problemas estacionarios no lineales de Leray–Lions [64, 65], problema de Stokes [3], ecuaciones incompresibles de Navier-Stokes [26], deformaciones finitas de materiales hiperelásticos [1], fuidos viscoplásticos de Bingham en tuberías [44], entre otros. Para una revisión de varios de estos trabajos y un detallado análisis de los mismos

consultar el libro dedicado al método [66].

Esta tesis busca complementar lo ya estudiado para HHO. Por ejemplo, el abordar condiciones Neumann puras, problemas de transmisión interior y una clase de problemas elípticos no lineales, por lo que el interés de este trabajo será:

- Estudiar matemáticamente modelos bien planteados de problemas de ingeniería que provienen de la mecánica del medio continuo.
- Desarrollar formulaciones variacionales apropiadas para establecer existencia y unicidad de la solución continua del problema.
- Establecer el esquema numérico basado en la filosofía HHO, para lo cual definimos espacios y operadores discretos apropiados.
- Analizar la solubilidad del esquema HHO y establecer los resultados de estabilidad y convergencia correspondientes del método.
- Validar los resultados teóricos obtenidos a través de ensayos y simulaciones numéricas ilustrativas.

La presente tesis se organiza de la siguiente manera:

En el Capítulo 1, presentamos las principales definiciones relativas a las mallas y sus geometrías. También algunos resultados usuales de análisis funcional para el tratamiento de formulaciones variacionales: primales y/o mixtas [69]. Se incluye, además, una descripción del método HHO para el problema de Poisson, con condiciones mixtas, incluyendo algunos ejemplos numéricos. Parte de esta discusión se encuentra en la publicación:

- Bustinza, R., Munguia, J.: *Revisión del método Híbrido de Alto Orden para un problema de difusión variable*. REVCIUNI 21(1), 6–14 (2018).

Como resultado, se prueba que el método HHO puede ser aplicado también a problemas con condición de frontera Neumann, es estable y converge de manera

óptima, bajo los mismos supuestos de regularidad de la solución exacta, consideradas para condiciones Dirichlet.

En el Capítulo 2, se analiza el problema de difusión variable bajo condiciones de frontera Neumann puras. Este mismo problema ha sido ya analizado, bajo condiciones de frontera Dirichlet en [72], y con condiciones mixtas en [76], pero no estaba completamente analizado para el caso Neumann. Se demuestra la convergencia del método HHO para el problem de Poisson con condición de frontera Neumann pura. Además, se explica cómo realizar la discretización y el ensamblaje de dicho problema, bajo la filosofía HHO. Los resultados de este capítulo han dado lugar a las publicaciones:

- Bustinza, R., Munguia, J.: *Revisión del método Híbrido de Alto Orden para un problema de difusión variable*. REVCIUNI 21(1), 6–14 (2018).
- Bustinza, R., Munguia-La-Cotera, J.: *A hybrid high-order formulation for a Neumann problem on polytopal meshes*. Numerical Methods for Partial Differential Equations 36, 3 (2020), 524–551. DOI 10.1002/num.22439

En el Capítulo 3, se propone una extensión del método HHO para problemas elípticos no lineales. Si bien se considera el caso de condiciones de frontera Dirichlet homogéneas, la metodología puede adaptarse, sin mayores dificultades, para condiciones Dirichlet no homogéneas, mixtas y hasta Neumann puro. El aporte de este análisis, es la deducción de la estima en norma L^2 del error del potencial, lo cual, hasta donde se sabe, no había sido establecido antes. Se incluyen ejemplos numéricos que validan la teoría. Este capítulo está contenido en el pre-print:

- Bustinza, R. and Munguia, J.: *An a priori error analysis for a class of nonlinear elliptic problems applying the hybrid high-order method*. Centro de Investigación en Ingeniería Matemática, Universidad de Concepción, Chile (2020). Pre-print 2020-08

En el Capítulo 4, introducimos un esquema HHO para analizar problemas de transmisión entre dos dominios que pueden respresentar medios porosos, gaseosos

o líquidos dependiendo del tipo de física que se esté analizando. En [31], los autores presentan un esquema unfitted HHO para problemas de transmisión interior, donde la frontera de transmisión puede ser curva. Sin embargo, no se incluyen ejemplos numéricos. Por esta razón, se decidió dedicar este capítulo al problema de transmisión lineal, con frontera de transmisión poligonal, donde se analiza un esquema HHO mixto, con un enfoque distinto de [31]. Se prueba la existencia y unicidad del esquema HHO, y se logran establecer las estimaciones de error a priori esperadas. Los resultados de este Capítulo se han plasmado en el pre-print:

- Bustinza, R. and Munguia, J.: *A mixed Hybrid High-Order formulation for linear interior transmission elliptic problems.* Centro de Investigación en Ingeniería Matemática, Universidad de Concepción, Chile (2020). Pre-print 2020-10

Finalmente, se hace un recuento de los trabajos realizados, enfatizando el/los aporte(s). Asimismo, se incluyen algunos problemas o aspectos teóricos a considerarse como trabajo a futuro.

Chapter 1

Preliminaries and basic results

In this chapter, we introduce the setting for the development and numerical analysis to deal with Hybrid High-Order (HHO) methods. These are built upon general meshes, possibly including polytope (or polytopal) elements and nonmatching interfaces.

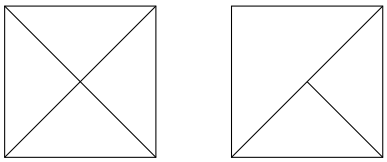

Figure 1.1: Left: Matching interfaces Right: Nonmatching interfaces

Here are the main concepts and properties used in this work, that can be found in more detail in [69, 66], for example.

1.1 General meshes

The HHO discretization of a PDE problem is a suitable decomposition (mesh) of the domain of the problem in study. The meshes supported by HHO methods are more general than those encountered in standard Finite Element methods, and possibly include general polytope elements and nonmatching interfaces.

The goal of this section is to introduce precise notions of mesh and h-refined mesh sequence suitable for the analysis.

Definition 1.1.1 (Polytope) *We say that the set P is a polytope in $\mathbb{R}^d$ if P is an open, connected, bounded subset of $\mathbb{R}^d$, such that its boundary ∂P is a finite union of parts of hyperplanes, say $\{H_i\}_{1\leq i\leq n_P}$. Moreover, for all $1 \leq i \leq n_P$, at each point in the interior of $\partial P \cap H_i$, the set P is assumed to lie on only one side of its boundary.*

An special polytope, is the convex polytope, which is the convex hull of finite number of points. See [111] for more details.

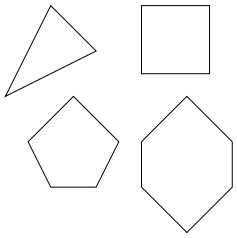

Figure 1.2: 2-polytopal elements

Definition 1.1.2 (Simplex) *Given a family $\{a_0, \cdots, a_d\}$ of $(d+1)$ points in $\mathbb{R}^d$ such that the vectors $\{a_1 - a_0, \cdots, a_d - a_0\}$ are linearly independent, the interior of the convex hull of $\{a_0, \cdots, a_d\}$ is called a non-degenerate simplex of $\mathbb{R}^d$, and the points $\{a_0, \cdots, a_d\}$ are called its vertices.*

Simplex is a convex polytope generated by the intersection of d independent hyperplanes. We often call a 2-polytope a polygon, and a 3-polytope a polyhedron.

Definition 1.1.3 (Simplex faces) *Let S be a non-degenerate simplex with vertices $\{a_0, \cdots, a_d\}$. For each $i \in \{0, \cdots, d\}$, the convex hull of $\{a_0, \cdots, a_d\}\backslash\{a_i\}$ is called a face of the simplex S.*

Definition 1.1.4 (Simplicial mesh) *A simplicial mesh $\mathcal{T}$ of the domain Ω (a polyhedron) is a finite collection of disjoint non-degenerate simplices $\mathcal{T} = \{T_j\}_{j\in I}$ with $I \subset \mathbb{N}$ finite, forming a partition of $\bar{\Omega}$.*

$$\bar{\Omega} = \bigcup_{T\in\mathcal{T}} T$$

Each $T \in \mathcal{T}$ is called a simplicial mesh element.

Definition 1.1.5 (General mesh) *A general mesh $\mathcal{T}$ of the domain Ω (a polyhedron) is a finite collection of disjoint polyhedra $\mathcal{T} = \{T\}$ forming a partition of $\bar{\Omega}$. Each $T \in \mathcal{T}$ is called a mesh element.*

Definition 1.1.6 (Element diameter, meshsize) *Let $\mathcal{T}$ be a general mesh of the domain Ω. For all $T \in \mathcal{T}$, h_T denotes the diameter of T, and the meshsize is defined as the real number*

$$h = \max_{T \in \mathcal{T}} h_T.$$

We use the notation $\mathcal{T}_h$ for a mesh $\mathcal{T}$ with meshsize h.

Definition 1.1.7 (Element outward normal) *Let $\mathcal{T}_h$ be a general mesh of the domain Ω (a polyhedron), and let $T \in \mathcal{T}_h$. We define $\boldsymbol{n}_T$ a.e. on ∂T as the (unit) outward normal to T.*

Definition 1.1.8 (Mesh faces) *Let $\mathcal{T}_h$ be a general mesh of the domain Ω (a polyhedron). We say that a (closed) subset F of $\bar{\Omega}$ is a mesh face if F has positive $(d-1)$-dimensional Hausdorff measure and if either one of the two following conditions is satisfied:*

1. *There are distinct mesh elements T_1 and T_2 such that $F = \partial T_1 \cap \partial T_2$. In such a case, F is called an interface.*

2. *There is $T \in \mathcal{T}$ such that $F = \partial T \cap \partial\Omega$. In such a case, F is called a boundary face.*

Interfaces are collected in the set $\mathcal{F}_h^i$, while boundary faces are collected in the set $\mathcal{F}_h^b$. Henceforth, we set the collection of faces inherited by $\mathcal{T}_h$ as

$$\mathcal{F}_h := \mathcal{F}_h^i \cup \mathcal{F}_h^b.$$

Moreover, for any mesh element $T \in \mathcal{T}_h$, the set

$$\mathcal{F}_T := \{F \in \mathcal{F}_h | F \subset \partial T\},$$

collects the mesh faces composing the boundary of T. The maximum number of mesh faces composing the boundary of mesh elements is denoted by

$$N_\partial := \max_{T \in \mathcal{T}_h} card(\mathcal{F}_T).$$

Finally, for any mesh face $F \in \mathcal{F}_h$, we define the set

$$\mathcal{T}_F := \{T \in \mathcal{T}_h | F \subset \partial T\},$$

that collects the mesh element of $\mathcal{T}_h$ sharing F.

Definition 1.1.9 (Face normals) *For all $F \in \mathcal{F}_h$ and a.e. $x \in F$, we define the normal $\boldsymbol{n}_F$ to F at x as*

1. *$\boldsymbol{n}_{T_1}$, the unit normal to F at x pointing from T_1 to T_2 if $F \in \mathcal{F}_h^i$ with $F = \partial T_1 \cap \partial T_2$; the orientation of $\boldsymbol{n}_F$ is arbitrary depending on the choice of T_1 and T_2, but fixed once and for all.*

2. *$\boldsymbol{n}$, the unit outward normal to Ω at x if $F \in \mathcal{F}_h^b$.*

In the following, we give the standard notion of matching simplicial mesh useful in the process of refining of a coarse mesh in the context of HHO methods.

Definition 1.1.10 (Matching simplicial mesh) *We say that $\mathcal{T}_h$ is a matching simplicial mesh if all the mesh element are simplices and if for any $T \in \mathcal{T}_h$ with vertices $\{a_0, \cdots, a_d\}$, the set $\partial T \cap \partial T'$ for any $T' \in \mathcal{T}_h$, $T' \neq T$, is the convex hull of a (possibly empty) subset of $\{a_0, \cdots, a_d\}$.*

Definition 1.1.11 (Matching simplicial submesh) *Let $\mathcal{T}_h$ be a general mesh. We say that $\mathcal{T}_h'$ is a matching simplicial submesh of $\mathcal{T}_h$ if*

1. *$\mathcal{T}_h'$ is a matching simplicial mesh,*

2. *For all $T' \in \mathcal{T}_h'$, there is only one $T \in \mathcal{T}_h$ such that $T' \subset T$,*

3. *For all $F' \in \mathcal{F}_h'$, the set collecting the mesh faces of $\mathcal{T}_h'$, there is at most one $F \in \mathcal{F}_h$ such that $F' \subset F$.*

Definition 1.1.12 (Shape and contact regularity) *Let $\mathcal{H} \subset \mathbb{R}^+ \cup \{0\}$ denote a countable set of meshsizes having 0 as its unique accumulation point. We consider h-refined general mesh sequences $(\mathcal{T}_h)_{h \in \mathcal{H}}$. We say that the mesh sequence $(\mathcal{T}_h)_{h \in \mathcal{H}}$ is shape- and contact-regular if for all $h \in \mathcal{H}$, $\mathcal{T}_h$ admits a matching simplicial submesh $\mathcal{T}_h'$ and there exists a real number $\rho > 0$, independent of h, such that, for all $h \in \mathcal{H}$:*

1. $\rho h_S \leq r_S$ *holds, for all simplex* $S \in \mathcal{T}_h'$ *of diameter* h_S*, and inradius* r_S*, and*

2. $\rho h_T \leq r_S$ *holds, for all* $T \in \mathcal{T}_h$ *and all* $S \in \mathcal{T}_h'$*, such that* $S \subset T$*.*

1.2 A review of theoretical framework on functional analysis

In this section, we give a review of important definitions and very well known theorems in Functional analysis, to deal with PDE problems written in weak sense.

Definition 1.2.1 (Lebesgue spaces) *Let* Ω *be an open bounded subset of* $\mathbb{R}^d$*,* $d \geq 1$*. Given* $1 \leq p \leq \infty$*, we define the Lebesgue space as*

$$L^p(\Omega) := \{v : \Omega \to \mathbb{R} \quad \text{Lebesgue measurable function s.t. } \|v\|_{L^p(\Omega)} < +\infty\}, \quad (1.1)$$

where, $\|\cdot\|_{L^p(\Omega)} : L^p(\Omega) \to \mathbb{R}$ *is a norm on* $L^p(\Omega)$*, given for each* $v \in L^p(\Omega)$*, by*

$$\|v\|_{L^p(\Omega)} := \begin{cases} \left(\displaystyle\int_\Omega |v|^p\right)^{1/p} & \text{if } p \in [1, +\infty), \\ \inf\{M > 0 \ : \ |v(x)| \leq M \ \text{ a.e. } x \in \Omega\} & \text{if } p = +\infty. \end{cases}$$

Definition 1.2.2 (Sobolev spaces) *Let* $m \geq 0$ *be an integer and let* $1 \leq p \leq \infty$ *be a real number. We introduce the Sobolev space*

$$W^{m,p}(\Omega) := \{v \in L^p(\Omega) \ : \ \partial^\alpha v \in L^p(\Omega) \, \forall \alpha \in \mathbb{N}^d : \ |\alpha| \leq m\}, \quad (1.2)$$

where, given a multi-index $\alpha = (\alpha_1, \alpha_2, \cdots, \alpha_d) \in \mathbb{N}^d$*,* $|\alpha| := \sum_{i=1}^d \alpha_i$*, and* $\partial^\alpha v$ *denotes the distributional derivative* $\partial^{\alpha_1} \cdots \partial^{\alpha_d} v$*. It is well known that the Sobolev space* $W^{m,p}(\Omega)$ *is a Banach space when is equipped with the norm* $\|\cdot\|_{W^{m,p}(\Omega)} : W^{m,p}(\Omega) \to \mathbb{R}$*, such that for all* $v \in W^{m,p}(\Omega)$*:*

$$\|v\|_{W^{m,p}(\Omega)} := \left(\sum_{|\alpha| \leq m} \|\partial^\alpha v\|_{L^p(\Omega)}\right)^{1/p} \qquad 1 \leq p < \infty,$$

and, when $p = +\infty$*,* $\|v\|_{W^{m,\infty}(\Omega)} := \max_{|\alpha| \leq m} \|\partial^\alpha v\|_{L^\infty(\Omega)}$*. We also consider the seminorm* $|\cdot|_{W^{m,p}(\Omega)}$ *by restricting the above definitions to multi-index* α*, with* $|\alpha| = m$*.*

For $p = 2$, we use the notation $H^m(\Omega) := W^{m,2}(\Omega)$. $H^m(\Omega)$ is a Hilbert space provided with the scalar product

$$(v, w)_{H^m(\Omega)} := \sum_{|\alpha| \leq m} (\partial^\alpha v, \partial^\alpha w)_{L^2(\Omega)} \quad \text{for all } v, w \in H^m(\Omega).$$

Now, we consider the following (abstract) problem: Seek $u \in U$ such that

$$a(u, v) = l(v) \text{ for all } v \in V, \tag{1.3}$$

where U and V are Hilbert spaces, $a : U \times V \to \mathbb{R}$ is a form and $l : V \to \mathbb{R}$ is a functional.

Theorem 1.2.1 (Banach–Nečas–Babuška (BNB)) *Let U be a Banach space and let V be a reflexive Banach space. Let $a : U \times V \to \mathbb{R}$ be a continuous bilinear form and let $l : V \to \mathbb{R}$ be a continuous linear functional. Then, problem (1.3) is well-posed if and only if:*

(i) There holds the inf-sup condition: there exists $C > 0$ such that

$$C \leq \inf_{u \in U \setminus \{0\}} \sup_{v \in V \setminus \{0\}} \frac{a(u, v)}{\|u\|_U \|v\|_V}. \tag{1.4}$$

(ii) For each $v \in V$, there holds

$$\Big(\forall\, w \in U,\ a(w, v) = 0\Big) \Rightarrow \Big(v = 0\Big). \tag{1.5}$$

Moreover, we have the continuous dependency:

$$\|u\|_U \leq \frac{1}{C} \|l\|_{V'}.$$

Proof. We refer to Theorem 2.6 in [86, page 85]. □

Definition 1.2.3 *Let H be a Hilbert space, and let $a : H \times H \to \mathrm{R}$ be a continuous bilinear form. We say that a is an H-elliptic (or coercive) operator if there is a constant $\alpha > 0$, such that*

$$\forall\, v \in H : \quad a(v, v) \geq \alpha \|v\|_H^2. \tag{1.6}$$

Lemma 1.2.1 *Under the assumptions of Definition 1.2.3, if a is H-elliptic, then there holds the following statements:*

(i) $\alpha \leq \inf_{w \in H\setminus\{0\}} \sup_{v \in H\setminus\{0\}} \dfrac{a(w,v)}{\|w\|_H \|v\|_H}$.

(ii) $\forall v \in H$: $\Big(\forall\, w \in H :\ a(w,v) = 0\Big) \Rightarrow \Big(v = 0\Big)$.

Proof. We refer to Lemma 2.8 in [86, page 85]. First, we fix $w \in H \setminus \{0\}$. Then, since a is H-ellipticity, we have

$$\alpha \|w\|_H \leq \frac{a(w,w)}{\|w\|_H} \leq \sup_{v \in H\setminus\{0\}} \frac{a(w,v)}{\|v\|_H},$$

and we derive (i) straightforwardly. Next, we prove (ii). We take $v \in H$, and by hypothesis, we have $a(v,v) = 0$. Thanks to coerciveness of a on H, we infer $v = 0$, and we end the proof. □

The following theorem is useful for establishing the well-posedness of variational formulations written as (1.3), with $V = U$.

Theorem 1.2.2 (Lax-Milgram Lemma) *Let V be a Hilbert space and let $a : V \times V \to \mathbb{R}$ be a V-elliptic continuous bilinear form. Then, for each continuous linear functional, $l : V \to \mathbb{R}$, there exists one and only one solution $u \in V$, such that*

$$a(u,v) = l(v), \quad \forall\, v \in V. \tag{1.7}$$

Proof. Problem (1.7) is equivalent to (1.3) when $U = V$. Then, the well-posedness of (1.7) follows from Lemma 1.2.1. □

Remark 1.2.1 *There is a generalized version of Lax-Milgram Lemma, to deal with (1.3) (i.e. $U \neq V$). We refer to [97, Theorem 4.2].*

In the following, we will give another result that helps us to proof the well-posedness of mixed variational formulations: Given functionals $f : U \to \mathbb{R}$, $g : P \to \mathbb{R}$, we seek $u \in U$ and $p \in P$, such that

$$a(u,v) + b(v,p) = f(v), \quad \forall\, v \in U, \tag{1.8a}$$

$$b(u,q) = g(q), \quad \forall\, q \in P. \tag{1.8b}$$

If we introduce $W := U \times P$, $A\big((u,p),(v,q)\big) := a(u,v) + b(v,p) + b(u,q)$, and $l(v,q) = f(v) + g(q)$, (1.8) is equivalent to the primal formulation: Find $(u,p) \in W$:

$$A\big((u,p),(v,q)\big) = l(v,q) \quad \forall (v,q) \in W. \tag{1.9}$$

Then, to establish well-posedness of the problem (1.8), we can take into account Theorem 1.2.1 to (1.9), under appropriate conditions. On the other hand, the following theorem could be useful to deal with linear mixed variational formulations of the type (1.8).

Theorem 1.2.3 (Well-posedness for linear mixed variational formulations) *Let U and P be two reflexive Banach spaces. Let $a : U \times U \to \mathbb{R}$, $b : U \times P \to \mathbb{R}$ be continuous bilinear forms and let $f : U \to \mathbb{R}$, $g : V \to \mathbb{R}$ be continuous linear functionals. Then, (1.8) is well-posed if and only if:*

(i) For each $v \in V := \{v \in U \ : \ \forall\, q \in P,\ b(v,q) = 0\}$, there holds

$$\Big(\forall\, w \in V,\ a(w,v) = 0\Big) \Rightarrow \Big(v = 0\Big). \tag{1.10}$$

(ii) There exists $\alpha > 0$ such that

$$\alpha \leq \inf_{u \in V\setminus\{0\}} \sup_{v \in V\setminus\{0\}} \frac{a(u,v)}{\|u\|_V \|v\|_V}. \tag{1.11}$$

(iii) and, there exists $\beta > 0$, such that

$$\beta \leq \inf_{q \in P\setminus\{0\}} \sup_{v \in U\setminus\{0\}} \frac{b(v,q)}{\|v\|_U \|q\|_P}. \tag{1.12}$$

Proof. We refer to the proof of Theorem 2.34 in [86, page 100] or Theorem 4.7 in [97, page 162]. □

Lemma 1.2.2 *Let V and W be two Banach spaces and let $A : V \to W$ be a continuous linear form. If A is surjective, then there exists $\alpha > 0$ such that*

$$\forall w \in W : \ \exists v_w \in V : \quad Av_w = w, \quad \text{and} \quad \alpha \|v_w\|_V \leq \|w\|_W\,. \tag{1.13}$$

Proof. We make a slightly adaptation of the proof of Theorem A.36 in [86, page 469]. Since A is surjective, thanks to Open Mapping Theorem, we deduce that $A\big(B_V(0,1)\big)$ is open in W, where $B_V(0,1)$ denotes the unit ball in V. Besides, by the linearity of A, we infer

$$\exists \gamma > 0 \text{ such that } \quad B_W(0,\gamma) \subset A\big(B_V(0,1)\big). \tag{1.14}$$

Now, taking $w \in W \setminus \{0\}$, we notice that $\frac{\gamma}{2}\frac{w}{\|w\|_W} \in B_W(0,\gamma)$, so that, from (1.14), $\exists z \in B_V(0,1)$ such that $Az = \frac{\gamma}{2}\frac{w}{\|w\|_W}$. Finally, we conclude (1.13) with $\alpha := \gamma/2$, and $v_w = \frac{2\|w\|_W}{\gamma} z \in V$. □

Definition 1.2.4 (Dual space, continuous linear functional) *Let X be a real Banach space . The dual space of X is defined as the set of continuous linear functional from X to $\mathbb{R}$, and is denoted by X'. Also, we provide to X' the following usual norm: for each $f \in X'$,*

$$\|f\|_{X'} := \sup_{x \in X \setminus \{0\}} \frac{|\langle f, x \rangle|_{X',X}}{\|x\|_X}, \tag{1.15}$$

where $\langle \cdot, \cdot \rangle_{X',X}$ denote the duality product between X' and X. Since $\pm x$ can be considered in the supremum, the absolute value can be omitted from the numerator.

Definition 1.2.5 (Dual operator) *Let V and W be two normed vector spaces and let $A : V \to W$ be a continuous linear operator. The dual operator $A^T : W' \to V'$ is defined by*

$$\forall v \in V : \forall w' \in W' : \quad \langle A^T w', v \rangle_{V',V} = \langle w', Av \rangle_{W',W}.$$

Lemma 1.2.3 *Let V and W be two Banach spaces and let $A : V \to W$ be a continuous linear form. If A is surjective, then, there holds the inf-sup condition:*

$$\exists \alpha > 0 : \quad \inf_{w' \in W'} \sup_{v \in V} \frac{\langle A^T w', v \rangle_{V',V}}{\|w'\|_{W'} \|v\|_V} \geq \alpha. \tag{1.16}$$

Proof. The proof is taken from [86, Lemma A.42]. We deduce, from Lemma 1.2.2, that there exists $\alpha > 0$, such that for each $w' \in W'$,

$$\langle w', w \rangle_{W',W} = \langle w', Av_w \rangle_{W',W} = \langle A^T w', v_w \rangle_{V',V} \leq \frac{1}{\alpha} \|A^T w'\|_{V'} \|w\|_W.$$

Hence,

$$\|w'\|_{W'} = \sup_{\substack{w \in W \\ \|w\|_W \leq 1}} \langle w', w \rangle_{W',W} \leq \frac{1}{\alpha} \|A^T w'\|_{V'},$$

and the conclusion follows from the definition of the norm in V'. □

Remark 1.2.2 *The converse holds when V is a reflexive space (Hilbert, in particular). We refer to Lemma A.42 in [86].*

The following corollary is useful for proving the well-posedness of the transmission problem of Chapter 4.

Corollary 1.2.1 *Under the same conditions of Theorem 1.2.3, the mixed problem (1.8) is well-posed if:*

(i) $\mathbb{B} : U \to P$ *is surjective, where* $\mathbb{B}$ *is the continuous linear operator induced by bilinear form* b*, as follows:*

$$\forall v \in U : \forall q \in P : \quad (\mathbb{B}v, q)_P = b(v, q),$$

(ii) and, a *is* W*-elliptic, where* $W := \mathbf{Ker}(\mathbb{B})$.

Proof. We are going to verify the three items from Theorem 1.2.3. It is easy to see that $V = W$, then from Lemma 1.2.1 and the W-ellipticy of a, we ensure that there holds the conditions (1.10) and (1.11). On the other hand, (1.12) follows from Lemma 1.2.3 and the surjectivity of $\mathbb{B}$. □

Remark 1.2.3 *It is possible to obtain:*

$$(i) \Longleftrightarrow \exists\, C > 0 \text{ s.t. } \sup_{v \in U \setminus \{0\}} \frac{b(v, q)}{\|v\|_U} \geq C \|q\|_P \ \ \forall q \in P.$$

We refer to the proof of Lemma 2.1 in [96] or Lemma 2.1 in [94].

1.3 A review on approximation theory in Banach spaces

Definition 1.3.1 (Polynomial Space) *Let* $k \geq 0$ *be an integer. We define the space of polynomials of* d *variables, of total degree at most* k*, as*

$$\mathbb{P}_d^k := \left\{ p : \mathbb{R}^d \ni x \to p(x) \in \mathbb{R} \ : \ \exists\, (c_\alpha)_{\alpha \in A_d^k} \in \mathbb{R}^{card(A_d^k)} \ s.t.\ p(x) = \sum_{\alpha \in A_d^k} c_\alpha x^\alpha \right\},$$

where $A_d^k := \{\alpha := (\alpha_1, \cdots, \alpha_d) \in \mathbb{N}^d \ : \ \sum_{j=1}^d \alpha_j \leq k\}$ *and for* $x = (x_1, \cdots, x_d) \in \mathbb{R}^d$*, we set* $x^\alpha := \prod_{i=1}^d x_i^{\alpha_i}$.

Definition 1.3.2 (The broken Polynomial Space) *We define the broken polynomial space as:*

$$\mathbb{P}_d^k(\mathcal{T}_h) := \{v \in L^2(\Omega) \ : \ \forall T \in \mathcal{T}_h : v_{|_T} \in \mathbb{P}_d^k(T)\},$$

where $\mathbb{P}_d^k(T)$ *is spanned by the restriction to* T *of polynomials in* $\mathbb{P}_d^k$.

Definition 1.3.3 (Optimal polynomial approximation) *We say that the mesh sequence $(\mathcal{T}_h)_{h\in\mathcal{H}}$ has optimal polynomial approximation properties if, for all $h \in \mathcal{H}$, all $T \in \mathcal{T}_h$, and all polynomial degree k, there is a linear interpolation operator $I_T^k : L^2(T) \to \mathbb{P}_d^k(T)$ such that, for all $s \in \{0, \cdots, k+1\}$ and all $v \in H^s(T)$, there holds*

$$|v - I_T^k v|_{H^m(T)} \leq C_{app} h_T^{s-m} |v|_{H^s(T)} \quad \forall m \in \{0, \cdots, s\}, \tag{1.17}$$

where $C_{app} > 0$ is independent of both T and h.

Definition 1.3.4 (Admissible mesh sequence) *The mesh sequence $(\mathcal{T}_h)_{h\in\mathcal{H}}$ is admissible, if it is shape- and contact-regular, and it has optimal polynomial approximation properties.*

We next show basic results, valid for admissible mesh sequences.

Lemma 1.3.1 (Diameters comparison) *Let $(\mathcal{T}_h)_{h\in\mathcal{H}}$ be an admissible mesh sequence. For all $h \in \mathcal{H}$, all $T \in \mathcal{T}_h$, and all $F \in \mathcal{F}_T$, h_F is comparable to h_T in the sense that*

$$\rho^2 h_T \leq h_F \leq h_T, \tag{1.18}$$

where h_F denotes the diameter of F.

Proof. We refer to Lemma 1.42 in [69]. □

Lemma 1.3.2 (Inverse inequality) *Let $(\mathcal{T}_h)_{h\in\mathcal{H}}$ be an admissible mesh sequence. For all $h \in \mathcal{H}$, all $v_h \in \mathbb{P}_d^k(\mathcal{T}_h)$, all $T \in \mathcal{T}_h$, and all $F \in \mathcal{F}_T$, there holds*

$$\|\nabla v_h\|_{[L^2(T)]^d} \leq C_{inv} h_T^{-1} \|v_h\|_{L^2(T)}, \tag{1.19}$$

where $C_{inv} > 0$, only depends on ρ, d, and k.

Proof. We refer to the proof of Lemma 1.44 in [69]. □

Lemma 1.3.3 (Continuous trace inequality) *Let $(\mathcal{T}_h)_{h\in\mathcal{H}}$ be an admissible mesh sequence. For all $h \in \mathcal{H}$, all $T \in \mathcal{T}_h$, all $v \in H^1(T)$, and all $F \in \mathcal{F}_T$, there holds*

$$\|v\|_{L^2(F)}^2 \leq C_{cti}(h_T \|\nabla v\|_{[L^2(T)]^d}^2 + h_T^{-1} \|v\|_{L^2(T)}^2), \tag{1.20}$$

where $C_{cti} > 0$, only depends on ρ.

Proof. We refer to the proof of Lemma 1.49 in [69]. □

Lemma 1.3.4 (Discrete trace inequality) *Let $(\mathcal{T}_h)_{h\in\mathcal{H}}$ be an admissible mesh sequence. For all $h \in \mathcal{H}$, all $v_h \in \mathbb{P}_d^k(\mathcal{T}_h)$, and all $T \in \mathcal{T}_h$, there holds*

$$\|v_h\|_{L^2(F)} \leq C_{tr} h_T^{-1/2} \|v_h\|_{L^2(T)}, \tag{1.21}$$

where $C_{tr} > 0$ only depends on ρ, d, and k.

Proof. We refer to the proof of Lemma 1.46 in [69]. □

Lemma 1.3.5 (Approximation properties of π_T^l) *Given $T \in \mathcal{T}_h$, let π_T^l be the L^2-orthogonal projection onto $\mathbb{P}_d^k(T)$. Then, for all $s \in \{0, \cdots, l+1\}$ and all $v \in H^s(T)$, there holds*

$$|v - \pi_T^l v|_{H^m(T)} \leq C'_{app} h_T^{s-m} |v|_{H^s(T)} \quad \forall m \in \{0, \cdots, s\}. \tag{1.22}$$

Moreover, assuming additionally that $s \geq 1$, there holds for all $F \in \mathcal{F}_T$,

$$|v - \pi_T^l v|_{H^m(F)} \leq C''_{app} h_T^{s-m-1/2} |v|_{H^s(T)} \quad \forall m \in \{0, \cdots, s-1\}. \tag{1.23}$$

Here $C'_{app} > 0$ and $C''_{app} > 0$ are independent of both T and h.

Proof. We refer to the proofs of Lemmas 1.58 and Lemma 1.59 in [69] or to the proof of Theorem 1.44 in [66]. □

Lemma 1.3.6 (Local Poincaré–Wintinger inequality) *For all $h \in \mathcal{H}$, all $T \in \mathcal{T}_h$, all $v \in H^1(T)$, such that $\int_T v = 0$, there holds*

$$\|v\|_{L^2(T)} \leq C_p h_T \|\nabla v\|_{[L^2(T)]^d}, \tag{1.24}$$

where $C_p > 0$ only depends on ρ (mesh regularity parameter) ($C_p = \pi^{-1}$ if T is convex).

Proof. We refer to the proof of Lemma 5.8 in [64] or Theorem 3.2 in [19]. The proof is based on Poincaré-Wintinger inequality. □

In the following section, we give a review of the HHO method when applied to Poisson problem, with Dirichlet and mixed boundary conditions.

1.4 An HHO method for Poisson problem with mixed boundary conditions

Several elliptic problems with Dirichlet boundary conditions have been analyzed in the context of HHO methods, see e.g. [75, 64, 72, 70]. Part of the description developed in the following, is taken from [76], where HHO is applied to a class of variable diffusion problems with mixed boundary conditions. We begin introducing the model problem. Let $\Omega \subset \mathbb{R}^d$, $d \in \{2,3\}$, be an open, connected, bounded polytopal domain. We assume that there exists a partition $\{\Gamma_D, \Gamma_N\}$ of boundary $\Gamma := \partial\Omega$, such that $\Gamma = \Gamma_N \cup \Gamma_D$, $\mathring{\Gamma}_N \cap \mathring{\Gamma}_D = \emptyset$ and $|\Gamma_D| > 0$. For any connected subset $X \subset \Omega$, with nonzero Lebesgue measure, the inner product and norm of the Lebesgue space $L^2(X)$ will be denoted by $(\cdot,\cdot)_X$ and $\|\cdot\|_X$, respectively. Furthermore, given $x, y > 0$, $x \lesssim y$ denotes the inequality $x \leq Cy$ with positive constant C independent of the diffusion tensor K and the meshsize h, and probably not independent of the polynomial degree k. The model problem reads: Find $u : \Omega \to \mathbb{R}$ such that

$$-\nabla \cdot (K\nabla u) = f \quad \text{in } \Omega\,, \tag{1.25a}$$

$$K\nabla u \cdot \boldsymbol{n} = g_N \quad \text{on } \Gamma_N\,, \tag{1.25b}$$

$$u = g_D \quad \text{on } \Gamma_D\,, \tag{1.25c}$$

where $f \in L^2(\Omega)$, $g_N \in L^2(\Gamma_N)$, $g_D \in H^{1/2}(\Gamma_D)$, $K \in [L^\infty(\Omega)]^{d\times d}$ be a tensor-valued diffusivity and $\boldsymbol{n}$ be unit outward normal. For simplicity, we assume K is piecewise constant on P_Ω (partition of Ω). Let $U := H^1(\Omega)$ and $U_0 := \{v \in U \ : \ \gamma_0(v) = 0 \text{ on } \Gamma_D\}$. We obtain the primal weak formulation: Find $u_0 \in U_0$ such that

$$(K\nabla u_0, \nabla v)_\Omega = (f, v)_\Omega - (K\nabla u_\partial, \nabla v)_\Omega + (g_N, v)_{\Gamma_N} \quad \forall v \in U_0, \tag{1.26}$$

where $u_\partial \in H^1(\Omega)$ such that $\gamma_0(u_\partial) = g_D$ on Γ_D. The weak solution $u \in U$ related to (1.25), is then computed as

$$u = u_0 + u_\partial. \tag{1.27}$$

Now, we introduce the discrete spaces:

$$\underline{\mathbf{U}}_h^k := \left(\prod_{T\in\mathcal{T}_h} \mathbb{P}_d^k(T)\right) \times \left(\prod_{F\in\mathcal{F}_h} \mathbb{P}_{d-1}^k(F)\right) \quad , \quad \underline{\mathbf{U}}_T^k := \mathbb{P}_d^k(T) \times \left(\prod_{F\in\mathcal{F}_T} \mathbb{P}_{d-1}^k(F)\right).$$

In addition, we will denote by $\underline{\mathbf{v}}_h := ((v_T)_{T\in\mathcal{T}_h}, (v_F)_{F\in\mathcal{F}_h})$ an element in $\underline{\mathbf{U}}_h^k$ and its restriction on $T \in \mathcal{T}_h$ by $\underline{\mathbf{v}}_T := (v_T, (v_F)_{F\in\mathcal{F}_T}) \in \underline{\mathbf{U}}_T^k$. Besides, we introduce over each $T \in \mathcal{T}_h$, the discrete operator $p_T^{k+1} : \underline{\mathbf{U}}_T^k \to \mathbb{P}_d^{k+1}(T)$ such that, for each $\underline{\mathbf{v}}_T := (v_T, (v_F)_{F\in\mathcal{F}_T}) \in \underline{\mathbf{U}}_T^k$, and each $w \in \mathbb{P}_d^{k+1}(T)$,

$$(K\nabla p_T^{k+1}\underline{\mathbf{v}}_T, \nabla w)_T = (K\nabla v_T, \nabla w)_T + \sum_{F\in\mathcal{F}_T} (v_F - v_T, K\nabla w\cdot \boldsymbol{n}_{TF})_F, \tag{1.28}$$

and

$$\int_T p_T^{k+1}\underline{\mathbf{v}}_T := \int_T v_T, \tag{1.29}$$

where, $\boldsymbol{n}_{TF}$ is the unit normal to F pointing out of T. Moreover, we define the bilinear form $a_h : \underline{\mathbf{U}}_h^k \times \underline{\mathbf{U}}_h^k \to \mathbb{R}$ as

$$a_h(\underline{\mathbf{u}}_h, \underline{\mathbf{v}}_h) := \sum_{T\in\mathcal{T}_h} a_T(\underline{\mathbf{u}}_T, \underline{\mathbf{v}}_T)\,, \tag{1.30}$$

where, for each $T \in \mathcal{T}_h$, the local bilinear forms a_T , $s_T : \underline{\mathbf{U}}_T^k \times \underline{\mathbf{U}}_T^k \to \mathbb{R}$, are given by

$$a_T(\underline{\mathbf{u}}_T, \underline{\mathbf{v}}_T) := (K\,\nabla\, p_T^{k+1}\,\underline{\mathbf{u}}_T, \nabla\, p_T^{k+1}\,\underline{\mathbf{v}}_T)_T \;+\; s_T(\underline{\mathbf{u}}_T, \underline{\mathbf{v}}_T), \tag{1.31a}$$

$$s_T(\underline{\mathbf{u}}_T, \underline{\mathbf{v}}_T) := \sum_{F\in\mathcal{F}_T} \frac{k_F}{h_F}(\pi_F^k(u_F - R_T^{k+1}\underline{\mathbf{u}}_T), \pi_F^k(v_F - R_T^{k+1}\underline{\mathbf{v}}_T))_F, \tag{1.31b}$$

where, $R_T^{k+1}\underline{\mathbf{v}}_T := v_T + (p_T^{k+1}\underline{\mathbf{v}}_T - \pi_T^k p_T^{k+1}\underline{\mathbf{v}}_T)$.

Then, the (primal) HHO discretization of problem (1.26) reads: Find $\underline{\mathbf{u}}_{0,h} \in \underline{\mathbf{U}}_{h,0}^k := \left\{\underline{\mathbf{v}}_h \in \underline{\mathbf{U}}_h^k \mid v_F \equiv 0\ \forall F \subset \Gamma_D\right\}$ such that

$$a_h(\underline{\mathbf{u}}_{0,h}, \underline{\mathbf{v}}_h) = \sum_{T\in\mathcal{T}_h}(f, v_T)_T - a_h(\underline{\mathbf{u}}_{\partial,h}, \underline{\mathbf{v}}_h) + \sum_{F\subset\Gamma_N}(g_N, v_F)_F \quad \forall \underline{\mathbf{v}}_h \in \underline{\mathbf{U}}_{h,0}^k, \tag{1.32}$$

where $\underline{\mathbf{u}}_{\partial,h} := \left((\pi_T^k u_\partial)_{T\in\mathcal{T}_h}, (\pi_F^k\gamma_0(u_\partial))_{F\in\mathcal{F}_h}\right)$. The discrete solution $\underline{\mathbf{u}}_h \in \underline{\mathbf{U}}_h^k$ is finally computed as

$$\underline{\mathbf{u}}_h = \underline{\mathbf{u}}_{0,h} + \underline{\mathbf{u}}_{\partial,h}, \tag{1.33}$$

The next result establishes an estimate of the error between the Projection operator of the exact solution u, $\underline{\mathbf{I}}_h^k u := \left((\pi_T^k u)_{T\in\mathcal{T}_h}, (\pi_F^k\gamma_0(u))_{F\in\mathcal{F}_h}\right)$, and the discrete solution $\underline{\mathbf{u}}_h$, measures in the energy norm, defined as $\|\cdot\|_{a,h} := a_h(\cdot,\cdot)^{1/2}$. We remark that this result has been mentioned, without proof, in [76, Theorem 3.1].

Theorem 1.4.1 (Energy-norm error estimate) *Let $u \in U$, defined in (1.27), be the weak solution, and let $\underline{\mathbf{u}}_h \in \underline{\mathbf{U}}_h^k$, defined in (1.33), the discrete solution. Assume that u further belongs to $H^{k+2}(P_\Omega)$, with P_Ω being a partition of $\overline{\Omega}$ associated with the diffusion tensor K. Then, the following holds:*

$$\|\underline{\mathbf{I}}_h^k u - \underline{\boldsymbol{u}}_h\|_{a,h} \lesssim \left\{ \sum_{T \in \mathcal{T}_h} \overline{K}_T \rho_T h_T^{2(k+1)} \|u\|^2_{H^{k+2}(T)} \right\}^{1/2}, \tag{1.34}$$

where, $\rho_T := \overline{K}_T / \underline{K}_T$, with $\underline{K}_T$ and $\overline{K}_T$ being the lowest and largest eigenvalues of tensor K in T, respectively.

Proof. The proof follows similar ideas to the proof of Theorems 3.19 and 4.16 in [66]. □

Next, we provide an estimate of $\|\pi_h^k u - u_h\|_\Omega$, where $u_h \in L^2(\Omega)$ and $\pi_h^k u \in L^2(\Omega)$, such that

$$u_h|_T := u_T \quad \text{and} \quad \pi_h^k u|_T := \pi_T^k u \qquad \forall\, T \in \mathcal{T}_h. \tag{1.35}$$

To this aim, we require an elliptic regularity property: Given $g \in L^2(\Omega)$, let $z \in U_0$ be the solution of

$$\Delta z = g \quad \text{in } \Omega\,, \tag{1.36a}$$

$$\nabla z \cdot \boldsymbol{n} = 0 \quad \text{on } \Gamma_N\,, \tag{1.36b}$$

$$z = 0 \quad \text{on } \Gamma_D\,, \tag{1.36c}$$

which satisfies the a priori estimate:

$$\|z\|_{H^2(P_\Omega)} \lesssim \underline{K}_T \|g\|_\Omega, \tag{1.37}$$

Theorem 1.4.2 (L^2-norm error estimate) *Under the same assumptions on u as in Theorem 1.4.1, the elliptic regularity property (1.37), and assuming that $f \in H^{k+\delta}(\Omega)$, $g_N \in W^{k+\delta,\infty}(\Gamma_N)$, with $\delta = 0$ for $k \geq 1$ and $\delta = 1$ for $k = 0$, there holds*

$$\begin{aligned} \underline{K}\|\pi_h^k u - u_h\|_\Omega \lesssim \overline{K}^{1/2} \rho^{1/2} h \left\{ \sum_{T \in \mathcal{T}_h} \overline{K}_T \rho_T h_T^{2(k+1)} \|u\|^2_{H^{k+2}(T)} \right\}^{1/2} \\ + h^{k+2} \left\{ \|f\|_{H^{k+\delta}(\Omega)} + \|g_N\|_{W^{k+\delta,\infty}(\Gamma_N)} \right\}, \end{aligned} \tag{1.38}$$

where, $\rho := \overline{K}/\underline{K}$, $\overline{K} := \max_{T \in \mathcal{T}_h} \overline{K}_T$, $\underline{K} := \min_{T \in \mathcal{T}_h} \underline{K}_T$, and $h := \max_{T \in \mathcal{T}_h} h_T$.

Proof. The proof follows similar ideas from the Theorem 2.4.2 in the Chapter 2, or it could be deduced from the proof of Theorem 4.21 in [66]. □

Next, we show several numerical examples of (1.25), considering different boundary conditions (cf. [38]).

1.4.1 Pure Dirichlet boundary condition

In this section, we consider the pure Dirichlet boundary condition, whose analysis is included in the analysis developed here, taking $\Gamma_N = \emptyset$.

Example 1

First, we solve (1.25), with $\Gamma_N = \emptyset$, on the unit square $\Omega = (0,1)^2$, with the following smooth function:

$$u(x,y) = \sin(\pi x)\sin(\pi y) \tag{1.39}$$

and heterogeneous anisotropic diffusion tensor:

$$K(x,y) = \begin{pmatrix} 1 & 0 \\ 0 & \epsilon \end{pmatrix}, \tag{1.40}$$

with $\epsilon = 10^{-3}$. Then, we test the problem with two families of meshes: triangular and hexagonal form (See Figure 1.3). In Figures 1.4, 1.5, and Tables 1.1, 1.2, we observe that the rates of convergence of the HHO scheme are in agreement with Theorems 1.4.1 and 1.4.2. We point out, that for $k = 4$, the rate of convergence is being lost, and is worse with the triangular family mesh. This phenomenon is possibly due to the high anisotropy of the diffusion tensor and the round-off errors.

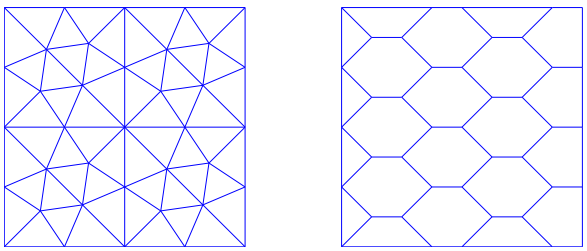

Figure 1.3: (Left) sequence of simplicial meshes and (Right) sequences of (predominantly) hexagonal meshes.

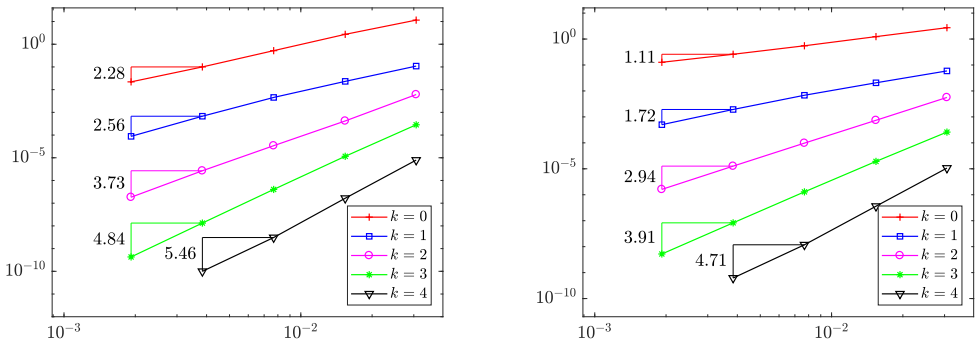

Figure 1.4: Convergence rates of potential (Left) and flux (Right) errors, considering a sequence of simplicial meshes.

Table 1.1: History of convergence of potential and flux errors, $k \in \{0, 1, 2, 3, 4\}$. (Family of simplicial meshes)

Potential										
	$k = 0$		$k = 1$		$k = 2$		$k = 3$		$k = 4$	
h	error	rate	error	rate	error	rate	error	rate	error	rate
3.07e-02	1.15e+01		1.09e-01		6.09e-03		2.83e-04		7.91e-06	
1.54e-02	2.72e+00	2.092	2.31e-02	2.245	4.18e-04	3.881	1.16e-05	4.632	1.65e-07	5.610
7.68e-03	5.21e-01	2.377	4.54e-03	2.343	3.40e-05	3.606	4.03e-07	4.830	3.07e-09	5.724
3.84e-03	1.00e-01	2.381	6.75e-04	2.747	2.68e-06	3.668	1.33e-08	4.917	9.96e-11	4.947
1.92e-03	2.20e-02	2.184	8.79e-05	2.943	1.83e-07	3.870	4.29e-10	4.958	2.68e-10	-1.428
Flux										
	$k = 0$		$k = 1$		$k = 2$		$k = 3$		$k = 4$	
h	error	rate	error	rate	error	rate	error	rate	error	rate
3.07e-02	2.74e+00		5.90e-02		5.62e-03		2.60e-04		1.07e-05	
1.54e-02	1.24e+00	1.148	2.06e-02	1.526	7.40e-04	2.939	1.93e-05	3.769	3.61e-07	4.906
7.68e-03	5.50e-01	1.168	6.82e-03	1.590	9.76e-05	2.911	1.29e-06	3.886	1.18e-08	4.917
3.84e-03	2.59e-01	1.086	1.93e-03	1.820	1.27e-05	2.944	8.27e-08	3.964	6.19e-10	4.254
1.92e-03	1.27e-01	1.028	5.02e-04	1.944	1.61e-06	2.977	5.22e-09	3.986	3.14e-09	-2.341

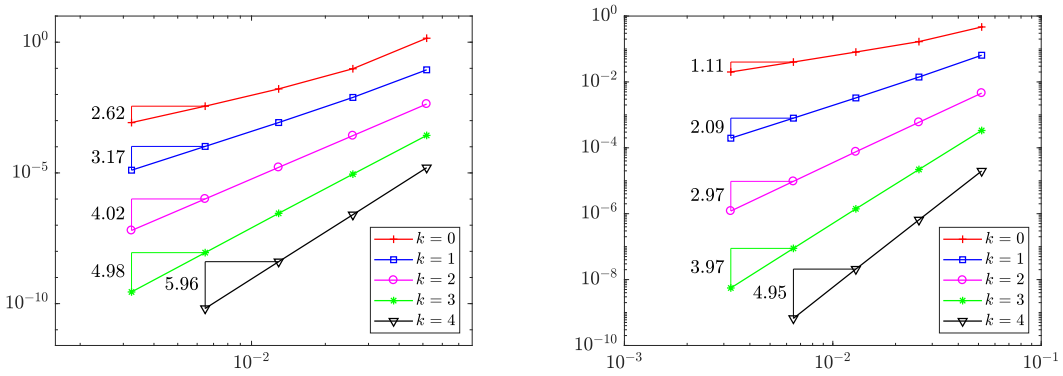

(a) Potential error

(b) Flux error

Figure 1.5: Convergence rates of potential and flux errors, considering a family of hexagonal meshes.

Table 1.2: History of convergence of potential and flux errors, $k \in \{0, 1, 2, 3, 4\}$. (Family of hexagonal meshes)

Potential										
	$k = 0$		$k = 1$		$k = 2$		$k = 3$		$k = 4$	
h	error	rate	error	rate	error	rate	error	rate	error	rate
5.18e-02	1.42e+00		8.77e-02		4.32e-03		2.72e-04		1.58e-05	
2.59e-02	9.65e-02	3.877	7.71e-03	3.507	2.66e-04	4.020	8.96e-06	4.921	2.52e-07	5.970
1.29e-02	1.63e-02	2.548	8.44e-04	3.173	1.63e-05	4.007	2.84e-07	4.952	4.02e-09	5.937
6.47e-03	3.57e-03	2.206	1.03e-04	3.047	1.01e-06	4.029	8.92e-09	5.016	6.52e-11	5.974
3.24e-03	8.40e-04	2.091	1.27e-05	3.027	6.29e-08	4.014	2.80e-10	5.007	3.54e-11	0.881
Flux										
	$k = 0$		$k = 1$		$k = 2$		$k = 3$		$k = 4$	
h	error	rate	error	rate	error	rate	error	rate	error	rate
5.18e-02	4.66e-01		6.46e-02		4.58e-03		3.36e-04		1.98e-05	
2.59e-02	1.67e-01	1.477	1.41e-02	2.199	5.95e-04	2.944	2.20e-05	3.931	6.50e-07	4.926
1.29e-02	8.08e-02	1.046	3.27e-03	2.094	7.58e-05	2.957	1.40e-06	3.949	2.08e-08	4.938
6.47e-03	4.01e-02	1.013	7.95e-04	2.049	9.58e-06	2.997	8.85e-08	4.004	6.62e-10	4.996
3.24e-03	2.00e-02	1.004	1.96e-04	2.025	1.21e-06	2.998	5.56e-09	4.002	3.98e-10	0.738

Example 2

Now, we consider (1.25) with pure Dirichlet conditions on the domain $\Omega = (-1,1)^2\backslash[0,1]\times[-1,0]$ (see Figure 1.6), such that the exact solution (in polar coordinates) is given by

$$u(r,\theta) = r^{2/3}\sin(2\theta/3), \tag{1.41}$$

where $u \in H^{1+\frac{2}{3}-s}$ for some $s > 0$ (see [108]), and homogeneous isotropic diffusion tensor K equal to the identity.

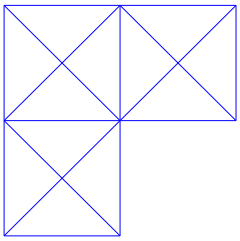

Figure 1.6: L-shaped domain.

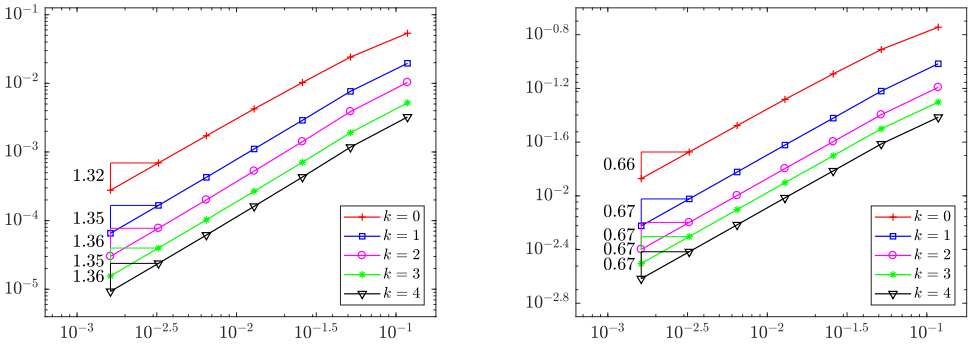

Figure 1.7: Convergence rates of potential (Left) and flux (Right) errors.

From Figure 1.7 and Table 1.3, it is observed that the HHO scheme always converges with order 4/3 for the potential and 2/3 for the flux, respectively. And this behavior is independent of the degree of approximation considered. This does not contradict the theoretical results from Theorems 1.4.1 and 1.4.2, due to the little regularity of the exact solution u in this case.

Table 1.3: History of convergence of potential and flux errors, $k \in \{0, 1, 2, 3, 4\}$.

Potential										
	$k=0$		$k=1$		$k=2$		$k=3$		$k=4$	
h	error	rate	error	rate	error	rate	error	rate	error	rate
1.18e-01	5.37e-02		1.96e-02		1.03e-02		5.19e-03		3.23e-03	
5.18e-02	2.41e-02	0.971	7.64e-03	1.143	3.87e-03	1.191	1.91e-03	1.213	1.17e-03	1.231
2.59e-02	1.03e-02	1.232	2.90e-03	1.401	1.41e-03	1.454	7.08e-04	1.433	4.31e-04	1.446
1.29e-02	4.24e-03	1.270	1.11e-03	1.381	5.28e-04	1.414	2.67e-04	1.397	1.61e-04	1.407
6.47e-03	1.72e-03	1.307	4.27e-04	1.378	2.01e-04	1.402	1.03e-04	1.388	6.16e-05	1.396
3.24e-03	6.92e-04	1.317	1.66e-04	1.362	7.73e-05	1.379	3.98e-05	1.369	2.38e-05	1.375
1.62e-03	2.77e-04	1.322	6.53e-05	1.350	3.01e-05	1.361	1.56e-05	1.355	9.28e-06	1.359
Flux										
	$k=0$		$k=1$		$k=2$		$k=3$		$k=4$	
h	error	rate	error	rate	error	rate	error	rate	error	rate
1.18e-01	1.80e-01		9.63e-02		6.42e-02		4.99e-02		3.85e-02	
5.18e-02	1.23e-01	0.466	6.02e-02	0.570	4.02e-02	0.570	3.16e-02	0.555	2.43e-02	0.556
2.59e-02	8.09e-02	0.603	3.79e-02	0.668	2.53e-02	0.666	1.99e-02	0.666	1.53e-02	0.667
1.29e-02	5.22e-02	0.628	2.39e-02	0.662	1.60e-02	0.663	1.25e-02	0.663	9.66e-03	0.663
6.47e-03	3.34e-02	0.649	1.51e-02	0.669	1.01e-02	0.670	7.89e-03	0.670	6.08e-03	0.670
3.24e-03	2.12e-02	0.656	9.48e-03	0.668	6.33e-03	0.668	4.97e-03	0.668	3.83e-03	0.668
1.62e-03	1.34e-02	0.659	5.97e-03	0.667	3.99e-03	0.667	3.13e-03	0.667	2.41e-03	0.667

1.4.2 Mixed boundary condition

We will consider the nonregular solution (1.41) in polar coordinates: for the mixed diffusion problem (1.25), and unity diffusion tensor again. This test is run over two mixed boundary conditions:

First, we consider the domain $\Omega = (-1, 1)^2 \backslash [0, 1] \times [-1, 0]$, with the following partition of the boundary $\Gamma := \partial\Omega$.

$$\Gamma_D = \{0\} \times [-1, 0] \cup [0, 1] \times \{0\} \quad \text{and} \quad \Gamma_N := \Gamma \backslash \Gamma_D. \tag{1.42}$$

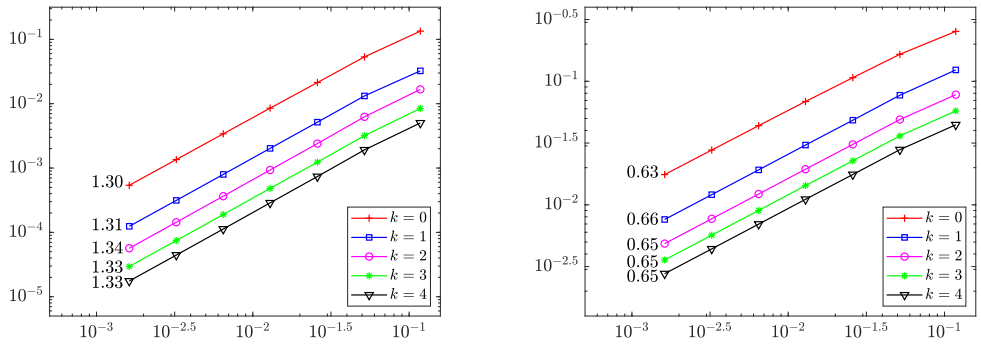

(a) Potential error

(b) Flux error

Figure 1.8: Convergence rates of potential and flux errors.

Table 1.4: History of convergence of potential and flux errors, $k \in \{0, 1, 2, 3, 4\}$.

Potential										
	$k = 0$		$k = 1$		$k = 2$		$k = 3$		$k = 4$	
h	error	rate	error	rate	error	rate	error	rate	error	rate
1.18e-01	1.34e-01		3.24e-02		1.67e-02		8.44e-03		5.02e-03	
5.18e-02	5.34e-02	1.119	1.32e-02	1.091	6.25e-03	1.194	3.19e-03	1.182	1.91e-03	1.171
2.59e-02	2.13e-02	1.324	5.16e-03	1.355	2.40e-03	1.380	1.23e-03	1.369	7.38e-04	1.375
1.29e-02	8.52e-03	1.316	2.02e-03	1.344	9.33e-04	1.356	4.82e-04	1.349	2.88e-04	1.353
6.47e-03	3.40e-03	1.331	7.96e-04	1.351	3.65e-04	1.359	1.89e-04	1.354	1.13e-04	1.357
3.24e-03	1.36e-03	1.331	3.14e-04	1.344	1.44e-04	1.349	7.47e-05	1.346	4.44e-05	1.348
1.62e-03	5.39e-04	1.329	1.24e-04	1.338	5.67e-05	1.341	2.95e-05	1.339	1.75e-05	1.341
Flux										
	$k = 0$		$k = 1$		$k = 2$		$k = 3$		$k = 4$	
h	error	rate	error	rate	error	rate	error	rate	error	rate
1.18e-01	2.54e-01		1.24e-01		7.79e-02		5.76e-02		4.45e-02	
5.18e-02	1.65e-01	0.519	7.71e-02	0.573	4.90e-02	0.562	3.61e-02	0.567	2.80e-02	0.564
2.59e-02	1.07e-01	0.629	4.84e-02	0.671	3.09e-02	0.669	2.27e-02	0.668	1.76e-02	0.668
1.29e-02	6.86e-02	0.637	3.05e-02	0.664	1.94e-02	0.664	1.43e-02	0.664	1.11e-02	0.663
6.47e-03	4.37e-02	0.652	1.92e-02	0.670	1.22e-02	0.670	9.02e-03	0.670	6.98e-03	0.670
3.24e-03	2.78e-02	0.657	1.21e-02	0.668	7.71e-03	0.668	5.68e-03	0.668	4.40e-03	0.668
1.62e-03	1.76e-02	0.660	7.61e-03	0.667	4.85e-03	0.667	3.58e-03	0.667	2.77e-03	0.667

In Figure 1.8 and Table 1.4, it is observed similar rate of convergence of 4/3 for the potential and 2/3 for the flux, respectively, as was found for the pure Dirichlet boundary condition.

Now, we consider the domain $\Omega = (-1,1)^2/[0,1]\times[-1,0]$, with $\Gamma = \Gamma_D \cup \Gamma_N$, where

$$\Gamma_N = \{0\}\times[-1,0]\cup[0,1]\times\{0\} \quad \text{and} \quad \Gamma_D := \Gamma\backslash\Gamma_N. \tag{1.43}$$

Table 1.5: History of convergence of potential and flux errors, $k \in \{0,1,2,3,4\}$.

Potential										
	$k=0$		$k=1$		$k=2$		$k=3$		$k=4$	
h	error	rate	error	rate	error	rate	error	rate	error	rate
1.18e-01	5.35e-02		2.41e-02		1.84e-02		1.46e-02		1.22e-02	
5.18e-02	2.85e-02	0.767	1.49e-02	0.582	1.11e-02	0.618	8.55e-03	0.650	6.93e-03	0.687
2.59e-02	1.63e-02	0.808	9.49e-03	0.654	6.88e-03	0.686	5.27e-03	0.697	4.23e-03	0.711
1.29e-02	9.79e-03	0.727	6.02e-03	0.654	4.32e-03	0.668	3.30e-03	0.671	2.65e-03	0.674
6.47e-03	6.06e-03	0.695	3.80e-03	0.666	2.72e-03	0.671	2.08e-03	0.672	1.66e-03	0.673
3.24e-03	3.79e-03	0.678	2.40e-03	0.667	1.71e-03	0.668	1.31e-03	0.669	1.05e-03	0.669
1.62e-03	2.38e-03	0.670	1.51e-03	0.666	1.08e-03	0.667	8.25e-04	0.667	6.60e-04	0.667
Flux										
	$k=0$		$k=1$		$k=2$		$k=3$		$k=4$	
h	error	rate	error	rate	error	rate	error	rate	error	rate
1.18e-01	2.38e-01		1.24e-01		8.17e-02		6.43e-02		5.10e-02	
5.18e-02	1.62e-01	0.469	7.94e-02	0.538	5.26e-02	0.536	4.13e-02	0.539	3.28e-02	0.536
2.59e-02	1.07e-01	0.595	5.13e-02	0.632	3.41e-02	0.625	2.67e-02	0.627	2.13e-02	0.627
1.29e-02	6.97e-02	0.614	3.31e-02	0.629	2.21e-02	0.624	1.73e-02	0.625	1.38e-02	0.625
6.47e-03	4.50e-02	0.633	2.13e-02	0.637	1.43e-02	0.632	1.12e-02	0.634	8.89e-03	0.633
3.24e-03	2.89e-02	0.640	1.37e-02	0.637	9.21e-03	0.632	7.20e-03	0.634	5.73e-03	0.634
1.62e-03	1.85e-02	0.643	8.83e-03	0.636	5.94e-03	0.633	4.64e-03	0.634	3.70e-03	0.634

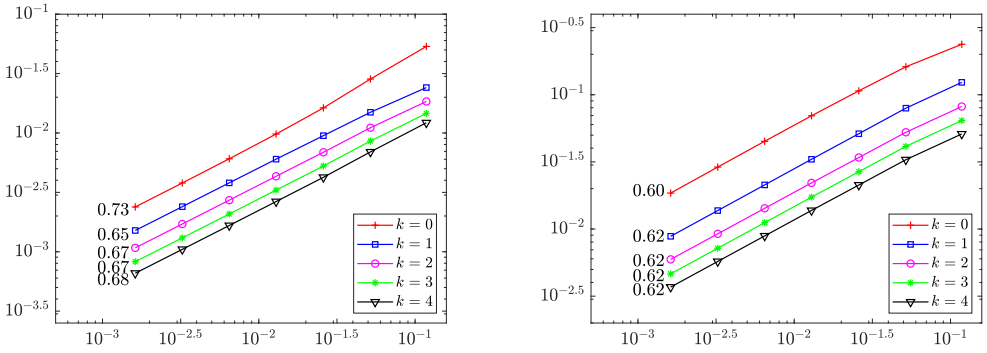

(a) Potential error

(b) Flux error

Figure 1.9: Convergence rates of potential and flux errors.

From Figure 1.9 and Table 1.5, we observe a rate of convergence of 2/3 for the potential and approximately 7/11 for the flux. These rates are lower possibly because the nonregularity of the gradient near the origin (Neumann boundary condition).

We remark that the pure Neumann boundary condition is not included in this analysis. The latter is analysed in [39] and it will be addressed in Chapter 2.

Chapter 2

An HHO formulation for a Neumann problem on general meshes

In this chapter, we study a Hybrid High-Oder (HHO) method for an elliptic diffusion problem with Neumann boundary condition. The proposed method has several features, such as: i) the support of arbitrary approximation order polynomial at mesh elements and faces on general polyhedral meshes, ii) the design of a local (element-wise) potential reconstruction operator and a local stabilization term, that weakly enforces the matching between local element- and face- based on degrees of Freedom (DOF), and iii) cheap computational cost, thanks to static condensation and compact stencil. We prove the well-posedness of our HHO formulation, and obtain the optimal error estimates, according to [72]. Implementation aspects are throughly discussed. Finally, some numerical examples are provided, which are in agreement with our theoretical results.

2.1 Introduction

The approximation of diffusive problems on general polyhedral meshes have received an increasing attention over the last few years, motivated in particular by applications in the geosciences, where the mesh is often adapted to geological layers, cracks and

faults leading to cells with polyhedral shape and to nonmatching interfaces. These considerations are included in the context of Hybrid High-Order methods, which are derived in terms of a primal formulation, and are designed from two key ingredients:

i) a potential reconstruction in each mesh cell, and

ii) a face-based stabilization consistent, with the high-order provided by the potential reconstruction.

This design relies on intermediate cell-based discrete unknowns, in addition to the face-based ones (hence, the term hybrid). We remark that the cell-based unknowns can be eliminated by static condensation, as it has already been pointed out in[75, 70]. As low-order methods on polyhedral meshes have been studied for quite some time, we mention that HHO can be seen as a Finite Volume method (FVM) (cf. [82], [88]) for polynomial of order $k = 0$ (see Section 2.5 in [75]). HHO can also be expressed into an equivalent mixed formulation (cf. [76], [73]). In [57], we find the identification of conservative numerical traces of the flux, and that HHO methods can be seen as a generalization of HDG methods. Moreover, in Section 2.4 in [57], we find a link between a nonconforming Virtual Element Method considered in [11], and HHO methods, by defining an isomorphism between the HHO degrees of freedom and a local virtual finite-dimensional space (containing those polynomial functions leading to optimal approximation properties), we identify the projection operator related to the elliptic operator of HHO.

In what follows, we describe the model problem. Let $\Omega \subset \mathbb{R}^d$, $d \in \{2, 3\}$, be an open, bounded, polytopic domain with Lipschitz-continuous boundary $\Gamma := \partial\Omega$ and unit outward normal $\boldsymbol{n}$. Let $K \in [L^\infty(\Omega)]^{d\times d}$ be a bounded, measurable, and symmetric tensor describing the material properties, $f \in L^2(\Omega)$ is the forcing term and $g \in L^2(\Gamma)$ is the flux through the boundary. We focus on the following variable-diffusion problem with Neumann boundary condition:

$$-\nabla \cdot (K\nabla u) = f \text{ in } \Omega\,, \tag{2.1a}$$

$$K\nabla u \cdot \boldsymbol{n} = g \text{ on } \Gamma\,, \tag{2.1b}$$

$$\int_\Omega u = 0. \tag{2.1c}$$

It is well known that the data f and g must satisfy the compatibility condition

$$\int_{\Omega} f + \int_{\Gamma} g = 0\,. \tag{2.2}$$

From here on, we assume that K is strongly elliptic, that is there exist two positive constants c_1 and c_2 such that

$$c_1|\boldsymbol{\xi}|^2 \leq \boldsymbol{\xi}^t\, K(x)\, \boldsymbol{\xi} \leq c_2|\boldsymbol{\xi}|^2 \quad \forall \boldsymbol{\xi} \in \mathbb{R}^d,\, \forall x \in \Omega,$$

where $|\cdot|$ represents the usual Euclidean norm. The strong ellipticity implies that matrix $K(x)$ is uniformly positive definite and thus nonsingular for every $x \in \Omega$.
For any connected subset $X \subset \bar{\Omega}$ with nonzero Lebesgue measure, the inner product and norm of the Lebesgue space $L^2(X)$ are denoted by $(\cdot,\cdot)_X$ and $||\cdot||_X$, respectively. Similar notations will be used for $L^2(X)^d$ and $L^2(\Gamma)$. It is not difficult to deduce that the weak formulation of (2.1) reads as: *Given* $f \in L^2(\Omega)$ *and* $g \in L^2(\Gamma)$, *we seek* $u \in U := \{v \in H^1(\Omega) \,:\, (v,1)_\Omega = 0\}$ *such that*

$$(K\nabla u, \nabla v)_\Omega = (f, v)_\Omega + (g, v)_\Gamma \quad \forall v \in U. \tag{2.3}$$

In addition, thanks to the Poincaré-Wintinger inequality and the Lax-Milgram lemma, we can ensure that the problem (2.3) is well-posed.
The application of HHO technique Poisson problem with Dirichlet conditions has been described in [72], while in [76] one can find the corresponding analysis for mixed boundary conditions. An extension of this approach for a certain class of nonlinear elliptic problems ($p-$Laplacian) has been developed in [64]. HHO method for elliptic problems with homogeneous Neumann boundary value condition, has already been used in [6], but without its corresponding a priori error analysis, which is a bit different that the one for mixed/Dirichlet boundary conditions, although it is reasonable to think that we also should expect similar theoretical results. For these reasons, the focus of the present work is to describe the Hybrid High-Order method for linear variable-diffusion problems with nonhomogeneous Neumann boundary conditions and to develop a complete error estimate. It is important to emphasize that the involved analysis described in this work is not contained in the context of [76].

In Section 2.2, we introduce any assumptions over the diffusion tensor, our main analysis tools, the degrees of freedom (DOFs) in the context of HHO method, and the potential reconstruction operator, with its key properties. In Section 2.3, we introduce the discrete problem and study its stability. In Section 2.4, we perform the error analysis, first in the energy-norm and then in the L^2-norm under additional elliptic regularity assumption. In Section 2.5, we discuss the computational implementation and, finally in Section 2.6, we present some numerical examples, which are in agreement with our theoretical results.

2.2 Discrete settings

Let $\mathcal{H} \subset \mathbb{R}^+$ denote a countable set of meshsizes having 0 as its unique accumulation point and $(\mathcal{T}_h)_{h\in\mathcal{H}}$ a h-refined admissible mesh sequence of $\overline{\Omega}$ (see Section 4.1 in [74]). Each mesh $\mathcal{T}_h$ of this sequence is a finite collection of nonempty, disjoint, open, polytopic elements such that $\overline{\Omega} = \bigcup_{T\in\mathcal{T}_h} \overline{T}$ and $h = \max_{T\in\mathcal{T}_h} h_T$ (with h_T the diameter of T), and there is a matching simplicial submesh of $\mathcal{T}_h$ with locally equivalent mesh size and which is shape-regular in the usual sense (γ is the mesh regularity parameter). We call a face any hyperplanar closed connected subset F of $\overline{\Omega}$ with positive $(d-1)$-dimensional measure and such that (i) either there exist T_1, $T_2 \in \mathcal{T}_h$ such that $F \subset \partial T_1 \cap \partial T_2$ (F is called an interior face) or (ii) there exists $T \in \mathcal{T}_h$ such that $F \subset \partial T \cap \partial\Omega$ (F is called a boundary face). Interior faces are collected in the set $\mathcal{F}_h^i$, boundary faces in $\mathcal{F}_h^b$, and we set $\mathcal{F}_h := \mathcal{F}_h^i \cup \mathcal{F}_h^b$. The diameter of a face $F \in \mathcal{F}_h$ is denoted by h_F. For each $T \in \mathcal{T}_h$, $\mathcal{F}_T := \{F \in \mathcal{F}_h \,|\, F \subset \partial T\}$ defines the set of faces lying on the boundary of T and, for each $F \in \mathcal{F}_T$, $\boldsymbol{n}_{TF}$ is the unit normal to F pointing out of T. In an admissible mesh sequence, for any $T \in \mathcal{T}_h$, and any $F \in \mathcal{F}_T$, h_F is uniformly comparable to h_T in the sense that, for all $h \in \mathcal{H}$ and all $T \in \mathcal{T}_h$

$$\gamma^2 h_T \leq h_F \leq h_T, \tag{2.4}$$

and the card$(\mathcal{F}_T)$ is uniformly bounded. The usual discrete and multiplicative trace inequalities hold on element faces. The following assumptions and notations will be taken into account in this work:

N.1 There is a partition P_Ω of Ω so that K is piecewise Lipschitz, and the mesh $\mathcal{T}_h$ fits the (polytopal) partition P_Ω associated with the diffusion tensor K in the sense that, there is a unique Ω_i in P_Ω containing T.

N.2 We denote by $\underline{\kappa}_T$ and $\overline{\kappa}_T$ the lowest and largest eigenvalues of K in T. We introduce the local heterogeneity/anisotropy ratio $\rho_T := \overline{\kappa}_T/\underline{\kappa}_T \geq 1$.

N.3 Furthermore, $A \lesssim B$ denotes the inequality $A \leq CB$ with positive constant C independent of the diffusion tensor K and the meshsize h, and probably not independent of the polynomial degree k.

N.4 To avoid the proliferation of symbols, we assume that for all $T \in \mathcal{T}_h$, the Lipschitz constant of K in T, say L_T^K, satisfies $L_T^K \lesssim \overline{\kappa}_T$.

In the following lemma, we show that the L^2-orthogonal projector onto polynomial spaces have optimal approximation properties on each mesh element.

Lemma 2.2.1 (L^2-orthogonal projector) *Given an integer $l \geq 0$, and $T \in \mathcal{T}_h$, we denote by π_T^l the L^2-orthogonal projector onto $\mathbb{P}_d^l(T)$. Then, for any $s, t \in \mathbb{R}$ with $0 \leq s \leq t \leq l+1$ there exists $C_{app} = C_{app}(\gamma, l) > 0$, such that*

$$|v - \pi_T^l v|_{H^s(T)} \leq C_{app} h_T^{t-s} |v|_{H^t(T)}, \quad \forall\, v \in H^t(T). \tag{2.5}$$

Besides, there exists $C'_{app} > 0$ such that, for all t, $1/2 < t \leq l+1$, there holds

$$\|v - \pi_T^l v\|_{\partial T} \leq C'_{app} h_T^{t-1/2} |v|_{H^t(T)}, \quad \forall\, v \in H^t(T), \tag{2.6}$$

where $|\cdot|_{H^t(T)}$ and $|\cdot|_{H^s(T)}$ denotes the corresponding seminorms on Sobolev spaces $H^t(T)$ and $H^s(T)$, respectively.

Proof. We refer to Theorems 3.2 and 3.3 in [102]. □

2.2.1 Degrees of freedom (DOFs)

Let a polynomial degree $k \geq 0$ be fixed. For all $T \in \mathcal{T}_h$, we define the local space of DOFs as $\underline{\boldsymbol{U}}_T^k := \mathbb{P}_d^k(T) \times \big(\bigtimes_{F \in \mathcal{F}_T} \mathbb{P}_{d-1}^k(F)\big)$, where $\mathbb{P}_d^k(T)$ (resp., $\mathbb{P}_{d-1}^k(F)$) is spanned

by the restrictions to T (resp., F) of d-variate (resp., $(d-1)$-variate) polynomials of total degree $\leq k$. And the global space of DOFs on the domain Ω.

$$\underline{\boldsymbol{U}}_h^k := \left(\bigtimes_{T\in\mathcal{T}_h} \mathbb{P}_d^k(T)\right) \times \left(\bigtimes_{F\in\mathcal{F}_h} \mathbb{P}_{d-1}^k(F)\right).$$

For all $T \in \mathcal{T}_h$, we define the local reduction operator $\underline{\mathbf{I}}_T^k : H^1(T) \to \underline{\boldsymbol{U}}_T^k$ such that, for all $v \in H^1(T)$,

$$\underline{\mathbf{I}}_T^k v := (\pi_T^k v, (\pi_F^k v)_{F\in\mathcal{F}_T}), \tag{2.7}$$

where π_T^k and π_F^k are the L^2-orthogonal projectors onto $\mathbb{P}_d^k(T)$ and $\mathbb{P}_{d-1}^k(F)$, respectively. The corresponding global interpolation operator $\underline{\mathbf{I}}_h^k : H^1(\Omega) \to \underline{\boldsymbol{U}}_h^k$ is such that, for all $v \in H^1(\Omega)$,

$$\underline{\mathbf{I}}_h^k v := ((\pi_T^k v)_{T\in\mathcal{T}_h}, (\pi_F^k v)_{F\in\mathcal{F}_h}). \tag{2.8}$$

2.2.2 Potential reconstruction operator

For all $T \in \mathcal{T}_h$, we define the potential reconstruction operator $p_T^{k+1} : \underline{\boldsymbol{U}}_T^k \to \mathbb{P}_d^{k+1}(T)$ such that, for each $\underline{\boldsymbol{v}}_T := (v_T, (v_F)_{F\in\mathcal{F}_T}) \in \underline{\boldsymbol{U}}_T^k$ and each $w \in \mathbb{P}_d^{k+1}(T)$,

$$(K\nabla p_T^{k+1}\underline{\boldsymbol{v}}_T, \nabla w)_T = (K\nabla v_T, \nabla w)_T + \sum_{F\in\mathcal{F}_T} (v_F - v_T, K\nabla w\cdot\boldsymbol{n}_{TF})_F, \tag{2.9}$$

and

$$\int_T p_T^{k+1}\underline{\boldsymbol{v}}_T := \int_T v_T, \tag{2.10}$$

where we recall that $\boldsymbol{n}_{TF}$ is the unit normal to F pointing out of T.

The following result characterizes the composition of the diffusion-dependent potential reconstruction with the local reduction operator and shows that $p_T^{k+1}\underline{\mathbf{I}}_T^k$ is the K-weighted elliptic projector onto $\mathbb{P}_d^{k+1}(T)$ only if K is constant in the cell.

Lemma 2.2.2 (Characterization of $p_T^{k+1}\underline{\mathbf{I}}_T^k$ and polynomial consistency) *For every $v \in H^1(T)$ and $w \in \mathbb{P}_d^{k+1}(T)$, there holds*

$$\begin{aligned}(K\nabla(v - p_T^{k+1}\underline{\mathbf{I}}_T^k v), \nabla w)_T = {}& ((K - \overline{K}_T)\nabla(v - \pi_T^k v), \nabla w)_T \\ & - \sum_{F\in\mathcal{F}_T} (\pi_F^k v - \pi_T^k v, (K - \overline{K}_T)\nabla w\cdot\boldsymbol{n}_{TF})_F,\end{aligned} \tag{2.11}$$

where $\overline{K}_T$ denotes the mean-value of K on T. In addition, if K is piecewise constant on P_Ω, we obtain the following orthogonality property:

$$(K\nabla(v - p_T^{k+1}\underline{\mathbf{I}}_T^k v), \nabla w)_T = 0, \tag{2.12}$$

and the polynomial consistency:

$$p_T^{k+1}\underline{\mathbf{I}}_T^k v = v \quad \forall\, v \in \mathbb{P}_d^{k+1}(T). \tag{2.13}$$

Proof. We will give a detailed proof of statements in Lemma 2.1 in [72] and Lemma 3.1 in [76].

Using the fact that $\overline{K}_T$ is a symmetric matrix and using integration by parts, we obtain that for each $w \in \mathbb{P}_d^{k+1}(T)$,

$$\begin{aligned}(\overline{K}_T\nabla\pi_T^k v, \nabla w)_T &= (\nabla\pi_T^k v, \overline{K}_T\nabla w)_T \\ &= -(\pi_T^k v, \nabla\cdot(\overline{K}_T\nabla w))_T + \sum_{F\in\mathcal{F}_T}(\pi_T^k v, \overline{K}_T\nabla w\cdot\boldsymbol{n}_{TF})_F,\end{aligned} \tag{2.14}$$

using the definition of L^2-orthogonal projector on $\mathbb{P}_d^k(T)$ with $\nabla\cdot(\overline{K}_T\nabla w) \in \mathbb{P}_d^{k-1}(T)$, we can write (2.14) as

$$(\overline{K}_T\nabla\pi_T^k v, \nabla w)_T = -(v, \nabla\cdot(\overline{K}_T\nabla w))_T + \sum_{F\in\mathcal{F}_T}(\pi_T^k v, \overline{K}_T\nabla w\cdot\boldsymbol{n}_{TF})_F, \tag{2.15}$$

performing integration by parts on the first addend of (2.15), and using L^2-orthogonal projector on $\mathbb{P}_{d-1}^k(F)$ with $\overline{K}_T\nabla w\cdot\boldsymbol{n}_{TF} \in \mathbb{P}_{d-1}^k(F)$ leads to

$$(\overline{K}_T\nabla\pi_T^k v, \nabla w)_T = (\overline{K}_T\nabla v, \nabla w)_T - \sum_{F\in\mathcal{F}_T}(\pi_F^k v - \pi_T^k v, \overline{K}_T\nabla w\cdot\boldsymbol{n}_{TF})_F, \tag{2.16}$$

using $\underline{\boldsymbol{v}}_T = \underline{\mathbf{I}}_T^k v$ in the definition of potential reconstruction operator, we obtain

$$(K\nabla p_T^{k+1}\underline{\mathbf{I}}_T^k v, \nabla w)_T = (K\nabla\pi_T^k v, \nabla w)_T + \sum_{F\in\mathcal{F}_T}(\pi_F^k v - \pi_T^k v, K\nabla w\cdot\boldsymbol{n}_{TF})_F, \tag{2.17}$$

then, subtracting $(K\nabla v, \nabla w)$ from both sides of (2.17), we obtain

$$\begin{aligned}(K\nabla(p_T^{k+1}\underline{\mathbf{I}}_T^k v - v), \nabla w)_T &= (K\nabla\pi_T^k v, \nabla w)_T - (K\nabla v, \nabla w) \\ &\quad + \sum_{F\in\mathcal{F}_T}(\pi_F^k v - \pi_T^k v, K\nabla w\cdot\boldsymbol{n}_{TF})_F,\end{aligned} \tag{2.18}$$

finally (2.11) follows from (2.16) and (2.18).

Furthermore, noticing that the right-hand side of (2.11) vanishes if K is piecewise constant on P_Ω, it follows the orthogonality property (2.12). In the case of $v \in \mathbb{P}_d^{k+1}(T)$, we can take $w = v - p_T^{k+1}\underline{\mathbf{I}}_T^k v$ in (2.12), and it follows that $v - p_T^{k+1}\underline{\mathbf{I}}_T^k v$ is constant on T. Then, from the definition of potential reconstruction operator and orthogonal projector, we infer that $(v - p_T^{k+1}\underline{\mathbf{I}}_T^k v, 1)_T = 0$, and finally we conclude (2.13). □

Lemma 2.2.3 (Approximation properties for $p_T^{k+1}\underline{\mathbf{I}}_T^k$) *There exists a real number $C > 0$, depending of γ (mesh regularity parameter) and d, but independent of the polynomial degree, the meshsize, and the diffusion tensor. So that for any $v \in H^{s+2}(T)$, $s \in \{0, \cdots, k\}$, there holds:*

$$\begin{aligned}\left\|v - p_T^{k+1}\underline{\mathbf{I}}_T^k v\right\|_T + h_T^{1/2}\left\|v - p_T^{k+1}\underline{\mathbf{I}}_T^k v\right\|_{\partial T} + h_T\left\|\nabla(v - p_T^{k+1}\underline{\mathbf{I}}_T^k v)\right\|_T \\ + h_T^{3/2}\left\|\nabla(v - p_T^{k+1}\underline{\mathbf{I}}_T^k v)\right\|_{\partial T} \leq C\rho_T^{\alpha} h_T^{s+2}\left\|v\right\|_{H^{s+2}(T)},\end{aligned} \tag{2.19}$$

Here, $\alpha = 1/2$ if K is piecewise constant, and $\alpha = 1$ otherwise.

Proof. In Lemma 2.1 in [72], we find a sketch of the proof, we will give a more detailed proof.

Using the same notation of lemma 2.2.2, and the fact that K is piecewise Lipschitz on T with Lipschitz constant L_T^K, we infer that

$$\left|(K - \overline{K}_T)(x)\right|_2 \lesssim L_T^K h_T, \quad \forall\, x \in \overline{T}. \tag{2.20}$$

Using Cauchy-Schwarz inequality on (2.11), we obtain

$$\begin{aligned}&\left|\left(K\nabla(v - p_T^{k+1}\underline{\mathbf{I}}_T^k v), \nabla w\right)_T\right| \leq \\ &\left\|(K - \overline{K}_T)\nabla(v - \pi_T^k v)\right\|_T \left\|\nabla w\right\|_T + \sum_{F\in\mathcal{F}_T}\left\|\pi_F^k v - \pi_T^k v\right\|_F \left\|(K - \overline{K}_T)\nabla w \cdot \boldsymbol{n}_{TF}\right\|_F,\end{aligned} \tag{2.21}$$

by (2.20) and the approximation properties of π_T^k, we infer that

$$\left\|(K - \overline{K}_T)\nabla(v - \pi_T^k v)\right\|_T \lesssim L_T^K h_T^{k+1}\left\|v\right\|_{H^{k+1}(T)}, \tag{2.22}$$

using Cauchy-Schwarz inequality on $(K-\overline{K}_T)\nabla w\cdot\boldsymbol{n}_{TF}$, again (2.20), the discrete trace inequality $\|\nabla w\|_F \lesssim h_F^{-1/2}\|\nabla w\|_T$, and (2.4), it holds

$$\left\|(K-\overline{K}_T)\nabla w\cdot\boldsymbol{n}_{TF}\right\|_F \lesssim L_T^K h_T^{1/2}\|\nabla w\|_T, \tag{2.23}$$

using polynomial approximation properties on mesh faces, we have

$$\left\|\pi_F^k v-\pi_T^k v\right\|_F \lesssim h_T^{k+1/2}\|v\|_{H^{k+1}(T)}. \tag{2.24}$$

Then, we deduce from (2.21) to (2.24), and the assumption $L_T^K \lesssim \overline{\kappa}_T$, that

$$\left|\left(K\nabla(v-p_T^{k+1}\underline{\mathbf{I}}_T^k v),\nabla w\right)_T\right| \lesssim \overline{\kappa}_T h_T^{k+1}\|v\|_{H^{k+1}(T)}\|\nabla w\|_T. \tag{2.25}$$

We also notice that

$$\begin{aligned}\left\|K^{1/2}\nabla(v-p_T^{k+1}\underline{\mathbf{I}}_T^k v)\right\|_T^2 &= \left(K\nabla(v-p_T^{k+1}\underline{\mathbf{I}}_T^k v),\nabla(v-\pi^{k+1}v)\right)_T\\ &\quad+\left(K\nabla(v-p_T^{k+1}\underline{\mathbf{I}}_T^k v),\nabla(\pi^{k+1}v-p_T^{k+1}\underline{\mathbf{I}}_T^k v)\right)_T.\end{aligned} \tag{2.26}$$

We denote by $\mathfrak{T}_1$ and $\mathfrak{T}_2$ the addends on the right-hand side of (2.26). Applying Cauchy Schwarz inequality, and approximation properties of π_T^{k+1}, we obtain

$$|\mathfrak{T}_1| \lesssim \left\|K^{1/2}\nabla(v-p_T^{k+1}\underline{\mathbf{I}}_T^k v)\right\|_T \overline{\kappa}_T{}^{1/2} h_T^{k+1}\|v\|_{H^{k+2}(T)}. \tag{2.27}$$

To bound $\mathfrak{T}_2$, we use (2.25) with $w=\pi^{k+1}v-p_T^{k+1}\underline{\mathbf{I}}_T^k v$, obtaining

$$|\mathfrak{T}_2| \lesssim \overline{\kappa}_T h_T^{k+1}\|v\|_{H^{k+1}(T)}\left\|\nabla(\pi^{k+1}v-p_T^{k+1}\underline{\mathbf{I}}_T^k v)\right\|_T, \tag{2.28}$$

also, it holds

$$\left\|\nabla(\pi_T^{k+1}v-p_T^{k+1}\underline{\mathbf{I}}_T^k v)\right\|_T \le \underline{\kappa}_T{}^{-1/2}\left\|K^{1/2}\nabla(v-p_T^{k+1}\underline{\mathbf{I}}_T^k v)\right\|_T, \tag{2.29}$$

where we have used the H^1-stability of the projector π_T^{k+1}, and $\left|K_T^{-1/2}\right|_2 \le \underline{\kappa}_T{}^{-1/2}$. Then, we infer from (2.28), (2.29) that

$$|\mathfrak{T}_2| \lesssim \left\|K^{1/2}\nabla(v-p_T^{k+1}\underline{\mathbf{I}}_T^k v)\right\|_T \rho_T^{1/2}\overline{\kappa}_T{}^{1/2} h_T^{k+1}\|v\|_{H^{k+2}(T)}. \tag{2.30}$$

Considering K piecewise constant in (2.26), we notice that $\mathfrak{T}_2$ vanishes, then it holds

$$\left\|K^{1/2}\nabla(v-p_T^{k+1}\underline{\mathbf{I}}_T^k v)\right\|_T \lesssim \overline{\kappa}_T{}^{1/2} h_T^{k+1}\|v\|_{H^{k+2}(T)}. \tag{2.31}$$

Considering K in the general case in (2.26), we obtain from (2.27) and (2.30) that

$$\left\|K^{1/2}\nabla(v-p_T^{k+1}\underline{\mathbf{I}}_T^k v)\right\|_T \lesssim \rho_T^{1/2}\overline{K}_T{}^{1/2}h_T^{k+1}\left\|v\right\|_{H^{k+2}(T)}, \tag{2.32}$$

finally, using the definition of α, and $\left|K_T^{-1/2}\right|_2 \leq \underline{K}_T{}^{-1/2}$ again, it concludes

$$\left\|\nabla(v-p_T^{k+1}\underline{\mathbf{I}}_T^k v)\right\|_T \lesssim \rho_T^{\alpha}h_T^{k+1}\left\|v\right\|_{H^{k+2}(T)}. \tag{2.33}$$

Now, we bound the first addend of (2.19) using the facts that $v-p_T^{k+1}\underline{\mathbf{I}}_T^k v \in H^1(T)\cap L_0^2(T)$, the local Poincaré inequality, and (2.33), we obtain

$$\left\|v-p_T^{k+1}\underline{\mathbf{I}}_T^k v\right\|_T \lesssim h_T\left\|\nabla(v-p_T^{k+1}\underline{\mathbf{I}}_T^k v)\right\|_T \lesssim \rho_T^{\alpha}h_T^{k+2}\left\|v\right\|_{H^{k+2}(T)}. \tag{2.34}$$

The consecutive application of the continuous trace inequality and (2.33)-(2.34) yields

$$h_T\left\|v-p_T^{k+1}\underline{\mathbf{I}}_T^k v\right\|_{\partial T}^2 \lesssim \left\|v-p_T^{k+1}\underline{\mathbf{I}}_T^k v\right\|_T^2+h_T^2\left\|\nabla(v-p_T^{k+1}\underline{\mathbf{I}}_T^k v)\right\|_T^2 \lesssim h_T^{2(k+2)}\left\|v\right\|_{H^{k+2}(T)}^2. \tag{2.35}$$

For bounding $\|K^{1/2}\nabla(v-p_T^{k+1}\underline{\mathbf{I}}_T^k v)\|_{\partial T}$, we notice that

$$\left\|K^{1/2}\nabla(v-p_T^{k+1}\underline{\mathbf{I}}_T^k v)\right\|_{\partial T} \leq \left\|K^{1/2}(\nabla v-\pi_T^k\nabla v)\right\|_{\partial T}+\left\|K^{1/2}(\pi_T^k\nabla v-\nabla p_T^{k+1}\underline{\mathbf{I}}_T^k v)\right\|_{\partial T}. \tag{2.36}$$

Applying componentwise the approximation property of π_T^k to ∇v, we obtain

$$\left\|K^{1/2}(\nabla v-\pi_T^k\nabla v)\right\|_{\partial T} \lesssim \overline{K}_T{}^{1/2}h_T^{k+1/2}\|v\|_{H^{k+2}(T)}. \tag{2.37}$$

Without loss of generality, we assume that K is piecewise polynomial, then, using discrete trace inequality, and the bound on $\mathrm{card}(\mathcal{F}_T)$, we infer that

$$\left\|K^{1/2}(\pi_T^k\nabla v-\nabla p_T^{k+1}\underline{\mathbf{I}}_T^k v)\right\|_{\partial T} \lesssim h_T^{-1/2}\left\|K^{1/2}(\pi_T^k\nabla v-\nabla p_T^{k+1}\underline{\mathbf{I}}_T^k v)\right\|_T. \tag{2.38}$$

If K is piecewise constant, it follows from the fact $\nabla p_T^{k+1}\underline{\mathbf{I}}_T^k v \in \left[\mathbb{P}_d^k(T)\right]^d$, and approximation property of π_T^k that

$$\left\|K^{1/2}(\pi_T^k\nabla v-\nabla p_T^{k+1}\underline{\mathbf{I}}_T^k v)\right\|_T \leq \left\|K^{1/2}\nabla(v-p_T^{k+1}\underline{\mathbf{I}}_T^k v)\right\|_T, \tag{2.39}$$

then, in the case of K piecewise constant, we infer from (2.36) to (2.39) that

$$\left\|K^{1/2}\nabla(v-p_T^{k+1}\underline{\mathbf{I}}_T^k v)\right\|_{\partial T} \lesssim \overline{K}_T{}^{1/2}h_T^{k+1/2}\|v\|_{H^{k+2}(T)}. \tag{2.40}$$

Otherwise, since $\left|K_T^{1/2}\right|_2 \leq \overline{K}_T{}^{1/2}$, it follows

$$\left\|K^{1/2}(\pi_T^k \nabla v - \nabla p_T^{k+1} \underline{\mathbf{I}}_T^k v)\right\|_T \lesssim \overline{K}_T{}^{1/2} \left\|\nabla(v - p_T^{k+1} \underline{\mathbf{I}}_T^k v)\right\|_T, \tag{2.41}$$

then, from (2.36), (2.37), (2.38), (2.41) and (2.33), we conclude for the general case that

$$\left\|K^{1/2}\nabla(v - p_T^{k+1} \underline{\mathbf{I}}_T^k v)\right\|_{\partial T} \lesssim \rho_T^{1/2} \overline{K}_T{}^{1/2} h_T^{k+1/2} \|v\|_{H^{k+2}(T)}. \tag{2.42}$$

Finally, it follows from (2.40) and (2.42) and the definition of ρ_T, the bound of $\left\|\nabla(v - p_T^{k+1} \underline{\mathbf{I}}_T^k v)\right\|_{\partial T}$.

□

2.3 Formulation

First, we introduce the discrete global space for our HHO formulation as

$$\underline{\boldsymbol{U}}_h^{k,0} := \left\{ \underline{\boldsymbol{v}}_h := ((v_T)_{T\in\mathcal{T}_h}, (v_F)_{F\in\mathcal{F}_h}) \in \underline{\boldsymbol{U}}_h^k \ : \ \sum_{T\in\mathcal{T}_h} (v_T, 1)_T = 0 \right\}. \tag{2.43}$$

Next, we consider the following discrete semi norm on $\underline{\boldsymbol{U}}_h^k$,

$$\|\underline{\boldsymbol{v}}_h\|_{K,h}^2 := \sum_{T\in\mathcal{T}_h} \rho_T^{-1} \|\underline{\boldsymbol{v}}_T\|_{K,T}^2, \quad \forall\, \underline{\boldsymbol{v}}_h \in \underline{\boldsymbol{U}}_h^k, \tag{2.44}$$

where $\|\underline{\boldsymbol{v}}_T\|_{K,T}^2 := \|K^{1/2}\nabla v_T\|_T^2 + |\underline{\boldsymbol{v}}_T|_{K,\partial T}^2$ and $|\underline{\boldsymbol{v}}_T|_{K,\partial T}^2 := \sum_{F\in\mathcal{F}_T} \dfrac{k_F}{h_F} \|v_F - v_T\|_F^2$, with $k_F := \|\boldsymbol{n}_{TF}^t K \boldsymbol{n}_{TF}\|_{L^\infty(F)}$, for all $\underline{\boldsymbol{v}}_T := (v_T, (v_F)_{F\in\mathcal{F}_T}) \in \underline{\boldsymbol{U}}_T^k$.

Proposition 2.3.1 *The map $\|\cdot\|_{K,h}$ defines a norm on $\underline{\boldsymbol{U}}_h^{k,0}$.*

Proof. It is enough to prove that $\forall \underline{\boldsymbol{v}}_h \in \underline{\boldsymbol{U}}_h^{k,0}$: $\|\underline{\boldsymbol{v}}_h\|_{K,h} = 0 \Rightarrow \underline{\boldsymbol{v}}_h = \underline{\mathbf{0}}_h$. Let $\underline{\boldsymbol{v}}_h \in \underline{\boldsymbol{U}}_h^{k,0}$ be such that $\|\underline{\boldsymbol{v}}_h\|_{K,h} = 0$. This implies (cf. (2.44)) that

$$\nabla v_T \equiv 0 \quad \text{and} \quad v_T|_F = v_F \quad \forall F \in \mathcal{F}_T \ \forall T \in \mathcal{T}_h. \tag{2.45}$$

Then, from (2.45) we infer that v_T is constant on each $T \in \mathcal{T}_h$. In addition, we notice that given any interior face $F \in \mathcal{F}_h$, there exist $T_1, T_2 \in \mathcal{T}_h$ with $F \subset \partial T_1 \cap \partial T_2$, such that $v_{T_1}|_F = v_F = v_{T_2}|_F$. This means that $v_T = \alpha \in \mathbb{R}$ for each $T \in \mathcal{T}_h$. Finally, taking into account the zero mean value condition that

characterizes $\underline{\boldsymbol{U}}_h^{k,0}$, we deduce that $\alpha = 0$ and thus $\underline{\boldsymbol{v}}_h = \underline{\mathbf{0}}_h$, and we end the proof. □

Hereafter, the local potential reconstruction $R_T^{k+1} : \underline{\boldsymbol{U}}_T^k \to \mathbb{P}_d^{k+1}(T)$ is defined such that, for all $\underline{\boldsymbol{v}}_T \in \underline{\boldsymbol{U}}_T^k$,

$$R_T^{k+1}\underline{\boldsymbol{v}}_T := v_T + (p_T^{k+1}\underline{\boldsymbol{v}}_T - \pi_T^k p_T^{k+1}\underline{\boldsymbol{v}}_T)\,. \tag{2.46}$$

Now, to discretize the left-hand of (2.3), we introduce the following bilinear form on $\underline{\boldsymbol{U}}_h^k \times \underline{\boldsymbol{U}}_h^k$

$$a_h(\underline{\boldsymbol{u}}_h, \underline{\boldsymbol{v}}_h) := \sum_{T\in\mathcal{T}_h} a_T(\underline{\boldsymbol{u}}_T, \underline{\boldsymbol{v}}_T)\,, \tag{2.47}$$

where, for each $T \in \mathcal{T}_h$, the local bilinear forms $a_T\,,\ s_T : \underline{\boldsymbol{U}}_T^k \times \underline{\boldsymbol{U}}_T^k \to \mathbb{R}$, are given by

$$a_T(\underline{\boldsymbol{u}}_T, \underline{\boldsymbol{v}}_T) := (K\,\nabla\, p_T^{k+1}\,\underline{\boldsymbol{u}}_T, \nabla\, p_T^{k+1}\,\underline{\boldsymbol{v}}_T)_T \;+\; s_T(\underline{\boldsymbol{u}}_T, \underline{\boldsymbol{v}}_T), \tag{2.48a}$$

$$s_T(\underline{\boldsymbol{u}}_T, \underline{\boldsymbol{v}}_T) := \sum_{F\in\mathcal{F}_T} \frac{k_F}{h_F}(\pi_F^k(u_F - R_T^{k+1}\underline{\boldsymbol{u}}_T), \pi_F^k(v_F - R_T^{k+1}\underline{\boldsymbol{v}}_T))_F. \tag{2.48b}$$

The linear functional on the right hand side in (2.3) is discretized by means of the linear functional on $\underline{\boldsymbol{U}}_h^k$ such that

$$b_h(\underline{\boldsymbol{v}}_h) := \sum_{T\in\mathcal{T}_h}(f, v_T)_T \;+\sum_{F\in\mathcal{F}_h^b}(g, v_F)_F \quad \forall\, \underline{\boldsymbol{v}}_h := ((v_T)_{T\in\mathcal{T}_h}, (v_F)_{F\in\mathcal{F}_h}) \in \underline{\boldsymbol{U}}_h^k\,. \tag{2.49}$$

Then, the discrete problem reads: Find $\underline{\boldsymbol{u}}_h \in \underline{\boldsymbol{U}}_h^{k,0}$ such that,

$$a_h(\underline{\boldsymbol{u}}_h, \underline{\boldsymbol{v}}_h) = b_h(\underline{\boldsymbol{v}}_h) \quad \forall\, \underline{\boldsymbol{v}}_h \in \underline{\boldsymbol{U}}_h^{k,0}. \tag{2.50}$$

To analyse the stability and solvability of the discrete problem, we introduce the local and global energy semi-norms as follows:

$$\|\underline{\boldsymbol{v}}_h\|_{a,h}^2 := \sum_{T\in\mathcal{T}_h} \|\underline{\boldsymbol{v}}_T\|_{a,T}^2\,, \quad \text{where} \quad \|\underline{\boldsymbol{v}}_T\|_{a,T}^2 := a_T(\underline{\boldsymbol{v}}_T.\underline{\boldsymbol{v}}_T)\,. \tag{2.51}$$

Next result establishes an important relation between $\|\cdot\|_{a,T}$ and $\|\cdot\|_{K,T}$.

Lemma 2.3.1 *For any $\underline{\boldsymbol{v}}_T \in \underline{\boldsymbol{U}}_T^k$, there holds:*

$$\rho_T^{-1}\|\underline{\boldsymbol{v}}_T\|_{K,T}^2 \lesssim \|\underline{\boldsymbol{v}}_T\|_{a,T}^2 \lesssim \rho_T\|\underline{\boldsymbol{v}}_T\|_{K,T}^2. \tag{2.52}$$

Consequently, for all $\underline{\boldsymbol{v}}_h \in \underline{\boldsymbol{U}}_h^k$, $\|\underline{\boldsymbol{v}}_h\|_{K,h} \lesssim \|\underline{\boldsymbol{v}}_h\|_{a,h}$, and then, problem (2.50) is well-posed.

Proof. We refer to the proof of Lemma 3.1 in [72]. □

We end this section, introducing the global potential reconstruction operator $p_h^{k+1} : \underline{\boldsymbol{U}}_h^k \to \mathbb{P}_d^{k+1}(\mathcal{T}_h)$, such that for all $\underline{\boldsymbol{v}}_h \in \underline{\boldsymbol{U}}_h^k$: $(p_h^{k+1}\underline{\boldsymbol{v}}_h)|_T := p_T^{k+1}\underline{\boldsymbol{v}}_T \quad \forall T \in \mathcal{T}_h$, and also the global stabilization term $s_h : \underline{\boldsymbol{U}}_h^k \times \underline{\boldsymbol{U}}_h^k \to \mathbb{R}$, given by

$$s_h(\underline{\boldsymbol{u}}_h, \underline{\boldsymbol{v}}_h) := \sum_{T\in\mathcal{T}_h} s_T(\underline{\boldsymbol{u}}_T, \underline{\boldsymbol{v}}_T) \quad \forall\, \underline{\boldsymbol{u}}_h, \underline{\boldsymbol{v}}_h \in \underline{\boldsymbol{U}}_h^k\,.$$

These operators will be invoked in the next sections.

2.4 Error analysis

In this section we prove error estimates in the energy-norm and also in L^2-norm, under additional regularity assumption on exact solution. First, we start by establishing some technical results.

Lemma 2.4.1 (Consistency of s_T) *Given $T \in \mathcal{T}_h$, let s_T be the stabilization bilinear form defined in (2.48b), consider α as in Lemma 2.2.3), and let $q \in \{0, \cdots, k\}$. Then, for all $v \in H^{q+2}(T)$,*

$$s_T(\underline{\mathbf{I}}_T^k v, \underline{\mathbf{I}}_T^k v)^{1/2} \lesssim \overline{K}_T{}^{1/2} \rho_T^{\alpha} h_T^{q+1} \left\| v \right\|_{H^{q+2}(T)}. \tag{2.53}$$

Proof. Let $q \in \{0, \cdots, k\}$ be fixed, and consider $v \in H^{q+2}(T)$. Taking into account (2.46), the definition of $\underline{\mathbf{I}}_T^k v$, triangle inequality, discrete trace inequality and the L^2-stability of the projectors, we deduce

$$h_F^{-1/2}\|\pi_F^k(v - R_T^{k+1}\underline{\mathbf{I}}_T^k v)\|_F \lesssim h_F^{-1/2}\|v - p_T^{k+1}\underline{\mathbf{I}}_T^k v\|_F + h_F^{-1}\|v - p_T^{k+1}\underline{\mathbf{I}}_T^k v\|_T. \tag{2.54}$$

Now, since $k_F \leq \overline{K}_T$ for all $F \in \mathcal{F}_T$, together with the fact that $\mathrm{card}(\mathcal{F}_T)$ is uniformly bounded, and the mesh regularity property (2.4), we infer from (2.54) that

$$\sum_{F\in\mathcal{F}_T} \frac{k_F}{h_F}\|\pi_F^k(v - R_T^{k+1}\underline{\mathbf{I}}_T^k v)\|_F^2 \lesssim \overline{K}_T\Big(h_T^{-1}\|v - p_T^{k+1}\underline{\mathbf{I}}_T^k v\|_{\partial T}^2 + h_T^{-2}\|v - p_T^{k+1}\underline{\mathbf{I}}_T^k v\|_T^2\Big). \tag{2.55}$$

Then, using (2.55), and the approximation property of $p_T^{k+1}\underline{\mathbf{I}}_T^k$ in Lemma 2.19, we conclude (2.53). We remark that in [66] (Proposition 2.14), there is a proof for stabilization terms satisfying three conditions, which are checked for s_T. □

The following result will help us to conclude the error estimates of the method. From now on, we let $u \in U$ be the exact solution of (2.3). We define the *consistency error* as the linear functional $\mathcal{E}_h(u;\cdot) : \underline{\boldsymbol{U}}_h^{k,0} \to \mathbb{R}$ such that $\mathcal{E}_h(u;\cdot) := a_h(\underline{\mathbf{I}}_h^k u, \cdot) - b_h(\cdot)$.

Lemma 2.4.2 (Consistency-error estimate) *Taking into account the definition of α (given in Lemma 2.2.3), and assuming, in addition, that the exact solution of (2.3), $u \in H^{q+2}(\mathcal{T}_h)$, with $q \in \{0, ..., k\}$, there holds*

$$\sup_{\underline{\boldsymbol{v}}_h \in \underline{\boldsymbol{U}}_h^{k,0},\, \|\underline{\boldsymbol{v}}_h\|_{a,h}=1} \mathcal{E}_h(u;\underline{\boldsymbol{v}}_h) \lesssim \left\{ \sum_{T\in\mathcal{T}_h} \overline{K}_T \rho_T^{2\alpha} h_T^{2(q+1)} \|u\|^2_{H^{q+2}(T)} \right\}^{1/2}. \tag{2.56}$$

Proof. We derive a bound for the consistency error for a generic $\underline{\boldsymbol{v}}_h \in \underline{\boldsymbol{U}}_h^{k,0}$. Taking $w := p_T^{k+1}\underline{\mathbf{I}}_T^k u$ in (2.9), and using (2.10), we infer that

$$\begin{aligned} a_h(\underline{\mathbf{I}}_h^k u, \underline{\boldsymbol{v}}_h) = &\sum_{T\in\mathcal{T}_h} \left\{ (\nabla v_T, K\nabla p_T^{k+1}\underline{\mathbf{I}}_T^k u)_T + \sum_{F\in\mathcal{F}_T} (v_F - v_T, K\nabla p_T^{k+1}\underline{\mathbf{I}}_T^k u \cdot \boldsymbol{n}_{TF})_F \right\} \\ &+ s_h(\underline{\mathbf{I}}_h^k u, \underline{\boldsymbol{v}}_h). \end{aligned} \tag{2.57}$$

Since $f = -\nabla\cdot(K\nabla u)$ in Ω (in distributional sense), an element-wise integration by parts in the first term of b_h yields

$$\sum_{T\in\mathcal{T}_h} (f, v_T)_T = \sum_{T\in\mathcal{T}_h} \left\{ (K\nabla u, \nabla v_T)_T - \sum_{F\in\mathcal{F}_T} (v_T, K\nabla u\cdot\boldsymbol{n}_{TF})_F \right\}. \tag{2.58}$$

In addition, from the fact that $g = K\nabla u\cdot\boldsymbol{n}$ on Γ (in distributional sense), we infer that the second term of b_h can be written as

$$\sum_{F\in\mathcal{F}_h^b} (g, v_F)_F = \sum_{F\in\mathcal{F}_h^b} (v_F, K\nabla u\cdot\boldsymbol{n}_{TF})_F. \tag{2.59}$$

Then, from (2.58), (2.59) and noticing that v_F is single-valued on $\mathcal{F}_h$, and the fluxes $K\nabla u\cdot\boldsymbol{n}$ are continuous at interior faces, we infer that

$$b_h(\underline{\boldsymbol{v}}_h) = \sum_{T\in\mathcal{T}_h} \left\{ (K\nabla u, \nabla v_T)_T + \sum_{F\in\mathcal{F}_T} (v_F - v_T, K\nabla u\cdot\boldsymbol{n}_{TF})_F \right\}. \tag{2.60}$$

Combining (2.57) with (2.60), we arrive at

$$\begin{aligned} \mathcal{E}_h(u;\underline{\boldsymbol{v}}_h) = \sum_{T\in\mathcal{T}_h} \Bigg\{ &\left(\nabla v_T, K\nabla(p_T^{k+1}\underline{\mathbf{I}}_T^k u - u)\right)_T \\ &+ \sum_{F\in\mathcal{F}_T} \left(v_F - v_T, K\nabla(p_T^{k+1}\underline{\mathbf{I}}_T^k u - u)\cdot\boldsymbol{n}_{TF}\right)_F \Bigg\} \quad + s_h(\underline{\mathbf{I}}_h^k u, \underline{\boldsymbol{v}}_h) := \mathfrak{T}_1 + \mathfrak{T}_2. \end{aligned} \tag{2.61}$$

Applying Cauchy-Schwarz inequality on each term of $\mathfrak{T}_1$, we obtain

$$|\mathfrak{T}_1| \leq \sum_{T\in\mathcal{T}_h} \Bigg\{ \rho_T^{-1/2} \|K^{1/2}\nabla v_T\|_T \, \rho_T^{1/2} \|K^{1/2}\nabla(p_T^{k+1}\underline{\mathbf{I}}_T^k u - u)\|_T$$
$$+ \sum_{F\in\mathcal{F}_T} \rho_T^{-1/2} \left(\left\{ \frac{k_F}{h_F} \right\}^{1/2} \|v_F - v_T\|_F \right) \rho_T^{1/2} \left(\left\{ \frac{h_F}{k_F} \right\}^{1/2} \| \, K\nabla(p_T^{k+1}\underline{\mathbf{I}}_T^k u - u)\, \boldsymbol{n}_{TF}\|_F \right) \Bigg\}. \tag{2.62}$$

Now, thanks to Minkowski inequality, recalling (2.44), and taking into account the inequality $\|K\nabla w \cdot \boldsymbol{n}_{TF}\|_F \leq k_F^{1/2}\|K^{1/2}\nabla w\|_F$, together with the mesh regularity property (2.4), we deduce

$$|\mathfrak{T}_1| \lesssim \left(\sum_{T\in\mathcal{T}_h} \rho_T \Big\{ \|K^{1/2}\nabla(p_T^{k+1}\underline{\mathbf{I}}_T^k u - u)\|_T^2 + h_T \|K^{1/2}\nabla(p_T^{k+1}\underline{\mathbf{I}}_T^k u - u)\|_{\partial T}^2 \Big\} \right)^{1/2} \|\underline{\boldsymbol{v}}_h\|_{K,h}\,. \tag{2.63}$$

Next, by the approximation properties (2.31), (2.32), (2.40), and (2.42) of $p_T^{k+1}\underline{\mathbf{I}}_T^k$, we infer that

$$\|K^{1/2}\nabla(p_T^{k+1}\underline{\mathbf{I}}_T^k u - u)\|_T^2 + h_T \|K^{1/2}\nabla(p_T^{k+1}\underline{\mathbf{I}}_T^k u - u)\|_{\partial T}^2 \lesssim \overline{K}_T \rho_T^{2\alpha-1} h_T^{2(q+1)} \|u\|_{H^{q+2}(T)}^2\,, \tag{2.64}$$

and thus, replacing (2.64) in (2.63), we derive

$$|\mathfrak{T}_1| \lesssim \left(\sum_{T\in\mathcal{T}_h} \overline{K}_T \rho_T^{2\alpha} h_T^{2(q+1)} \|u\|_{H^{q+2}(T)}^2 \right)^{1/2} \|\underline{\boldsymbol{v}}_h\|_{K,h}\,. \tag{2.65}$$

Next, in order to bound $\mathfrak{T}_2$, we first notice that

$$\left| s_h(\underline{\mathbf{I}}_h^k u, \underline{\boldsymbol{v}}_h) \right| \leq s_h(\underline{\mathbf{I}}_h^k u, \underline{\mathbf{I}}_h^k u)^{1/2}\, s_h(\underline{\boldsymbol{v}}_h, \underline{\boldsymbol{v}}_h)^{1/2}\,, \tag{2.66}$$

and then, invoking Lemma 2.4.1 in (2.66), we obtain

$$|\mathfrak{T}_2| \lesssim \left(\sum_{T\in\mathcal{T}_h} \overline{K}_T \rho_T^{2\alpha} h_T^{2(q+1)} \|u\|_{H^{q+2}(T)}^2 \right)^{1/2} s_h(\underline{\boldsymbol{v}}_h, \underline{\boldsymbol{v}}_h)^{1/2}\,. \tag{2.67}$$

As consequence, we have established that

$$\mathcal{E}_h(u;\underline{\boldsymbol{v}}_h) \lesssim \left(\sum_{T\in\mathcal{T}_h} \overline{K}_T \rho_T^{2\alpha} h_T^{2(q+1)} \|u\|_{H^{q+2}(T)}^2 \right)^{1/2} \left(\|\underline{\boldsymbol{v}}_h\|_{K,h} + s_h(\underline{\boldsymbol{v}}_h, \underline{\boldsymbol{v}}_h)^{1/2} \right). \tag{2.68}$$

Thus, (2.56) follows from the fact that $\|\underline{\boldsymbol{v}}_h\|_{K,h} \lesssim \|\underline{\boldsymbol{v}}_h\|_{a,h}$ (cf. Lemma 2.3.1), $s_h(\underline{\boldsymbol{v}}_h, \underline{\boldsymbol{v}}_h)^{1/2} \leq \|\underline{\boldsymbol{v}}_h\|_{a,h}$, and recalling that $\|\underline{\boldsymbol{v}}_h\|_{a,h} = 1$.

□

Theorem 2.4.1 (Energy-error estimate) *Let* $\underline{\boldsymbol{u}}_h \in \underline{\boldsymbol{U}}_h^{k,0}$ *be the solution of* (2.50)*, and recall the definition of* α *(given in Lemma 2.2.3). If, in addition, we assume that the exact solution of* (2.3)*,* $u \in H^{q+2}(\mathcal{T}_h)$*, for some* $q \in \{0, ..., k\}$*, then there holds*

$$\|\underline{\mathbf{I}}_h^k u - \underline{\boldsymbol{u}}_h\|_{a,h} \lesssim \left\{ \sum_{T \in \mathcal{T}_h} \overline{K}_T \rho_T^{2\alpha} h_T^{2(q+1)} \|u\|_{H^{q+2}(T)}^2 \right\}^{1/2}. \tag{2.69}$$

Moreover, applying Lemma 2.2.3, there holds

$$\|K^{1/2}(\nabla u - \nabla_h p_h^{k+1} \underline{\boldsymbol{u}}_h)\|_\Omega \lesssim \left\{ \sum_{T \in \mathcal{T}_h} \overline{K}_T \rho_T^{2\alpha} h_T^{2(q+1)} \|u\|_{H^{q+2}(T)}^2 \right\}^{1/2}. \tag{2.70}$$

Proof. Since a_h is coercive on $\underline{\boldsymbol{U}}_h^{k,0}$, provided with the norm $\|\cdot\|_{a,h}$ (consequence of Lemma 2.3.1), we are able to apply the Third Strang Lemma A.7 in the appendix in [66], and obtain

$$\|\underline{\mathbf{I}}_h^k u - \underline{\boldsymbol{u}}_h\|_{a,h} \quad \leq \sup_{\underline{\boldsymbol{v}}_h \in \underline{\boldsymbol{U}}_h^{k,0},\, \|\underline{\boldsymbol{v}}_h\|_{a,h}=1} \mathcal{E}_h(u; \underline{\boldsymbol{v}}_h)\,.$$

Then, (2.69) is derived by applying Lemma 2.4.2. Now, in order to deduce (2.70), we first apply triangle inequality, and obtain

$$\|K^{1/2}(\nabla u - \nabla_h p_h^{k+1} \underline{\boldsymbol{u}}_h)\|_\Omega \leq \|K^{1/2}(\nabla u - \nabla_h p_h^{k+1} \underline{\mathbf{I}}_h^k u)\|_\Omega + \|K^{1/2} \nabla_h p_h^{k+1}(\underline{\mathbf{I}}_h^k u - \underline{\boldsymbol{u}}_h))\|_\Omega\,. \tag{2.71}$$

Finally, (2.70) follows from (2.71), (2.51), (2.69), and (2.64). We omit further details. □

Next, we provide an estimate of the L^2-error between $u_h \in L^2(\Omega)$ and $\pi_h^k u \in L^2(\Omega)$, where

$$u_h|_T := u_T \quad \text{and} \quad \pi_h^k u|_T := \pi_T^k u \qquad \forall\, T \in \mathcal{T}_h. \tag{2.72}$$

To this end, we need an additional elliptic regularity assumption in the following form: Given $w \in L_0^2(\Omega) := \{q \in L^2(\Omega) \,:\, (q,1)_\Omega = 0\}$, we let $z_w \in U$ be the unique function such that

$$(K \nabla z_w, \nabla v)_\Omega = (w, v)_\Omega \quad \forall v \in U, \tag{2.73}$$

which satisfies the a priori estimate:

$$\|z_w\|_{H^2(\Omega)} \lesssim \underline{K}^{-1} \|w\|_\Omega\,, \quad \underline{K} := \min_{T \in \mathcal{T}_h} \underline{K}_T. \tag{2.74}$$

This assumption holds when, for example, the domain Ω is convex and K is Lipschitz continuous [109]. For simplicity, we assume for the rest of analysis, that K is constant on Ω. According to Lemma 2.2.3, the latter implies that $\alpha = 1/2$.

Theorem 2.4.2 (L^2-error estimate) *Let $\underline{\boldsymbol{u}}_h \in \underline{\boldsymbol{U}}_h^{k,0}$ be the solution of (2.50), and assume that the exact solution of (2.3), $u \in H^{q+2}(\mathcal{T}_h)$, for some $q \in \{0, ..., k\}$. Then, when $k \geq 1$, there holds*

$$\|\pi_h^k u - u_h\|_\Omega \lesssim \underline{K}^{-1}\, \overline{K}^{1/2} \rho^{1/2} h \left(\sum_{T \in \mathcal{T}_h} \overline{K}_T \rho_T h_T^{2(q+1)} \|u\|^2_{H^{q+2}(T)} \right)^{1/2}. \tag{2.75}$$

Moreover, when $k = 0$, and assuming in addition that $f \in H^1(\mathcal{T}_h)$ and $g \in W^{1,\infty}(\mathcal{F}_h^b)$, there holds

$$\begin{aligned} \|\pi_h^0 u - u_h\|_\Omega \lesssim\ & \underline{K}^{-1} \overline{K}^{1/2} \rho^{1/2}\, h \left\{ \sum_{T \in \mathcal{T}_h} \overline{K}_T \rho_T h_T^2 \|u\|^2_{H^2(T)} \right\}^{1/2} \\ & + \underline{K}^{-1}\, h \left(\sum_{T \in \mathcal{T}_h} h_T^2 \, ||f||^2_{H^1(T)} \right)^{1/2} + \underline{K}^{-1}\, h^{1/2} \left(\sum_{F \in \mathcal{F}_h^b} h_F^{d+1} \, ||g||^2_{W^{1,\infty}(F)} \right)^{1/2}, \end{aligned} \tag{2.76}$$

where, $\overline{K} := \max_{T \in \mathcal{T}_h} \overline{K}_T$, $\rho := \overline{K}/\underline{K}$, and $h := \max_{T \in \mathcal{T}_h} h_T$.

Proof. First, we invoke the Aubin-Nitsche Lemma A.10 in the appendix in [66], with $\mathtt{U} := U = H^1(\Omega) \cap L_0^2(\Omega)$, $\mathtt{a}(u, v) = (K\nabla u, \nabla v)_\Omega$, $\mathtt{l}(v) := (f, v)_\Omega + (g, v)_\Gamma$, $\mathtt{U}_h := \underline{\boldsymbol{U}}_h^{k,0}$, $\|\cdot\|_{\mathtt{U}_h} := \|\cdot\|_{a,h}$, $\mathtt{a}_h := a_h$, $\mathtt{l}_h := b_h$, and $\mathtt{I}_h u := \underline{\mathbf{I}}_h^k u$. Moreover, we take $\mathtt{L} := L_0^2(\Omega)$ and introduce the *linear reconstruction operator* $\mathtt{r}_h : \underline{\boldsymbol{U}}_h^{k,0} \to L_0^2(\Omega)$, which given $\underline{\boldsymbol{v}}_h := ((v_T)_{T \in \mathcal{T}_h}, (v_F)_{F \in \mathcal{F}_h}) \in \underline{\boldsymbol{U}}_h^{k,0}$, $\mathtt{r}_h(\underline{\boldsymbol{v}}_h) := v_h$, where $v_h \in L_0^2(\Omega)$ is such that $v_h|_T := v_T \quad \forall T \in \mathcal{T}_h$. It is not difficult to check that $\mathtt{r}_h$ is continuous, and thanks to the symmetry of a_h, the dual consistency error of z_w, $\mathcal{E}_h^{\mathtt{d}}(z_w; \cdot)$, verifies,

$$\mathcal{E}_h^{\mathtt{d}}(z_w; \cdot) := a_h(\cdot, \underline{\mathbf{I}}_h^k z_w) - (w, \mathtt{r}_h(\cdot))_\Omega = a_h\left(\underline{\mathbf{I}}_h^k z_w - \underline{\boldsymbol{z}}_{\boldsymbol{w}_h}, \cdot\right), \tag{2.77}$$

with $\underline{\boldsymbol{z}}_{\boldsymbol{w}_h} \in \underline{\boldsymbol{U}}_h^{k,0}$ being the unique solution of the HHO scheme related to (2.73). Now, denoting by $\|\cdot\|_{a,h,*}$ the dual norm of $\|\cdot\|_{a,h}$, the referred Aubin-Nitsche

Lemma A.10 yields us to

$$\|I_h^k u - u_h\|_\Omega \leq \underbrace{\|\underline{\mathbf{I}}_h^k u - \underline{\boldsymbol{u}}_h\|_{a,h} \sup_{w\in L_0^2(\Omega)\,,\,\|w\|\leq 1} \|\mathcal{E}_h^{\mathtt{d}}(z_w;\cdot)\|_{a,h,*}}_{\mathfrak{T}_1} + \underbrace{\sup_{w\in L_0^2(\Omega)\,,\,\|w\|\leq 1} \mathcal{E}_h(u;\underline{\mathbf{I}}_h^k z_w)}_{\mathfrak{T}_2}\,. \tag{2.78}$$

We now bound $\mathfrak{T}_1$. Thanks to (2.77), and after applying Theorem 2.4.1 to the HHO scheme related to (2.73), with $q=0$, and *elliptic regularity* (2.74), we have that

$$\|\mathcal{E}_h^{\mathtt{d}}(z_w;\cdot)\|_{a,h,*} \leq \|\underline{\mathbf{I}}_h^k z_w - \underline{\boldsymbol{z_w}}_h\|_{a,h} \lesssim (\overline{\kappa})^{1/2}\,\rho^{1/2}\,h\,\|z_w\|_{H^2(\Omega)} \lesssim \underline{\kappa}^{-1}\,(\overline{\kappa})^{1/2}\,\rho^{1/2}\,h\,\|w\|_\Omega\,.$$

Next, invoking (2.69), we derive a bound of $\mathfrak{T}_1$:

$$\mathfrak{T}_1 \lesssim \underline{\kappa}^{-1}\,(\overline{\kappa})^{1/2}\,\rho^{1/2}\,h\,\left\{\sum_{T\in\mathcal{T}_h} \overline{K}_T\rho_T\,h_T^{2(q+1)}\|u\|^2_{H^{q+2}(T)}\right\}^{1/2}. \tag{2.79}$$

It remains to bound $\mathfrak{T}_2$. To this aim, we need to analyze the cases: $k\geq 1$ and $k=0$.

Case $k\geq 1$. Taking into account the orthogonality property (2.12), we proceed as in the deduction of (2.68), with $\underline{\boldsymbol{v}}_h := \underline{\mathbf{I}}_h^k z_w$, and obtain

$$\mathcal{E}_h(u;\underline{\mathbf{I}}_h^k z_w) \lesssim \left(\sum_{T\in\mathcal{T}_h} \overline{K}_T\rho_T\,h_T^{2(q+1)}\|u\|^2_{H^{q+2}(T)}\right)^{1/2} \times \left[\left(\sum_{T\in\mathcal{T}_h} |\underline{\mathbf{I}}_T^k z_w|^2_{K,\partial T}\right)^{1/2} + s_h(\underline{\mathbf{I}}_h^k z_w, \underline{\mathbf{I}}_h^k z_w)^{1/2}\right]. \tag{2.80}$$

Applying Lemma 2.4.1, with $q=0$, we have

$$s_h(\underline{\mathbf{I}}_h^k z_w, \underline{\mathbf{I}}_h^k z_w)^{1/2} \lesssim (\overline{\kappa})^{1/2}\,\rho^{1/2}\,h\,\|z_w\|_{H^2(\Omega)}\,. \tag{2.81}$$

Next, recalling the definition of $|\cdot|_{K,\partial T}$, we have for any $T\in\mathcal{T}_h$

$$\begin{aligned}
|\underline{\mathbf{I}}_T^k z_w|^2_{K,\partial T} &= \sum_{F\in\mathcal{F}_T} \rho_T^{-1/2}\left(\frac{\kappa_F}{h_F}\right)^{1/2}\|\pi_F^k z_w - \pi_T^k z_w\|_F^2\\
&= \sum_{F\in\mathcal{F}_T} \rho_T^{-1/2}\left(\frac{\kappa_F}{h_F}\right)^{1/2}\|\pi_F^k\left(z_w - \pi_T^k z_w\right)\|_F^2\\
&\leq \sum_{F\in\mathcal{F}_T} \rho_T^{-1/2}\left(\frac{\kappa_F}{h_F}\right)^{1/2}\|z_w - \pi_T^k z_w\|_F^2\\
&\lesssim \sum_{F\in\mathcal{F}_T} (\overline{\kappa}_T)^{1/2}\,h_T^2\,\|z_w\|^2_{H^2(T)}\,,
\end{aligned} \tag{2.82}$$

after applying Lemma 2.2.1, with t=2 (since $l := k \geq 1$), and $s = 0$. Then, plugging estimates (2.82) and (2.81) into (2.80), together with the *elliptic regularity* (2.74), we deduce

$$\mathfrak{T}_2 \lesssim \underline{\kappa}^{-1} (\overline{\kappa})^{1/2} \rho^{1/2} h \left\{ \sum_{T \in \mathcal{T}_h} \overline{K}_T \rho_T h_T^{2(q+1)} \|u\|^2_{H^{q+2}(T)} \right\}^{1/2},$$

and thus, we conclude the proof of (2.75) in the case $k \geq 1$.

Case $k = 0$. Considering the definition of a_h and b_h, we have

$$\begin{aligned} \mathcal{E}_h(u; \underline{\mathrm{I}}_h^0 z_w) &= a_h(\underline{\mathrm{I}}_h^0 u, \underline{\mathrm{I}}_h^0 z_w) - \sum_{T \in \mathcal{T}_h} (f, \pi_T^0 z_w)_T - \sum_{F \in \mathcal{F}_h^b} (g, \pi_F^0 z_w)_F \\ &= \sum_{T \in \mathcal{T}_h} (K \nabla p_T^1 \underline{\mathrm{I}}_T^0 u, \nabla p_T^1 \underline{\mathrm{I}}_T^0 z_w)_T + s_h(\underline{\mathrm{I}}_h^0 u, \underline{\mathrm{I}}_h^0 z_w) \\ &\quad - \sum_{T \in \mathcal{T}_h} (f, \pi_T^0 z_w)_T - \sum_{F \in \mathcal{F}_h^b} (g, \pi_F^0 z_w)_F . \end{aligned} \tag{2.83}$$

On the other hand, we know

$$(K \nabla u, \nabla z_w)_\Omega = (f, z_w)_\Omega + (g, z_w)_\Gamma . \tag{2.84}$$

Now, thanks to the orthogonality property of π_T^0, and (2.84), we derive

$$\begin{aligned} \sum_{T \in \mathcal{T}_h} (f, \pi_T^0 z_w)_T &= \sum_{T \in \mathcal{T}_h} (\pi_T^0 f, z_w)_T \\ &= \sum_{T \in \mathcal{T}_h} (\pi_T^0 f - f, z_w)_T + (f, z_w)_\Omega \\ &= \sum_{T \in \mathcal{T}_h} (\pi_T^0 f - f, z_w - \pi_T^0 z_w)_T + (K \nabla u, \nabla z_w)_\Omega - (g, z_w)_\Gamma . \end{aligned} \tag{2.85}$$

Plugging (2.85) into (2.83), we obtain

$$\begin{aligned} \mathcal{E}_h(u; \underline{\mathrm{I}}_h^0 z_w) &= \underbrace{\sum_{T \in \mathcal{T}_h} \left[(K \nabla p_T^1 \underline{\mathrm{I}}_T^0 u, \nabla p_T^1 \underline{\mathrm{I}}_T^0 z_w)_T - (K \nabla u, \nabla z_w)_T \right]}_{\mathfrak{T}_{2,1}} + \underbrace{s_h(\underline{\mathrm{I}}_h^0 u, \underline{\mathrm{I}}_h^0 z_w)}_{\mathfrak{T}_{2,2}} \\ &\quad + \underbrace{\sum_{T \in \mathcal{T}_h} (\pi_T^0 f - f, z_w - \pi_T^0 z_w)_T}_{\mathfrak{T}_{2,3}} + \underbrace{\sum_{F \in \mathcal{F}_h^b} (g - \pi_F^0 g, z_w - \pi_F^0 z_w)_F}_{\mathfrak{T}_{2,4}} . \end{aligned} \tag{2.86}$$

Now, we notice that

$$
\begin{aligned}
(K\nabla u, \nabla z_w)_T - \left(K\nabla p_T^1 \underline{\mathrm{I}}_T^0 u, \nabla p_T^1 \underline{\mathrm{I}}_T^0 z_w\right)_T &= \left(K\nabla(u - p_T^1 \underline{\mathrm{I}}_T^0 u), \nabla(z_w - p_T^1 \underline{\mathrm{I}}_T^0 z_w)\right)_T + \\
&\left(K\nabla(u - p_T^1 \underline{\mathrm{I}}_T^0 u), \nabla p_T^1 \underline{\mathrm{I}}_T^0 z_w)\right)_T + \left(K\nabla p_T^1 \underline{\mathrm{I}}_T^0 u, K\nabla(z_w - p_T^1 \underline{\mathrm{I}}_T^0 z_w)\right)_T \\
&= \left(K\nabla(u - p_T^1 \underline{\mathrm{I}}_T^0 u), \nabla(z_w - p_T^1 \underline{\mathrm{I}}_T^0 z_w)\right)_T \ ,
\end{aligned}
$$

where the two last terms vanish by orthogonality property (2.12). Then, by approximation property (2.31), Cauchy-Schwarz inequality, and (2.74) we deduce

$$
\begin{aligned}
|\mathfrak{T}_{2,1}| &\lesssim \left(\sum_{T\in\mathcal{T}_h} \overline{K}_T \rho_T h_T^2 \|u\|_{H^2(T)}^2\right)^{1/2} \left(\sum_{T\in\mathcal{T}_h} \overline{K}_T \rho_T h_T^2 \|z_w\|_{H^2(T)}^2\right)^{1/2} \\
&\lesssim \underline{K}^{-1} \overline{K}^{1/2} \rho^{1/2}\, h \left\{\sum_{T\in\mathcal{T}_h} \overline{K}_T \rho_T h_T^2 \|u\|_{H^2(T)}^2\right\}^{1/2} \|w\|_\Omega \ . \qquad (2.87)
\end{aligned}
$$

Concerning $\mathfrak{T}_{2,2}$, we have, after applying Lemma 2.4.1

$$
\begin{aligned}
s_T(\underline{\mathrm{I}}_T^0 u, \underline{\mathrm{I}}_T^0 z_w) &\leq \left[s_T(\underline{\mathrm{I}}_T^0 u, \underline{\mathrm{I}}_T^0 u)\right]^{1/2} \left[s_T(\underline{\mathrm{I}}_T^0 z_w, \underline{\mathrm{I}}_T^0 z_w)\right]^{1/2} \\
&\leq \left(\overline{K}_T{}^{1/2} \rho_T^{1/2} h_T \left\|u\right\|_{H^2(T)}\right) \left(\overline{K}_T{}^{1/2} \rho_T^{1/2} h_T \left\|z_w\right\|_{H^2(T)}\right) .
\end{aligned}
$$

Then, with the help of Minkowski inequality and (2.74), we obtain

$$
|\mathfrak{T}_{2,2}| \lesssim \underline{K}^{-1} \overline{K}^{1/2} \rho^{1/2}\, h \left\{\sum_{T\in\mathcal{T}_h} \overline{K}_T \rho_T h_T^2 \|u\|_{H^2(T)}^2\right\}^{1/2} \|w\|_\Omega \ . \qquad (2.88)
$$

Next, applying Cauchy-Schwarz inequality, Minkowski inequality, approximation property (2.5), and (2.74), we deduce

$$
\begin{aligned}
|\mathfrak{T}_{2,3}| &\leq \sum_{T\in\mathcal{T}_h} ||\pi_T^0 f - f||_T \, ||z_w - \pi_T^0 z_w||_T \\
&\leq \left(\sum_{T\in\mathcal{T}_h} ||\pi_T^0 f - f||_T^2\right)^{1/2} \left(\sum_{T\in\mathcal{T}_h} ||z_w - \pi_T^0 z_w||_T^2\right)^{1/2} \\
&\lesssim \left(\sum_{T\in\mathcal{T}_h} h_T^2 \, ||f||_{H^1(T)}^2\right)^{1/2} \left(\sum_{T\in\mathcal{T}_h} h_T^2 \, |z_w|_{H^1(T)}^2\right)^{1/2} \\
&\lesssim \underline{K}^{-1}\, h \left(\sum_{T\in\mathcal{T}_h} h_T^2 \, ||f||_{H^1(T)}^2\right)^{1/2} ||w||_\Omega \, . \qquad (2.89)
\end{aligned}
$$

Now, applying Theorem 1.45 in [66], for $p = \infty$, $s = 1$, and $m = 0$, we obtain

$$
\|g - \pi_F^0 g\|_{L^\infty(F)} \lesssim h_F \|g\|_{W^{1,\infty}(F)} \quad \forall F \in \mathcal{F}_h^b. \qquad (2.90)
$$

Also, thanks to that fact that $|F| \lesssim h_F^{d-1}$ ($d = 2$ or 3), there holds

$$\|g - \pi_F^0 g\|_{L^2(F)} \leq h_F^{(d-1)/2} \|g - \pi_F^0 g\|_{L^\infty(F)} \,. \tag{2.91}$$

Then, taking into account (2.90)-(2.91), and proceeding as in the deduction of (2.89), we have

$$\begin{aligned}
|\mathfrak{T}_{2,4}| &\leq \sum_{F \in \mathcal{F}_h^b} ||g - \pi_F^0 g||_F \, ||z_w - \pi_F^0 z_w||_F \\
&\lesssim \left(\sum_{F \in \mathcal{F}_h^b} ||g - \pi_F^0 g||_F^2 \right)^{1/2} \left(\sum_{F \in \mathcal{F}_h^b} ||z_w - \pi_F^0 z_w||_F^2 \right)^{1/2} \\
&\lesssim \left(\sum_{F \in \mathcal{F}_h^b} h_F^{d+1} \, ||g||_{W^{1,\infty}(F)}^2 \right)^{1/2} \left(\sum_{F \in \mathcal{F}_h^b} h_T \, |z_w|_{H^1(T_F)}^2 \right)^{1/2} \\
&\lesssim \underline{K}^{-1} \, h^{1/2} \left(\sum_{F \in \mathcal{F}_h^b} h_F^{d+1} \, ||g||_{W^{1,\infty}(F)}^2 \right)^{1/2} ||w||_\Omega \,.
\end{aligned} \tag{2.92}$$

Therefore, (2.87)-(2.89), in connection with (2.92), allow us to conclude that

$$\begin{aligned}
|\mathfrak{T}_2| \lesssim \underline{K}^{-1} \overline{K}^{1/2} \rho^{1/2} \, h \left\{ \sum_{T \in \mathcal{T}_h} \overline{K}_T \rho_T h_T^2 \|u\|_{H^2(T)}^2 \right\}^{1/2} \\
+ \underline{K}^{-1} \, h \left(\sum_{T \in \mathcal{T}_h} h_T^2 \, ||f||_{H^1(T)}^2 \right)^{1/2} + \underline{K}^{-1} \, h^{1/2} \left(\sum_{F \in \mathcal{F}_h^b} h_F^{d+1} \, ||g||_{W^{1,\infty}(F)}^2 \right)^{1/2} .
\end{aligned} \tag{2.93}$$

The proof of (2.76) follows from (2.79) (with $q = k = 0$) and (2.93). We omit further details. □

Remark 2.4.1 *If $g \in \mathbb{P}_{d-1}^0(\mathcal{F}_h^b)$, (2.76) reduces to*

$$\begin{aligned}
\|\pi_h^0 u - u_h\|_\Omega \lesssim \underline{K}^{-1} \overline{K}^{1/2} \rho^{1/2} \, h \left\{ \sum_{T \in \mathcal{T}_h} \overline{K}_T \rho_T h_T^2 \|u\|_{H^2(T)}^2 \right\}^{1/2} \\
+ \underline{K}^{-1} \, h \left(\sum_{T \in \mathcal{T}_h} h_T^2 \, ||f||_{H^1(T)}^2 \right)^{1/2} .
\end{aligned} \tag{2.94}$$

Remark 2.4.2 *It is possible to establish a similar result to Theorem 2.4.2, for non-piecewise constant diffusion coefficient K. In essence, we need to assume an*

elliptic regularity property for locally variable K *(cf. Assumption 4.21 in [66]), and extend/adapt the theoretical arguments applied for Poisson equation with Dirichlet boundary condition, as described in Section 4.2 in [66].*

The following section, take as reference [50], where, we will discuss several issues of the implementation of Neumann boundary conditions.

2.5 Implementation

An essential step in the implementation consists in selecting suitable bases for the polynomial spaces on elements and faces. Particular care is required to make sure that the resulting local problems are well-conditioned, since the accuracy of the local computations may affect the overall quality of the approximation. Let $T \in \mathcal{T}_h$ and denote by $\underline{x}_T$ a point with respect to which T is star-shaped (in the numerical test, the barycenter of T was used). For a given polynomial degree $l \in \{k, k+1\}$, one possibility leading to a hierarchical basis for $\mathbb{P}_d^l(T)$, $T \in \mathcal{T}_h$, is to choose the following family of monomial functions:

$$\mathcal{B}_T^l := \left\{ \prod_{i=1}^{d} \eta_{T,i}^{\alpha_i} |\ \eta_{T,i} := \frac{x_i - x_{T,i}}{h_T}\ \forall\, 1 \le i \le d,\ \underline{\alpha} \in \mathbb{N}^d,\ \|\underline{\alpha}\|_{l^1} \le l \right\}. \tag{2.95}$$

The characteristics of this bases are

i) Basis functions are expressed with respect to a reference frame local to each element, which ensures that the basis does not depend on the position of the element.

ii) Using the length scale equal to h_T ensures that the basis functions take values in an interval close to $[-1, 1]$.

A basis for the polynomial space of vector-valued functions $\mathbb{P}_d^l(T)^d$ is then obtained by the Cartesian product of $\mathcal{B}_T^l$. Similarly, a hierarchical monomial basis can be defined for the spaces $\mathbb{P}_d^l(F)^d$, $F \in \mathcal{F}_h$, using the face barycenter x_F and the face diameter h_F.

For computational implementation purposes, finding a basis for $\underline{\boldsymbol{U}}_h^{k,0}$ could be a hard task, due to the zero mean value condition that must satisfy all its elements. One

way to circumvent this difficulty, is to impose this restriction with the help of a Lagrange multiplier. This lets us to introduce the following discrete scheme, which reads as: Find $(\underline{\boldsymbol{u}}_h, \lambda) \in \underline{\boldsymbol{U}}_h^k \times \mathbb{R}$ such that

$$a_h(\underline{\boldsymbol{u}}_h, \underline{\boldsymbol{v}}_h) + \lambda(v_h, 1)_\Omega + \mu(u_h, 1)_\Omega = b_h(\underline{\boldsymbol{v}}_h) \quad \forall\, (\underline{\boldsymbol{v}}_h, \mu) \in \underline{\boldsymbol{U}}_h^k \times \mathbb{R}. \tag{2.96}$$

Theorem 2.5.1 *The problems (2.50) and (2.96) are equivalent, in the sense:*

1. *If $(\underline{\boldsymbol{u}}_h, \lambda)$ is a solution of (2.96), then $\lambda = 0$ and $\underline{\boldsymbol{u}}_h \in \underline{\boldsymbol{U}}_h^{k,0}$ is a solution of (2.50).*

2. *If $\underline{\boldsymbol{u}}_h \in \underline{\boldsymbol{U}}_h^{k,0}$ is a solution of (2.50), then $(\underline{\boldsymbol{u}}_h, 0) \in \underline{\boldsymbol{U}}_h^k \times \mathbb{R}$ is a solution of (2.96).*

Proof. It is immediate from the compatibility condition (2.2). □

To deduce the linear system associated to (2.96), we rewrite the term b_h as

$$b_h(\underline{\boldsymbol{v}}_h) := \sum_{T \in \mathcal{T}_h} b_T(\underline{\boldsymbol{v}}_T) \quad , \quad b_T(\underline{\boldsymbol{v}}_T) := (f, v_T)_T + \sum_{F \in \mathcal{F}_T \cap \mathcal{F}_h^\partial} (g, v_F)_F. \tag{2.97}$$

For integers $l \geq 0$ and $n \geq 0$, we denote by $N_n^l := \begin{pmatrix} l+n \\ l \end{pmatrix}$ the dimension of the space composed of n-variate polynomials of degree at most l.

For any $\underline{\boldsymbol{v}}_h$ in the global discrete space $\underline{\boldsymbol{U}}_h^k$, we collect its components with respect to the polynomial bases attached to the mesh cells and faces in a global component vector denoted by $V_{\mathcal{TF}} \in \mathbb{R}^{N_\mathcal{T}^k} \times \mathbb{R}^{N_\mathcal{F}^k}$ with

$$N_\mathcal{T}^k := \mathrm{card}(\mathcal{T}_h) \times N_d^k \quad \text{and} \quad N_\mathcal{F}^k := \mathrm{card}(\mathcal{F}_h) \times N_{d-1}^k, \tag{2.98}$$

where N_d^k and N_{d-1}^k denote the dimension of the local cell and face bases, respectively, while d represents the space dimension. We can decompose the global vector of coefficients as

$$V_{\mathcal{TF}} = \begin{bmatrix} V_\mathcal{T} \\ \hdashline V_\mathcal{F} \end{bmatrix}, \tag{2.99}$$

where the vectors $V_{\mathcal{T}} \in \mathbb{R}^{N_{\mathcal{T}}^k}$ and $V_{\mathcal{F}} \in \mathbb{R}^{N_{\mathcal{F}}^k}$ collect the coefficients associated to element-based and face-based DOFS, respectively.

Also, we can collect, for every $\underline{\boldsymbol{v}}_T \in \underline{\boldsymbol{U}}_T^k$, its components associated to T and ∂T, in a local component vector denoted by $V_{T\mathcal{F}_T} \in \mathbb{R}^{N_T^k}$, and in the similar way, we split the local vector of coefficients associated to the element T as

$$V_{T\mathcal{F}_T} = \left[\begin{array}{c} V_T \\ \hdashline V_{\mathcal{F}_T} \end{array}\right], \tag{2.100}$$

with V_T and $V_{\mathcal{F}_T}$ collecting the coefficients associated to the bases of the element and faces linked to T, respectively.

Expressing the functions in the discrete formulation (2.96) as a linear combination of its respective basis functions, we obtain the following system

$$\sum_{T\in\mathcal{T}_h} V_{T\mathcal{F}_T}^t A(T) U_{T\mathcal{F}_T} + \lambda \sum_{T\in\mathcal{T}_h} V_T^t M_T + \mu \sum_{T\in\mathcal{T}_h} M_T^t U_T = \sum_{T\in\mathcal{T}_h} V_{T\mathcal{F}_T}^t B(T). \tag{2.101}$$

Here, the local matrix $A(T)$ represents the local bilinear form a_T, the local vector $B(T)$ represents the linear functional b_T, and the vector $M_T \in \mathbb{R}^{N_d^k}$ collects the average of the local base functions on T:

$$A(T) = \left[\begin{array}{c:c} A_{TT} & A_{T\mathcal{F}_T} \\ \hdashline A_{T\mathcal{F}_T}^t & A_{\mathcal{F}_T\mathcal{F}_T} \end{array}\right], \qquad B(T) = \left[\begin{array}{c} B_T \\ \hdashline B_{\mathcal{F}_T} \end{array}\right], \tag{2.102}$$

Arranging the equation (2.101) in a matrix form, in order to eliminate the element-based DOFS (by static condensation), we obtain the following linear global system corresponding to the discrete problem (2.96): Find $(U_{\mathcal{T}}, U_{\mathcal{F}}, \lambda) \in \mathbb{R}^{N_{\mathcal{T}}^k} \times \mathbb{R}^{N_{\mathcal{F}}^k} \times \mathbb{R}$ such that

$$\left[\begin{array}{c:c:c} A_{\mathcal{T}\mathcal{T}} & A_{\mathcal{T}\mathcal{F}} & M_{\mathcal{T}} \\ \hdashline A_{\mathcal{T}\mathcal{F}}^t & A_{\mathcal{F}\mathcal{F}} & 0_{\mathcal{F}} \\ \hdashline M_{\mathcal{T}}^t & 0_{\mathcal{F}}^t & 0 \end{array}\right] \left[\begin{array}{c} U_{\mathcal{T}} \\ \hdashline U_{\mathcal{F}} \\ \hdashline \lambda \end{array}\right] = \left[\begin{array}{c} B_{\mathcal{T}} \\ \hdashline B_{\mathcal{F}} \\ \hdashline 0 \end{array}\right], \tag{2.103}$$

where the vector $M_{\mathcal{T}} \in \mathbb{R}^{N_{\mathcal{T}}^k}$ denote the vector collecting the average of the functions of the element-based DOFs, and $0_{\mathcal{F}}$ is the zero vector in $\mathbb{R}^{N_{\mathcal{F}}^k}$. Instead of assembling

the full system (2.103), we can effectively compute the Schur complement of $A_{\mathcal{TT}}$, following the system

$$A_{\mathcal{TT}}U_{\mathcal{T}} + \widehat{A}_{\mathcal{TF}}\widehat{U}_{\mathcal{F}} = B_{\mathcal{T}}, \tag{2.104}$$

$$\widehat{A}^t_{\mathcal{TF}}U_{\mathcal{T}} + \widehat{A}_{\mathcal{FF}}\widehat{U}_{\mathcal{F}} = \widehat{B}_{\mathcal{F}}, \tag{2.105}$$

where $\widehat{A}_{\mathcal{FF}} = \left[\begin{array}{c|c} A_{\mathcal{FF}} & 0_{\mathcal{F}} \\ \hline 0^t_{\mathcal{F}} & 0 \end{array}\right]$, $\widehat{A}_{\mathcal{TF}} = \left[\begin{array}{c|c} A_{\mathcal{TF}} & M_{\mathcal{T}} \end{array}\right]$, $\widehat{U}_{\mathcal{F}} = \left[\begin{array}{c|c} U_{\mathcal{F}} & \lambda \end{array}\right]^t$, and $\widehat{B}_{\mathcal{F}} = \left[\begin{array}{c|c} B_{\mathcal{F}} & 0 \end{array}\right]^t$. From (2.104), we obtain

$$U_{\mathcal{T}} = A^{-1}_{\mathcal{TT}}\left[B_{\mathcal{T}} - \widehat{A}_{\mathcal{TF}}\widehat{U}_{\mathcal{F}}\right]. \tag{2.106}$$

Then, replacing (2.106) in (2.105), we derive

$$\left[\widehat{A}_{\mathcal{FF}} - \widehat{A}^t_{\mathcal{TF}}A^{-1}_{\mathcal{TT}}\widehat{A}_{\mathcal{TF}}\right]\widehat{U}_{\mathcal{F}} = \left[\widehat{B}_{\mathcal{F}} - \widehat{A}^t_{\mathcal{TF}}A^{-1}_{\mathcal{TT}}B_{\mathcal{T}}\right]. \tag{2.107}$$

After simplifying the system (2.107), we obtain the following reduced system, where the element-based DOFs collected in the vector $U_{\mathcal{T}}$ no longer appears:

$$\left[\begin{array}{c|c} A_{\mathcal{FF}} - A^t_{\mathcal{TF}}A^{-1}_{\mathcal{TT}}A_{\mathcal{TF}} & -A^t_{\mathcal{TF}}A^{-1}_{\mathcal{TT}}M_{\mathcal{T}} \\ \hline -M^t_{\mathcal{T}}A^{-1}_{\mathcal{TT}}A_{\mathcal{TF}} & -M^t_{\mathcal{T}}A^{-1}_{\mathcal{TT}}M_{\mathcal{T}} \end{array}\right]\left[\begin{array}{c} U_{\mathcal{F}} \\ \hline \lambda \end{array}\right] = \left[\begin{array}{c} B_{\mathcal{F}} - A^t_{\mathcal{TF}}A^{-1}_{\mathcal{TT}}B_{\mathcal{T}} \\ \hline -M^t_{\mathcal{T}}A^{-1}_{\mathcal{TT}}B_{\mathcal{T}} \end{array}\right]. \tag{2.108}$$

The advantage of implementing (2.108) instead of (2.103) is that the number of unknowns in (2.108) is reduced from $N^k_{\mathcal{T}} + N^k_{\mathcal{F}} + 1$ to $N^k_{\mathcal{F}} + 1$.

Denoting by $\underset{T\in\mathcal{T}_h}{\longleftarrow\!\!\!\!\!\!\longleftarrow}$ the usual assembling procedure based on a global DOF map, we can assemble all matrix products appearing in (2.108) directly from their local counterparts, as

$$B_{\mathcal{F}} - A^t_{\mathcal{TF}}A^{-1}_{\mathcal{TT}}B_{\mathcal{T}} \underset{T\in\mathcal{T}_h}{\longleftarrow\!\!\!\!\!\!\longleftarrow} B_{\mathcal{F}_T} - A^t_{T\mathcal{F}_T}A^{-1}_{TT}B_T \quad , \quad A^t_{\mathcal{TF}}A^{-1}_{\mathcal{TT}}M_{\mathcal{T}} \underset{T\in\mathcal{T}_h}{\longleftarrow\!\!\!\!\!\!\longleftarrow} A^t_{T\mathcal{F}_T}A^{-1}_{TT}M_T,$$

$$A_{\mathcal{FF}} - A^t_{\mathcal{TF}}A^{-1}_{\mathcal{TT}}A_{\mathcal{TF}} \underset{T\in\mathcal{T}_h}{\longleftarrow\!\!\!\!\!\!\longleftarrow} A_{\mathcal{F}_T\mathcal{F}_T} - A^t_{T\mathcal{F}_T}A^{-1}_{TT}A_{T\mathcal{F}_T},$$

$$M^t_{\mathcal{T}}A^{-1}_{\mathcal{TT}}M_{\mathcal{T}} = \sum_{T\in\mathcal{T}_h} M^t_T A^{-1}_{TT}M_T, \text{and} \quad M^t_{\mathcal{T}}A^{-1}_{\mathcal{TT}}B_{\mathcal{T}} = \sum_{T\in\mathcal{T}_h} M^t_T A^{-1}_{TT}B_T.$$

Besides, the global vector $U_{\mathcal{T}}$ can be recovered from (2.104), letting $\lambda = 0$ in $\widehat{U}_{\mathcal{F}}$, so that

$$U_{\mathcal{T}} = A^{-1}_{\mathcal{TT}}\Big(B_{\mathcal{T}} - A_{\mathcal{TF}}U_{\mathcal{F}}\Big), \tag{2.109}$$

Finally, for all $T \in \mathcal{T}_h$, the local vector U_T of element-based DOFs can be recovered from (2.109) following element-by-element post-processing:

$$U_T = A_{TT}^{-1}\Big(B_T - A_{T\mathcal{F}_T}U_{\mathcal{F}_T}\Big). \tag{2.110}$$

2.6 Numerical test

In this section we present a comprehensive set of numerical tests to assess the properties of our method. We use different meshes for the numerical tests, which were originally prosed for the FVCA5 benchmark [119].

We based our code on the one developed by Di Pietro [75, 70], where the implementation of local potential reconstruction operator (2.9), L^2-orthogonal projectors π_T^k and π_F^k, are based on the linear algebra facilities (robust Cholesky factorization) provided by the Eigen3 library [112]. The reduced system on the skeleton (2.108) is solved using SuperLU [63] through the PETSc 3.4 interface [14].

For each one of the examples presented here, we consider four families of meshes, which are depicted in Figure 2.1. We also approximate the exact solution considering piecewise polynomials of degree at most k, with $k \in \{0, 1, 2, 3, 4\}$. In addition, we compute the experimental order of convergence (r) as

$$r = \log(e_{\mathcal{T}_1}/e_{\mathcal{T}_2})/\log(h_{\mathcal{T}_1}/h_{\mathcal{T}_2})\,,$$

where $e_{\mathcal{T}_1}$ and $e_{\mathcal{T}_2}$ are the errors associated to the corresponding variable considering two consecutive meshsizes $h_{\mathcal{T}_1}$ and $h_{\mathcal{T}_2}$, respectively.

2.6.1 Example 1: Constant diffusivity

First, we consider a Neumann problem defined in $\Omega := (0,1)^2$, whose data are such that its exact solution is given by the smooth function

$$u(x,y) = \sin(\pi x)\sin(\pi y) - \frac{4}{\pi^2}\,, \tag{2.111}$$

with diffusivity tensor $K := \boldsymbol{I}$. Tables 2.1 and 2.2 show the behavior of potential an flux errors, for each one of the described family of meshes. In all cases, it is noticed the convergence of the method, at the expected optimal rates of convergence: $k+2$ for

the potential, and $k+1$ for the flux, when the solution is approximated by piecewise polynomials of degree at most k. This is in agreement with Theorems 2.4.1 and 2.4.2, and it can also be observed in Figure 2.2. However, for each one of the family of meshes, the errors (for potencial and flux) in the last mesh and $k = 4$ are probably being affected by round-off errors.

2.6.2 Example 2: Polynomial diffusivity

The aim here is to check the robustness of the method, when we solve on the unit square domain $\Omega = (0,1)^2$ the nonhomogeneous Neumann problem with

$$u(x,y) = \sin(\pi x)\sin(\pi y) - \frac{4}{\pi^2}, \tag{2.112}$$

and diffusion tensor (from [137]):

$$K(x,y) = \begin{pmatrix} (y-\bar{y})^2 + \epsilon(x-\bar{x})^2 & -(1-\epsilon)(x-\bar{x})(y-\bar{y}) \\ -(1-\epsilon)(x-\bar{x})(y-\bar{y}) & (x-\bar{x})^2 + \epsilon(y-\bar{y})^2 \end{pmatrix}, \tag{2.113}$$

where $(\bar{x},\bar{y}) = -(0.1,0.1)$. This defines an anisotropic diffusion problem, where the principal axes of the diffusion tensor vary at each point of the domain. For the case $\epsilon = 10^{-1}$, we obtain an anisotropic ratio $\rho = 10$. Figure 2.3 exhibits the well behavior of the L^2-error approximations of the potential (first column) and flux (second column), with respect to the mesh size h, and for each one of the four families of meshes we have considered. Their corresponding histories of convergence are given in Tables 2.3 and 2.4, and they are in agreement with Theorems 2.4.1 and 2.4.2, despite the fact that it is not covered (at all) by the theory since K is not constant (as required for proving Theorem 2.4.2). This gives some numerical evidence that our results could be improved for a general kind of diffusivity tensor, as we pointwise in Remark 2.4.2. As in Example 1, we also observe in this case, for each one of the family of meshes, that the round-off errors are probably affecting the errors (for potencial and flux) in the last hexagonal mesh and $k = 4$.

2.6.3 Example 3: Neumann problem with numerical singularity

Here, we consider the Neumann problem on the unit square domain $\Omega = (0,1)^2$, where its data are such that the exact solution is given by the potential function:

$$u(x,y) = \frac{xy}{(x+0.05)^2 + y^2} - \overline{u}\,, \tag{2.114}$$

with homogeneous (constant) anisotropic diffusion tensor:

$$K(x,y) = \begin{pmatrix} 1.5 & 0.5 \\ 0.5 & 1.5 \end{pmatrix}. \tag{2.115}$$

We remark here that $\overline{u}$ represents the mean value of u in Ω, and notice that u has a singularity at $(-0.05, 0)$, which is close to $\partial\Omega$. The history of errors for potential and flux are shown in Tables 2.5 and 2.6, for $k \in \{0,1,2,3\}$, and for each of the four considered family of meshes. For the first three family of meshes, they exhibit that the HHO method converges with the corresponding optimal rate of convergence $k+2$ and $k+1$ for the potential and flux error, respectively. This is also observed in Figure 2.4. For the latter family of meshes, we observe that the order of convergence behaves as $k+1$ and k, respectively. This phenomena could be explained since the sequence of uniformed hexagonal meshes does not refine enough in the neighborhood of $(-0.05, 0)$, and then it is not capable of capturing the induced numerical singularity. This should be improve by performing certain a posteriori error adaptivity procedure, which would be the subject of future work.

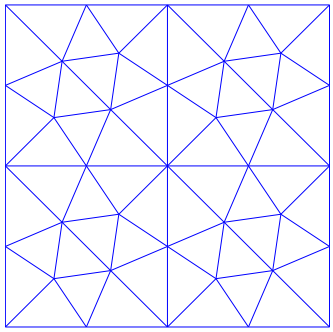

(a) Triangular

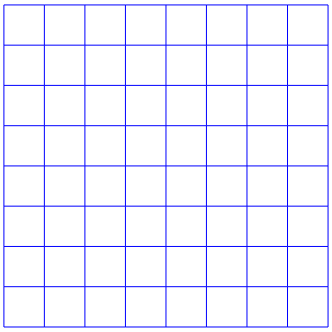

(b) Cartesian

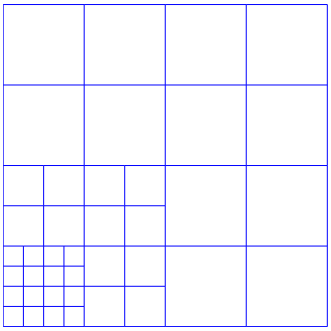

(c) Refined

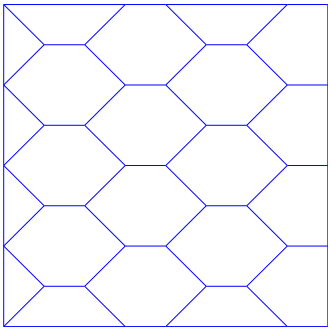

(d) Hexagonal

Figure 2.1: Triangular, Cartesian, Refined and Hexagonal initial meshes that define the family of meshes considered for the numerical examples.

2.6.4 Example 4: Nonregular test

In this section, we will consider the nonregular solution in polar coordinates:

$$u(r,\theta) = r^{2/3}\sin(2\theta/3), \tag{2.116}$$

for the Neumann diffusion problem (2.1), where $u \in H^{1+\frac{2}{3}-s}$ for some $s > 0$ (see [108]), and homogeneous isotropic diffusion tensor K as the identity is considered. This test run over the domain $\Omega = (-1,1)^2/[0,1]\times[-1,0]$, see Figure 2.6.

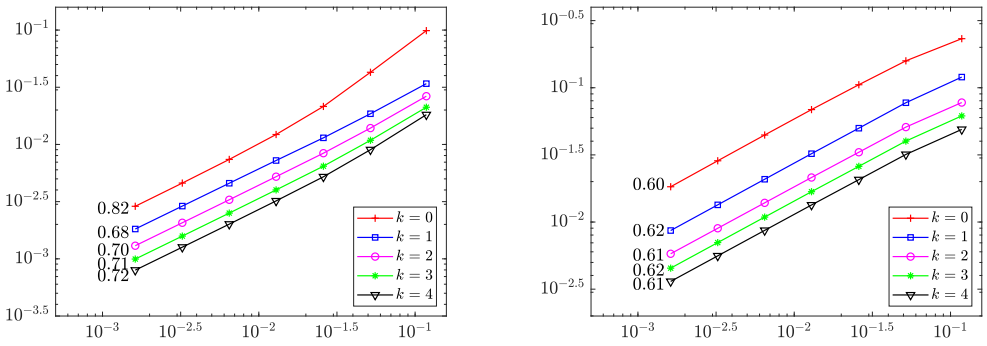

(a) Potential error

(b) Flux error

Figure 2.5: Convergence rates of potential and flux errors.

Table 2.7: History of convergence of potential and flux errors, $k \in \{0, 1, 2, 3, 4\}$.

Potential										
	$k = 0$		$k = 1$		$k = 2$		$k = 3$		$k = 4$	
h	error	rate	error	rate	error	rate	error	rate	error	rate
1.18e-01	9.89e-02		3.40e-02		2.64e-02		2.11e-02		1.82e-02	
5.18e-02	4.28e-02	1.018	1.86e-02	0.736	1.39e-02	0.780	1.09e-02	0.808	9.00e-03	0.856
2.59e-02	2.15e-02	0.992	1.14e-02	0.699	8.39e-03	0.729	6.46e-03	0.752	5.21e-03	0.787
1.29e-02	1.22e-02	0.811	7.24e-03	0.655	5.23e-03	0.679	4.00e-03	0.686	3.21e-03	0.696
6.47e-03	7.40e-03	0.727	4.58e-03	0.663	3.28e-03	0.674	2.51e-03	0.676	2.01e-03	0.678
3.24e-03	4.59e-03	0.688	2.89e-03	0.665	2.07e-03	0.669	1.58e-03	0.670	1.26e-03	0.670
1.62e-03	2.88e-03	0.674	1.82e-03	0.666	1.30e-03	0.667	9.95e-04	0.667	7.96e-04	0.667
Flux										
	$k = 0$		$k = 1$		$k = 2$		$k = 3$		$k = 4$	
h	error	rate	error	rate	error	rate	error	rate	error	rate
1.18e-01	2.32e-01		1.20e-01		7.76e-02		6.17e-02		4.90e-02	
5.18e-02	1.59e-01	0.461	7.73e-02	0.534	5.09e-02	0.511	4.01e-02	0.525	3.19e-02	0.522
2.59e-02	1.05e-01	0.591	5.00e-02	0.630	3.31e-02	0.622	2.60e-02	0.625	2.07e-02	0.624
1.29e-02	6.88e-02	0.612	3.23e-02	0.627	2.15e-02	0.621	1.68e-02	0.623	1.34e-02	0.623
6.47e-03	4.45e-02	0.632	2.08e-02	0.635	1.39e-02	0.630	1.09e-02	0.632	8.66e-03	0.631
3.24e-03	2.86e-02	0.639	1.34e-02	0.635	8.99e-03	0.630	7.03e-03	0.632	5.60e-03	0.632
1.62e-03	1.83e-02	0.642	8.64e-03	0.635	5.80e-03	0.631	4.53e-03	0.632	3.61e-03	0.632

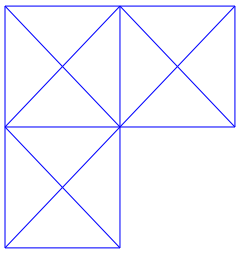

Figure 2.6: L-shaped domain.

From Figure 2.5 and Table 2.7, we observe that the order of convergence of the potential and flux is less than or equal that 2/3. It does not surprise us because the function is not regular, this does not contradict the Theorems 2.4.1 and 2.4.2. These results are similar to those found in the Figure 1.9 and Table 1.5 in Section 1.4.2.

Conclusions

In this work we have developed an a priori error analysis (valid for any dimension $d \in \{2, 3\}$) for a pure Neumann problem, when applying HHO method. We have proved the convergence of the method, with the optimal rates of convergence when the exact solution is smooth enough: order k + 1 for the flux error, and k + 2 for potential error, when piecewise polynomial of degree at most k are considered for the corresponding approximations. This technique can deal with hanging nodes, as in the Refined mesh (Figure 1c), and also with triangular, quadrilateral an hexagonal meshes (Figures 1a, 1b and 1d, respectively). There are several computational libraries that can be used for HHO methods. For example, DiSk++ (Discontinuous Skeletal C++, `https://github.com/datafl4sh/diskpp`) which has four levels of abstraction that allow us to work indirectly over general polytopal meshes in 1D, 2D, and 3D, and with different mesh input formats, such as: FVCA5, NETGEN, GMESH. The mesh structure of DiSk++ allows us to use Discontinuous Skeletal methods such as DG, HDG, as well as standard FEM. This library has been used to solve many problems as those described in [50], [53], [42], [1], [2], [44], [45], [31] and [51]. On the other hand, HArDCore (Hybrid Arbitrary Degree::Core, `https://github.com/jdroniou/HArDCore`) is a C++ code focused on HHO (Hybrid High Order) methods, but it

can be useful for a wide range of hybrid methods. It is implemented in two parts, one for 2D and another for 3D, on general polytopal meshes. It supports the FVCA5 format [119], and their implementation principles are described in Appendix B in [66]. HArDCore allows us to work on Diffusion problems with Dirichlet or Neumann boundary conditions, with diffusion tensors that can be piecewise constant or variable on each cell. We also mention the source codes POLYPHO (`http://www.comphys.com`), written in Fortran by Specogna and Di Pietro, and SpaFEDTe (`https://github.com/SpaFEDTe/spafedte.github.com`), written in C++, and developed for Discontinuous Finite Element Spaces by L. Botti.

Numerical results presented here, are in agreement with our theoretical results, even in a case not covered by the current analysis (cf. Example 2). We refer to Remark 2.4.2 for the tools/ideas we required to extend the validity of Theorem 2.4.2 for locally variable tensor K. On the other hand, we notice that in Example 3, the numerical results obtained for hexagonal meshes are not the optimal ones. This is probably due to the presence of a numerical singularity of the exact solution in a neighborhood of $(0, 0)$ that affects the accuracy of the method. Then, it would be better to deduce an a posteriori error estimator for problems having singularities, inner or boundary layers. Thus, we can perform an adaptive refinement, with the purpose of recognizing the region of the domain where the singularities/layers are, improving the quality of approximation in the process. These are the subject of ongoing work.

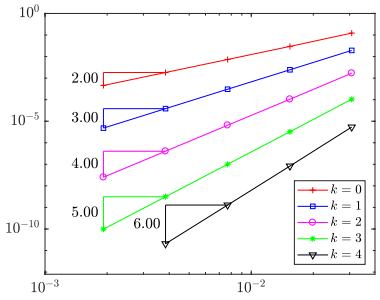

(a) Potential error, Triangular meshes

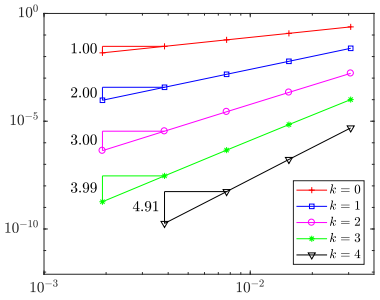

(b) Flux error, Triangular meshes

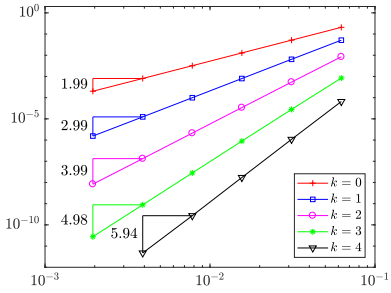

(c) Potential error, Cartesian meshes

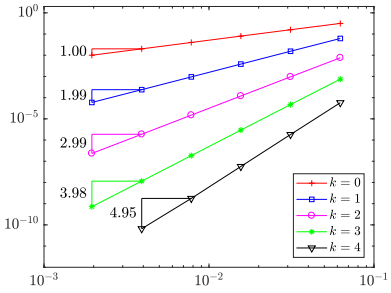

(d) Flux error, Cartesian meshes

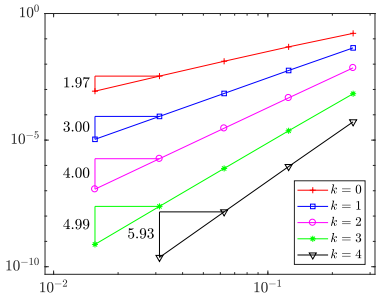

(e) Potential error, Refined meshes

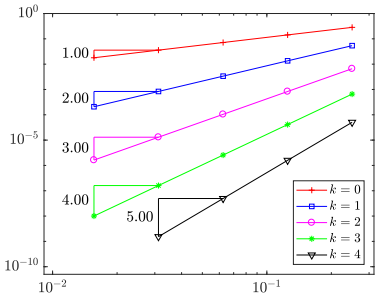

(f) Flux error, Refined meshes

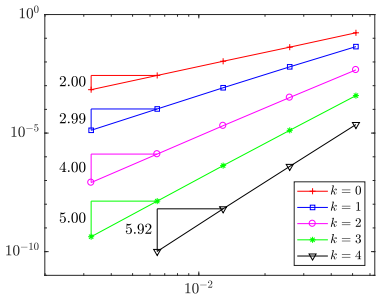

(g) Potential error, Hexagonal meshes

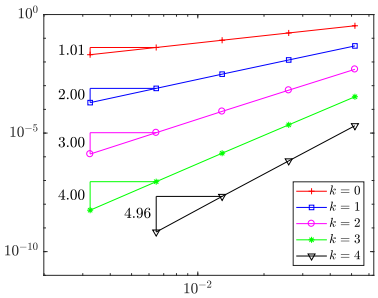

(h) Flux error, Hexagonal meshes

Figure 2.2: Rates of convergence of Potential and Flux errors, considering each one of the family of meshes (Example 1).

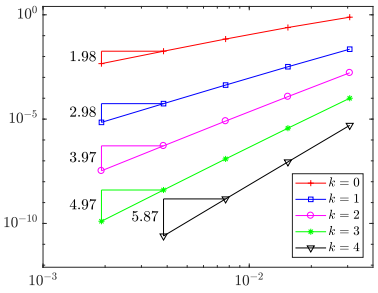

(a) Potential error, Triangular meshes

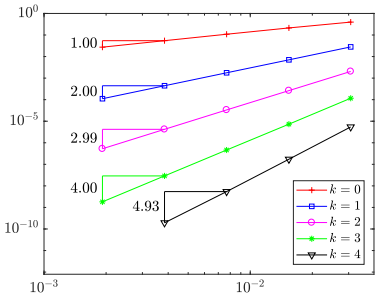

(b) Flux error, Triangular meshes

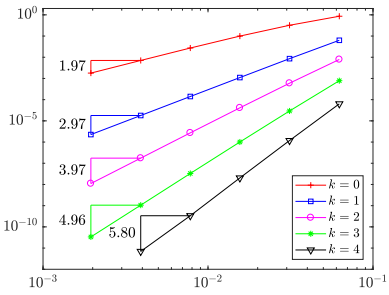

(c) Potential error, Cartesian meshes

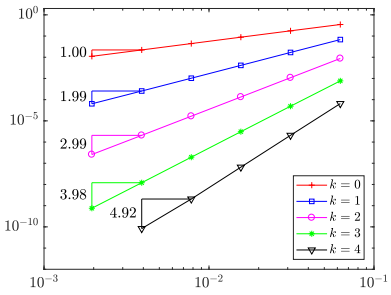

(d) Flux error, Cartesian meshes

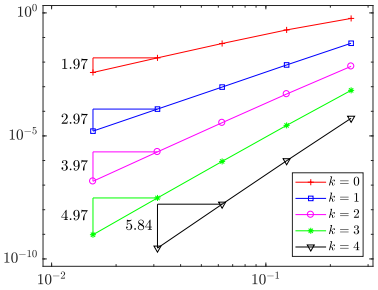

(e) Potential error, Refined meshes

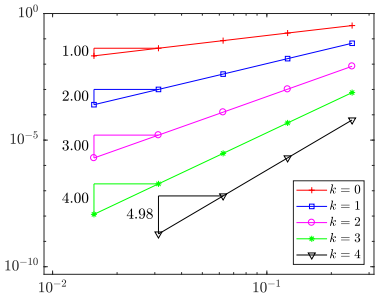

(f) Flux error, Refined meshes

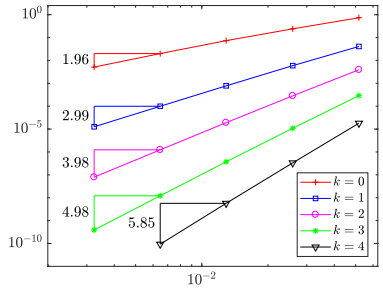

(g) Potential error, Hexagonal meshes

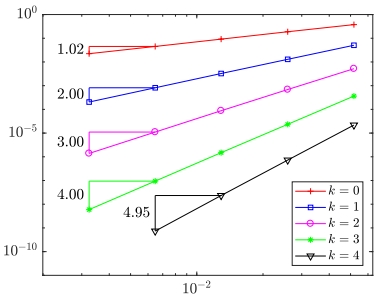

(h) Flux error, Hexagonal meshes

Figure 2.3: Rates of convergence of potential and flux errors, considering each one of the family of meshes (Example 2).

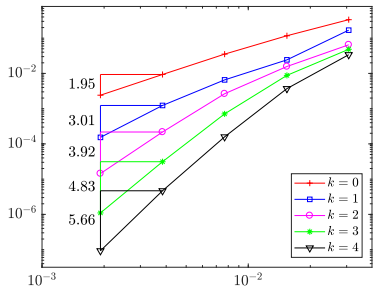

(a) Potential error, Triangular meshes

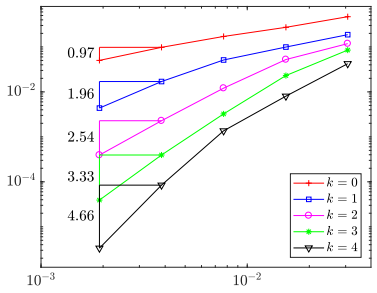

(b) Flux error, Triangular meshes

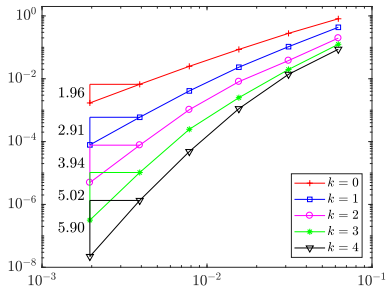

(c) Potential error, Cartesian meshes

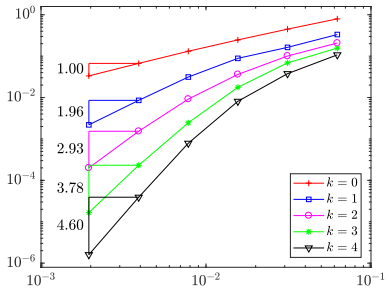

(d) Flux error, Cartesian meshes

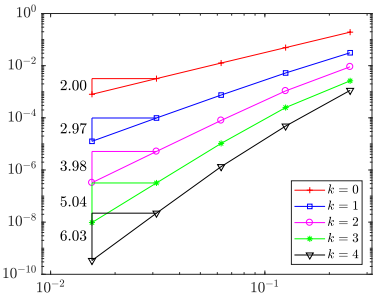

(e) Potential error, Refined meshes

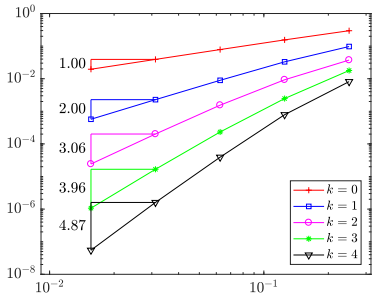

(f) Flux error, Refined meshes

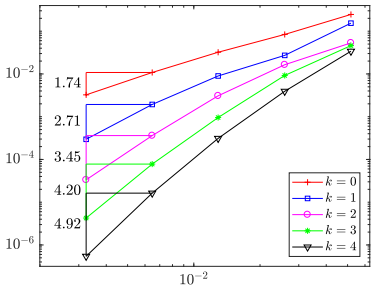

(g) Potential error, Hexagonal meshes

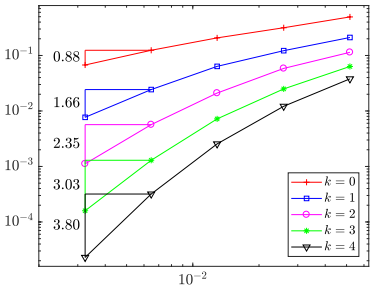

(h) Flux error, Hexagonal meshes

Figure 2.4: Rates of convergence of potential and flux errors, considering each one of the family of meshes (Example 3).

Table 2.1: History of convergence of L^2-norm of the Potential error, for each one of the family of meshes and $k \in \{0, 1, 2, 3, 4\}$ (Example 1).

Triangles										
	$k=0$		$k=1$		$k=2$		$k=3$		$k=4$	
h	error	rate	error	rate	error	rate	error	rate	error	rate
3.07e-02	1.23e-01		1.93e-02		1.69e-03		1.05e-04		5.36e-06	
1.54e-02	2.95e-02	2.065	2.43e-03	2.999	1.05e-04	4.034	3.24e-06	5.036	8.30e-08	6.041
7.68e-03	7.32e-03	2.005	3.06e-04	2.982	6.49e-06	3.995	1.01e-07	4.991	1.29e-09	5.986
3.84e-03	1.82e-03	2.004	3.83e-05	2.997	4.04e-07	4.005	3.13e-09	5.006	2.05e-11	5.974
1.92e-03	4.56e-04	2.001	4.79e-06	2.999	2.52e-08	4.003	9.77e-11	5.003	7.42e-12	1.468
Cartesian										
	$k=0$		$k=1$		$k=2$		$k=3$		$k=4$	
h	error	rate	error	rate	error	rate	error	rate	error	rate
6.25e-02	2.07e-01		5.13e-02		8.47e-03		8.41e-04		6.57e-05	
3.12e-02	5.15e-02	2.004	6.44e-03	2.987	5.41e-04	3.959	2.79e-05	4.903	1.08e-06	5.912
1.56e-02	1.29e-02	2.002	7.97e-04	3.015	3.40e-05	3.992	8.91e-07	4.969	1.72e-08	5.973
7.81e-03	3.21e-03	2.004	9.92e-05	3.013	2.13e-06	4.005	2.81e-08	4.996	2.71e-10	6.000
3.91e-03	8.03e-04	2.004	1.24e-05	3.008	1.33e-07	4.007	8.82e-10	5.003	4.73e-12	5.851
1.95e-03	2.01e-04	1.993	1.55e-06	2.990	8.32e-09	3.985	2.77e-11	4.975	8.77e-12	-0.889
Refined										
	$k=0$		$k=1$		$k=2$		$k=3$		$k=4$	
h	error	rate	error	rate	error	rate	error	rate	error	rate
2.50e-01	1.65e-01		4.39e-02		7.15e-03		6.79e-04		5.28e-05	
1.25e-01	4.82e-02	1.773	5.62e-03	2.964	4.66e-04	3.940	2.34e-05	4.861	9.03e-07	5.868
6.25e-02	1.30e-02	1.890	6.96e-04	3.014	2.94e-05	3.986	7.59e-07	4.944	1.46e-08	5.947
3.12e-02	3.37e-03	1.943	8.63e-05	3.004	1.84e-06	3.987	2.41e-08	4.963	2.33e-10	5.963
1.56e-02	8.57e-04	1.975	1.08e-05	3.005	1.15e-07	3.999	7.60e-10	4.988	5.72e-12	5.346
Hexagonal										
	$k=0$		$k=1$		$k=2$		$k=3$		$k=4$	
h	error	rate	error	rate	error	rate	error	rate	error	rate
5.18e-02	1.70e-01		4.43e-02		4.63e-03		3.81e-04		2.29e-05	
2.59e-02	4.21e-02	2.013	6.22e-03	2.832	3.17e-04	3.872	1.31e-05	4.866	3.93e-07	5.867
1.29e-02	1.07e-02	1.965	8.16e-04	2.915	2.05e-05	3.927	4.24e-07	4.917	6.39e-09	5.909
6.47e-03	2.70e-03	1.996	1.04e-04	2.984	1.30e-06	3.995	1.35e-08	4.997	1.02e-10	6.000
3.24e-03	6.77e-04	1.999	1.31e-05	2.993	8.20e-08	3.998	4.25e-10	4.999	1.74e-12	5.878

Table 2.2: History of convergence of L^2-norm of the Flux error, for each one of the family of meshes, and $k \in \{0, 1, 2, 3, 4\}$ (Example 1).

Triangles										
	$k=0$		$k=1$		$k=2$		$k=3$		$k=4$	
h	error	rate	error	rate	error	rate	error	rate	error	rate
3.07e-02	2.38e-01		2.42e-02		1.67e-03		1.01e-04		4.89e-06	
1.54e-02	1.19e-01	1.003	6.02e-03	2.013	2.18e-04	2.954	6.98e-06	3.874	1.68e-07	4.883
7.68e-03	5.96e-02	0.998	1.50e-03	1.995	2.75e-05	2.973	4.56e-07	3.921	5.43e-09	4.935
3.84e-03	2.98e-02	1.001	3.76e-04	2.001	3.45e-06	2.995	2.91e-08	3.970	1.81e-10	4.908
1.92e-03	1.49e-02	1.001	9.39e-05	2.000	4.31e-07	2.998	1.84e-09	3.986	1.70e-10	0.085
Cartesian										
	$k=0$		$k=1$		$k=2$		$k=3$		$k=4$	
h	error	rate	error	rate	error	rate	error	rate	error	rate
6.25e-02	3.17e-01		6.18e-02		7.60e-03		7.44e-04		5.77e-05	
3.12e-02	1.60e-01	0.986	1.54e-02	1.996	9.58e-04	2.980	4.71e-05	3.972	1.82e-06	4.972
1.56e-02	8.01e-02	0.997	3.83e-03	2.013	1.20e-04	2.998	2.95e-06	3.996	5.68e-08	5.005
7.81e-03	4.01e-02	1.001	9.52e-04	2.010	1.50e-05	3.005	1.85e-07	4.006	1.77e-09	5.014
3.91e-03	2.00e-02	1.002	2.38e-04	2.006	1.88e-06	3.005	1.16e-08	4.007	6.57e-11	4.760
1.95e-03	1.00e-02	0.996	5.94e-05	1.993	2.34e-07	2.989	7.22e-10	3.985	9.24e-11	-0.492
Refined										
	$k=0$		$k=1$		$k=2$		$k=3$		$k=4$	
h	error	rate	error	rate	error	rate	error	rate	error	rate
2.50e-01	2.84e-01		5.37e-02		6.61e-03		6.57e-04		5.05e-05	
1.25e-01	1.43e-01	0.990	1.35e-02	1.991	8.32e-04	2.990	4.11e-05	3.998	1.59e-06	4.989
6.25e-02	7.15e-02	0.999	3.36e-03	2.009	1.04e-04	2.999	2.57e-06	4.002	4.94e-08	5.009
3.12e-02	3.58e-02	0.997	8.34e-04	2.004	1.30e-05	2.993	1.60e-07	3.992	1.53e-09	4.996
1.56e-02	1.79e-02	1.000	2.08e-04	2.004	1.63e-06	3.000	1.00e-08	4.001	1.51e-10	3.342
Hexagonal										
	$k=0$		$k=1$		$k=2$		$k=3$		$k=4$	
h	error	rate	error	rate	error	rate	error	rate	error	rate
5.18e-02	3.36e-01		4.75e-02		4.90e-03		3.41e-04		2.04e-05	
2.59e-02	1.67e-01	1.007	1.21e-02	1.967	6.45e-04	2.926	2.22e-05	3.937	6.72e-07	4.927
1.29e-02	8.24e-02	1.014	3.06e-03	1.977	8.23e-05	2.954	1.41e-06	3.953	2.13e-08	4.950
6.47e-03	4.08e-02	1.021	7.68e-04	2.003	1.04e-05	3.000	8.91e-08	4.006	6.70e-10	5.014
3.24e-03	2.02e-02	1.013	1.92e-04	2.002	1.30e-06	3.001	5.59e-09	4.003	2.38e-11	4.827

Table 2.3: History of convergence of L^2-norm of the potential error, for each one of the family of meshes, and $k \in \{0, 1, 2, 3, 4\}$ (Example 2).

Triangles										
	$k=0$		$k=1$		$k=2$		$k=3$		$k=4$	
h	error	rate	error	rate	error	rate	error	rate	error	rate
3.07e-02	7.69e-01		2.25e-02		1.66e-03		1.00e-04		5.02e-06	
1.54e-02	2.46e-01	1.652	3.24e-03	2.809	1.20e-04	3.812	3.67e-06	4.790	8.89e-08	5.847
7.68e-03	6.89e-02	1.829	4.29e-04	2.905	8.06e-06	3.877	1.23e-07	4.877	1.50e-09	5.870
3.84e-03	1.80e-02	1.938	5.51e-05	2.959	5.23e-07	3.946	4.00e-09	4.948	2.50e-11	5.904
1.92e-03	4.57e-03	1.977	6.99e-06	2.980	3.33e-08	3.973	1.27e-10	4.974	6.91e-12	1.854
Cartesian										
	$k=0$		$k=1$		$k=2$		$k=3$		$k=4$	
h	error	rate	error	rate	error	rate	error	rate	error	rate
6.25e-02	8.59e-01		6.31e-02		7.87e-03		7.84e-04		6.35e-05	
3.12e-02	3.22e-01	1.412	8.58e-03	2.873	5.97e-04	3.711	2.92e-05	4.733	1.18e-06	5.737
1.56e-02	9.95e-02	1.696	1.10e-03	2.960	4.12e-05	3.857	1.01e-06	4.862	2.04e-08	5.857
7.81e-03	2.72e-02	1.872	1.41e-04	2.974	2.72e-06	3.930	3.30e-08	4.939	3.35e-10	5.935
3.91e-03	7.06e-03	1.952	1.79e-05	2.982	1.74e-07	3.969	1.06e-09	4.974	6.97e-12	5.598
1.95e-03	1.79e-03	1.972	2.26e-06	2.975	1.10e-08	3.966	3.36e-11	4.958	4.74e-12	0.555
Refined										
	$k=0$		$k=1$		$k=2$		$k=3$		$k=4$	
h	error	rate	error	rate	error	rate	error	rate	error	rate
2.50e-01	5.96e-01		5.84e-02		6.74e-03		7.11e-04		5.22e-05	
1.25e-01	2.03e-01	1.552	7.66e-03	2.930	5.04e-04	3.740	2.68e-05	4.732	9.78e-07	5.737
6.25e-02	5.70e-02	1.836	9.65e-04	2.988	3.44e-05	3.873	9.18e-07	4.864	1.68e-08	5.865
3.12e-02	1.49e-02	1.934	1.23e-04	2.964	2.24e-06	3.930	3.01e-08	4.921	2.75e-10	5.919
1.56e-02	3.78e-03	1.974	1.57e-05	2.975	1.43e-07	3.971	9.62e-10	4.966	6.02e-12	5.512
Hexagonal										
	$k=0$		$k=1$		$k=2$		$k=3$		$k=4$	
h	error	rate	error	rate	error	rate	error	rate	error	rate
5.18e-02	7.34e-01		4.08e-02		3.92e-03		2.90e-04		1.80e-05	
2.59e-02	2.41e-01	1.610	5.91e-03	2.790	2.83e-04	3.791	1.08e-05	4.743	3.33e-07	5.756
1.29e-02	7.33e-02	1.704	7.75e-04	2.914	1.91e-05	3.873	3.71e-07	4.842	5.68e-09	5.841
6.47e-03	1.99e-02	1.887	9.93e-05	2.978	1.24e-06	3.961	1.21e-08	4.956	9.28e-11	5.962
3.24e-03	5.13e-03	1.963	1.26e-05	2.989	7.90e-08	3.979	3.88e-10	4.978	1.93e-12	5.597

Table 2.4: History of convergence of L^2-norm of the flux error, for each one of the family of meshes, and $k \in \{0, 1, 2, 3, 4\}$ (Example 2).

Triangles										
	$k=0$		$k=1$		$k=2$		$k=3$		$k=4$	
h	error	rate	error	rate	error	rate	error	rate	error	rate
3.07e-02	3.97e-01		2.80e-02		2.04e-03		1.16e-04		5.43e-06	
1.54e-02	2.13e-01	0.902	7.05e-03	2.002	2.63e-04	2.970	7.30e-06	4.013	1.73e-07	5.000
7.68e-03	1.09e-01	0.968	1.77e-03	1.989	3.34e-05	2.966	4.61e-07	3.970	5.43e-09	4.971
3.84e-03	5.46e-02	0.993	4.42e-04	1.997	4.21e-06	2.989	2.90e-08	3.992	1.93e-10	4.813
1.92e-03	2.73e-02	0.999	1.11e-04	1.998	5.28e-07	2.995	1.82e-09	3.995	1.97e-10	-0.024
Cartesian										
	$k=0$		$k=1$		$k=2$		$k=3$		$k=4$	
h	error	rate	error	rate	error	rate	error	rate	error	rate
6.25e-02	3.50e-01		6.81e-02		8.77e-03		7.69e-04		6.53e-05	
3.12e-02	1.76e-01	0.987	1.68e-02	2.011	1.08e-03	3.008	4.91e-05	3.960	2.08e-06	4.960
1.56e-02	8.84e-02	0.996	4.14e-03	2.025	1.34e-04	3.022	3.09e-06	3.991	6.55e-08	4.989
7.81e-03	4.42e-02	1.001	1.03e-03	2.016	1.66e-05	3.014	1.93e-07	4.005	2.06e-09	5.003
3.91e-03	2.21e-02	1.002	2.56e-04	2.008	2.07e-06	3.008	1.21e-08	4.006	8.31e-11	4.638
1.95e-03	1.11e-02	0.996	6.39e-05	1.994	2.59e-07	2.990	7.56e-10	3.984	1.37e-10	-0.718
Refined										
	$k=0$		$k=1$		$k=2$		$k=3$		$k=4$	
h	error	rate	error	rate	error	rate	error	rate	error	rate
2.50e-01	3.34e-01		6.69e-02		8.25e-03		7.53e-04		6.24e-05	
1.25e-01	1.69e-01	0.982	1.65e-02	2.019	1.03e-03	3.009	4.77e-05	3.982	1.98e-06	4.976
6.25e-02	8.50e-02	0.995	4.05e-03	2.026	1.27e-04	3.017	2.99e-06	3.996	6.25e-08	4.989
3.12e-02	4.25e-02	0.997	1.00e-03	2.008	1.58e-05	3.000	1.87e-07	3.990	1.96e-09	4.982
1.56e-02	2.12e-02	1.000	2.50e-04	2.004	1.97e-06	3.002	1.17e-08	3.999	8.28e-11	4.565
Hexagonal										
	$k=0$		$k=1$		$k=2$		$k=3$		$k=4$	
h	error	rate	error	rate	error	rate	error	rate	error	rate
5.18e-02	3.76e-01		5.06e-02		5.20e-03		3.63e-04		2.18e-05	
2.59e-02	1.88e-01	0.999	1.29e-02	1.970	6.88e-04	2.919	2.34e-05	3.953	7.26e-07	4.907
1.29e-02	9.18e-02	1.030	3.25e-03	1.978	8.76e-05	2.956	1.49e-06	3.951	2.32e-08	4.937
6.47e-03	4.51e-02	1.030	8.15e-04	2.006	1.10e-05	3.001	9.42e-08	4.004	7.35e-10	5.006
3.24e-03	2.23e-02	1.016	2.04e-04	2.003	1.39e-06	3.001	5.92e-09	4.002	2.60e-11	4.834

Table 2.5: History of convergence of L^2-norm of the potential error, for each one of the family of meshes, and $k \in \{0, 1, 2, 3, 4\}$ (Example 3).

Triangles										
	$k=0$		$k=1$		$k=2$		$k=3$		$k=4$	
h	error	rate	error	rate	error	rate	error	rate	error	rate
3.07e-02	3.35e-01		1.69e-01		6.49e-02		4.83e-02		3.39e-02	
1.54e-02	1.17e-01	1.522	2.42e-02	2.813	1.57e-02	2.056	8.80e-03	2.468	3.70e-03	3.211
7.68e-03	3.52e-02	1.727	6.55e-03	1.881	2.65e-03	2.558	7.10e-04	3.617	1.58e-04	4.530
3.84e-03	9.32e-03	1.918	1.23e-03	2.411	2.17e-04	3.607	3.12e-05	4.508	4.68e-06	5.082
1.92e-03	2.41e-03	1.953	1.53e-04	3.007	1.44e-05	3.915	1.10e-06	4.828	9.27e-08	5.657
Cartesian										
	$k=0$		$k=1$		$k=2$		$k=3$		$k=4$	
h	error	rate	error	rate	error	rate	error	rate	error	rate
6.25e-02	8.11e-01		4.34e-01		1.97e-01		1.25e-01		8.68e-02	
3.12e-02	2.79e-01	1.538	1.05e-01	2.043	3.79e-02	2.369	1.97e-02	2.655	1.38e-02	2.642
1.56e-02	8.57e-02	1.699	2.33e-02	2.173	8.09e-03	2.229	2.50e-03	2.982	1.11e-03	3.636
7.81e-03	2.49e-02	1.790	4.10e-03	2.509	1.04e-03	2.971	2.46e-04	3.350	4.81e-05	4.542
3.91e-03	6.65e-03	1.906	5.94e-04	2.792	7.70e-05	3.756	1.04e-05	4.574	1.34e-06	5.175
1.95e-03	1.70e-03	1.962	7.85e-05	2.910	4.96e-06	3.941	3.17e-07	5.018	2.21e-08	5.903
Refined										
	$k=0$		$k=1$		$k=2$		$k=3$		$k=4$	
h	error	rate	error	rate	error	rate	error	rate	error	rate
2.50e-01	1.93e-01		3.13e-02		9.06e-03		2.62e-03		1.13e-03	
1.25e-01	4.93e-02	1.969	5.25e-03	2.575	1.08e-03	3.074	2.48e-04	3.404	4.82e-05	4.547
6.25e-02	1.26e-02	1.964	7.46e-04	2.813	7.95e-05	3.758	1.04e-05	4.569	1.34e-06	5.168
3.12e-02	3.19e-03	1.983	9.85e-05	2.914	5.13e-06	3.945	3.18e-07	5.024	2.21e-08	5.911
1.56e-02	7.99e-04	1.996	1.26e-05	2.969	3.25e-07	3.981	9.65e-09	5.042	3.39e-10	6.027
Hexagonal										
	$k=0$		$k=1$		$k=2$		$k=3$		$k=4$	
h	error	rate	error	rate	error	rate	error	rate	error	rate
5.18e-02	2.46e-01		1.54e-01		5.33e-02		4.60e-02		3.40e-02	
2.59e-02	8.40e-02	1.553	2.72e-02	2.503	1.64e-02	1.697	9.21e-03	2.321	3.93e-03	3.113
1.29e-02	3.22e-02	1.376	8.97e-03	1.592	3.08e-03	2.402	9.56e-04	3.251	3.11e-04	3.639
6.47e-03	1.08e-02	1.580	1.93e-03	2.224	3.62e-04	3.104	7.79e-05	3.633	1.63e-05	4.273
3.24e-03	3.24e-03	1.742	2.96e-04	2.712	3.33e-05	3.447	4.26e-06	4.203	5.43e-07	4.917

Table 2.6: History of convergence of L^2-norm of the flux error, for each one of the family of meshes, and $k \in \{0, 1, 2, 3, 4\}$ (Example 3).

Triangles										
	$k=0$		$k=1$		$k=2$		$k=3$		$k=4$	
h	error	rate	error	rate	error	rate	error	rate	error	rate
3.07e-02	4.70e-01		1.87e-01		1.18e-01		8.50e-02		4.24e-02	
1.54e-02	2.73e-01	0.788	9.94e-02	0.918	5.24e-02	1.181	2.31e-02	1.889	8.04e-03	2.410
7.68e-03	1.71e-01	0.672	5.12e-02	0.952	1.21e-02	2.107	3.24e-03	2.823	1.36e-03	2.553
3.84e-03	9.79e-02	0.804	1.70e-02	1.592	2.28e-03	2.407	3.95e-04	3.036	8.44e-05	4.011
1.92e-03	5.02e-02	0.965	4.36e-03	1.961	3.93e-04	2.537	3.92e-05	3.331	3.35e-06	4.655
Cartesian										
	$k=0$		$k=1$		$k=2$		$k=3$		$k=4$	
h	error	rate	error	rate	error	rate	error	rate	error	rate
6.25e-02	7.96e-01		3.33e-01		2.08e-01		1.56e-01		1.08e-01	
3.12e-02	4.49e-01	0.823	1.63e-01	1.029	1.01e-01	1.040	6.89e-02	1.181	3.77e-02	1.508
1.56e-02	2.47e-01	0.864	8.85e-02	0.881	3.62e-02	1.479	1.77e-02	1.961	8.12e-03	2.217
7.81e-03	1.31e-01	0.911	3.13e-02	1.502	9.19e-03	1.981	2.46e-03	2.854	7.87e-04	3.373
3.91e-03	6.68e-02	0.977	8.56e-03	1.874	1.53e-03	2.587	2.32e-04	3.413	3.91e-05	4.338
1.95e-03	3.34e-02	0.997	2.19e-03	1.959	2.00e-04	2.928	1.66e-05	3.784	1.60e-06	4.595
Refined										
	$k=0$		$k=1$		$k=2$		$k=3$		$k=4$	
h	error	rate	error	rate	error	rate	error	rate	error	rate
2.50e-01	2.97e-01		9.71e-02		3.73e-02		1.78e-02		8.14e-03	
1.25e-01	1.55e-01	0.936	3.30e-02	1.559	9.28e-03	2.007	2.46e-03	2.857	7.87e-04	3.370
6.25e-02	7.83e-02	0.986	8.93e-03	1.884	1.54e-03	2.588	2.32e-04	3.408	3.91e-05	4.330
3.12e-02	3.91e-02	1.000	2.28e-03	1.967	2.01e-04	2.933	1.67e-05	3.790	1.60e-06	4.602
1.56e-02	1.95e-02	1.003	5.71e-04	1.996	2.42e-05	3.056	1.07e-06	3.963	5.49e-08	4.866
Hexagonal										
	$k=0$		$k=1$		$k=2$		$k=3$		$k=4$	
h	error	rate	error	rate	error	rate	error	rate	error	rate
5.18e-02	4.95e-01		2.11e-01		1.14e-01		6.34e-02		3.79e-02	
2.59e-02	3.16e-01	0.647	1.22e-01	0.790	5.85e-02	0.964	2.50e-02	1.344	1.21e-02	1.643
1.29e-02	2.07e-01	0.604	6.36e-02	0.934	2.10e-02	1.468	7.20e-03	1.785	2.55e-03	2.240
6.47e-03	1.24e-01	0.745	2.43e-02	1.395	5.67e-03	1.899	1.29e-03	2.488	3.18e-04	3.015
3.24e-03	6.74e-02	0.883	7.69e-03	1.664	1.12e-03	2.351	1.59e-04	3.029	2.30e-05	3.802

Chapter 3

An HHO formulation for a class of nonlinear elliptic problems

In this chapter, we analyse a nonlinear elliptic problem in a bounded domain, applying the already known hybrid high-order (HHO) method. Our analysis follows known approaches to deal with diffusion linear problems, and take into account a nonlinear HHO work in elasticity (which considers a particular nonlinear coefficient). This approach allows us to obtain high-order approximation of unknowns, by assembling a nonconforming discrete space based on degrees of freedom over the interior volume of each element and on the faces of its boundary, through L^2-projections. The principal feature is the use of a gradient reconstruction operator, whose codomain in the current context, is bigger than the considered in the linear case. On the other hand, the stabilization term is the same as for the linear case. In addition, the construction does not depend on the spatial dimension, and it offers the possibility to use general meshes with polytopal cells and nonmatching interfaces. The discrete unknowns are chosen such that they are supported over each element and its boundary. It is important to emphasize that the cell-based unknowns can be eliminated locally by a Schur complement technique (also known as static condensation). This allows us to obtain a more compact system, reducing significantly its size, which is solved by Newton's method. We establish the well-posedness of the nonlinear discrete scheme, the stability of the method, and confirm that it is optimally convergent in the energy norm and in the L^2-norm,

for the potential and its gradient, for smooth enough solutions. In addition, we also establish the convergence of the L^2-projection of the potential error and the super convergence of the reconstructive potential error, under the same additional regularity assumption of the exact solution. The latter results, up to the author's knowledge, have not been proved before. Several numerical experiments confirm our theoretical results. We point out that this approach can be also applied/extended to deal with other boundary conditions (such as nonhomogeneous Dirichlet, mixed or pure Neumann).

3.1 Introduction

The numerical resolution of nonlinear elliptic partial differential equations (PDEs) is nowadays of great interest in the engineering practice. These arise in many areas, including differential geometry (the Monge-Ampère equation) [93], mass transportation (the Monge-Kantorovich problem) [5, 139], dynamic programming (Bellman's equation), fluid dynamics (the geostrophic equations) [129], phase change problems governed by Stefan's model [95], the modelling of phenomena such as: glacier motion [106], incompressible turbulent flows in porous media [78], and airfoil design [105]. We consider a class of nonlinear elliptic problems arising in heat conduction and fluid mechanics, that reads as: *Find u such that*

$$-\mathrm{div}(\mathbf{a}(\cdot, \nabla u)) = f \quad \text{in } \Omega, \tag{3.1a}$$

$$u = 0 \quad \text{on } \partial\Omega, \tag{3.1b}$$

where $\Omega \subset \mathbb{R}^d$, $d \in \{2, 3\}$, is a polytopal bounded connected domain, with Lipschitz boundary $\partial\Omega$, $\mathbf{a} : \Omega \times \mathbb{R}^d \to \mathbb{R}^d$ is a nonlinear function, and f represents the source term. The design of convergent numerical schemes for the solution of such equations, is thus an important and very active research topic. In this work, we focus in particular, in the well-known HHO method, under certain hypothesis on nonlinear function $\mathbf{a}$ that will be described in the Section 3.2. The homogeneous Dirichlet boundary condition (3.1b) is considered only for the sake of simplicity. We can modify appropriately the mathematical analysis, to deal with more general

boundary conditions such as mixed boundary conditions, nonhomogeneous Dirichlet boundary condition, and also Neumann boundary condition.

This approach has several advantageous features, initially described in [75, 70]: (i) it is independent of the spatial dimension; (ii) it supports arbitrary polynomial orders $k \geq 0$ on fairly general meshes including, e.g., polyhedral elements and nonmatching interfaces; (iii) it is devised from local reconstruction operators and a linear local stabilization term; (iv) it is efficiently parallelable (the local stencil only connects a mesh element with its faces); (v) it has moderate computational costs, thanks to the possibility of locally eliminating, by static condensation, the volumetric unknowns for linearized versions of the problem (encountered, e.g., when solving the corresponding system of nonlinear algebraic equations by the Newton method or Kačanov's one).

It is important to point out that a kind of nonlinear elasticity problem, under weak hypotheses, has been analysed with HHO approach in [27]. For a more general context, we refer to [64, 65], where the authors analyse the p-Laplacian problem in Banach spaces, with a stabilization term depending also of the nonlinearity. In the case of $p = 2$, we obtain the linear diffusion problem described in [73], but with a slightly different definition for the reconstruction operator. The case of p-Laplacian and Leray–Lions equations with pure Neumann boundary conditions is analyse in [66, Chapter 7]. Albeit, in [64, 27] we can find part of the HHO analysis for (3.1), in this paper we propose another mathematical analysis (taking into account that we are dealing only with the case $p = 2$). Moreover, we are able to deduce an a priori error estimate for L^2-error of reconstructive potential, which, up to author's knowledgement, has not been established yet.

Conforming finite element methods on standard meshes have been considered in [99, 104], in the context of elasticity for mixed formulation, while in [17], the authors deal with the p-laplacian applying a continuous piecewise linear finite element approximation. Discontinuous Galerkin (DG) methods on standard meshes

have been considered in [135], while in [33], the authors apply local discontinuous Galerkin (LDG) method for the same class of nonlinear elliptic problem we study. Polytopal meshes have been considered in DG methods in [24], and also with in Virtual Element (VE) method [23], based on a low-order approximation of the displacement field.

The lowest-order version of the HHO method ($k = 0$), can be linked with Hybrid Finite Volume (HFV) methods in [75], when face unknowns are not eliminated by interpolation. Also, HHO approach is related to Hybrid Mixed Mimetic (HMM) methods in [67]. Here, HMM methods can be seen as the unified formulation for the Hybrid Finite Volume (HFV, [88]) methods, the Mixed Finite Volume (MFV, [82]) methods, and the Mimetic Finite Difference (MFD, [22]) methods proposed in [21, 83]. It is important to mention that in [65] , the authors extend the analysis proposed in [81] for Leray–Lions equations. Moreover, in the case of fully nonlinear models, one strategy to recover the high-order rate of convergence, seems to be defining the gradient reconstruction operator in the full polynomial space $\mathbb{P}^k(T)^d$. For more details, we refer to Section 4 in [68].

There is also a connection of HHO technique with other approaches, such as Hybridizable Discontinuous Galerkin (HDG) methods in [57, Section 4], with the help of an equivalent mixed formulation is necessary. Also, in [57, Section 2.4], we find a link with High-order mimetic (HOM) approach, introduced in [127], and with the nonconforming version of the VE method introduced in [11]. In addition, we find a unified analysis between HHO and VE methods in [125], but differs from the standard VE method described in [20].
Finally, in [68], the authors show that the HHO method [75, 64], the nonconforming versions of MFD [127] and VE [20, 43] methods, can be included in the generic framework of Gradient scheme (GS), which was originally developed for encompassing low numerical methods ($k = 0$). We point out that our analysis is not included, since the stabilization term is not embedded into the discrete symmetric gradient operator. We refer to Remark 24 in [68], for further details.

The rest of the paper is organized as follows. In Section 3.2, we introduce the continuous model problem and discuss the well-posedness of a weak formulation of this one. In Section 3.3, we introduce the discrete approximation spaces, where the unknowns of the HHO scheme will be looked for. Moreover, we also introduce the potential and gradient reconstruction operators, emphasizing their key properties. In Section 3.4, we introduce the discrete problem and study its stability. In Section 3.5, we establish the well-posedness of the discrete problem, while in Section 3.6 we perform the a priori error analysis. First, in the energy-norm, and then in the L^2-norm, under additional elliptic regularity assumptions. Section 3.7 contains a brief description of how we can adapt the approach for other types of boundary conditions. Finally, in Section 3.8, we present some examples, which are in agreement with our theoretical results.

3.2 Continuous setting

In this section, we present the continuous problem, and give appropriate assumptions on the function $\mathbf{a}$ that will let us to prove the well-posedness of the corresponding weak formulation. Then, given $f \in L^2(\Omega)$, we look for $u : \Omega \to \mathbb{R}$, solution of the following class of nonlinear elliptic problem:

$$-\mathrm{div}(\mathbf{a}(\cdot, \nabla u)) = f \quad \text{in } \Omega, \tag{3.2a}$$

$$u = 0 \quad \text{on } \partial\Omega, \tag{3.2b}$$

where $\Omega \subset \mathbb{R}^d$, $d \in \{2, 3\}$, is a polytopal bounded connected domain, with Lipschitz boundary $\partial\Omega$, while $\mathbf{a} : \Omega \times \mathbb{R}^d \to \mathbb{R}^d$ is a nonlinear function.

Assumption 3.2.1 *The vectorial nonlinear function* $\mathbf{a}$ *satisfies the following properties/hypotheses (see [33]):*

(H.1) *Carathéodory condition: The function* $\mathrm{a}_j(x, \cdot)$, $j = 1, ..., d$, *is continuous in* $\mathbb{R}^d$ *for almost all* $x \in \Omega$, *and* $\mathrm{a}_j(\cdot, \boldsymbol{\zeta})$, $j = 1, ..., d$, *is measurable in* Ω *for all* $\boldsymbol{\zeta} \in \mathbb{R}^d$.

(H.2) *Growth condition: There exist* $\phi_j \in L^2(\Omega)$, $j = 1, ..., d$, *and* $C > 0$ *such that* $|\mathrm{a}_j(x, \boldsymbol{\zeta})| \leq C(1 + |\boldsymbol{\zeta}|) + |\phi_j(x)|$, *for almost all* $x \in \Omega$ *and for all* $\boldsymbol{\zeta} \in \mathbb{R}^d$.

(H.3) *Ellipticity condition: The function* $\mathbf{a} = (\mathrm{a}_1, \cdots, \mathrm{a}_d)$ *has continuous first order partial derivatives in* $\mathbb{R}^d$*, for almost all* $x \in \Omega$*. In addition, there exists* $C > 0$ *such that*

$$\sum_{i,j=1}^{d} \frac{\partial}{\partial \zeta_j} \mathrm{a}_i(x, \zeta) \tilde{\zeta}_i \tilde{\zeta}_j \geq C |\tilde{\zeta}|^2,$$

for all $\zeta := (\zeta_i, \zeta_j)^{\mathsf{t}}$, $\tilde{\zeta} := (\tilde{\zeta}_i, \tilde{\zeta}_j)^{\mathsf{t}} \in \mathbb{R}^2$ *and for almost all* $x \in \Omega$*.*

(H.4) *Regularity condition: The function* $\mathrm{a}_i(x, \cdot)$*,* $i = 1, ..., d$*, has continuous first order partial derivatives in* $\mathbb{R}^d$ *for almost all* $x \in \Omega$*. In addition, there exists* $C > 0$ *such that for each* $i, j \in \{1, \cdots, d\}$*,* $\frac{\partial}{\partial \zeta_j} \mathrm{a}_i(x, \boldsymbol{\zeta})$ *satisfies the Carathéodory condition* ***(H.1)****, and* $\left| \frac{\partial}{\partial \zeta_j} \mathrm{a}_i(x, \boldsymbol{\zeta}) \right| \leq C$*, for all* $\boldsymbol{\zeta} \in \mathbb{R}^d$*, and for almost all* $x \in \Omega$*.*

The weak formulation of problem (3.2), that will serve as a starting point for the development and analysis of the HHO method, reads: *Find* $u \in U := H_0^1(\Omega)$ *such that*

$$\int_\Omega \mathbf{a}(x, \nabla u(x)) \cdot \nabla v(x)\, dx = \int_\Omega f(x)\, v(x)\, dx \quad \forall\, v \in U. \tag{3.3}$$

We remark that ***(H.1)*** - ***(H.2)*** guarantee that $\mathbf{a}$ is well defined, while ***(H.3)*** - ***(H.4)*** ensure that the nonlinear operator in the left-hand side of (3.3) is strongly monotone and Lipschitz-continuous, thanks to Theorem 32.6 in [144, page 240]. Finally, the well-posedness of the problem (3.3) follows after invoking Theorem 34.1 in [144, page 245].

3.3 Discrete settings

In this section, we recall the notion of admissible mesh sequences, and reasonable assumptions on such meshes, which are required to define the HHO scheme. First, we let $(\mathcal{T}_h)_{h \in \mathcal{H}}$ be an h-refined regular mesh sequence of $\overline{\Omega}$, consisting of polytopal meshes (cf. Chapter 1 in [66]), with $\mathcal{H}$ being a countable set of positive numbers having 0 as its only accumulation point. Next, for any $h \in \mathcal{H}$, $\mathcal{T}_h$ is a finite collection of nonempty, disjoint, open, polytope elements T with diameter h_T, such that $\cup_{T \in \mathcal{T}_h} \overline{T} = \overline{\Omega}$, and there is a matching simplicial submesh $\mathfrak{J}_h$ such that any

simplex and any face in $\mathfrak{J}_h$ belongs to just one element and face of $\mathcal{T}_h$. Besides, there exists $\rho > 0$ (called the mesh regularity parameter), that is independent of h, such that for every $h \in \mathcal{H}$: (i) for any simplex $S \in \mathfrak{J}_h$ of diameter h_S and inradius r_S, there holds $\rho\, h_S \leq r_S$; and (ii) $\forall\, T \in \mathcal{T}_h\,,\, \forall\, S \in \mathfrak{J}_h\, :\, (S \subseteq T \,\Rightarrow\, \rho\, h_T \leq h_S)$. As usual, we introduce $h := \max_{T\in\mathcal{T}_h} h_T$. The regularity condition of the mesh sequence, ensures important geometric bounds on $\mathcal{T}_h$ and $\mathcal{F}_h$, for any $h \in \mathcal{H}$. We refer to Lemma 1.2 in [66] for more details in this context.

Given any $\mathcal{T}_h$, with $h \in \mathcal{H}$, we call a face any hyperplanar closed connected subset F of $\overline{\Omega}$ with positive $(d-1)$-dimensional measure, and such that: (1) either there exists $T \in \mathcal{T}_h$ such that $F \subset \partial T \cap \partial\Omega$ (in this case, F is called a boundary face), or (2) there exist $T_1, T_2 \in \mathcal{T}_h$ such that $F \subset \partial T_1 \cap \partial T_2$ (and then, F is called an interior face). Boundary faces are collected in $\mathcal{F}_h^{\mathtt{b}}$, interior faces are callected in the set $\mathcal{F}_h^{\mathtt{int}}$, and we set $\mathcal{F}_h := \mathcal{F}_h^{\mathtt{int}} \cup \mathcal{F}_h^{\mathtt{b}}$. Now, by h_F we denote the diameter of a face $F \in \mathcal{F}_h$. For each $T \in \mathcal{T}_h$, we define $\mathcal{F}_T := \{F \in \mathcal{F}_h \,:\, F \subset \partial T\}$, and then, given $F \in \mathcal{F}_T$, by $\boldsymbol{n}_{TF}$ we denote the unit normal to F, outward to T.

Throughout this paper, given two different non-negative numbers x, y, by $x \lesssim y$, we denote the inequality $x \leq C\, y$, where C is a positive constant that is independent of the meshsize, but may depend on the mesh regularity parameter ρ. In addition, we also introduce the notation $x \approx y$, which means that $y \lesssim x$ and $x \lesssim y$.

It is important to emphasize that in this context, the very well-known inequalities and embeddings, are also valid. We remind here the discrete Poincaré-Wirtinger inequality [66, Remark 1.46], i.e. given any $T \in \mathcal{T}_h$:

$$||w||_T \lesssim h_T\, ||\nabla w||_T \quad \forall\, w \in H^1(T) \cap L^2_0(T)\,, \tag{3.4}$$

which will be invoked in this paper. Other know results are, for example, the discrete Sobolev embedding [64, Proposition 5.4], the discrete inverse inequality [69, Lemma 1.44], the discrete and continuous trace inequalities [69, Lemmas 1.46 and 1.49].

Now, we recall the definition and properties of the L^2-orthogonal projector. Given any $T \in \mathcal{T}_h$ and any integer $l \geq 0$, we define the L^2-orthogonal projector $\pi_T^l : L^1(T) \to \mathbb{P}_d^l(T)$ such that: For all $v \in L^1(T)$, $\pi_T^l v$ is the unique polynomial in $\mathbb{P}_d^l(T)$

that satisfies

$$(\pi_T^l v - v, \nabla w)_T = 0 \quad \forall w \in \mathbb{P}_d^l(T)\,.$$

We also introduce the so called elliptic projector $\pi_T^{1,l} : W^{1,1}(T) \to \mathbb{P}_d^l(T)$ such that: For all $v \in W^{1,1}(T)$, $\pi_T^{1,l} v$ is a polynomial in $\mathbb{P}_d^l(T)$ that satisfies (cf. Definition 1.39 in [66])

$$\begin{aligned}\big(\nabla(\pi_T^{1,l} v - v), \nabla w\big)_T = 0 \quad \forall w \in \mathbb{P}_d^l(T)\,,\\ (\pi_T^{1,l} v - v, 1)_T = 0\,.\end{aligned}$$

For the next result, we set $\pi_T^{0,l} := \pi_T^l$.

Lemma 3.3.1 (Approximation properties) *Given an integer $l \geq 0$, $T \in \mathcal{T}_h$ and $\kappa \in \{0, 1\}$. Let $\pi_T^{\kappa,l}$ be the L^2-orthogonal projection or elliptic projector onto $\mathbb{P}_d^k(T)$. Then, for all $s \in \{\kappa, \cdots, l+1\}$ and all $v \in H^s(T)$, there holds*

$$|v - \pi_T^{\kappa,l} v|_{H^m(T)} \leq C'_{app} h_T^{s-m} |v|_{H^s(T)} \quad \forall m \in \{0, \cdots, s\}. \tag{3.5}$$

Moreover, assuming additionally that $s \geq 1$, there holds for all $F \in \mathcal{F}_T$,

$$|v - \pi_T^{\kappa,l} v|_{H^m(F)} \leq C''_{app} h_T^{s-m-1/2} |v|_{H^s(T)} \quad \forall m \in \{0, \cdots, s-1\}. \tag{3.6}$$

Here $C'_{app} > 0$ and $C''_{app} > 0$ depend only on d, the regularity of the mesh, l, and s.

Proof. We refer to the proofs of Theorems 1.45 and 1.48 in [66]. □

3.3.1 Degrees of freedom (DOFs)

Let $k \geq 0$ be fixed. For all $T \in \mathcal{T}_h$, we define the local space of DOFs as $\underline{\mathbf{U}}_T^k := \mathbb{P}_d^k(T) \times \big(\prod_{F \in \mathcal{F}_T} \mathbb{P}_{d-1}^k(F)\big)$, where $\mathbb{P}_d^k(T)$ (resp., $\mathbb{P}_{d-1}^k(F)$) is spanned by the restrictions to T (resp., to F) of d-variate (resp., $(d-1)$-variate) polynomials of total degree $\leq k$. The global space of DOFs on the domain Ω, is

$$\underline{\mathbf{U}}_h^k := \left(\prod_{T \in \mathcal{T}_h} \mathbb{P}_d^k(T)\right) \times \left(\prod_{F \in \mathcal{F}_h} \mathbb{P}_{d-1}^k(F)\right)\,.$$

The space $\underline{\mathbf{U}}_h^k$ is equipped with the following discrete semi-norm, $\|\cdot\|_{\epsilon,h} : \underline{\mathbf{U}}_h^k \to \mathbb{R}$

$$\|\underline{\mathbf{v}}_h\|_{\epsilon,h}^2 := \sum_{T \in \mathcal{T}_h} \|\underline{\mathbf{v}}_T\|_{\epsilon,T}^2 \quad , \quad \|\underline{\mathbf{v}}_T\|_{\epsilon,T}^2 := \|\nabla v_T\|_T^2 + \sum_{F \in \mathcal{F}_T} h_F^{-1} \|v_F - v_T\|_F^2\,. \tag{3.7}$$

For each $T \in \mathcal{T}_h$, we define the local reduction operator $\underline{\mathbf{I}}_T^k : H^1(T) \to \underline{\mathbf{U}}_T^k$ such that, for all $v \in H^1(T)$,

$$\underline{\mathbf{I}}_T^k v \;:=\; \big(\pi_T^k v, (\pi_F^k v)_{F\in\mathcal{F}_T}\big) \;\in\; \underline{\mathbf{U}}_T^k\,, \tag{3.8}$$

where π_T^k and π_F^k denote the usual L^2-orthogonal projectors onto $\mathbb{P}_d^k(T)$ and $\mathbb{P}_{d-1}^k(F)$, respectively. The corresponding global interpolation operator $\underline{\mathbf{I}}_h^k : H^1(\Omega) \to \underline{\mathbf{U}}_h^k$ is then defined, such that for all $v \in H^1(\Omega)$,

$$\underline{\mathbf{I}}_h^k v \;:=\; \big((\pi_T^k v)_{T\in\mathcal{T}_h}, (\pi_F^k v)_{F\in\mathcal{F}_h}\big) \in \underline{\mathbf{U}}_h^k\,. \tag{3.9}$$

3.3.2 Gradient and Potential reconstruction operators

Based on the local DOFs, we introduce reconstructions of the gradient and of the potential that will be helpful in the formulation of the method. In what follows, $(\cdot,\cdot)_T$ and $(\cdot,\cdot)_F$ will denote the usual L^2-inner products on $T \in \mathcal{T}_h$ and $F \in \mathcal{F}_h$, respectively. We define the **local discrete gradient operator** $G_T^k : \underline{\mathbf{U}}_T^k \to [\mathbb{P}_d^k(T)]^d$ such that, given $\underline{\mathbf{v}}_T \in \underline{\mathbf{U}}_T^k$, then, $G_T^k \underline{\mathbf{v}}_T \in [\mathbb{P}_d^k(T)]^d$ satisfies

$$(G_T^k \underline{\mathbf{v}}_T, \boldsymbol{\phi})_T = (\nabla v_T, \boldsymbol{\phi})_T + \sum_{F\in\mathcal{F}_T} (v_F - v_T, \boldsymbol{\phi}\cdot\boldsymbol{n}_{TF})_F \quad \forall \boldsymbol{\phi} \in [\mathbb{P}_d^k(T)]^d, \tag{3.10}$$

where, we recall that $\boldsymbol{n}_{TF}$ is the unit normal to F pointing out of T. The following proposition shows us the relation between the exact gradient and the discrete gradient operators.

Proposition 3.3.1 (Commuting property) *For all $v \in H^1(T)$, there holds*

$$G_T^k \underline{\mathbf{I}}_T^k v = \pi_T^k(\nabla v)\,, \tag{3.11}$$

where π_T^k acts componentwise.

Proof. For the sake of completeness, we rewrite the proof of Proposition 10 in [65]. First, we fix $T \in \mathcal{T}_h$ and $\boldsymbol{\phi} \in [\mathbb{P}_d^k(T)]^d$. Then, plugging the definition (3.8) of $\underline{\mathbf{I}}_T^k$ into (3.10), and applying integration by parts, taking into account the definition of orthogonal projection, together with the fact that $\operatorname{div}\boldsymbol{\phi} \in \mathbb{P}_d^{k-1}(T) \subset \mathbb{P}_d^k(T)$ and that

$\boldsymbol{\phi}|_F \cdot \boldsymbol{n}_{TF} \in \mathbb{P}^k_{d-1}(F)$ for all $F \in \mathcal{F}_T$, we have

$$\begin{aligned}(G^k_T \underline{\mathbf{I}}^k_T v, \boldsymbol{\phi})_T &= (\nabla \pi^k_T v, \boldsymbol{\phi})_T + \sum_{F\in\mathcal{F}_T} (\pi^k_F v - \pi^k_T v, \boldsymbol{\phi}\cdot\boldsymbol{n}_{TF})_F \\ &= -(\pi^k_T v, \operatorname{div}\boldsymbol{\phi})_T + \sum_{F\in\mathcal{F}_T} (\pi^k_F v, \boldsymbol{\phi}\cdot\boldsymbol{n}_{TF})_F \\ &= -(v, \operatorname{div}\boldsymbol{\phi})_T + \sum_{F\in\mathcal{F}_T} (v, \boldsymbol{\phi}\cdot\boldsymbol{n}_{TF})_F \\ &= (\nabla v, \boldsymbol{\phi})_T\,,\end{aligned}$$

where, we have applied integration by parts again. Then, the conclusion is derived and we end the proof. □

Remark 3.3.1 *In the Appendix of this paper, we show the relevance of introducing* (3.10)*, with a numerical example.*

We also define the **local potential reconstruction operator** $p^{k+1}_T : \underline{\boldsymbol{U}}^k_T \to \mathbb{P}^{k+1}_d(T)$ such that, for all $\underline{\mathbf{v}}_T := (v_T, (v_F)_{F\in\mathcal{F}_T}) \in \underline{\mathbf{U}}^k_T$, $p^{k+1}_T \underline{\mathbf{v}}_T \in \mathbb{P}^{k+1}_d(T)$ is the unique solution of

$$(\nabla p^{k+1}_T \underline{\mathbf{v}}_T - G^k_T \underline{\mathbf{v}}_T, \nabla w)_T = 0\,, \quad \forall\, w \in \mathbb{P}^{k+1}_d(T), \tag{3.12a}$$

$$(p^{k+1}_T \underline{\mathbf{v}}_T - v_T, 1)_T = 0\,. \tag{3.12b}$$

This operator satisfies the following orthogonal property (cf. Section 4 in [64]).

Corollary 3.3.1 (Euler equation) *For all $v \in H^1(T)$, there holds*

$$(\nabla(p^{k+1}_T \underline{\mathbf{I}}^k_T v - v), \nabla w)_T = 0 \quad \forall\, w \in \mathbb{P}^{k+1}_d(T). \tag{3.13}$$

Proof. We have the following identity

$$(\nabla(p^{k+1}_T \underline{\mathbf{I}}^k_T v - v), \nabla w)_T = (\nabla p^{k+1}_T \underline{\mathbf{I}}^k_T v - G^k_T \underline{\mathbf{I}}^k_T v, \nabla w)_T + (G^k_T \underline{\mathbf{I}}^k_T v - \nabla v, \nabla w)_T \quad \forall\, w \in \mathbb{P}^{k+1}_d(T).$$

Then, the conclusion follows from (3.12a) and the commuting property (3.11). □

Remark 3.3.2 *We observe from* (3.12b) *and the definition of π^k_T, that $\left(p^{k+1}_T \underline{\mathbf{I}}^k_T v, 1\right)_T = (\pi^k_T v, 1)_T = (v, 1)_T$. Then, there holds*

$$\left(p^{k+1}_T \underline{\mathbf{I}}^k_T v - v, 1\right)_T = 0 \quad \forall\, T \in \mathcal{T}_h\,. \tag{3.14}$$

The following lemma is similar to the one established for the original Gradient reconstruction operator (defined for linear elliptic problems), and will be applied later in this paper (cf. proof of Theorem 3.6.3).

Lemma 3.3.2 (Approximation properties for $p_T^{k+1}\underline{\mathbf{I}}_T^k$) *There exists a real number $C > 0$, depending on ρ (mesh regularity parameter) and d, but independent of the polynomial degree, and the meshsize. So that for any $v \in H^{s+2}(T)$, $s \in \{0, \cdots, k\}$, there holds:*

$$\left\|v - p_T^{k+1}\underline{\mathbf{I}}_T^k v\right\|_T + h_T^{1/2}\left\|v - p_T^{k+1}\underline{\mathbf{I}}_T^k v\right\|_{\partial T} + h_T\left\|\nabla(v - p_T^{k+1}\underline{\mathbf{I}}_T^k v)\right\|_T + h_T^{3/2}\left\|\nabla(v - p_T^{k+1}\underline{\mathbf{I}}_T^k v)\right\|_{\partial T} \leq C h_T^{s+2}\left\|v\right\|_{H^{s+2}(T)}. \tag{3.15}$$

Proof. The proof follows immediately from Theorems 1.1 and 1.2 in [65], and observing that $p_T^{k+1}\underline{\mathbf{I}}_T^k$ is an elliptic projector, thanks to the Euler equation (3.13), fixing its constant by (3.14). □

3.4 Formulation

Here, we introduce the following subspace of $\underline{\mathbf{U}}_h^k$, which strongly incorporates the homogeneous Dirichlet boundary condition (3.2b):

$$\underline{\mathbf{U}}_{h,0}^k := \left\{\underline{\mathbf{v}}_h \in \underline{\mathbf{U}}_h^k \,:\, v_F = 0 \quad \forall\, F \in \mathcal{F}_h^b\right\}. \tag{3.16}$$

Proposition 3.4.1 *The map $\|\cdot\|_{\epsilon,h} : \underline{\mathbf{U}}_h^k \to \mathbb{R}$, given in (3.7), defines a norm on $\underline{\mathbf{U}}_{h,0}^k$.*

Proof. The proof follows the same ideas from the proof of Corollary 2.16 in [66].For the sake of completeness, we proceed to establish this result. First, we notice that it is enough to prove

$$\forall\, \underline{\mathbf{v}}_h := \left((v_T)_{T\in\mathcal{T}_h}, (v_F)_{F\in\mathcal{F}_h}\right) \in \underline{\mathbf{U}}_{h,0}^k \,:\, \left(\|\underline{\mathbf{v}}_h\|_{\epsilon,h} = 0 \quad \Rightarrow \quad \underline{\mathbf{v}}_h = 0 \in \underline{\mathbf{U}}_{h,0}^k\right).$$

We let $\underline{\mathbf{v}}_h := \left((v_T)_{T\in\mathcal{T}_h}, (v_F)_{F\in\mathcal{F}_h}\right) \in \underline{\mathbf{U}}_{h,0}^k$ be such that $\|\underline{\mathbf{v}}_h\|_{\epsilon,h} = 0$. This implies, from (3.7), that there exists $C_0 \in \mathbb{R}$, such that

$$v_F = v_T = C_0 \quad \forall F \in \mathcal{F}_T\,, \quad \forall\, T \in \mathcal{T}_h\,.$$

Since v_F is single value on each $F \in \mathcal{F}_h$ and $v_F = 0$ on $\mathcal{F}_h^{\mathsf{b}}$, we conclude that $\underline{\mathbf{v}}_h = 0 \in \underline{\mathbf{U}}_{h,0}^k$, and we end the proof. □

Hereafter, we recall that given $\underline{\mathbf{v}}_h := \big((v_T)_{T\in\mathcal{T}_h}, (v_F)_{F\in\mathcal{F}_h}\big) \in \underline{\mathbf{U}}_h^k$, we set $v_h \in \mathbb{P}_d^k(\mathcal{T}_h)$ such that $v_h|_T := v_T$, for all $T \in \mathcal{T}_h$.

Now, we consider the following discrete variational formulation of (3.3): Find $\underline{\mathbf{u}}_h \in \underline{\mathbf{U}}_{h,0}^k$ such that, for any $\underline{\mathbf{v}}_h \in \underline{\mathbf{U}}_{h,0}^k$,

$$A_h(\underline{\mathbf{u}}_h, \underline{\mathbf{v}}_h) := N_h(\underline{\mathbf{u}}_h, \underline{\mathbf{v}}_h) + s_h(\underline{\mathbf{u}}_h, \underline{\mathbf{v}}_h) = (f, v_h)_{0,\Omega} =: b_h(\underline{\mathbf{v}}_h), \tag{3.17}$$

where the nonlinear form $N_h : \underline{\mathbf{U}}_h^k \times \underline{\mathbf{U}}_h^k \to \mathbb{R}$ and the bilinear form $s_h : \underline{\mathbf{U}}_h^k \times \underline{\mathbf{U}}_h^k \to \mathbb{R}$, are assembled element-wise as

$$N_h(\underline{\mathbf{u}}_h, \underline{\mathbf{v}}_h) := \sum_{T\in\mathcal{T}_h} N_T(\underline{\mathbf{u}}_T, \underline{\mathbf{v}}_T), \quad \text{and} \quad s_h(\underline{\mathbf{u}}_h, \underline{\mathbf{v}}_h) := \sum_{T\in\mathcal{T}_h} s_T(\underline{\mathbf{u}}_T, \underline{\mathbf{v}}_T), \tag{3.18}$$

from the local contributions $N_T : \underline{\mathbf{U}}_T^k \times \underline{\mathbf{U}}_T^k \to \mathbb{R}$, and $s_T : \underline{\mathbf{U}}_T^k \times \underline{\mathbf{U}}_T^k \to \mathbb{R}$, $T \in \mathcal{T}_h$, given by

$$N_T(\underline{\mathbf{u}}_T, \underline{\mathbf{v}}_T) := \int_T \mathrm{a}(x, G_T^k \underline{\mathbf{u}}_T(x)) \cdot G_T^k \underline{\mathbf{v}}_T(x)\, dx, \tag{3.19a}$$

$$s_T(\underline{\mathbf{u}}_T, \underline{\mathbf{v}}_T) := \sum_{F\in\mathcal{F}_T} h_F^{-1} \Big(\pi_F^k(u_F - P_T^k \underline{\mathbf{u}}_T), \pi_F^k(v_F - P_T^k \underline{\mathbf{v}}_T)\Big)_F. \tag{3.19b}$$

We recall that the local potential reconstruction $P_T^k : \underline{\mathbf{U}}_T^k \to \mathbb{P}_d^{k+1}(T)$ is defined such that, for all $\underline{\mathbf{v}}_T \in \underline{\mathbf{U}}_T^k$,

$$P_T^k \underline{\mathbf{v}}_T := v_T + (p_T^{k+1} \underline{\mathbf{v}}_T - \pi_T^k p_T^{k+1} \underline{\mathbf{v}}_T). \tag{3.20}$$

Next, we introduce the global discrete gradient operator $G_h^k : \underline{\mathbf{U}}_h^k \to [\mathbb{P}_d^k(\mathcal{T}_h)]^d$ such that, for all $\underline{\mathbf{v}}_h \in \underline{\mathbf{U}}_h^k$,

$$G_h^k \underline{\mathbf{v}}_h|_T := G_T^k \underline{\mathbf{v}}_T \quad \forall T \in \mathcal{T}_h. \tag{3.21}$$

Lemma 3.4.1 *Let $(\mathcal{T}_h)_{h\in\mathcal{H}}$ be an admissible mesh sequence and $k \geq 0$. For any $T \in \mathcal{T}_h$, there holds the following equivalence of local semi norms on $\underline{\mathbf{U}}_T^k$*

$$\|\underline{\mathbf{v}}_T\|_{\epsilon,T}^2 \approx \|G_T^k \underline{\mathbf{v}}_T\|_T^2 + s_T(\underline{\mathbf{v}}_T, \underline{\mathbf{v}}_T) \quad \forall \underline{\mathbf{v}}_T \in \underline{\mathbf{U}}_T^k \tag{3.22}$$

$$\approx \|p_T^{k+1} \underline{\mathbf{v}}_T\|_T^2 + s_T(\underline{\mathbf{v}}_T, \underline{\mathbf{v}}_T) \quad \forall \underline{\mathbf{v}}_T \in \underline{\mathbf{U}}_T^k. \tag{3.23}$$

Besides, the hidden constant is independent of the meshsize and $\underline{\mathbf{v}}_T$. *Consequently, for all* $\underline{\mathbf{v}}_h \in \underline{\mathbf{U}}_h^k$, *there holds*

$$\|\underline{\mathbf{v}}_h\|_{\epsilon,h}^2 \approx \|G_h^k \underline{\mathbf{v}}_h\|_\Omega^2 + s_h(\underline{\mathbf{v}}_h, \underline{\mathbf{v}}_h)\,. \tag{3.24}$$

Proof. We refer to the proofs of Lemma 4 in [75] and Lemma 5.2 in [64]. □

Remark 3.4.1 $\|G_h^k \underline{\mathbf{v}}_h\|_\Omega^2 + s_h(\underline{\mathbf{v}}_h, \underline{\mathbf{v}}_h)$ *is usually called energy norm.*

Lemma 3.4.2 *The nonlinear form* N_h, *defined in* (3.18), *is strongly monotone on* $\underline{\mathbf{U}}_h^k$.

Proof. The strong monotonicity of N_h follows straightforwardly from (3.22) and ***(H.3)***. □

Lemma 3.4.3 (Consistency of s_T**)** *Given* $T \in \mathcal{T}_h$, *we let* s_T *be the stabilization bilinear form defined in* (3.18). *Then, for each* $v \in H^{r+2}(T)$, *with* $r \in \{0, \cdots, k\}$, *there holds*

$$s_T(\underline{\mathbf{I}}_T^k v, \underline{\mathbf{I}}_T^k v)^{1/2} \lesssim h_T^{r+1} \|v\|_{H^{r+2}(T)}\,. \tag{3.25}$$

Proof. We refer to the proof of Lemma 2.14 in [66]. We omit further details. □

3.5 Well-posedness of (3.17)

Our purpose here, is to establish the unique solvability of (3.17). To this aim, we notice that the assumptions ***(H.3)*** and ***(H.4)*** on the coefficients a_i, imply that the nonlinear operator induced by $\mathbf{a}$ is strongly monotone and Lipschitz continuous on $[L^2(\Omega)]^d$ (see, e.g. [98, 101]). This ensures the existence of $C_1\,, C_2 > 0$, such that for all $\boldsymbol{\theta}\,, \tilde{\boldsymbol{\theta}} \in [L^2(\Omega)]^d$, there hold

$$\int_\Omega \Big(\mathbf{a}(\cdot, \boldsymbol{\theta}) - \mathbf{a}(\cdot, \tilde{\boldsymbol{\theta}})\Big) \cdot (\boldsymbol{\theta} - \tilde{\boldsymbol{\theta}}) \geq C_1 \, ||\boldsymbol{\theta} - \tilde{\boldsymbol{\theta}}||_\Omega^2\,, \tag{3.26}$$

and

$$||\mathbf{a}(\cdot, \boldsymbol{\theta}) - \mathbf{a}(\cdot, \tilde{\boldsymbol{\theta}})||_\Omega \leq C_2 \, ||\boldsymbol{\theta} - \tilde{\boldsymbol{\theta}}||_\Omega\,. \tag{3.27}$$

Next result shows that the nonlinear operator A_h is also Lipschitz continuous.

Lemma 3.5.1 *There exists $C_{\mathtt{LC}} > 0$, independent of the meshsize, such that*

$$||A_h(\underline{\mathbf{v}}_h, \cdot) - A_h(\underline{\mathbf{w}}_h, \cdot)||_{\underline{\mathbf{U}}_{h,0}^{k,*}} \leq C_{\mathtt{LC}} \, ||\underline{\mathbf{v}}_h - \underline{\mathbf{w}}_h||_{\epsilon,h} \quad \forall \, \underline{\mathbf{v}}_h \, , \, \underline{\mathbf{w}}_h \in \underline{\mathbf{U}}_{h,0}^k \, , \tag{3.28}$$

where $\underline{\mathbf{U}}_{h,0}^{k,*}$ represents the dual of $\underline{\mathbf{U}}_{h,0}^k$.

Proof. Given $\underline{\mathbf{v}}_h \, , \, \underline{\mathbf{w}}_h \, , \, \underline{\mathbf{z}}_h \in \underline{\mathbf{U}}_{h,0}^k$, we notice that

$$A_h(\underline{\mathbf{v}}_h, \underline{\mathbf{z}}_h) - A_h(\underline{\mathbf{w}}_h, \underline{\mathbf{z}}_h) \, = \, \sum_{T \in \mathcal{T}_h} \Bigg[\Big(\mathbf{a}(\cdot, G_T^k \underline{\mathbf{v}}_T) - \mathbf{a}(\cdot, G_T^k \underline{\mathbf{w}}_T), G_T^k \underline{\mathbf{z}}_T \Big)_T + s_T(\underline{\mathbf{v}}_T - \underline{\mathbf{w}}_T, \underline{\mathbf{z}}_T) \Bigg] \, .$$

Now, noticing that ***(H.4)*** also implies that $\mathbf{a}$ is Lipschitz continuous on $[L^2(T)]^d$, for each $T \in \mathcal{T}_h$, we have, after applying Cauchy-Schwarz inequality, that

$$|A_h(\underline{\mathbf{v}}_h, \underline{\mathbf{z}}_h) - A_h(\underline{\mathbf{w}}_h, \underline{\mathbf{z}}_h)| \lesssim \sum_{T \in \mathcal{T}_h} ||G_T^k(\underline{\mathbf{v}}_T - \underline{\mathbf{w}}_T)||_T \, ||G_h^k \underline{\mathbf{z}}_T||_T \, + \, s_T(\underline{\mathbf{v}}_T - \underline{\mathbf{w}}_T, \underline{\mathbf{z}}_T) \, .$$

Next, we take into account Minkowski inequality, to derive

$$|A_h(\underline{\mathbf{v}}_h, \underline{\mathbf{z}}_h) - A_h(\underline{\mathbf{w}}_h, \underline{\mathbf{z}}_h)| \lesssim \left(\sum_{T \in \mathcal{T}_h} ||G_T^k(\underline{\mathbf{v}}_T - \underline{\mathbf{w}}_T)||_T^2 \, + \, s_T(\underline{\mathbf{v}}_T - \underline{\mathbf{w}}_T, \underline{\mathbf{v}}_T - \underline{\mathbf{w}}_T) \right)^{1/2} \times \left(\sum_{T \in \mathcal{T}_h} ||G_T^k \underline{\mathbf{z}}_T||_T^2 \, + \, s_T(\underline{\mathbf{z}}_T, \underline{\mathbf{z}}_T) \right)^{1/2} \, .$$

Then, (3.28) follows after invoking Lemma 3.4.1. □

Lemma 3.5.2 *There exists $C_{\mathtt{SM}} > 0$, independent of the meshsize, such that*

$$A_h(\underline{\mathbf{v}}_h, \underline{\mathbf{v}}_h - \underline{\mathbf{w}}_h) - A_h(\underline{\mathbf{w}}_h, \underline{\mathbf{v}}_h - \underline{\mathbf{w}}_h) \, \geq \, C_{\mathtt{SM}} \, ||\underline{\mathbf{v}}_h - \underline{\mathbf{w}}_h||_{\epsilon,h}^2 \quad \forall \, \underline{\mathbf{v}}_h \, , \, \underline{\mathbf{w}}_h \in \underline{\mathbf{U}}_h^k \, . \tag{3.29}$$

Proof. Let $\underline{\mathbf{v}}_h \, , \, \underline{\mathbf{w}}_h \in \underline{\mathbf{U}}_h^k$. Thanks to the definition of A_h, we derive

$$\begin{aligned} &A_h(\underline{\mathbf{v}}_h, \underline{\mathbf{v}}_h - \underline{\mathbf{w}}_h) - A_h(\underline{\mathbf{w}}_h, \underline{\mathbf{v}}_h - \underline{\mathbf{w}}_h) \\ &= \sum_{T \in \mathcal{T}_h} \Big(\mathbf{a}(\cdot, G_T^k \underline{\mathbf{v}}_T) - \mathbf{a}(\cdot, G_T^k \underline{\mathbf{w}}_T), G_T^k \underline{\mathbf{v}}_T - G_T^k \underline{\mathbf{w}}_T \Big)_T \, + \, s_h(\underline{\mathbf{v}}_h - \underline{\mathbf{w}}_h, \underline{\mathbf{v}}_h - \underline{\mathbf{w}}_h) \, . \end{aligned}$$

Next, applying (3.26), we obtain

$$A_h(\underline{\mathbf{v}}_h, \underline{\mathbf{v}}_h - \underline{\mathbf{w}}_h) - A_h(\underline{\mathbf{w}}_h, \underline{\mathbf{v}}_h - \underline{\mathbf{w}}_h) \, \geq \, C_1 \sum_{T \in \mathcal{T}_h} ||G_T^k(\underline{\mathbf{v}}_T - \underline{\mathbf{w}}_T)||_T^2 + s_h(\underline{\mathbf{v}}_h - \underline{\mathbf{w}}_h, \underline{\mathbf{v}}_h - \underline{\mathbf{w}}_h) \, .$$

Finally, applying Lemma 3.4.1 again, (3.29) is concluded. □

In order to exhibit that $b_h \in \underline{\mathbf{U}}_{h,0}^{k,*}$, we require the following result.

Lemma 3.5.3 *There exists $C_{\mathtt{P}} > 0$, independent of the meshsize, such that*

$$||v_h||_\Omega \leq C_{\mathtt{P}} ||\underline{\mathbf{v}}_h||_{\epsilon,h} \quad \forall \underline{\mathbf{v}}_h \in \underline{\mathbf{U}}_{h,0}^k . \tag{3.30}$$

Proof. We refer to the proof of Lemma 2.15 in [66] □

An immediate consequence of Lemma 3.5.3, is the boundedness of linear functional b_h. This allows us to ensure the unique solvability of the nonlinear HHO formulation (3.17).

Theorem 3.5.1 *There is one and only one solution $\underline{\mathbf{u}}_h \in \underline{\mathbf{U}}_{h,0}^k$ of (3.17), which satisfies*

$$||\underline{\mathbf{u}}_h||_{\epsilon,h} \leq \frac{1}{C_{\mathtt{SM}}} \left(C_{\mathtt{P}} ||f||_\Omega + ||A_h(0,\cdot)||_{\underline{\mathbf{U}}_{h,0}^{k,*}} \right) . \tag{3.31}$$

Proof. Thanks to Lemmas 3.5.1 and 3.5.2, the existence and uniqueness of the solution of (3.17) is consequence of a well known result in nonlinear functional analysis (see, e.g. Theorem 3.3.23 in Chapter III of [133, page 50], or Theorem 35.4 in [144, page 251]). On the other hand, (3.31) is obtained taking into account the strong monotonicity of A_h, (3.17), and Lemma 3.5.3. We omit further details. □

3.6 Error analysis

In this Section, we obtain a priori error estimates of the method, in the energy-norm and also in L^2-norm, under additional regularity assumption on exact solution. We emphasize that the analysis presented here is quite different to the one shown/described in [64], since we are dealing just with a kind of nonlinear version of the 2-Laplacian problem.

The following result will help us to conclude the error estimates of the method. From now on, we let $u \in U$ be the exact solution of (3.3), and $\underline{\mathbf{u}}_h \in \underline{\mathbf{U}}_{h,0}^k$ be the unique solution of (3.17) on the mesh $\mathcal{T}_h$. We define the *consistency error* as the linear functional $\mathcal{E}_h(u;\cdot) : \underline{\mathbf{U}}_{h,0}^k \to \mathbb{R}$ such that $\mathcal{E}_h(u;\cdot) := A_h(\underline{\mathbf{I}}_h^k u, \cdot) - b_h(\cdot)$.

For the sake of completeness, we introduce the following notations for the flux and potential fields, and their approximations. First, we recall that $\boldsymbol{\sigma} := \mathbf{a}(\cdot, \nabla u)$ and $\widehat{\underline{\mathbf{u}}}_h := \underline{\mathbf{I}}_h^k u$. Next, for each $T \in \mathcal{T}_h$, we introduce

$$\boldsymbol{\sigma}_T := \mathbf{a}(\cdot, G_T^k \underline{\mathbf{u}}_T) , \qquad \widehat{\underline{\mathbf{u}}}_T := \underline{\mathbf{I}}_T^k u \quad \text{and} \quad \widehat{\boldsymbol{\sigma}}_T := \mathbf{a}(\cdot, G_T^k \widehat{\underline{\mathbf{u}}}_T) .$$

Lemma 3.6.1 (Consistency error estimate) *Let $u \in H_0^1(\Omega)$ be the unique solution of (3.3). Let $(\mathcal{T}_h)_{h\in\mathcal{H}}$ be a regular mesh family. Let a polynomial degree $k \geq 0$ be fixed, and for all $h \in \mathcal{H}$, we take the additional regularity $u \in H^{r+2}(\mathcal{T}_h)$ and $\mathrm{a}(\cdot, \nabla u) \in H^{r+1}(\mathcal{T}_h)$, for some $r \in \{0, \cdots, k\}$. Then, there holds*

$$\sup_{\underline{\mathbf{v}}_h \in \underline{\mathbf{U}}_{h,0}^k,\, \|\underline{\mathbf{v}}_h\|_{\epsilon,h}=1} \mathcal{E}_h(u;\underline{\mathbf{v}}_h) \lesssim h^{r+1}\Big(\|u\|_{H^{r+2}(\mathcal{T}_h)} + \|\mathbf{a}(\cdot,\nabla u)\|_{H^{r+1}(\mathcal{T}_h)^d}\Big). \tag{3.32}$$

Proof. We adapt the proof of Theorem 16 in [27]. Using the definition (3.17), fixing $\underline{\mathbf{v}}_h \in \underline{\mathbf{U}}_{h,0}^k$, we obtain

$$\begin{aligned}
\mathcal{E}_h(u;\underline{\mathbf{v}}_h) &= \sum_{T\in\mathcal{T}_h} \big(\widehat{\boldsymbol{\sigma}}_T, G_T^k\underline{\mathbf{v}}_T\big)_T + s_h(\widehat{\underline{\mathbf{u}}}_h, \underline{\mathbf{v}}_h) - (f, v_h)_{0,\Omega} \\
&= \sum_{T\in\mathcal{T}_h} \big(\widehat{\boldsymbol{\sigma}}_T - \boldsymbol{\sigma}, G_T^k\underline{\mathbf{v}}_T\big)_T + s_h(\widehat{\underline{\mathbf{u}}}_h, \underline{\mathbf{v}}_h) \\
&\quad + \sum_{T\in\mathcal{T}_h} \big(\boldsymbol{\sigma}, G_T^k\underline{\mathbf{v}}_T\big)_T - (f, v_h)_{0,\Omega}\,.
\end{aligned} \tag{3.33}$$

Considering, for any $T \in \mathcal{T}_h$, the definition (3.10) of G_T^k with $\boldsymbol{\phi} := \pi_T^k\boldsymbol{\sigma} \in [\mathbb{P}_d^k(T)]^d$, we have that

$$\sum_{T\in\mathcal{T}_h} \big(G_T^k\underline{\mathbf{v}}_T, \boldsymbol{\sigma}\big)_T = \sum_{T\in\mathcal{T}_h}\Big\{\big(\boldsymbol{\sigma}, \nabla v_T\big)_T + \sum_{F\in\mathcal{F}_T}\big(\pi_T^k\boldsymbol{\sigma}\cdot\boldsymbol{n}_{TF}, v_F - v_T\big)_F\Big\}, \tag{3.34}$$

where we have used the fact that $\nabla v_T \in [\mathbb{P}_d^{k-1}(T)]^d$, together with the definition of the L^2-orthogonal projector π_T^k componentwise.

On the other hand, knowing that $v_h|_T = v_T$ for all $T \in \mathcal{T}_h$, and $f = -\nabla\cdot\boldsymbol{\sigma}$ a.e. in Ω, and after integrating by parts element by element, we get that

$$(f, v_h)_{0,\Omega} = \sum_{T\in\mathcal{T}_h}\Big\{\big(\boldsymbol{\sigma}, \nabla v_T\big)_T + \sum_{F\in\mathcal{F}_T}\big(\boldsymbol{\sigma}\cdot\boldsymbol{n}_{TF}, v_F - v_T\big)_F\Big\}, \tag{3.35}$$

where we have additionally taken into account that $\boldsymbol{\sigma} \in H(\mathrm{div};\Omega)$, $(v_F)_{F\in\mathcal{F}_h}$ is single valued, and $v_F = 0 \quad \forall\, F \in \mathcal{F}_h^{\mathsf{b}}$.

Now, replacing (3.34) and (3.35) in (3.33), we deduce

$$\begin{aligned}
\mathcal{E}_h(u;\underline{\mathbf{v}}_h) &= \sum_{T\in\mathcal{T}_h}\big(\mathbf{a}(\cdot, G_T^k\widehat{\underline{\mathbf{u}}}_T) - \mathbf{a}(\cdot,\nabla u), G_T^k\underline{\mathbf{v}}_T\big)_T + s_h(\widehat{\underline{\mathbf{u}}}_h, \underline{\mathbf{v}}_h) \\
&\quad + \sum_{T\in\mathcal{T}_h}\sum_{F\in\mathcal{F}_T}\Big(\mathbf{a}(\cdot,\nabla u) - \pi_T^k\mathbf{a}(\cdot,\nabla u)\cdot\boldsymbol{n}_{TF}, v_F - v_T\Big)_F\,.
\end{aligned} \tag{3.36}$$

Then, after applying Cauchy-Schwarz and Minkowski inequalities, we obtain

$$|\mathcal{E}_h(u;\underline{\mathbf{v}}_h)| \lesssim \mathfrak{T}^{1/2}\,||\underline{\mathbf{v}}_h||_{\epsilon,h}\,, \tag{3.37}$$

where

$$\mathfrak{T} := \underbrace{\sum_{T\in\mathcal{T}_h} ||\mathbf{a}(\cdot,G_T^k\widehat{\underline{\mathbf{u}}}_T)-\mathbf{a}(\cdot,\nabla u)||_T^2}_{\mathfrak{T}_1} + \underbrace{\sum_{T\in\mathcal{T}_h}\sum_{F\in\mathcal{F}_T} h_F||\mathbf{a}(\cdot,\nabla u)-\pi_T^k\mathbf{a}(\cdot,\nabla u)||_F^2}_{\mathfrak{T}_2}$$
$$+ \underbrace{s_h(\widehat{\underline{\mathbf{u}}}_h,\widehat{\underline{\mathbf{u}}}_h)}_{\mathfrak{T}_3}\,. \tag{3.38}$$

To bound $\mathfrak{T}_1$, we apply the Lipschitz continuity (3.27) with $\boldsymbol{\theta} := \nabla u$, $\tilde{\boldsymbol{\theta}} := G_h^k\widehat{\underline{\mathbf{u}}}_h$, and invoke the optimal approximation properties of $G_T^k\underline{\mathbf{I}}_T^k$ (cf. (3.11)) and Lemma 3.3.1 (taking $m=1$ and $s=r+2$), to deduce

$$\mathfrak{T}_1 \lesssim \sum_{T\in\mathcal{T}_h}\|\nabla u - G_T^k\widehat{\underline{\mathbf{u}}}_T\|_T^2 \lesssim \sum_{T\in\mathcal{T}_h} h_T^{2(r+1)}\|u\|_{H^{r+2}(T)}^2\,. \tag{3.39}$$

Now, thanks to (3.11) again, we derive

$$\mathfrak{T}_2 \lesssim \sum_{T\in\mathcal{T}_h} h_T^{2(r+1)}||\mathbf{a}(\cdot,\nabla u)||_{[H^{r+1}(T)]^d}^2\,. \tag{3.40}$$

Finally, invoking Lemma 3.4.3, we bound $\mathfrak{T}_3$, and (3.32) is straightforwardly implied. We end the proof. □

Theorem 3.6.1 (Energy error estimate) *Under the same assumptions and notations given in Lemma 3.6.1, there holds, for some $r\in\{0,\cdots,k\}$:*

$$\|\underline{\mathbf{u}}_h - \underline{\mathbf{I}}_h^k u\|_{\epsilon,h} \lesssim h^{r+1}\Big(\|u\|_{H^{r+2}(\mathcal{T}_h)} + \|\mathbf{a}(\cdot,\nabla u)\|_{[H^{r+1}(\mathcal{T}_h)]^d}\Big)\,. \tag{3.41}$$

Moreover, applying Lemma 3.4.1, there holds

$$\|\nabla u - G_h^k\underline{\mathbf{u}}_h\|_{0,\Omega} + s_h(\underline{\mathbf{u}}_h,\underline{\mathbf{u}}_h)^{1/2} \lesssim h^{r+1}\Big(\|u\|_{H^{r+2}(\mathcal{T}_h)} + \|\mathbf{a}(\cdot,\nabla u)\|_{[H^{r+1}(\mathcal{T}_h)]^d}\Big)\,. \tag{3.42}$$

Proof. First, we take into account the strong monotonicity of nonlinear form A_h, and obtain

$$\begin{aligned}
||\underline{\mathbf{u}}_h - \underline{\mathbf{I}}_h^k u||_{\epsilon,h}^2 &\lesssim A_h(\underline{\mathbf{u}}_h,\underline{\mathbf{u}}_h-\underline{\mathbf{I}}_h^k u) \;-\; A_h(\underline{\mathbf{I}}_h^k u,\underline{\mathbf{u}}_h-\underline{\mathbf{I}}_h^k u)\\
&= b_h(\underline{\mathbf{u}}_h-\underline{\mathbf{I}}_h^k u) \;-\; A_h(\underline{\mathbf{I}}_h^k u,\underline{\mathbf{u}}_h-\underline{\mathbf{I}}_h^k u)\\
&= \mathcal{E}_h(u;\underline{\mathbf{I}}_h^k u-\underline{\mathbf{u}}_h)\\
&\lesssim \sup_{\underline{\mathbf{v}}_h\in\underline{\mathbf{U}}_{h,0}^k,\,\|\underline{\mathbf{v}}_h\|_{\epsilon,h}=1} \mathcal{E}_h(u;\underline{\mathbf{v}}_h)\,||\underline{\mathbf{u}}_h-\underline{\mathbf{I}}_h^k u||_{\epsilon,h}\,,
\end{aligned}$$

and then, we deduce

$$||\underline{\mathbf{u}}_h - \underline{\mathbf{I}}_h^k u||_{\epsilon,h} \lesssim \sup_{\underline{\mathbf{v}}_h \in \underline{\mathbf{U}}_{h,0}^k,\, \|\underline{\mathbf{v}}_h\|_{\epsilon,h}=1} \mathcal{E}_h(u;\underline{\mathbf{v}}_h)\,. \tag{3.43}$$

Thus, (3.41) follows once we apply Lemma 3.6.1. The proof of (3.42) relies on Lemma 3.4.1. We omit further details. □

3.6.1 L^2-norm error estimate

Let us turn our attention to the L^2-norm for the volumetric part of the error $\underline{\mathbf{u}}_h - \underline{\mathbf{I}}_h^k u$, that is $e_h := \pi_h^k u - u_h$, where $\pi_h^k u|_T := \pi_T^k u$ and $u_h|_T := u_T$. To this aim, we rewrite problem (3.17) as: Find $\underline{\mathbf{u}}_h \in V_h := \underline{\mathbf{U}}_{h,0}^k$ such that, for any $\underline{\mathbf{v}}_h \in V_h$,

$$[\mathbb{A}_h(\underline{\mathbf{u}}_h), \underline{\mathbf{v}}_h] := [\mathbb{N}_h(\underline{\mathbf{u}}_h), \underline{\mathbf{v}}_h] + s_h(\underline{\mathbf{u}}_h, \underline{\mathbf{v}}_h) = (f, v_h)_{0,\Omega} =: [F_h, \underline{\mathbf{v}}_h], \tag{3.44}$$

where $[\cdot,\cdot]$ represents the duality product, $V(h) := \underline{\mathbf{U}}_h^k$, $\mathbb{A}_h : V(h) \to V(h)'$ and $\mathbb{N}_h : V(h) \to V(h)'$ are the nonlinear operators induced by A_h and N_h, respectively. In particular,

$$[\mathbb{N}_h(\underline{\mathbf{w}}_h), \underline{\mathbf{v}}_h] := \int_\Omega \mathbf{a}(\cdot, G_h^k \underline{\mathbf{w}}_h) \cdot G_h^k \underline{\mathbf{v}}_h \quad \forall\, \underline{\mathbf{w}}_h\,,\, \underline{\mathbf{v}}_h \in V(h).$$

Now, we can ensure the existence of the Gâteaux derivative of $\mathbb{N}_h$ at each $\underline{\mathbf{z}}_h \in V(h)$, thanks to the assumption ***(H.1)***, as the bounded bilinear form $D\mathbb{N}_h(\underline{\mathbf{z}}_h) : V(h) \times V(h) \to \mathbb{R}$, given by

$$\begin{aligned}
D\mathbb{N}_h(\underline{\mathbf{z}}_h)(\underline{\mathbf{v}}_h, \underline{\mathbf{w}}_h) &= \lim_{t\to 0} \frac{[\mathbb{N}_h(\underline{\mathbf{z}}_h + t\underline{\mathbf{v}}_h), \underline{\mathbf{w}}_h] - [\mathbb{N}_h(\underline{\mathbf{z}}_h), \underline{\mathbf{w}}_h]}{t} \\
&= \lim_{t\to 0} \frac{\displaystyle\sum_{T\in\mathcal{T}_h} \Big\{ \big(\mathbf{a}(\cdot, G_T^k \underline{\mathbf{z}}_T + t G_T^k \underline{\mathbf{v}}_T), G_T^k \underline{\mathbf{w}}_T\big)_T - \big(\mathbf{a}(\cdot, G_T^k \underline{\mathbf{z}}_T), G_T^k \underline{\mathbf{w}}_T\big)_T \Big\}}{t} \\
&= \sum_{T\in\mathcal{T}_h} \left(\lim_{t\to 0} \frac{\mathbf{a}(\cdot, G_T^k \underline{\mathbf{z}}_T + t G_T^k \underline{\mathbf{v}}_T) - \mathbf{a}(\cdot, G_T^k \underline{\mathbf{z}}_T)}{t}, G_T^k \underline{\mathbf{w}}_T \right)_T \\
&= \sum_{T\in\mathcal{T}_h} \int_T (G_T^k \underline{\mathbf{v}}_T)^{\mathtt{t}}\, D\mathbf{a}(\cdot, G_T^k \underline{\mathbf{z}}_T)\, G_T^k \underline{\mathbf{w}}_T \\
&= \int_\Omega \big(G_h^k \underline{\mathbf{w}}_h\big)^{\mathtt{t}}\, D\mathbf{a}(\cdot, G_h^k \underline{\mathbf{z}}_h)\, G_h^k \underline{\mathbf{v}}_h \quad \forall\, \underline{\mathbf{w}}_h, \underline{\mathbf{v}}_h \in V(h)\,,
\end{aligned} \tag{3.45}$$

where $D\mathbf{a}(\cdot, G_h^k \underline{\mathbf{z}}_h)$ denotes the jacobian matrix of $\mathbf{a}$ at $G_h^k \underline{\mathbf{z}}_h$. As consequence, we define $D\mathbb{A}_h(\underline{\mathbf{z}}_h) : V(h) \times V(h) \to \mathbb{R}$ as the bilinear form

$$D\mathbb{A}_h(\underline{\mathbf{z}}_h)(\underline{\mathbf{v}}_h, \underline{\mathbf{w}}_h) := D\mathbb{N}_h(\underline{\mathbf{z}}_h)(\underline{\mathbf{v}}_h, \underline{\mathbf{w}}_h) + s_h(\underline{\mathbf{v}}_h, \underline{\mathbf{w}}_h) \quad \forall\, \underline{\mathbf{v}}_h\,,\, \underline{\mathbf{w}}_h \in V(h)\,. \tag{3.46}$$

In what follows, we assume that the jacobian tensor $D\mathbf{a}(\cdot,\boldsymbol{\theta})$ is symmetric for all $\boldsymbol{\theta} \in [L^2(\Omega)]^d$, and that $D\mathbb{N}_h$ is *hemi-continuous*, that is for any $\underline{\mathbf{v}}_h\,,\,\underline{\mathbf{w}}_h \in V(h)$, the mapping $\mathbb{R} \ni \mu \to D\mathbb{N}_h(\underline{\mathbf{v}}_h + \mu\,\underline{\mathbf{w}}_h)(\underline{\mathbf{w}}_h,\cdot) \in V(h)'$ is continuous. Thus, applying the mean value theorem to the referred mapping of real variable, there exists $\mu_0 \in (0,1)$ such that

$$\begin{aligned}
[\mathbb{N}_h(\underline{\mathbf{I}}_h^k u) - \mathbb{N}_h(\underline{\mathbf{u}}_h), \underline{\mathbf{v}}_h] &= \int_0^1 \frac{d}{d\mu}\Big\{[\mathbb{N}_h(\mu\,\underline{\mathbf{I}}_h^k u + (1-\mu)\,\underline{\mathbf{u}}_h), \underline{\mathbf{v}}_h]\Big\} d\mu \\
&= \int_0^1 D\mathbb{N}_h(\mu\,\underline{\mathbf{I}}_h^k u + (1-\mu)\,\underline{\mathbf{u}}_h)(\underline{\mathbf{I}}_h^k u - \underline{\mathbf{u}}_h, \underline{\mathbf{v}}_h)\, d\mu \\
&= D\mathbb{N}_h(\mu_0\,\underline{\mathbf{I}}_h^k u + (1-\mu_0)\,\underline{\mathbf{u}}_h)(\underline{\mathbf{I}}_h^k u - \underline{\mathbf{u}}_h, \underline{\mathbf{v}}_h) \quad \forall\, \underline{\mathbf{v}}_h \in V(h)\,.
\end{aligned}$$

Then by introducing $\tilde{\underline{\mathbf{u}}}_h := \mu_0\,\underline{\mathbf{I}}_h^k u + (1-\mu_0)\,\underline{\mathbf{u}}_h \in V(h)$, which is a convex combination of $\underline{\mathbf{I}}_h^k u$ and $\underline{\mathbf{u}}_h$, we have that

$$D\mathbb{N}_h(\tilde{\underline{\mathbf{u}}}_h)(\underline{\mathbf{I}}_h^k u - \underline{\mathbf{u}}_h, \underline{\mathbf{v}}_h) = [\mathbb{N}_h(\underline{\mathbf{I}}_h^k u) - \mathbb{N}_h(\underline{\mathbf{u}}_h), \underline{\mathbf{v}}_h] \quad \forall\, \underline{\mathbf{v}}_h \in V(h)\,. \tag{3.47}$$

Further, it follows from (3.46) and (3.47), that

$$D\mathbb{A}_h(\tilde{\underline{\mathbf{u}}}_h)(\underline{\mathbf{I}}_h^k u - \underline{\mathbf{u}}_h, \underline{\mathbf{v}}_h) = [\mathbb{A}_h(\underline{\mathbf{I}}_h^k u) - \mathbb{A}_h(\underline{\mathbf{u}}_h), \underline{\mathbf{v}}_h] \quad \forall\, \underline{\mathbf{v}}_h \in V(h)\,. \tag{3.48}$$

Next, we establish the following linear auxiliary problem with additional elliptic regularity assumption: Given $g \in L^2(\Omega)$, we let $z \in U := H_0^1(\Omega)$ be the unique solution of

$$-\mathrm{div}(\widetilde{\boldsymbol{K}}\nabla z)) = g \quad \text{in } \Omega, \tag{3.49a}$$

$$z = 0 \quad \text{on } \partial\Omega, \tag{3.49b}$$

with $\widetilde{\boldsymbol{K}} \in [L^\infty(\mathcal{T}_h)]^{d\times d}$, such that $\widetilde{\boldsymbol{K}}|_T := D\mathbf{a}(\cdot, G_T^k \underline{\mathbf{u}}_T)$, for each $T \in \mathcal{T}_h$. Assuming further regularity on $\widetilde{\boldsymbol{K}}$ so that $z \in U \cap H^2(\Omega)$ and $\widetilde{\boldsymbol{K}}\,\nabla z \in [H^1(\Omega)]^d$, there exists $C_{\mathrm{ell}} > 0$ only depending on Ω, such that:

$$||z||_{H^2(\Omega)} \le C_{\mathrm{ell}}\,||g||_{0,\Omega} \quad \text{and} \quad ||\widetilde{\boldsymbol{K}}\,\nabla z||_{H^1(\Omega)^d} \le C_{\mathrm{ell}}\,||g||_{0,\Omega}\,. \tag{3.50}$$

This holds, for example, when Ω is convex, and the tensor $\widetilde{\boldsymbol{K}}$ is symmetric and Lipschitz continuous (cf. [110]). We also consider the HHO formulation of problem (3.49): *Find* $\underline{\mathbf{z}}_h \in V_h$ *such that*

$$D\mathbb{A}_h(\tilde{\underline{\mathbf{u}}}_h)(\underline{\mathbf{z}}_h, \underline{\mathbf{v}}_h) = (g, v_h)_{0,\Omega} =: [\tilde{F}_h, \underline{\mathbf{v}}_h] \quad \forall\, \underline{\mathbf{v}}_h \in V_h. \tag{3.51}$$

We emphasize that invoking Theorem 4.16 in [66] with $r = 0$, and applying (3.50), we derive

$$||\underline{\mathbf{I}}_h^k z - \underline{\mathbf{z}}_h||_{\epsilon,h} \lesssim h\,||g||_{0,\Omega}\,. \tag{3.52}$$

Further, we introduce another nonlinear operator $\widehat{\mathbb{N}}_h : [L^2(\Omega)]^d \to [L^2(\Omega)]^d$ as

$$[\widehat{\mathbb{N}}_h(\boldsymbol{\theta}), \boldsymbol{\zeta}] := \sum_{T\in\mathcal{T}_h} \big(\mathbf{a}(\cdot, \boldsymbol{\theta}|_T), \boldsymbol{\zeta}\big)_T \quad \forall\, \boldsymbol{\theta}\,, \boldsymbol{\zeta} \in [L^2(\Omega)]^d. \tag{3.53}$$

Then, the corresponding Gâteaux derivative of $\widehat{\mathbb{N}}_h$ at each $\boldsymbol{\theta} \in [L^2(\Omega)]^d$ is given by

$$D\widehat{\mathbb{N}}_h(\boldsymbol{\theta})(\boldsymbol{\eta}, \boldsymbol{\zeta}) := \sum_{T\in\mathcal{T}_h} \big(D\mathbf{a}(\cdot, \boldsymbol{\theta}|_T)\,\boldsymbol{\eta}, \boldsymbol{\zeta}\big)_T, \quad \forall\, \boldsymbol{\eta}\,, \boldsymbol{\zeta} \in [L^2(\Omega)]^d. \tag{3.54}$$

Now, assuming that $D\widehat{\mathbb{N}}_h$ is hemi-continuous, we ensure that there exists $\widehat{\boldsymbol{\theta}} \in [L^2(\Omega)]^d$, a convex combination of ∇u and $\pi_h^k \nabla u$, such that

$$D\widehat{\mathbb{N}}_h(\widehat{\boldsymbol{\theta}})(\nabla u - \pi_h^k \nabla u, \boldsymbol{\zeta}) = [\widehat{\mathbb{N}}_h(\nabla u) - \widehat{\mathbb{N}}_h(\pi_h^k \nabla u), \boldsymbol{\zeta}] \quad \forall\, \boldsymbol{\zeta} \in [L^2(\Omega)]^d. \tag{3.55}$$

Then, introducing $\widehat{\boldsymbol{\theta}}_T := \widehat{\boldsymbol{\theta}}|_T$, we set $\widehat{\boldsymbol{K}} \in [L^\infty(\mathcal{T}_h)]^{d\times d}$ such that $\widehat{\boldsymbol{K}}|_T := D\mathbf{a}(\cdot, \widehat{\boldsymbol{\theta}}_T)$, and we can derive the following representation of $D\widehat{\mathbb{N}}_h(\widehat{\boldsymbol{\theta}})$ as the bilinear form

$$D\widehat{\mathbb{N}}_h(\widehat{\boldsymbol{\theta}})(\boldsymbol{\eta}, \boldsymbol{\zeta}) := \sum_{T\in\mathcal{T}_h} \big(\widehat{\boldsymbol{K}}\boldsymbol{\eta}, \boldsymbol{\zeta}\big)_T, \quad \forall\, \boldsymbol{\eta}\,, \boldsymbol{\zeta} \in [L^2(\Omega)]^d\,. \tag{3.56}$$

Theorem 3.6.2 (Error estimate of L^2-projection of the potential) *Under the same hypothesis given in Theorem 3.6.1, and assuming that $\widehat{\boldsymbol{K}} \in [W^{1,\infty}(\mathcal{T}_h)]^{d\times d}$. Let a integer $k \geq 0$ be fixed, and for all $h \in \mathcal{H}$, we take the additional regularity $u \in H^{q+2}(\mathcal{T}_h)$ and $\mathbf{a}(\cdot, \nabla u) \in H^{q+1}(\mathcal{T}_h)$, for some $q \in \{0, \cdots, k\}$. Then, for $k \geq 1$, there holds*

$$\|\pi_h^k u - u_h\|_{0,\Omega} \lesssim h^{q+2}\Big(\big(1 + |\widehat{\boldsymbol{K}}|_{[W^{1,\infty}(\mathcal{T}_h)]^{d\times d}}\big)\,\|u\|_{H^{q+2}(\mathcal{T}_h)} + \|\mathbf{a}(\cdot, \nabla u)\|_{[H^{q+1}(\mathcal{T}_h)]^d}\Big). \tag{3.57}$$

Moreover, when $k = 0$, assuming that $f \in H^1(\mathcal{T}_h)$, there holds

$$\|\pi_h^0 u - u_h\|_{0,\Omega} \lesssim h^2\Big(\big(1 + |\widehat{\boldsymbol{K}}|_{[W^{1,\infty}(\mathcal{T}_h)]^{d\times d}}\big)\,\|u\|_{H^2(\mathcal{T}_h)} + \|\mathbf{a}(\cdot, \nabla u)\|_{[H^1(\mathcal{T}_h)]^d} + \|f\|_{H^1(\mathcal{T}_h)}\Big). \tag{3.58}$$

Proof. From problem (3.51), with $g := \pi_h^k u - u_h \in L^2(\Omega)$ and $\underline{\mathbf{v}}_h := \underline{\mathbf{I}}_h^k u - \underline{\mathbf{u}}_h \in V_h$, we derive

$$||\pi_h^k u - u_h||_{0,\Omega}^2 = [\tilde{F}_h, \underline{\mathbf{I}}_h^k u - \underline{\mathbf{u}}_h] \;=\; D\mathbb{A}_h(\tilde{\underline{\mathbf{u}}}_h)(\underline{\mathbf{z}}_h, \underline{\mathbf{I}}_h^k u - \underline{\mathbf{u}}_h)\,.$$

Now, as $D\mathbb{A}_h(\tilde{\underline{\mathbf{u}}}_h)$ is symmetric, we apply (3.48) to deduce

$$\begin{aligned} ||\pi_h^k u - u_h||_{0,\Omega}^2 &= [\mathbb{A}_h(\underline{\mathbf{I}}_h^k u) - \mathbb{A}_h(\underline{\mathbf{u}}_h), \underline{\mathbf{z}}_h] \\ &= \underbrace{\Big\{[\mathbb{A}_h(\underline{\mathbf{I}}_h^k u), \underline{\mathbf{z}}_h - \underline{\mathbf{I}}_h^k z] \;-\; [F_h, \underline{\mathbf{z}}_h - \underline{\mathbf{I}}_h^k z]\Big\}}_{\mathfrak{T}_1} + \underbrace{\Big\{[\mathbb{A}_h(\underline{\mathbf{I}}_h^k u), \underline{\mathbf{I}}_h^k z] \;-\; [F_h, \underline{\mathbf{I}}_h^k z]\Big\}}_{\mathfrak{T}_2}\,. \end{aligned} \tag{3.59}$$

Since $\mathfrak{T}_1$ in (3.59) corresponds to the consistency error of (3.44), $\mathcal{E}_h(u; \underline{\mathbf{z}}_h - \underline{\mathbf{I}}_h^k z)$, we invoke (3.32) with $r = q$, and after taking into account (3.52), we obtain

$$\begin{aligned} |\mathfrak{T}_1| &\lesssim h^{q+1}\Big(\|u\|_{H^{q+2}(\mathcal{T}_h)} + \|\mathbf{a}(\cdot, \nabla u)\|_{[H^{q+1}(\mathcal{T}_h)]^d}\Big)\, \|\underline{\mathbf{I}}_h^k z - \underline{\mathbf{z}}_h\|_{\epsilon,h} \\ &\lesssim h^{q+1}\Big(\|u\|_{H^{q+2}(\mathcal{T}_h)} + \|\mathbf{a}(\cdot, \nabla u)\|_{[H^{q+1}(\mathcal{T}_h)]^d}\Big)\, h\, \|\pi_h^k u - u_h\|_{0,\Omega}\,. \end{aligned} \tag{3.60}$$

On the other hand, we notice that $\mathfrak{T}_2$ in (3.59) is the consistence term $\mathcal{E}_h(u; \underline{\mathbf{I}}_h^k z)$. Here, we consider two cases.

(i.A) $\boldsymbol{k \geq 1}$**.** We proceed as in the derivation of (3.36), to have

$$\begin{aligned} \mathcal{E}_h(u; \underline{\mathbf{I}}_h^k z) = &\underbrace{\sum_{T\in\mathcal{T}_h} \big(\mathbf{a}(\cdot, \pi_T^k \nabla u) - \mathbf{a}(\cdot, \nabla u), \pi_T^k \nabla z\big)_T}_{\mathfrak{J}_1} \\ &\underbrace{+ \sum_{T\in\mathcal{T}_h}\sum_{F\in\mathcal{F}_T} \big([\mathbf{a}(\cdot, \nabla u) - \pi_T^k \mathbf{a}(\cdot, \nabla u)] \cdot \boldsymbol{n}_{TF}, \pi_F^k z - \pi_T^k z\big)_F}_{\mathfrak{J}_2} \\ &\underbrace{- s_h(\underline{\mathbf{I}}_h^k u, \underline{\mathbf{I}}_h^k z).}_{\mathfrak{J}_3} \end{aligned} \tag{3.61}$$

We bound $\mathfrak{J}_2$ applying Cauchy-Schwarz, resulting

$$|\mathfrak{J}_2| \leq \left(\sum_{T\in\mathcal{T}_h}\sum_{F\in\mathcal{F}_T} \|\mathbf{a}(\cdot, \nabla u) - \pi_T^k \mathbf{a}(\cdot, \nabla u)\|_F^2\right)^{1/2} \left(\sum_{T\in\mathcal{T}_h}\sum_{F\in\mathcal{F}_T} \|\pi_F^k z - \pi_T^k z\|_F^2\right)^{1/2},$$

By approximation property (3.6), with $m = 0$ and $s := q + 1$, we obtain

$$\|\mathbf{a}(\cdot, \nabla u) - \pi_T^k \mathbf{a}(\cdot, \nabla u)\|_F \;\lesssim\; h_T^{q+1/2} ||\mathbf{a}(\cdot, \nabla u)||_{H^{q+1}(T)^d}\,. \tag{3.62}$$

Similarly, applying approximation property (3.6), we infer

$$\|\pi_F^k z - \pi_T^k z\|_F \leq ||z - \pi_T^k z||_F \lesssim h_T^{3/2} \|z\|_{H^2(T)}. \tag{3.63}$$

Then, from (3.62), (3.63), and (3.50), with $g := \pi_h^k u - u_h$, we derive

$$|\mathfrak{J}_2| \lesssim h^{q+2} ||\mathbf{a}(\cdot, \nabla u)||_{H^{q+1}(\mathcal{T}_h)} \|\pi_h^k u - u_h\|_{0,\Omega}. \tag{3.64}$$

Now, we bound $\mathfrak{J}_3$, using (3.25) with $r := q$ for u, and $r := 0$ for z, and the first elliptic regularity estimate in (3.50), yielding to

$$\begin{aligned} |\mathfrak{J}_3| &\leq s_h(\underline{\mathbf{I}}_h^k u, \underline{\mathbf{I}}_h^k u)^{1/2} \, s_h(\underline{\mathbf{I}}_h^k z, \underline{\mathbf{I}}_h^k z)^{1/2} \\ &\lesssim h^{q+1} \, \|u\|_{H^{q+2}(\mathcal{T}_h)} \, h \, \|z\|_{H^2(\Omega)} \\ &\lesssim h^{q+2} \, \|u\|_{H^{q+2}(\mathcal{T}_h)} \, \|\pi_h^k u - u_h\|_{0,\Omega}. \end{aligned} \tag{3.65}$$

Finally, to bound $\mathfrak{J}_1$, we invoke the bilinear form (3.56), obtaining

$$\begin{aligned} \mathfrak{J}_1 &= D\widehat{\mathbb{N}}_h(\widehat{\boldsymbol{\theta}})(\nabla u - \pi_h^k \nabla u, \pi_h^k \nabla z) \\ &= \sum_{T \in \mathcal{T}_h} \big(\widehat{\boldsymbol{K}}(\nabla u - \pi_T^k \nabla u), \pi_T^k \nabla z\big)_T \\ &= \underbrace{\sum_{T \in \mathcal{T}_h} \big(\widehat{\boldsymbol{K}}(\nabla u - \pi_T^k \nabla u), \pi_T^k \nabla z - \pi_T^0 \nabla z\big)_T}_{\mathfrak{J}_{1,1}} \\ &\quad + \underbrace{\sum_{T \in \mathcal{T}_h} \big(\nabla u - \pi_T^k \nabla u, \widehat{\boldsymbol{K}} \pi_T^0 \nabla z - \pi_T^0(\widehat{\boldsymbol{K}} \pi_T^0 \nabla z)\big)_T}_{\mathfrak{J}_{1,2}}. \end{aligned}$$

Invoking ***(H.4)***, the fact that $||\pi_T^k \nabla z - \pi_T^0 \nabla z||_T \leq ||\nabla z - \pi_T^0 \nabla z||_T$, and that $\widehat{\boldsymbol{K}}$ is uniformly bounded, we apply approximation property (3.5) and the first elliptic regularity estimate in (3.50), and deduce

$$|\mathfrak{J}_{1,1}| \lesssim h^{q+2} \, ||u||_{H^{q+2}(\mathcal{T}_h)} \, ||\pi_h^k u - u_h||_{0,\Omega}. \tag{3.66}$$

In order to bound $\mathfrak{J}_{1,2}$, we notice that $\pi_T^0(\widehat{\boldsymbol{K}} \pi_T^0 \nabla z) = (\pi_T^0 \widehat{\boldsymbol{K}})(\pi_T^0 \nabla z)$, where $\pi_T^0 \widehat{\boldsymbol{K}}$ is defined componentwise. Then, since $\widehat{\boldsymbol{K}} \in [W^{1,\infty}(\mathcal{T}_h)]^{d \times d}$, we invoke the *tensorial version of* Theorem 1.45 in [66], and establish that $||\widehat{\boldsymbol{K}} - \pi_T^0 \widehat{\boldsymbol{K}}||_{[W^{0,\infty}(T)]^{d \times d}} \lesssim h_T \, |\widehat{\boldsymbol{K}}|_{[W^{1,\infty}(\mathcal{T}_h)]^{d \times d}}$. Now, after applying again approximation properties (3.5) as in (3.66), it yields

$$|\mathfrak{J}_{1,2}| \lesssim |\widehat{\boldsymbol{K}}|_{[W^{1,\infty}(\mathcal{T}_h)]^{d \times d}} \, h^{q+2} \, \|u\|_{H^{q+2}(\mathcal{T}_h)} \, \|\pi_h^k u - u_h\|_{0,\Omega}. \tag{3.67}$$

Then, from (3.64), (3.65), (3.66), and (3.67), we deduce the estimate for $\mathcal{E}_h(u;\underline{\mathbf{I}}_h^k z)$ in (3.61), and (3.57) is concluded.

(i.B) $\boldsymbol{k=0}$. We can rewrite

$$\begin{aligned}\mathcal{E}_h(u;\underline{\mathbf{I}}_h^0 z) =&[\mathbb{A}(\underline{\mathbf{I}}_h^0 u)-\mathbb{A}(\underline{\mathbf{u}}_h),\underline{\mathbf{I}}_h^0 z]\\ &=\sum_{T\in\mathcal{T}_h}\left(\mathbf{a}(\cdot,\pi_T^0\nabla u),\pi_T^0\nabla z\right)_T+s_h(\underline{\mathbf{I}}_h^0 u,\underline{\mathbf{I}}_h^0 z)-\sum_{T\in\mathcal{T}_h}(f,\pi_T^0 z)_T\,. \end{aligned}\tag{3.68}$$

Playing with the definition of π_T^0, we obtain

$$(f,\pi_T^0 z)_T=(\pi_T^0 f,z)_T=(\pi_T^0 f-f,z-\pi_T^0 z)+(f,z)_T\,.\tag{3.69}$$

Then, from (3.68) and (3.69), and the fact $(\pi_T^0\nabla z-\nabla z,\pi_T^0\mathbf{a}(\cdot,\nabla u))_T=0$ for all $T\in\mathcal{T}_h$, we deduce

$$\begin{aligned}\mathcal{E}_h(u;\underline{\mathbf{I}}_h^0 z)=&\sum_{T\in\mathcal{T}_h}\left(\mathbf{a}(\cdot,\pi_T^0\nabla u),\pi_T^0\nabla z\right)_T-(f,z)_\Omega\\ &+s_h(\underline{\mathbf{I}}_h^0 u,\underline{\mathbf{I}}_h^0 z)+\sum_{T\in\mathcal{T}_h}(\pi_T^0 f-f,\pi_T^0 z-z)_T\\ =&\underbrace{\sum_{T\in\mathcal{T}_h}\left(\mathbf{a}(\cdot,\pi_T^0\nabla u)-\mathbf{a}(\cdot,\nabla u),\pi_T^0\nabla z\right)_T}_{\mathfrak{T}_1}\\ &+\underbrace{\sum_{T\in\mathcal{T}_h}\left(\mathbf{a}(\cdot,\nabla u)-\pi_T^0\mathbf{a}(\cdot,\nabla u),\pi_T^0\nabla z-\nabla z\right)_T}_{\mathfrak{T}_2}\\ &+\underbrace{s_h(\underline{\mathbf{I}}_h^0 u,\underline{\mathbf{I}}_h^0 z)}_{\mathfrak{T}_3}+\underbrace{\sum_{T\in\mathcal{T}_h}(\pi_T^0 f-f,\pi_T^0 z-z)_T}_{\mathfrak{T}_4}\,. \end{aligned}\tag{3.70}$$

$\mathfrak{T}_2$, $\mathfrak{T}_3$ and $\mathfrak{T}_4$ are bounded by applying Cauchy-Schwarz inequality and very well-known approximation property (3.5). Then, after take into account the first elliptic regularity estimate in (3.50), we find

$$|\mathfrak{T}_2|\lesssim h^2\,||\mathbf{a}(\cdot,\nabla u)||_{[H^1(\mathcal{T}_h)]^d}\,||\pi_h^0 u-u_h||_{0,\Omega}\tag{3.71}$$

$$|\mathfrak{T}_3|\lesssim h^2\,||u||_{H^2(\mathcal{T}_h)}\,||\pi_h^0 u-u_h||_{0,\Omega}\tag{3.72}$$

$$|\mathfrak{T}_4|\lesssim h^2\,||f||_{H^1(\mathcal{T}_h)}\,||\pi_h^0 u-u_h||_{0,\Omega}\,.\tag{3.73}$$

Now, we aim to bound the remaining term $\mathfrak{T}_1$. First, we notice that

$$\begin{aligned}\mathfrak{T}_1 &= D\widehat{\mathbb{N}}_h(\widehat{\boldsymbol{\theta}})(\nabla u - \pi_h^0\nabla u, \pi_h^0\nabla z)\\ &= \sum_{T\in\mathcal{T}_h}\big(\widehat{\boldsymbol{K}}(\nabla u - \pi_T^0\nabla u), \pi_T^0\nabla z\big)_T\\ &= \sum_{T\in\mathcal{T}_h}\big(\nabla u - \pi_T^0\nabla u, \widehat{\boldsymbol{K}}\pi_T^0\nabla z - \pi_T^0(\widehat{\boldsymbol{K}}\pi_T^0\nabla z)\big)_T\,.\end{aligned}$$

Then, proceeding in analogous way for bounding $\mathfrak{J}_{1,2}$, we derive

$$|\mathfrak{T}_1| \lesssim |\widehat{\boldsymbol{K}}|_{[W^{1,\infty}(\mathcal{T}_h)]^{d\times d}}\, h^2\, \|u\|_{H^2(\mathcal{T}_h)}\, \|\pi_h^k u - u_h\|_{0,\Omega}\,. \tag{3.74}$$

As a result, we establish

$$|\mathcal{E}_h(u;\underline{\mathbf{I}}_h^0 z)| \lesssim h^2\Big(\big(1+|\widehat{\boldsymbol{K}}|_{[W^{1,\infty}(\mathcal{T}_h)]^{d\times d}}\big)\,\|u\|_{H^2(\mathcal{T}_h)} + \|\mathbf{a}(\cdot,\nabla u)\|_{[H^1(\mathcal{T}_h)]^d} + \|f\|_{H^1(\mathcal{T}_h)}\Big)\,, \tag{3.75}$$

and the estimate (3.58) is implied. □

Now, we establish another important result.

Theorem 3.6.3 (L^2-error estimate of reconstructive potential) *Under the same assumptions of Theorem 3.6.2, elliptic regularity (3.50), we have, for $k\geq 1$:*

$$\|p_h^{k+1}\underline{\mathbf{u}}_h - u\|_{0,\Omega} \lesssim h^{q+2}\Big(\big(1+|\widehat{\boldsymbol{K}}|_{[W^{1,\infty}(\mathcal{T}_h)]^{d\times d}}\big)\,\|u\|_{H^{q+2}(\mathcal{T}_h)} + \|\mathbf{a}(\cdot,\nabla u)\|_{H^{q+1}(\mathcal{T}_h)^d}\Big)\,, \tag{3.76}$$

for some $q\in\{0,\cdots,k\}$. Moreover, when $k=0$, assuming that $f\in H^1(\mathcal{T}_h)$, there holds

$$\|p_h^1\underline{\mathbf{u}}_h - u\|_{0,\Omega} \lesssim h^2\Big(\big(1+|\widehat{\boldsymbol{K}}|_{[W^{1,\infty}(\mathcal{T}_h)]^{d\times d}}\big)\,\|u\|_{H^2(\mathcal{T}_h)} + \|\mathbf{a}(\cdot,\nabla u)\|_{H^1(\mathcal{T}_h)^d} + \|f\|_{H^1(\mathcal{T}_h)}\Big)\,. \tag{3.77}$$

Proof. We proceed as in the proof of Theorem 2.32 from [66]. First, we take $\breve{u}_h := p_h^{k+1}\underline{\mathbf{I}}_h^k(u)$, and applying triangle inequality, we have

$$\|p_h^{k+1}\underline{\mathbf{u}}_h - u\|_{0,\Omega} \leq \underbrace{\|u-\breve{u}_h\|_{0,\Omega}}_{\mathfrak{T}_1} + \underbrace{\|p_h^{k+1}(\widehat{\underline{\mathbf{u}}}_h - \underline{\mathbf{u}}_h)\|_{0,\Omega}}_{\mathfrak{T}_2}\,. \tag{3.78}$$

Next, after invoking (3.15) with $s:=q$, we derive

$$\mathfrak{T}_1 \lesssim h^{q+2}\|u\|_{H^{q+2}(\mathcal{T}_h)}\,. \tag{3.79}$$

Now, using the local Poincaré–Wirtinger (3.4) and the fact

$$\Big(p_T^{k+1}(\widehat{\underline{\mathbf{u}}}_T - \underline{\mathbf{u}}_T) - \pi_T^0(\widehat{u}_T - u_T), 1\Big)_T = 0 \quad \forall T \in \mathcal{T}_h\,,$$

we obtain, after applying triangle inequality

$$\begin{aligned}\mathfrak{T}_2^2 &\lesssim \sum_{T\in\mathcal{T}_h} \big\{\|p_h^{k+1}(\widehat{\underline{\mathbf{u}}}_h - \underline{\mathbf{u}}_h) - \pi_T^0(\widehat{u}_T - u_T)\|_T^2 \;+\; ||\pi_T^0(\widehat{u}_T - u_T)||_T^2\big\} \\ &\lesssim \underbrace{\sum_{T\in\mathcal{T}_h} h_T^2\|\nabla p_T^{k+1}(\widehat{\underline{\mathbf{u}}}_T - \underline{\mathbf{u}}_T)\|_T^2}_{\mathfrak{E}_1} + \underbrace{\sum_{T\in\mathcal{T}_h} \|\pi_T^0(\widehat{u}_T - u_T)\|_T^2}_{\mathfrak{E}_2}\,. \end{aligned} \tag{3.80}$$

We observe that, $\mathfrak{E}_1$ is bounded thanks to Lemma 3.4.1 and Theorem 3.6.1, while the boundedness of $\mathfrak{E}_2$ is deduced by invoking Theorem 3.6.2. Finally, (3.79) and (3.80) help us to bound (3.78), and we conclude the proof.

□

3.7 Other boundary conditions

Here, we briefly discuss how the HHO scheme is written for nonhomogeneous Dirichlet, mixed, and nonhomogeneous Neumann boundary conditions, and hint at the modifications required for establishing the corresponding a priori error estimates.

3.7.1 Nonhomogeneous Dirichlet boundary conditions

We consider the nonlinear problem

$$-\operatorname{div}(\mathbf{a}(\cdot,\nabla u)) \;=\; f \quad \text{in} \quad \Omega\,, \qquad u = g \quad \text{on} \quad \partial\Omega\,, \tag{3.81}$$

with $g \in H^{1/2}(\partial\Omega)$. Denoting by $\gamma : H^1(\Omega) \to H^{1/2}(\partial\Omega)$ the trace operator, the continuous weak formulation is expressed as: *Find* $u \in H_g^1(\Omega) := \{w \in H^1(\Omega) : \gamma(w) = g\}$ *such that*

$$(\mathbf{a}(\cdot,\nabla u), \nabla v)_\Omega = (f, v)_\Omega \quad \forall v \in H_0^1(\Omega)\,. \tag{3.82}$$

Now, if we decompose $u = u_0 + u_g$, such that $u_0 \in H_0^1(\Omega)$ and $u_g \in H_g^1(\Omega)$, then we can rewrite (3.82) as: *Find* $u_0 \in H_0^1(\Omega)$ *such that*

$$(\mathbf{a}(\cdot,\nabla u_0 + \nabla u_g), \nabla v)_\Omega = (f, v)_\Omega \quad \forall v \in H_0^1(\Omega)\,. \tag{3.83}$$

The problem (3.83) is well-posed, since its associated nonlinear form results to be also Lipschitz continuous and strongly monotone in $H_0^1(\Omega)$. Now, to establish the HHO discrete scheme corresponding to (3.83), we follow the ideas given in Subsection 7.1 in [64], and introduce $\underline{\mathbf{w}}_{g,h} := \Big((w_{g,T})_{T\in\mathcal{T}_h}, (w_{g,F})_{F\in\mathcal{F}_h}\Big) \in \underline{\mathbf{U}}_h^k$ such that

$$w_{g,T} = 0 \quad \forall T \in \mathcal{T}_h\,, \qquad w_{g,F} = 0 \quad \forall F \in \mathcal{F}_h^{\mathtt{int}}\,, \qquad w_{g,F} = \pi_F^k g \quad \forall F \in \mathcal{F}_h^{\mathtt{b}}\,.$$

In order to show a procedure to compute $\underline{\mathbf{u}}_h$, the HHO-approximation of the solution of (3.83), we decompose it as $\underline{\mathbf{u}}_h := \underline{\mathbf{u}}_{0,h} + \underline{\mathbf{w}}_{g,h}$, with $\underline{\mathbf{u}}_{0,h} \in \underline{\mathbf{U}}_{h,0}^k$. As a result, the proposed HHO formulation reads as: *Find* $\underline{\mathbf{u}}_{0,h} \in \underline{\mathbf{U}}_{h,0}^k$ *such that*

$$A_h(\underline{\mathbf{u}}_{0,h} + \underline{\mathbf{w}}_{g,h}, \underline{\mathbf{v}}_h) = b_h(\underline{\mathbf{v}}_h) \quad \forall \underline{\mathbf{v}}_h \in \underline{\mathbf{U}}_{h,0}^k\,, \tag{3.84}$$

with A_h and b_h defined as in (3.17). The well-posedness of (3.84) also relies on Lipschitz continuity and strong monotonocity properties. It is not difficult to establish similar results to Theorems 3.6.1, 3.6.2 and 3.6.3 in this situation.

3.7.2 Mixed boundary conditions

We consider a nonlinear problem (3.2) with mixed boundary conditions, for which we assume that there exists a partition $\{\Gamma_D, \Gamma_N\}$ of the boundary $\Gamma := \partial\Omega$, such that $\Gamma = \Gamma_N \cup \Gamma_D$, $\mathring{\Gamma}_N \cap \mathring{\Gamma}_D = \emptyset$ and $|\Gamma_D| > 0$. Then, the nonlinear problem with mixed boundary conditions reads as: *Find* $u : \Omega \to \mathbb{R}$ *such that*

$$-\mathrm{div}(\mathbf{a}(\cdot, \nabla u)) = f \quad \text{in } \Omega\,, \tag{3.85a}$$

$$\mathbf{a}(\cdot, \nabla u)\cdot \boldsymbol{n} = g_N \quad \text{on } \Gamma_N\,, \tag{3.85b}$$

$$u = g_D \quad \text{on } \Gamma_D\,, \tag{3.85c}$$

where $f \in L^2(\Omega)$, $g_N \in L^2(\Gamma_N)$, $g_D \in H^{1/2}(\Gamma_D)$, and $\boldsymbol{n}$ denotes the exterior unit normal to Γ. We notice that (3.85) does not degenerate into the pure Neumann case. The continuous weak formulation of (3.85) reads as: *Find* $u \in H_*^1(\Omega) := \{w \in H^1(\Omega) \,:\, w|_{\Gamma_D} = g_D\}$ *such that*

$$(\mathbf{a}(\cdot, \nabla u), \nabla v)_\Omega = (f, v)_\Omega + (g_N, v)_{\Gamma_N} \quad \forall v \in H_D^1(\Omega) := \{w \in H^1(\Omega) \,:\, w|_{\Gamma_D} = 0\}\,. \tag{3.86}$$

The well-posedness of (3.86) follows from [92]. Next, for the HHO discretization, we require the following hypothesis.

Assumption 3.7.1 *$\mathcal{T}_h$ fits the partition $\{\Gamma_D, \Gamma_N\}$, in the sense that we can define two sets, $\mathcal{F}_h^{\mathtt{D}} := \{F \in \mathcal{F}_h^{\mathtt{b}} \,:\, F \subset \Gamma_D\}$ and $\mathcal{F}_h^{\mathtt{N}} := \{F \in \mathcal{F}_h^{\mathtt{b}} \,:\, F \subset \Gamma_N\}$, such that $\mathcal{F}_h^{\mathtt{D}} \cup \mathcal{F}_h^{\mathtt{N}} = \mathcal{F}_h^{\mathtt{b}}$.*

Next, we introduce the discrete spaces

$$\underline{\mathbf{U}}_{h,g_D,D}^k := \{\underline{\mathbf{w}}_h \in \underline{\mathbf{U}}_h^k \,:\, w_F = \pi_F^k g_D \;\forall F \in \mathcal{F}_h^{\mathtt{D}}\}\,. \tag{3.87}$$

Then, the HHO discretization of (3.86) reads as: Find $\underline{\mathbf{u}}_h \in \underline{\mathbf{U}}_{h,g_D,D}^k$ such that

$$A_h(\underline{\mathbf{u}}_h, \underline{\mathbf{v}}_h) = (f, v_h)_\Omega + \sum_{F\in\mathcal{F}_h^{\mathtt{N}}} (g_N, v_F)_F =: b_h(\underline{\mathbf{v}}_h) \quad \forall \underline{\mathbf{v}}_h \in \underline{\mathbf{U}}_{h,0,D}^k\,. \tag{3.88}$$

with A_h defined as in (3.17). Now, to compute $\underline{\mathbf{u}}_h$, we can proceed as described in the previous subsection. This motivates the introduction of $\underline{\mathbf{w}}_{g_D,h} := \Big((w_{g_D,T})_{T\in\mathcal{T}_h}, (w_{g_D,F})_{F\in\mathcal{F}_h}\Big) \in \underline{\mathbf{U}}_{h,g_D,D}^k$, such that

$$w_{g_D,T} = 0 \quad \forall T \in \mathcal{T}_h\,, \qquad w_{g_D,F} = 0 \quad \forall F \in \mathcal{F}_h^{\mathtt{int}}\,, \qquad w_{g_D,F} = 0 \quad \forall F \in \mathcal{F}_h^{\mathtt{N}}\,.$$

After that, we compute $\underline{\mathbf{u}}_h = \underline{\mathbf{u}}_{0,h} + \underline{\mathbf{w}}_{g_D,h}$, where $\underline{\mathbf{u}}_{0,h} \in \underline{\mathbf{U}}_{h,0,D}^k$ verifies

$$A_h(\underline{\mathbf{u}}_{0,h} + \underline{\mathbf{w}}_{g_D,h}, \underline{\mathbf{v}}_h) = (f, v_h)_\Omega + \sum_{F\in\mathcal{F}_h^{\mathtt{N}}} (g_N, v_F)_F =: b_h(\underline{\mathbf{v}}_h) \quad \forall \underline{\mathbf{v}}_h \in \underline{\mathbf{U}}_{h,0,D}^k\,, \tag{3.89}$$

where the nonlinear form A_h is defined as in (3.17).

3.7.3 Nonhomogeneous Neumann boundary condition

Now, we consider a nonlinear problem with pure Neumann condition: Find $u : \Omega \to \mathbb{R}$ such that

$$-\mathrm{div}(\mathbf{a}(\cdot, \nabla u)) = f \quad \text{in } \Omega\,, \tag{3.90a}$$

$$\mathbf{a}(\cdot, \nabla u)\cdot\mathbf{n} = g \quad \text{on } \Gamma\,, \tag{3.90b}$$

$$\int_\Omega u = 0\,, \tag{3.90c}$$

where $f \in L^2(\Omega)$, $g \in L^2(\Gamma)$. We look for the continuous weak solution in the Hilbert space

$$U := \{v \in H^1(\Omega) \,:\, (v,1)_\Omega = 0\}\,. \tag{3.91}$$

The corresponding weak formulation to (3.90) is given as: *Find* $u \in U$ *such that*

$$(\mathbf{a}(\cdot,\nabla u),\nabla v)_\Omega = (f,v)_\Omega + (g,v)_\Gamma \quad \forall v \in U\,. \tag{3.92}$$

Now, applying the HHO approach, we seek the discrete weak solution of (3.92) in the discrete space

$$\underline{\mathbf{U}}_h^{k,0} := \left\{ \underline{\mathbf{v}}_h \in \underline{\mathbf{U}}_h^k \,:\, \sum_{T\in\mathcal{T}_h} (v_T,1)_T = 0 \right\}. \tag{3.93}$$

Then, the associated discrete HHO scheme reads as: *Find* $\underline{\mathbf{u}}_h \in \underline{\mathbf{U}}_h^{k,0}$ *such that*

$$A_h(\underline{\mathbf{u}}_h,\underline{\mathbf{v}}_h) = (f,v_h)_\Omega + \sum_{F\in\mathcal{F}_h} (g,v_F)_F =: b_h(\underline{\mathbf{v}}_h) \quad \forall\, \underline{\mathbf{v}}_h \in \underline{\mathbf{U}}_h^{k,0}\,. \tag{3.94}$$

with the nonlinear form A_h given as in (3.17). The problem (3.94) has been analised in a more general context in [66, Chapter 6], but the authors have only developed the a priori error analysis for the p-Laplacian nonlinear operator, which does not satisfy our hypotheses here, unless $p = 2$ (that is the linear Laplacian operator). Their a priori error analysis does not cover our proposed kind of nonlinear operators.

3.8 Numerical results

In this section, we present a comprehensive set of numerical tests with different boundary conditions, each of one with its corresponding explicit exact solution. We start by introducing the families of polytopal meshes we consider in our numerical computations. We call them: Simplicial I (cf. Figure 3.14), Cartesian (cf. Figure 3.15), Hexagonal (cf. Figure 3.18), and Tilted hexagonal (cf. Figure 3.19), which can be downloaded from `https://github.com/wareHHOuse/diskpp`. Other families of meshes are called Graduated (Cartesian with hanging nodes) as in Figure 3.16 and Fractured (cf. Figure 3.20), which can be founded in FVCA 5 benchmark [119]. We

also consider a family of Trapezoidal (cf. Figure 3.17) and uniform refined simplicial (Simplicial II) meshes (cf. Figure 3.21).

We remark that Example (3.8.1) provides HHO approximations for the nonlinear model problem (3.2), while Examples (3.8.2)-(3.8.5) solve (3.84), testing the robustness of the scheme considering smooth and nonsmooth solutions. Examples (3.8.6)-(3.8.7) deal with (3.85) and (3.90), respectively. In all examples, we compute the following errors:

- L^2-projection of potential error: $\|\pi_h^k u - u_h\|_{0,\Omega}$,
- Flux error: $\|\nabla u - G_h^k \underline{\mathbf{u}}_h\|_{0,\Omega}$,
- Reconstructive potential error: $\|u - p_h^{k+1}\underline{\mathbf{u}}_h\|_{0,\Omega}$.

We also remak that we have considered different families of polytopal meshes, and three nonlinear functions $\mathbf{a}$, that satisfy the hypotheses ***(H.1)***, ***(H.2)***, ***(H.3)***, and ***(H.4)***. The list of examples with their corresponding nonlinear function $\mathbf{a}$, the exact solution, domain, polytopal meshes considered (see Section 3.8.8), and type of boundary conditions (B.C.), are resumed in Table 3.1.

For each one of the examples presented here, we approximate the exact solution with piecewise polynomials of degree at most k, with $k \in \{0, 1, 2, 3, 4\}$. Besides, the experimental order of convergence ($rate$), is computed as

$$rate = \log(e_{\mathcal{T}}/e_{\widetilde{\mathcal{T}}})/\log(h_{\mathcal{T}}/h_{\widetilde{\mathcal{T}}}),$$

where $e_{\mathcal{T}}$ and $e_{\widetilde{\mathcal{T}}}$ represent the errors associated to two consecutive meshes $\mathcal{T}$ and $\widetilde{\mathcal{T}}$, respectively.

The nonlinear algebraic system, obtained from (3.17), is solved by Newton's method with the initial guess given by the solution of the associated Poisson problem. This choice leads to a considerable reduction of the number of iterations, instead of using the usual null initial guess. We also consider a tolerance of 10^{-10} for the corresponding residual, and fixed the maximum number of Newton's iterations in 10. The number of iterations needed to attain the prescribed tolerance, in all the examples presented here, is ≤ 5.

Ex.	$\mathbf{a}(\cdot,\boldsymbol{\zeta})$	u	Ω	Polytopal Mesh	B.C.
1	$\left(1+\frac{1}{1+\lvert\boldsymbol{\zeta}\rvert^2}\right)\boldsymbol{\zeta}$	$\sin(\pi x)\sin(\pi y)$	Square	Fractured Hexagonal	Dirichlet
2	$\left(1+\exp(-\lvert\boldsymbol{\zeta}\rvert^2)\right)\boldsymbol{\zeta}$	$\exp(x+\pi y)$	Square	Graduated	Dirichlet
3	$\left(2+\frac{1}{1+\lvert\boldsymbol{\zeta}\rvert}\right)\boldsymbol{\zeta}$	$\cos\left(\frac{\pi}{2}y\right)+\chi(x)x^{3.5}$	Square	Simplicial III	Dirichlet
4	$\left(2+\frac{1}{1+\lvert\boldsymbol{\zeta}\rvert}\right)\boldsymbol{\zeta}$	$\cos\left(\frac{\pi}{2}y\right)+\chi(x)x^{3.5}$	L-shaped	Simplicial II	Dirichlet
5	$\left(2+\frac{1}{1+\lvert\boldsymbol{\zeta}\rvert}\right)\boldsymbol{\zeta}$	$r^{2/3}\sin(2\theta/3)$	L-shaped	Simplicial II	Dirichlet
6	$\left(1+\exp(-\lvert\boldsymbol{\zeta}\rvert^2)\right)\boldsymbol{\zeta}$	$\sin(\pi x)\sin(\pi y)$	Square	Cartesian Hexagonal	Mixed
7	$\left(1+\frac{1}{1+\lvert\boldsymbol{\zeta}\rvert^2}\right)\boldsymbol{\zeta}$	$\exp(x+\pi y)-\text{Cte.}$	Square	Trapezoidal Tilted	Neumann

Table 3.1: Summary of data for the 7 examples

The computational code is based on the one developed by Di Pietro in [75], which is described in [39]. However, we have implemented the computations of the modified versions of the discrete gradient and potential operators (cf. (3.10) and (3.12)). The static condensation procedure has been implemented right after the assembling of the local matrices of the linearized problem over the global system. This allows us to recompute, on each iteration, the volumetric terms.

3.8.1 Example 1

We consider the nonlinear problem (3.2) with homogeneous Dirichlet boundary condition, defined in the convex domain $\Omega := (0,1)^2$, and with nonlinear coeffcient $\mathbf{a}(\cdot,\boldsymbol{\zeta}) := \left(1+\frac{1}{1+|\boldsymbol{\zeta}|^2}\right)\boldsymbol{\zeta}$, for all $\boldsymbol{\zeta}\in\mathbb{R}^2$. The datum f is chosen so that the exact solution is given by the smooth function $u(x,y)=\sin(\pi x)\sin(\pi y)$. Here, we consider two families of polytopal meshes: a nonconforming one, that we have called Fractured in Table 3.1 (cf. Figure 3.20), and conforming meshes with hexagonal-dominant cells (cf. Figure 3.18). Tables 3.2 and 3.3 show the history of convergence of potential, flux, and reconstructive potential errors, when the exact solution is approximated with piecewise polynomials of degree at most $k\in\{0,1,2,3,4\}$,

computed using families of Fractured and Hexagonal meshes, respectively. From both tables, we notice that the scheme converges with the order of convergence of the aforementioned errors behaves as $\mathcal{O}(h^{k+2})$, $\mathcal{O}(h^{k+1})$ and $\mathcal{O}(h^{k+2})$, respectively. These are in agreement with Theorems 3.6.1 and 3.6.2. Figures 3.1 and 3.3 resume the information provided in Tables 3.2 and 3.3, respectively.

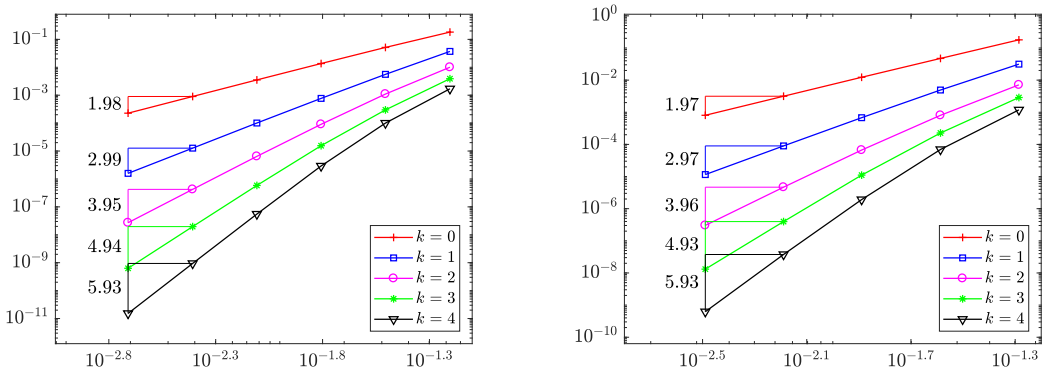

(a) Fractured

(b) Hexagonal

Figure 3.1: Rates of convergence of potential error vs. h (Example 1)

Table 3.2: Histories of convergence of potential, flux, and reconstructive potential errors, considering $k \in \{0, 1, 2, 3, 4\}$ (Example 1 - Fractured meshes)

Potential										
	$k=0$		$k=1$		$k=2$		$k=3$		$k=4$	
h	error	rate	error	rate	error	rate	error	rate	error	rate
6.25e-02	1.82e-01		3.70e-02		1.00e-02		3.89e-03		1.70e-03	
3.12e-02	5.14e-02	1.821	5.58e-03	2.725	1.10e-03	3.185	2.98e-04	3.701	1.00e-04	4.074
1.56e-02	1.36e-02	1.917	7.69e-04	2.860	9.06e-05	3.600	1.55e-05	4.262	2.91e-06	5.103
7.81e-03	3.53e-03	1.952	1.01e-04	2.937	6.45e-06	3.819	5.86e-07	4.737	5.52e-08	5.733
3.91e-03	9.00e-04	1.976	1.27e-05	2.994	4.24e-07	3.936	1.96e-08	4.907	9.41e-10	5.885
1.95e-03	2.27e-04	1.979	1.59e-06	2.990	2.71e-08	3.954	6.31e-10	4.943	1.52e-11	5.927
Flux										
	$k=0$		$k=1$		$k=2$		$k=3$		$k=4$	
h	error	rate	error	rate	error	rate	error	rate	error	rate
6.25e-02	1.04e-01		3.08e-02		9.07e-03		3.40e-03		1.36e-03	
3.12e-02	2.91e-02	1.837	7.68e-03	1.999	1.88e-03	2.265	4.20e-04	3.013	1.39e-04	3.284
1.56e-02	7.80e-03	1.898	1.78e-03	2.106	2.60e-04	2.855	3.57e-05	3.556	7.19e-06	4.268
7.81e-03	2.08e-03	1.907	3.53e-04	2.343	2.81e-05	3.215	2.39e-06	3.904	2.20e-07	5.041
3.91e-03	5.39e-04	1.955	6.15e-05	2.523	2.46e-06	3.519	1.27e-07	4.248	5.91e-09	5.227
1.95e-03	1.37e-04	1.972	9.97e-06	2.617	1.88e-07	3.701	6.38e-09	4.295	1.50e-10	5.275
Reconstructive potential										
	$k=0$		$k=1$		$k=2$		$k=3$		$k=4$	
h	error	rate	error	rate	error	rate	error	rate	error	rate
6.25e-02	1.94e-01		3.82e-02		1.01e-02		3.90e-03		1.70e-03	
3.12e-02	5.37e-02	1.850	5.71e-03	2.737	1.10e-03	3.189	2.98e-04	3.702	1.00e-04	4.075
1.56e-02	1.41e-02	1.926	7.83e-04	2.868	9.08e-05	3.601	1.55e-05	4.262	2.91e-06	5.103
7.81e-03	3.65e-03	1.956	1.02e-04	2.942	6.46e-06	3.820	5.86e-07	4.737	5.52e-08	5.733
3.91e-03	9.30e-04	1.977	1.29e-05	2.997	4.24e-07	3.937	1.96e-08	4.907	9.41e-10	5.885
1.95e-03	2.35e-04	1.980	1.60e-06	2.992	2.71e-08	3.954	6.31e-10	4.943	1.52e-11	5.927

Table 3.3: Histories of convergence of potential, flux, and reconstructive potential errors, considering $k \in \{0, 1, 2, 3, 4\}$ (Example 1 - Hexagonal meshes)

Potential										
	$k=0$		$k=1$		$k=2$		$k=3$		$k=4$	
h	error	rate	error	rate	error	rate	error	rate	error	rate
5.18e-02	1.79e-01		3.14e-02		7.13e-03		2.88e-03		1.19e-03	
2.59e-02	4.73e-02	1.920	4.92e-03	2.675	8.04e-04	3.148	2.26e-04	3.669	6.94e-05	4.096
1.29e-02	1.23e-02	1.939	6.78e-04	2.844	6.67e-05	3.572	1.11e-05	4.329	1.92e-06	5.151
6.47e-03	3.15e-03	1.968	8.98e-05	2.930	4.67e-06	3.854	3.97e-07	4.824	3.75e-08	5.699
3.24e-03	8.06e-04	1.973	1.15e-05	2.969	3.02e-07	3.959	1.31e-08	4.927	6.22e-10	5.927
Flux										
	$k=0$		$k=1$		$k=2$		$k=3$		$k=4$	
h	error	rate	error	rate	error	rate	error	rate	error	rate
5.18e-02	1.96e-01		2.05e-02		6.27e-03		2.53e-03		1.34e-03	
2.59e-02	7.63e-02	1.361	4.83e-03	2.082	1.18e-03	2.412	3.10e-04	3.027	1.18e-04	3.499
1.29e-02	2.87e-02	1.404	1.11e-03	2.114	1.83e-04	2.676	3.15e-05	3.280	5.72e-06	4.346
6.47e-03	1.08e-02	1.416	2.07e-04	2.428	2.53e-05	2.865	2.66e-06	3.584	2.32e-07	4.646
3.24e-03	3.99e-03	1.438	3.28e-05	2.666	3.09e-06	3.039	1.94e-07	3.785	8.22e-09	4.828
Reconstructive potential										
	$k=0$		$k=1$		$k=2$		$k=3$		$k=4$	
h	error	rate	error	rate	error	rate	error	rate	error	rate
5.18e-02	1.96e-01		3.19e-02		7.17e-03		2.88e-03		1.19e-03	
2.59e-02	5.04e-02	1.960	4.97e-03	2.682	8.06e-04	3.153	2.26e-04	3.670	6.95e-05	4.097
1.29e-02	1.28e-02	1.962	6.83e-04	2.847	6.67e-05	3.575	1.11e-05	4.329	1.92e-06	5.151
6.47e-03	3.27e-03	1.981	9.03e-05	2.932	4.67e-06	3.855	3.97e-07	4.824	3.75e-08	5.699
3.24e-03	8.31e-04	1.981	1.16e-05	2.970	3.02e-07	3.959	1.31e-08	4.927	6.22e-10	5.927

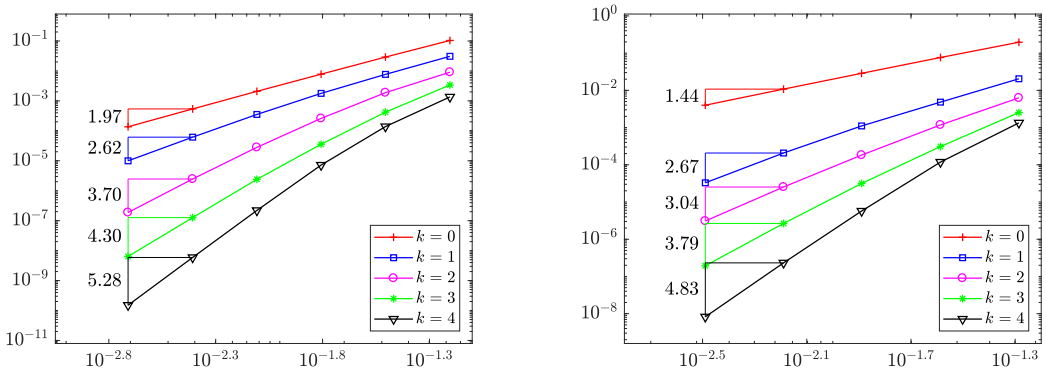

(a) Fractured (b) Hexagonal

Figure 3.2: Rates of convergence of flux error vs. h (Example 1)

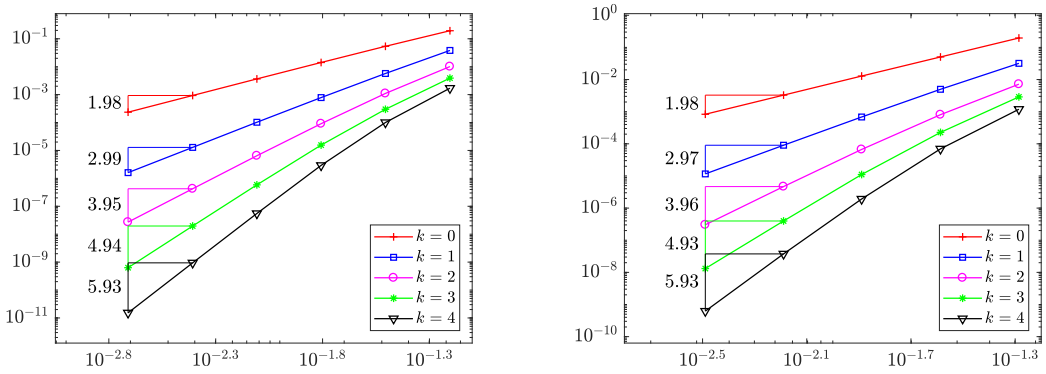

(a) Fracture (b) Hexagonal

Figure 3.3: Rates of convergence of reconstructive potential errors (Example 1)

3.8.2 Example 2

Here, we solve the HHO discrete nonlinear scheme (3.84), corresponding to the nonlinear problem (3.81). We take $\Omega := (0,1)^2$ as the domain, and the nonlinear coefficient $\mathbf{a}(\cdot,\boldsymbol{\zeta}) := \big(1+\exp(-|\boldsymbol{\zeta}|^2)\big)\boldsymbol{\zeta}$, for all $\boldsymbol{\zeta} \in \mathbb{R}^2$. We choose the data f and g so that the solution u is the smooth function given by $u(x,y) := \exp(x + \pi\, y)$. The family of meshes considered for this example, corresponds to a (nonconforming) graduated rectangular meshes (cf. Figure 3.16). Figure 3.4 shows the well behavior of the potential, flux and reconstructive potential errors, measure in the L^2-norm, with respect to the nonhomogeneous. Table 3.4 contains their respective histories

of convergence, which are in agreement with Theorems 3.6.1, 3.6.2 and 3.6.3. We point out that for $k = 4$, round-off errors are probably affecting the flux error in the last refinement iteration mesh. On the other hand, the apparent super-convergence phenomenon for the flux error (for $k \in \{0, 1, 2\}$) meshes, could be linked to the fact that the mesh quality improves when refining.

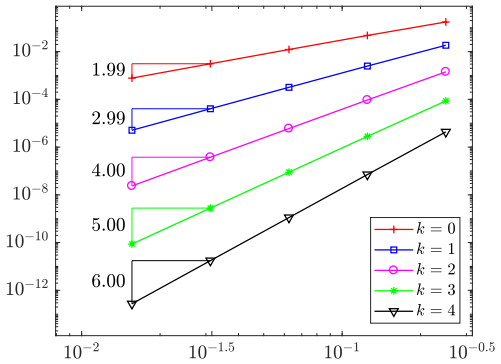

(a) Potential error vs. h

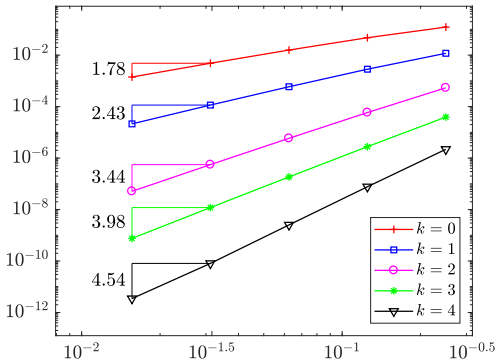

(b) Flux error vs. h

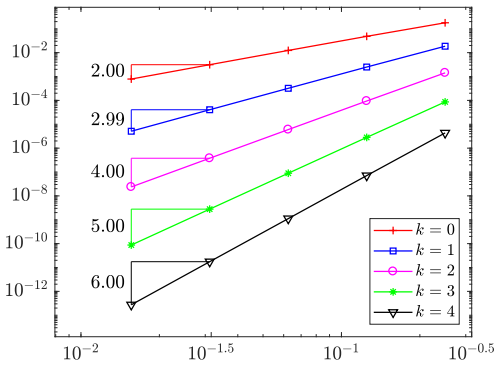

(c) Reconstructive potential error vs. h

Figure 3.4: Rates of convergence of potential, flux and reconstructive potential errors (Example 2)

Table 3.4: Histories of convergence of potential, flux, and reconstructive potential errors, considering $k \in \{0, 1, 2, 3, 4\}$ (Example 2 - Graduated meshes)

Potential										
	$k=0$		$k=1$		$k=2$		$k=3$		$k=4$	
h	error	rate	error	rate	error	rate	error	rate	error	rate
2.50e-01	1.74e-01		1.84e-02		1.42e-03		8.61e-05		4.33e-06	
1.25e-01	4.74e-02	1.878	2.48e-03	2.895	9.37e-05	3.921	2.81e-06	4.940	7.05e-08	5.939
6.25e-02	1.22e-02	1.953	3.19e-04	2.959	5.97e-06	3.973	8.86e-08	4.985	1.11e-09	5.984
3.12e-02	3.10e-03	1.979	4.03e-05	2.975	3.76e-07	3.980	2.78e-09	4.984	1.75e-11	5.982
1.56e-02	7.77e-04	1.995	5.07e-06	2.992	2.36e-08	3.995	8.69e-11	4.999	2.72e-13	6.004
Flux										
	$k=0$		$k=1$		$k=2$		$k=3$		$k=4$	
h	error	rate	error	rate	error	rate	error	rate	error	rate
2.50e-01	1.23e-01		1.18e-02		5.38e-04		3.92e-05		2.20e-06	
1.25e-01	4.75e-02	1.372	2.84e-03	2.054	5.88e-05	3.192	2.78e-06	3.818	7.69e-08	4.835
6.25e-02	1.58e-02	1.592	5.92e-04	2.263	5.86e-06	3.327	1.85e-07	3.910	2.53e-09	4.927
3.12e-02	4.84e-03	1.700	1.15e-04	2.360	5.57e-07	3.389	1.19e-08	3.945	8.09e-11	4.955
1.56e-02	1.41e-03	1.778	2.13e-05	2.427	5.12e-08	3.443	7.58e-10	3.977	3.47e-12	4.543
Reconstructive Potential										
	$k=0$		$k=1$		$k=2$		$k=3$		$k=4$	
h	error	rate	error	rate	error	rate	error	rate	error	rate
2.50e-01	1.79e-01		1.86e-02		1.43e-03		8.64e-05		4.33e-06	
1.25e-01	4.82e-02	1.889	2.50e-03	2.896	9.41e-05	3.922	2.81e-06	4.940	7.07e-08	5.939
6.25e-02	1.24e-02	1.959	3.21e-04	2.960	6.00e-06	3.973	8.89e-08	4.985	1.12e-09	5.984
3.12e-02	3.13e-03	1.982	4.06e-05	2.976	3.78e-07	3.980	2.79e-09	4.984	1.75e-11	5.982
1.56e-02	7.85e-04	1.996	5.10e-06	2.992	2.37e-08	3.995	8.71e-11	4.999	2.74e-13	5.998

3.8.3 Example 3

Now, we consider a nonhomogeneous Dirichlet nonlinear problem, defined in the convex domain $\Omega = (-1, 1)^2$. The nonlinear coefficient is setting as $\mathbf{a}(\cdot, \boldsymbol{\zeta}) := \big(2 +$

$\frac{1}{1+|\boldsymbol{\zeta}|}\big)\boldsymbol{\zeta}$, for all $\boldsymbol{\zeta} \in \mathbb{R}^2$, and the exact solution is given by $u(x,y) = \cos\left(\frac{\pi}{2}y\right) + \chi(x)x^{3.5}$, where $\chi(x)$ denotes the characteristic function on $[0,1]$ with respect to x. The HHO approximations are computed considering a family of uniform refined simplicial meshes, that we have called Simplicial-III (cf. Figure 3.22). We remark that $u \in H^4(\Omega)$ but does not belong to $H^{4+\epsilon}(\Omega)$, for all $\epsilon > 0$. We report the histories of convergence of the potential, flux and reconstructive potential errors, with respect to the nonhomogeneous, in Table 3.5. The results are in agreement with the corresponding versions of Theorems 3.6.1, 3.6.2 and 3.6.3, since the solution u has a limited regularity. This is the reason why we observe the optimal rates of convergence only for $k \in \{0,1,2\}$. In Figure 3.5 we display convergence results for the refined triangulations and polynomial degrees up to 4.

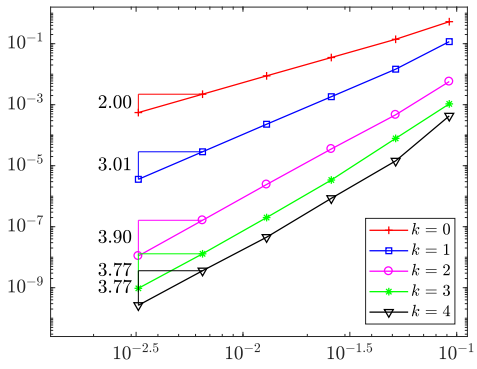

(a) Potential error vs. h

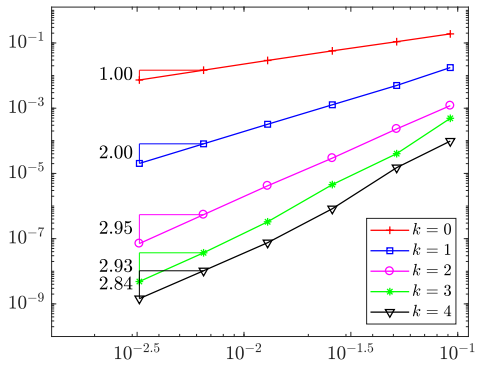

(b) Flux error vs. h

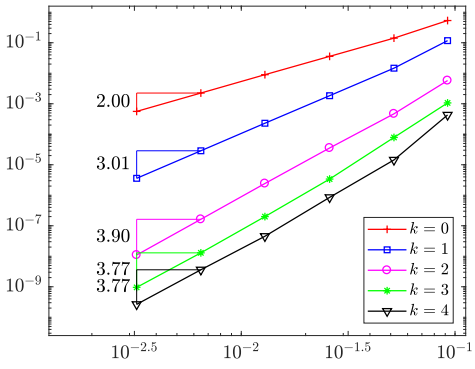

(c) Reconstructive potential error vs. h

Figure 3.5: Rates of convergence of potential, flux and reconstructive potential errors (Example 3)

Table 3.5: Histories of convergence of potential, flux, and reconstructive potential errors, considering $k \in \{0, 1, 2, 3, 4\}$ (Example 3 - Simplicial-III meshes)

Potential										
	$k=0$		$k=1$		$k=2$		$k=3$		$k=4$	
h	error	rate	error	rate	error	rate	error	rate	error	rate
9.23e-02	5.27e-01		1.17e-01		5.74e-03		1.06e-03		4.29e-04	
5.18e-02	1.39e-01	2.302	1.46e-02	3.600	4.66e-04	4.346	7.85e-05	4.512	1.44e-05	5.881
2.59e-02	3.52e-02	1.985	1.83e-03	2.997	3.54e-05	3.720	3.39e-06	4.531	8.51e-07	4.077
1.29e-02	8.82e-03	1.985	2.29e-04	2.982	2.42e-06	3.848	1.99e-07	4.067	4.52e-08	4.211
6.47e-03	2.21e-03	2.008	2.86e-05	3.013	1.62e-07	3.915	1.29e-08	3.965	3.60e-09	3.667
3.24e-03	5.52e-04	2.004	3.58e-06	3.007	1.10e-08	3.897	9.54e-10	3.768	2.65e-10	3.774
Flux										
	$k=0$		$k=1$		$k=2$		$k=3$		$k=4$	
h	error	rate	error	rate	error	rate	error	rate	error	rate
9.23e-02	1.90e-01		1.76e-02		1.20e-03		4.90e-04		9.81e-05	
5.18e-02	1.09e-01	0.953	4.98e-03	2.187	2.32e-04	2.845	4.04e-05	4.321	1.50e-05	3.246
2.59e-02	5.73e-02	0.934	1.27e-03	1.967	2.95e-05	2.973	4.55e-06	3.149	8.28e-07	4.183
1.29e-02	2.91e-02	0.971	3.22e-04	1.973	4.17e-06	2.805	3.29e-07	3.768	7.52e-08	3.441
6.47e-03	1.46e-02	0.997	8.09e-05	2.001	5.44e-07	2.952	3.69e-08	3.171	1.04e-08	2.873
3.24e-03	7.33e-03	1.000	2.03e-05	2.000	7.08e-08	2.950	4.85e-09	2.933	1.45e-09	2.844
Reconstructive potential										
	$k=0$		$k=1$		$k=2$		$k=3$		$k=4$	
h	error	rate	error	rate	error	rate	error	rate	error	rate
9.23e-02	5.35e-01		1.17e-01		5.77e-03		1.06e-03		4.29e-04	
5.18e-02	1.42e-01	2.301	1.47e-02	3.600	4.68e-04	4.348	7.85e-05	4.513	1.44e-05	5.881
2.59e-02	3.58e-02	1.984	1.84e-03	2.997	3.55e-05	3.721	3.40e-06	4.531	8.51e-07	4.077
1.29e-02	8.97e-03	1.985	2.30e-04	2.982	2.43e-06	3.848	1.99e-07	4.067	4.52e-08	4.211
6.47e-03	2.24e-03	2.008	2.87e-05	3.013	1.63e-07	3.915	1.29e-08	3.965	3.60e-09	3.667
3.24e-03	5.61e-04	2.004	3.59e-06	3.007	1.10e-08	3.897	9.55e-10	3.769	2.65e-10	3.774

3.8.4 Example 4

Here, we consider the same problem as in Example 3.8.3, but defined in the L-shaped domain $\Omega = (-1,1)^2/[0,1]\times[-1,0]$, which is clearly nonconvex. We choose a family of uniform refined simplicial meshes (named Simplicial-II) (cf. Figure 3.21), to establish the HHO formulation. In Figure 3.6 we display convergence results for the refined triangulations and polynomial degrees up to 4. Despite the nonconvexity of the domain, which could not help to ensure the additional regularity require for the L^2-error estimate of the potential as well as of the reconstructive potential, the obtained results behave similarly to the ones provided in Example (3.8.3) (in a convex domain), and are still in agreement with Theorems 3.6.1, 3.6.2 and 3.6.3.

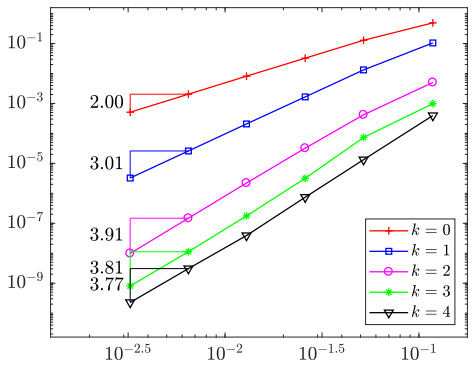

(a) Potential error vs. h

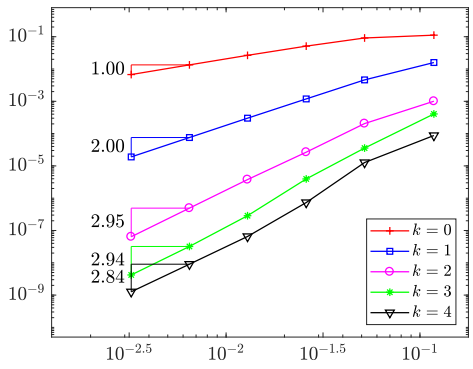

(b) Flux error vs. h

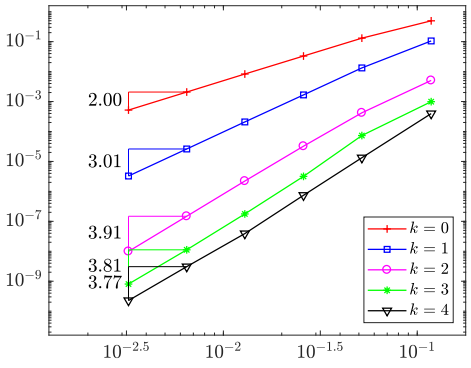

(c) Reconstructive potential error vs. h

Figure 3.6: Rates of convergence of potential, flux and reconstructive potential errors (Example 4)

Table 3.6: Histories of convergence of potential, flux, and reconstructive potential errors, considering $k \in \{0, 1, 2, 3, 4\}$ (Example 4 - Simplicial-II meshes)

Potential										
	$k = 0$		$k = 1$		$k = 2$		$k = 3$		$k = 4$	
h	error	rate	error	rate	error	rate	error	rate	error	rate
1.18e-01	4.91e-01		1.05e-01		5.05e-03		9.89e-04		3.96e-04	
5.18e-02	1.29e-01	1.624	1.32e-02	2.520	4.19e-04	3.023	7.32e-05	3.163	1.33e-05	4.123
2.59e-02	3.26e-02	1.985	1.66e-03	2.994	3.22e-05	3.701	3.17e-06	4.530	7.41e-07	4.164
1.29e-02	8.17e-03	1.985	2.08e-04	2.981	2.21e-06	3.846	1.76e-07	4.143	3.89e-08	4.227
6.47e-03	2.04e-03	2.008	2.60e-05	3.013	1.47e-07	3.922	1.12e-08	3.996	3.06e-09	3.683
3.24e-03	5.11e-04	2.004	3.25e-06	3.006	9.87e-09	3.910	8.05e-10	3.806	2.27e-10	3.766
Flux										
	$k = 0$		$k = 1$		$k = 2$		$k = 3$		$k = 4$	
h	error	rate	error	rate	error	rate	error	rate	error	rate
1.18e-01	1.12e-01		1.59e-02		1.01e-03		4.06e-04		8.74e-05	
5.18e-02	9.14e-02	0.244	4.60e-03	1.505	2.05e-04	1.936	3.57e-05	2.955	1.27e-05	2.343
2.59e-02	5.11e-02	0.838	1.19e-03	1.957	2.66e-05	2.942	3.95e-06	3.176	7.34e-07	4.114
1.29e-02	2.65e-02	0.942	3.00e-04	1.969	3.77e-06	2.804	2.87e-07	3.761	6.52e-08	3.472
6.47e-03	1.34e-02	0.987	7.56e-05	1.999	4.93e-07	2.949	3.20e-08	3.176	9.05e-09	2.863
3.24e-03	6.74e-03	0.997	1.90e-05	2.000	6.40e-08	2.951	4.20e-09	2.938	1.27e-09	2.845
Reconstructive potential										
	$k = 0$		$k = 1$		$k = 2$		$k = 3$		$k = 4$	
h	error	rate	error	rate	error	rate	error	rate	error	rate
1.18e-01	4.96e-01		1.06e-01		5.07e-03		9.90e-04		3.96e-04	
5.18e-02	1.31e-01	1.620	1.33e-02	2.520	4.20e-04	3.025	7.32e-05	3.164	1.33e-05	4.123
2.59e-02	3.31e-02	1.984	1.67e-03	2.994	3.23e-05	3.702	3.17e-06	4.530	7.41e-07	4.164
1.29e-02	8.29e-03	1.984	2.08e-04	2.981	2.21e-06	3.846	1.76e-07	4.143	3.89e-08	4.227
6.47e-03	2.08e-03	2.008	2.61e-05	3.013	1.48e-07	3.922	1.12e-08	3.996	3.07e-09	3.683
3.24e-03	5.19e-04	2.004	3.26e-06	3.006	9.89e-09	3.910	8.05e-10	3.806	2.27e-10	3.766

3.8.5 Example 5

We consider again the L-shaped domain $\Omega := (-1,-1)^2 \backslash [0,1] \times [-1,0]$, with $\Gamma := \partial\Omega$, and another nonlinear coefficient, given by $\mathbf{a}(\cdot,\boldsymbol{\zeta}) := \left(2 + \frac{1}{1+|\boldsymbol{\zeta}|}\right)\boldsymbol{\zeta}$, for all $\boldsymbol{\zeta} \in \mathbb{R}^2$. We choose the data f and g, so that the exact solution u is the nonsmooth function given (in polar coordinates) by $u(r,\theta) = r^{2/3}\sin(2\theta/3)$.

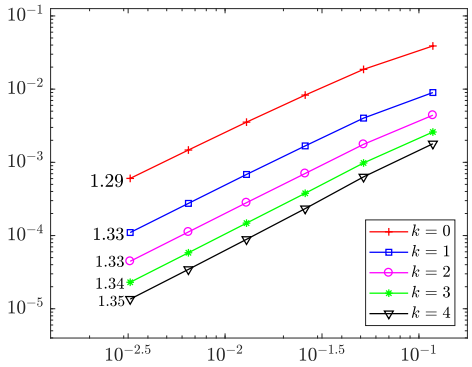

(a) Potential error vs. h

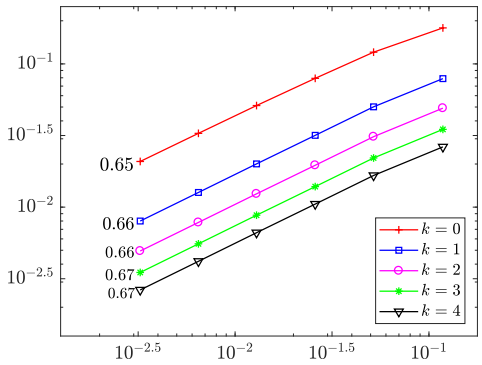

(b) Flux error vs. h

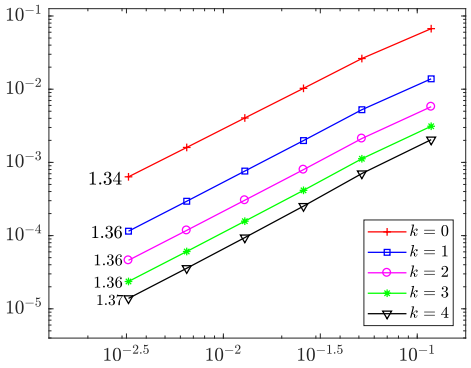

(c) Reconstructive potential error vs. h

Figure 3.7: Rates of convergence of potential, flux and reconstructive potential errors (Example 5)

We point out that $u \in H^{1+\frac{2}{3}-s}(\Omega)$, for an arbitrary small number $s > 0$. We test again over a family of uniform refined simplicial meshes (cf. Figure 3.21). In Figure 3.7 we display the rates of convergence corresponding to the potential, flux and reconstructive potential errors, vs. h, considering polynomials degrees up to 4. The histories of convergence of these errors, are reported in Table 3.7. We observe that

the potential and reconstructive potential errors go to zero at a rate that behaves as $\mathcal{O}(h^{4/3})$, while the flux error decreases to zero as $\mathcal{O}(h^{2/3})$.

Table 3.7: Histories of convergence of potential, flux, and reconstructive potential errors, considering $k \in \{0, 1, 2, 3, 4\}$ (Example 5 - Simplicial II meshes)

Potential										
	$k=0$		$k=1$		$k=2$		$k=3$		$k=4$	
h	error	rate	error	rate	error	rate	error	rate	error	rate
1.18e-01	3.89e-02		8.98e-03		4.41e-03		2.60e-03		1.79e-03	
5.18e-02	1.86e-02	0.894	4.02e-03	0.977	1.76e-03	1.112	9.80e-04	1.183	6.33e-04	1.265
2.59e-02	8.30e-03	1.166	1.68e-03	1.261	7.05e-04	1.323	3.78e-04	1.375	2.33e-04	1.441
1.29e-02	3.54e-03	1.222	6.83e-04	1.288	2.81e-04	1.318	1.48e-04	1.347	8.87e-05	1.386
6.47e-03	1.47e-03	1.271	2.75e-04	1.319	1.12e-04	1.334	5.82e-05	1.350	3.45e-05	1.370
3.24e-03	6.03e-04	1.291	1.10e-04	1.326	4.45e-05	1.334	2.30e-05	1.342	1.35e-05	1.352
Flux										
	$k=0$		$k=1$		$k=2$		$k=3$		$k=4$	
h	error	rate	error	rate	error	rate	error	rate	error	rate
1.18e-01	1.78e-01		7.89e-02		4.91e-02		3.49e-02		2.63e-02	
5.18e-02	1.21e-01	0.474	5.02e-02	0.551	3.10e-02	0.557	2.20e-02	0.559	1.66e-02	0.559
2.59e-02	7.93e-02	0.607	3.17e-02	0.661	1.96e-02	0.663	1.39e-02	0.664	1.05e-02	0.664
1.29e-02	5.12e-02	0.628	2.00e-02	0.659	1.24e-02	0.659	8.78e-03	0.660	6.63e-03	0.660
6.47e-03	3.27e-02	0.648	1.27e-02	0.665	7.82e-03	0.666	5.54e-03	0.667	4.18e-03	0.667
3.24e-03	2.08e-02	0.654	8.00e-03	0.664	4.94e-03	0.665	3.50e-03	0.666	2.64e-03	0.665
Reconstructive potential										
	$k=0$		$k=1$		$k=2$		$k=3$		$k=4$	
h	error	rate	error	rate	error	rate	error	rate	error	rate
1.18e-01	6.71e-02		1.39e-02		5.77e-03		3.12e-03		2.04e-03	
5.18e-02	2.62e-02	1.142	5.24e-03	1.180	2.12e-03	1.216	1.12e-03	1.242	7.04e-04	1.294
2.59e-02	1.03e-02	1.352	1.99e-03	1.401	7.96e-04	1.412	4.15e-04	1.434	2.53e-04	1.479
1.29e-02	4.04e-03	1.337	7.61e-04	1.376	3.05e-04	1.379	1.57e-04	1.392	9.39e-05	1.420
6.47e-03	1.60e-03	1.344	2.95e-04	1.375	1.18e-04	1.375	6.06e-05	1.382	3.58e-05	1.397
3.24e-03	6.35e-04	1.336	1.15e-04	1.362	4.60e-05	1.361	2.36e-05	1.363	1.39e-05	1.371

3.8.6 Example 6

Here, we consider the nonlinear problem with mixed boundary conditions (3.85), defined in the domain $\Omega := (0,1)^2$, with $\Gamma_N = \{1\} \times [0,1]$ and $\Gamma_D := \Gamma \backslash \Gamma_N$. The chosen nonlinear coefficient is given by $\mathbf{a}(\cdot, \boldsymbol{\zeta}) := \big(1 + \exp(-|\boldsymbol{\zeta}|^2)\big)\boldsymbol{\zeta}$, for all $\boldsymbol{\zeta} \in \mathbb{R}^2$, while the data f, g_D and g_N are chosen such that the solution u is given again by $u(x,y) = \sin(\pi x)\sin(\pi y)$. We remark that with this choice, $g_D = 0$. We solve the HHO nonlinear scheme 3.88, considering two families of polytopal meshes. The first one is a family of Cartesian meshes (cf. Figure 3.15), and the second one is a family of Hexagonal-dominant meshes (cf. Figure 3.18). Tables 3.8 and 3.9 report the histories of convergence of the potential, flux and reconstructive potential errors, for the family of Cartesian and the Hexagonal meshes, respectively. We notice certain super-convergence phenomenon for the flux error on the Cartesian (for $k \in \{0,1,2\}$) and Hexagonal (for $k \in \{0,1\}$) meshes, which could be related to the fact that the mesh quality improves when refining. The numerical results provided by this example support the conjecture that the present approach might behave quite well even in a case not fully covered by the theoretical results.

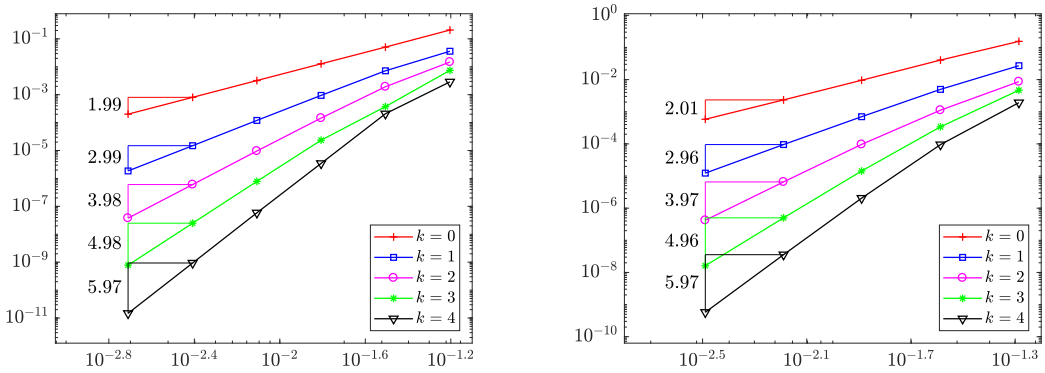

(a) Cartesian

(b) Hexagonal

Figure 3.8: Rates of convergence of potential error vs. h (Example 6)

Table 3.8: Histories of convergence of potential, flux, and reconstructive potential errors, considering $k \in \{0, 1, 2, 3, 4\}$ (Example 6 - Cartesian meshes)

Potential										
	$k=0$		$k=1$		$k=2$		$k=3$		$k=4$	
h	error	rate	error	rate	error	rate	error	rate	error	rate
6.25e-02	2.07e-01		3.60e-02		1.48e-02		7.43e-03		2.88e-03	
3.12e-02	5.06e-02	2.029	7.17e-03	2.321	1.93e-03	2.933	3.74e-04	4.303	2.07e-04	3.786
1.56e-02	1.28e-02	1.985	9.43e-04	2.927	1.45e-04	3.731	2.34e-05	3.996	3.45e-06	5.909
7.81e-03	3.21e-03	1.995	1.20e-04	2.982	9.60e-06	3.924	7.85e-07	4.908	5.87e-08	5.889
3.91e-03	8.04e-04	2.002	1.49e-05	3.014	6.05e-07	3.996	2.49e-08	4.986	9.36e-10	5.982
1.95e-03	2.01e-04	1.992	1.86e-06	2.994	3.78e-08	3.984	7.82e-10	4.976	1.47e-11	5.970
Flux										
	$k=0$		$k=1$		$k=2$		$k=3$		$k=4$	
h	error	rate	error	rate	error	rate	error	rate	error	rate
6.25e-02	9.31e-02		3.61e-02		1.14e-02		6.26e-03		2.88e-03	
3.12e-02	3.76e-02	1.306	9.57e-03	1.910	3.08e-03	1.882	9.44e-04	2.723	2.19e-04	3.712
1.56e-02	1.12e-02	1.749	2.47e-03	1.956	4.10e-04	2.911	5.91e-05	3.999	8.69e-06	4.653
7.81e-03	2.97e-03	1.916	4.91e-04	2.332	4.16e-05	3.309	3.39e-06	4.130	2.48e-07	5.143
3.91e-03	7.60e-04	1.970	7.68e-05	2.682	3.28e-06	3.670	1.76e-07	4.279	6.40e-09	5.284
1.95e-03	1.91e-04	1.984	1.04e-05	2.872	2.24e-07	3.857	9.53e-09	4.187	1.75e-10	5.173
Reconstructive potential										
	$k=0$		$k=1$		$k=2$		$k=3$		$k=4$	
h	error	rate	error	rate	error	rate	error	rate	error	rate
6.25e-02	2.19e-01		3.76e-02		1.48e-02		7.44e-03		2.88e-03	
3.12e-02	5.32e-02	2.035	7.30e-03	2.360	1.93e-03	2.936	3.75e-04	4.301	2.08e-04	3.787
1.56e-02	1.34e-02	1.993	9.58e-04	2.930	1.45e-04	3.731	2.34e-05	3.999	3.45e-06	5.909
7.81e-03	3.35e-03	1.999	1.21e-04	2.986	9.61e-06	3.925	7.85e-07	4.908	5.87e-08	5.889
3.91e-03	8.38e-04	2.003	1.50e-05	3.017	6.05e-07	3.997	2.49e-08	4.986	9.36e-10	5.982
1.95e-03	2.09e-04	1.993	1.87e-06	2.995	3.78e-08	3.984	7.82e-10	4.976	1.47e-11	5.970

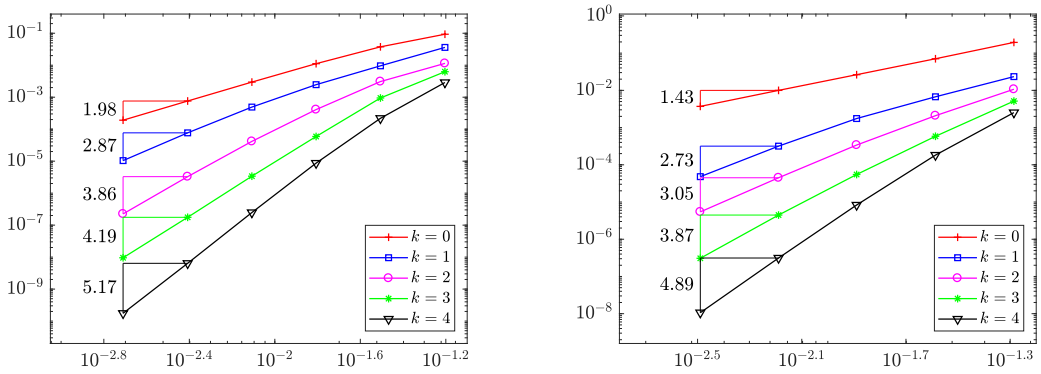

(a) Cartesian (b) Hexagonal

Figure 3.9: Rates of convergence of flux error vs. h (Example 6)

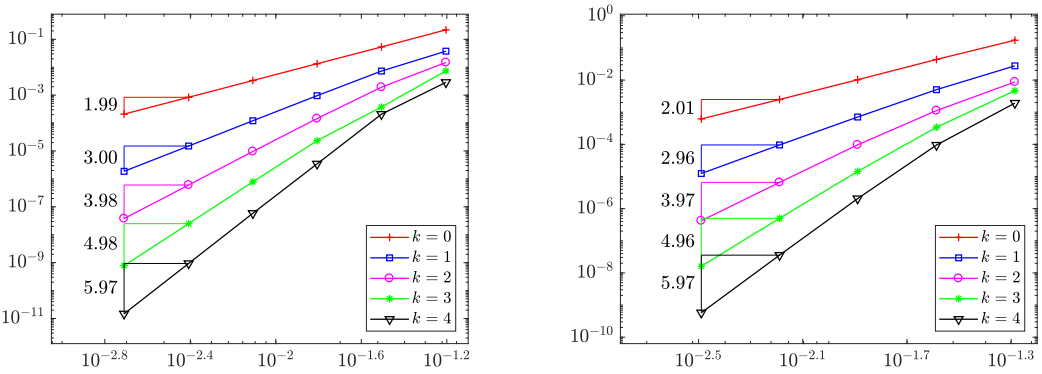

(a) Cartesian (b) Hexagonal

Figure 3.10: Rates of convergence of reconstructive potential errors (Example 6)

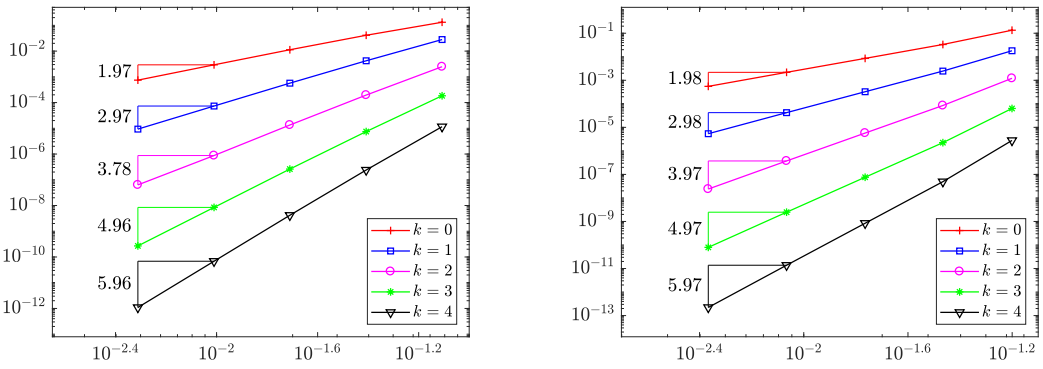

(a) Trapezoidal (b) Tilted

Figure 3.11: Rates of convergence of potential error vs. h (Example 7)

Table 3.9: Histories of convergence of potential, flux, and reconstructive potential errors, considering $k \in \{0, 1, 2, 3, 4\}$ (Example 6 - Hexagonal)

Potential										
	$k=0$		$k=1$		$k=2$		$k=3$		$k=4$	
h	error	rate	error	rate	error	rate	error	rate	error	rate
5.18e-02	1.55e-01		2.71e-02		8.64e-03		4.68e-03		1.92e-03	
2.59e-02	4.05e-02	1.935	4.97e-03	2.446	1.12e-03	2.949	3.39e-04	3.786	9.48e-05	4.340
1.29e-02	9.55e-03	2.073	7.01e-04	2.811	9.64e-05	3.517	1.43e-05	4.540	2.05e-06	5.502
6.47e-03	2.34e-03	2.041	9.53e-05	2.893	6.55e-06	3.897	5.00e-07	4.863	3.57e-08	5.870
3.24e-03	5.84e-04	2.005	1.23e-05	2.958	4.20e-07	3.971	1.62e-08	4.962	5.76e-10	5.966
Flux										
	$k=0$		$k=1$		$k=2$		$k=3$		$k=4$	
h	error	rate	error	rate	error	rate	error	rate	error	rate
5.18e-02	1.94e-01		2.34e-02		1.07e-02		5.15e-03		2.53e-03	
2.59e-02	7.06e-02	1.460	6.72e-03	1.800	2.09e-03	2.360	5.84e-04	3.140	1.82e-04	3.793
1.29e-02	2.63e-02	1.415	1.75e-03	1.931	3.39e-04	2.607	5.49e-05	3.392	8.31e-06	4.430
6.47e-03	9.98e-03	1.406	3.17e-04	2.474	4.48e-05	2.932	4.47e-06	3.635	3.13e-07	4.751
3.24e-03	3.71e-03	1.431	4.80e-05	2.730	5.43e-06	3.053	3.08e-07	3.867	1.06e-08	4.891
Reconstructive potential										
	$k=0$		$k=1$		$k=2$		$k=3$		$k=4$	
h	error	rate	error	rate	error	rate	error	rate	error	rate
5.18e-02	1.74e-01		2.77e-02		8.74e-03		4.69e-03		1.92e-03	
2.59e-02	4.38e-02	1.989	5.03e-03	2.462	1.12e-03	2.960	3.40e-04	3.787	9.49e-05	4.341
1.29e-02	1.02e-02	2.085	7.08e-04	2.814	9.66e-05	3.521	1.44e-05	4.540	2.05e-06	5.503
6.47e-03	2.49e-03	2.051	9.59e-05	2.898	6.56e-06	3.898	5.00e-07	4.864	3.57e-08	5.870
3.24e-03	6.18e-04	2.014	1.24e-05	2.960	4.20e-07	3.972	1.62e-08	4.963	5.76e-10	5.966

3.8.7 Example 7

This example, as the previous one, is also not covered by the current analysis. We are interested in solving the nonhomogeneous Neumann nonlinear problem

(3.90), with $\Omega := (0,1)^2$, and $\mathbf{a}(\cdot,\boldsymbol{\zeta}) := \left(1+\frac{1}{1+|\boldsymbol{\zeta}|^2}\right)\boldsymbol{\zeta}$, for all $\boldsymbol{\zeta} \in \mathbb{R}^2$. The data f and g are chosen so that the solution u is given by the smooth function $u(x,y) = \exp(x+\pi y) - (\exp(1+\pi) - \exp(\pi) - \exp(1) + 1)/\pi$. Following what we discussed in Subsection 3.7.3, we proceed to solve the nonlinear HHO scheme (3.94), considering one family of Trapezoidal meshes (cf. Figure 3.17), and another of Tilted hexagonal-dominant meshes (cf. Figure 3.19). Since the HHO discrete space includes the zero mean value condition of its elements, and knowing that it is not simple to find a basis of such space, we circumvent this searching by imposing this restriction through a Lagrange multiplier. We have applied this strategy in [39], where we have solved the Poisson problem with Neumann boundary condition applying the HHO method. The numerical results are displayed in Figure 3.12, while the histories of convergence of the potential, flux and reconstructive potential errors, with respect to the nonhomogeneous, are reported in Tables 3.10 (for the family of Trapezoidal meshes), and 3.11 (for the family of Tilted meshes). They give numerical evidence that the current a priori error analysis could be extended to this kind of boundary conditions.

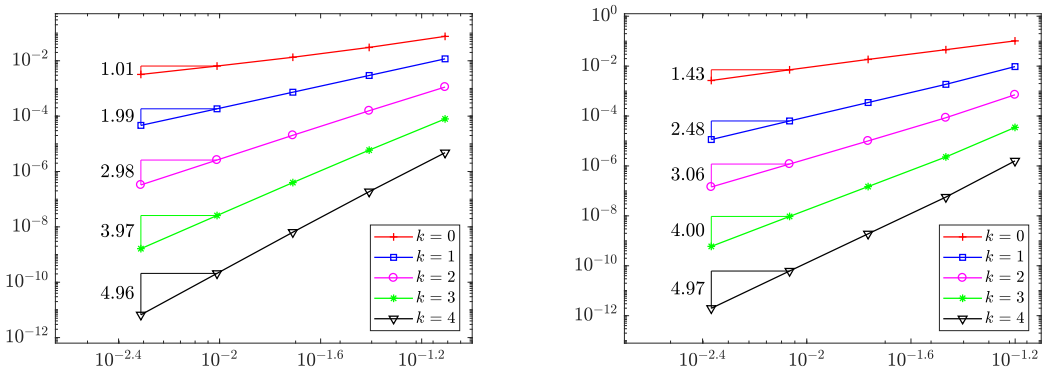

(a) Trapezoidal (b) Tilted

Figure 3.12: Rates of convergence of flux error vs. h (Example 7)

Table 3.10: Histories of convergence of potential, flux, and reconstructive potential errors, considering $k \in \{0, 1, 2, 3, 4\}$ (Example 7 - Trapezoidal meshes)

Potential										
	$k=0$		$k=1$		$k=2$		$k=3$		$k=4$	
h	error	rate	error	rate	error	rate	error	rate	error	rate
6.30e-02	1.32e-01		2.81e-02		2.48e-03		1.84e-04		1.16e-05	
3.42e-02	4.12e-02	1.907	4.20e-03	3.109	1.95e-04	4.156	7.46e-06	5.244	2.39e-07	6.347
1.72e-02	1.13e-02	1.885	5.68e-04	2.914	1.34e-05	3.896	2.60e-07	4.882	4.18e-09	5.890
8.59e-03	2.93e-03	1.943	7.33e-05	2.948	8.74e-07	3.935	8.44e-09	4.938	6.84e-11	5.923
4.30e-03	7.44e-04	1.979	9.30e-06	2.984	6.33e-08	3.795	2.69e-10	4.980	1.09e-12	5.979
Flux										
	$k=0$		$k=1$		$k=2$		$k=3$		$k=4$	
h	error	rate	error	rate	error	rate	error	rate	error	rate
6.30e-02	7.61e-02		1.17e-02		1.13e-03		7.94e-05		4.78e-06	
3.42e-02	3.04e-02	1.505	2.94e-03	2.265	1.57e-04	3.229	5.92e-06	4.250	1.87e-07	5.305
1.72e-02	1.34e-02	1.191	7.32e-04	2.025	2.04e-05	2.968	3.98e-07	3.928	6.41e-09	4.907
8.59e-03	6.45e-03	1.051	1.84e-04	1.988	2.59e-06	2.968	2.57e-08	3.946	2.09e-10	4.933
4.30e-03	3.21e-03	1.009	4.63e-05	1.992	3.27e-07	2.991	1.63e-09	3.984	6.66e-12	4.979
Potential reconstructive										
	$k=0$		$k=1$		$k=2$		$k=3$		$k=4$	
h	error	rate	error	rate	error	rate	error	rate	error	rate
6.30e-02	1.44e-01		2.84e-02		2.49e-03		1.85e-04		1.16e-05	
3.42e-02	4.36e-02	1.954	4.25e-03	3.108	1.97e-04	4.156	7.50e-06	5.243	2.40e-07	6.347
1.72e-02	1.19e-02	1.895	5.74e-04	2.913	1.35e-05	3.896	2.62e-07	4.882	4.19e-09	5.890
8.59e-03	3.07e-03	1.945	7.42e-05	2.947	8.81e-07	3.934	8.44e-09	4.946	6.87e-11	5.923
4.30e-03	7.81e-04	1.980	9.42e-06	2.983	6.37e-08	3.798	2.71e-10	4.972	1.10e-12	5.980

Table 3.11: Histories of convergence of potential, flux, and reconstructive potential errors, considering $k \in \{0, 1, 2, 3, 4\}$ (Example 7 - Tilted meshes)

Potential										
	$k=0$		$k=1$		$k=2$		$k=3$		$k=4$	
h	error	rate	error	rate	error	rate	error	rate	error	rate
6.30e-02	1.34e-01		1.80e-02		1.21e-03		6.35e-05		1.16e-05	
3.42e-02	3.32e-02	2.287	2.46e-03	3.259	8.48e-05	4.357	2.23e-06	5.480	2.39e-07	6.347
1.72e-02	8.52e-03	1.979	3.26e-04	2.939	5.72e-06	3.924	7.57e-08	4.924	4.18e-09	5.890
8.59e-03	2.18e-03	1.964	4.22e-05	2.947	3.73e-07	3.931	2.48e-09	4.925	6.84e-11	5.923
4.30e-03	5.52e-04	1.984	5.36e-06	2.980	2.39e-08	3.974	7.93e-11	4.973	1.09e-12	5.979
Flux										
	$k=0$		$k=1$		$k=2$		$k=3$		$k=4$	
h	error	rate	error	rate	error	rate	error	rate	error	rate
6.30e-02	1.03e-01		9.57e-03		7.12e-04		3.50e-05		4.78e-06	
3.42e-02	4.56e-02	1.327	1.86e-03	2.681	8.55e-05	3.470	2.29e-06	4.460	1.87e-07	5.305
1.72e-02	1.85e-02	1.309	3.48e-04	2.442	1.00e-05	3.115	1.49e-07	3.977	6.41e-09	4.907
8.59e-03	7.13e-03	1.377	6.35e-05	2.449	1.19e-06	3.071	9.49e-09	3.966	2.09e-10	4.933
4.30e-03	2.65e-03	1.428	1.14e-05	2.478	1.44e-07	3.057	5.98e-10	3.995	6.66e-12	4.979
Potential reconstructive										
	$k=0$		$k=1$		$k=2$		$k=3$		$k=4$	
h	error	rate	error	rate	error	rate	error	rate	error	rate
6.30e-02	1.50e-01		1.82e-02		1.22e-03		6.37e-05		1.16e-05	
3.42e-02	3.67e-02	2.308	2.48e-03	3.265	8.52e-05	4.358	2.24e-06	5.481	2.40e-07	6.347
1.72e-02	9.16e-03	2.018	3.28e-04	2.941	5.74e-06	3.925	7.59e-08	4.924	4.19e-09	5.890
8.59e-03	2.29e-03	1.995	4.24e-05	2.948	3.75e-07	3.932	2.48e-09	4.925	6.87e-11	5.923
4.30e-03	5.74e-04	2.003	5.39e-06	2.980	2.39e-08	3.974	7.95e-11	4.973	1.10e-12	5.980

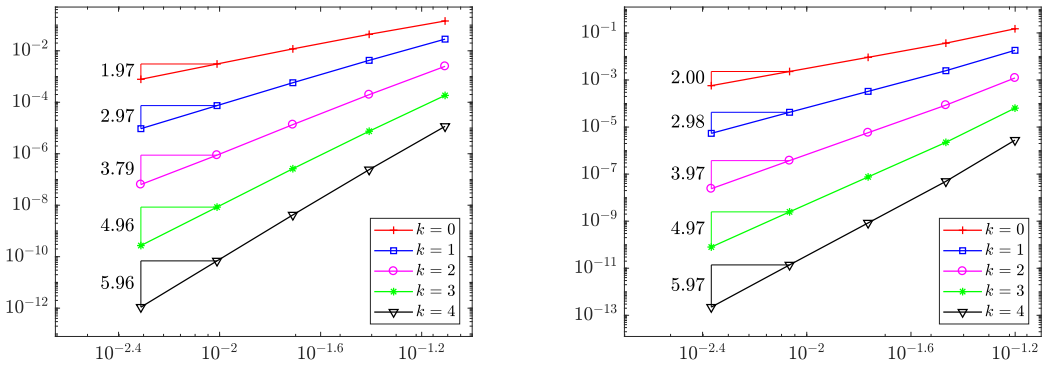

(a) Trapezoidal

(b) Tilted

Figure 3.13: Rates of convergence of reconstructive potential error vs. h (Ex 7)

3.8.8 Families of polytopal meshes

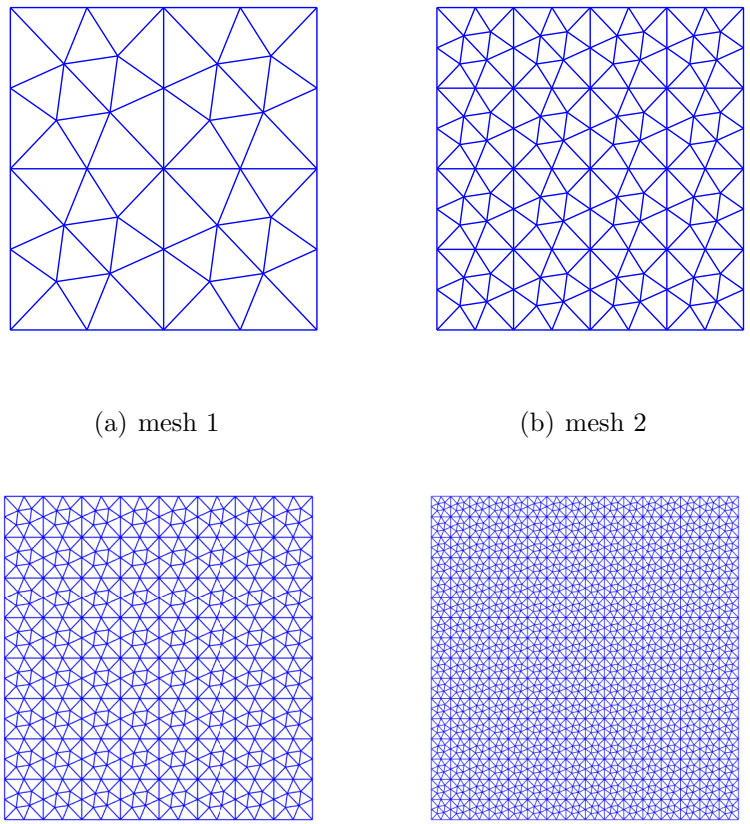

(a) mesh 1

(b) mesh 2

(c) mesh 3

(d) mesh 4

Figure 3.14: Family of Simplicial-I meshes in a square domain

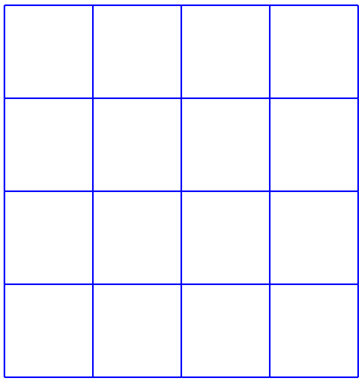

(a) mesh 1

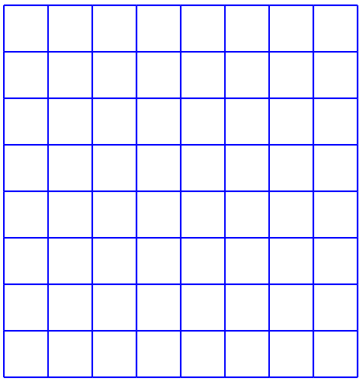

(b) mesh 2

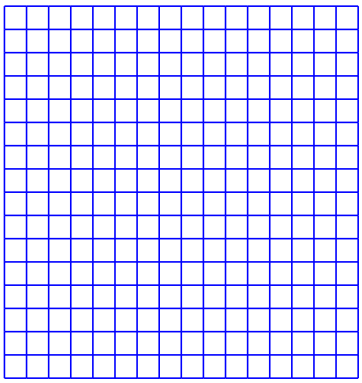

(c) mesh 3

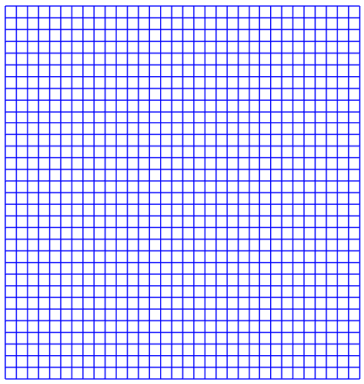

(d) mesh 4

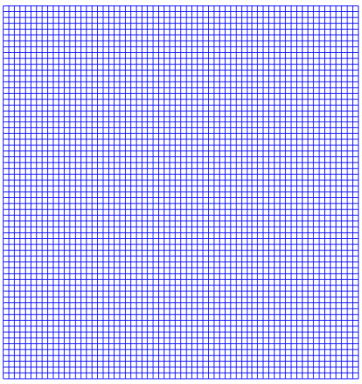

(e) mesh 5

Figure 3.15: Family of Cartesian meshes in a square domain

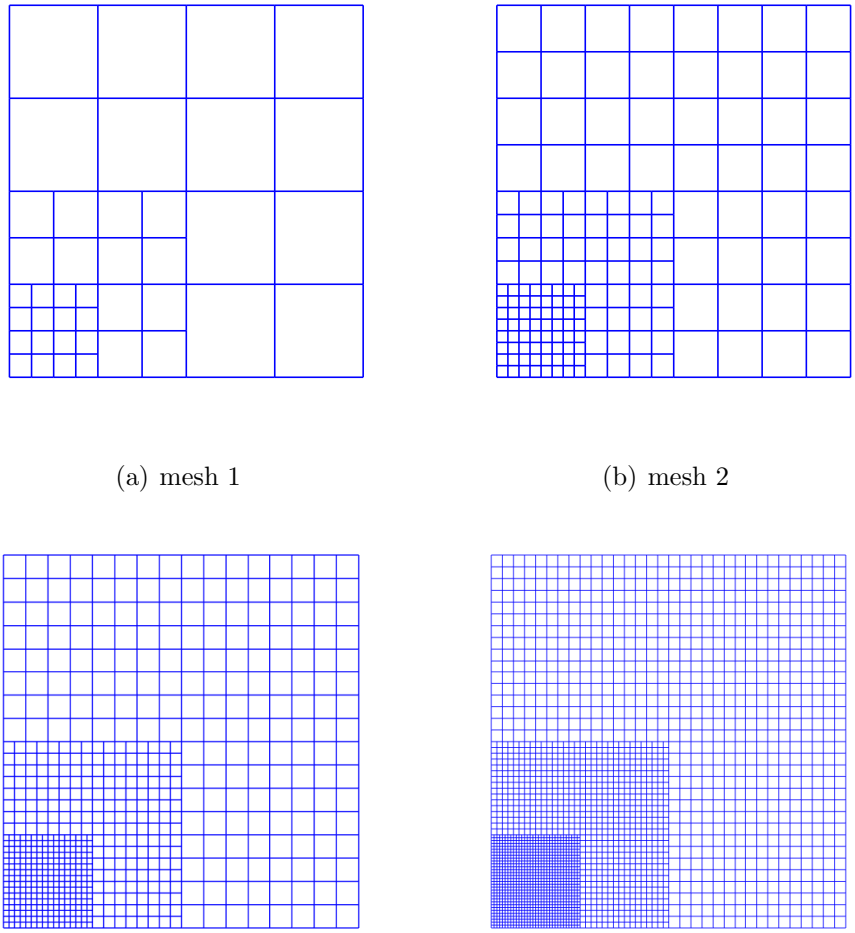

(a) mesh 1

(b) mesh 2

(c) mesh 3

(d) mesh 4

Figure 3.16: Family of Graduated meshes (with hanging nodes) in a square domain

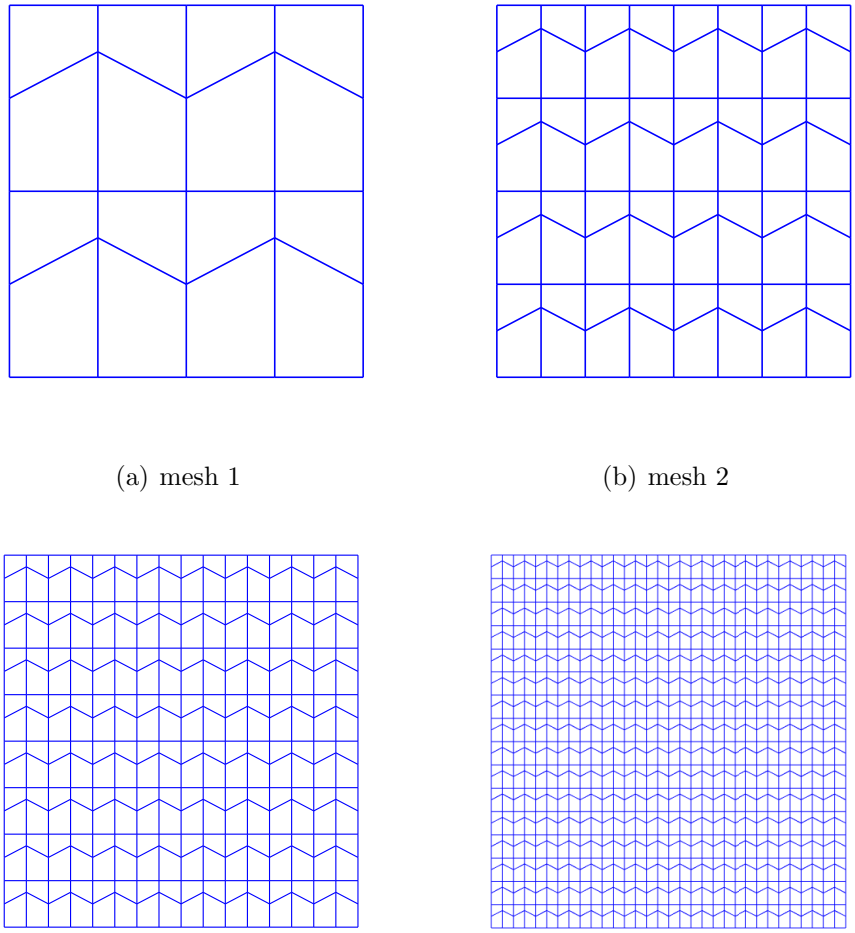

(a) mesh 1

(b) mesh 2

(c) mesh 3

(d) mesh 4

Figure 3.17: Family of Trapezoidal meshes in a square domain

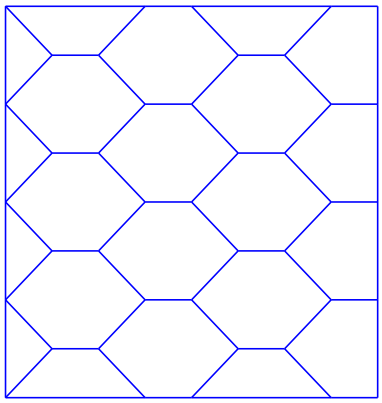

(a) mesh 1

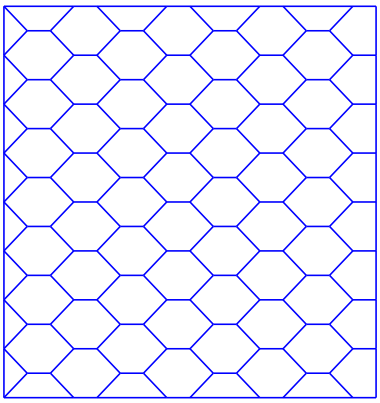

(b) mesh 2

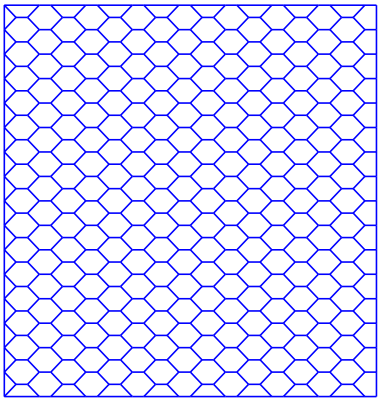

(c) mesh 3

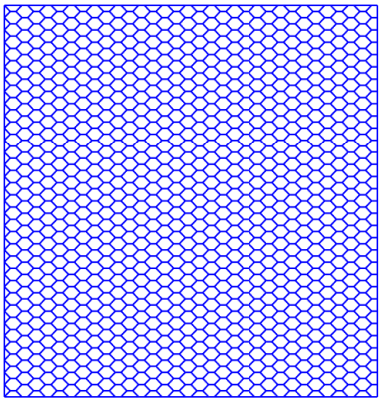

(d) mesh 4

Figure 3.18: Family of Hexagonal meshes in a square domain

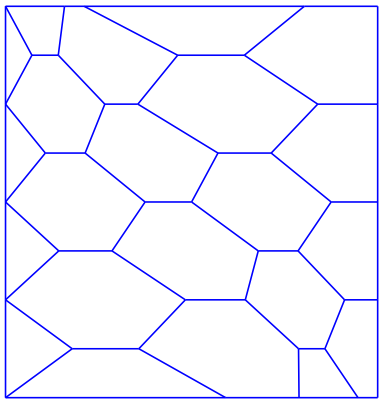

(a) mesh 1

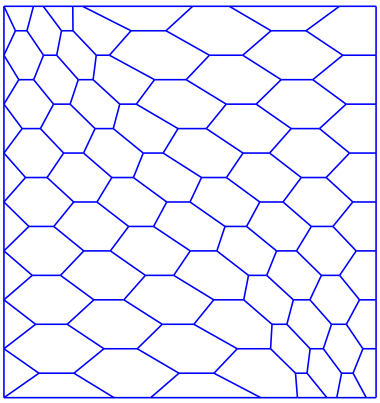

(b) mesh 2

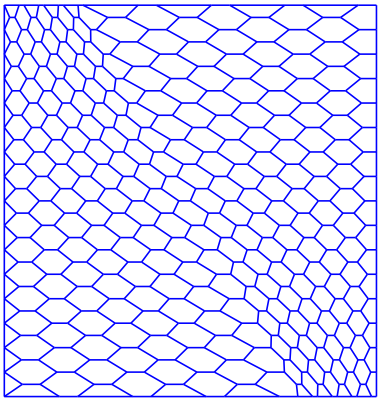

(c) mesh 3

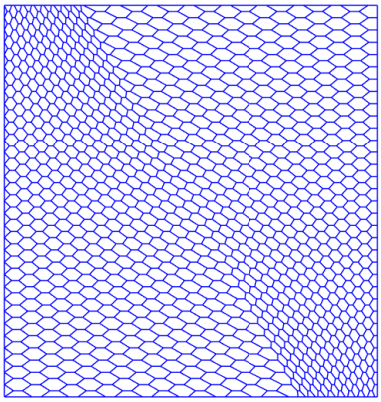

(d) mesh 4

Figure 3.19: Family of Tilted Hexagonal meshes in a square domain

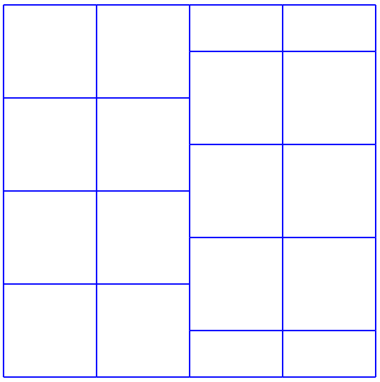

(a) mesh 1

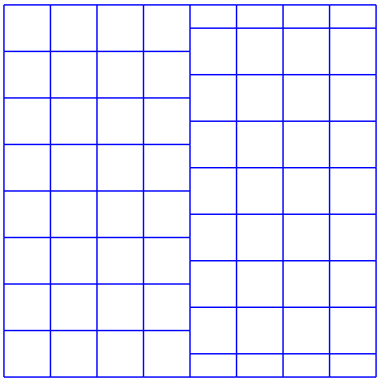

(b) mesh 2

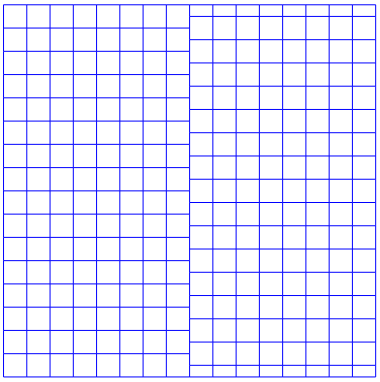

(c) mesh 3

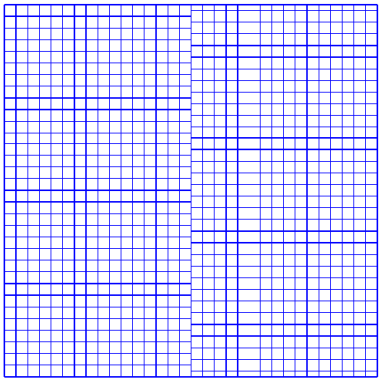

(d) mesh 4

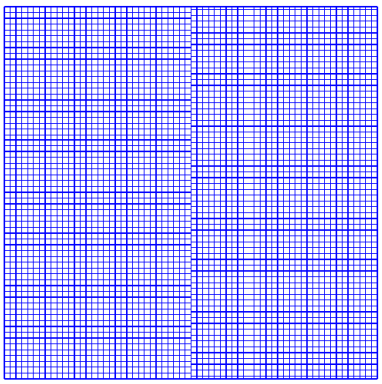

(e) mesh 5

Figure 3.20: Family of Fractured meshes in a square domain.

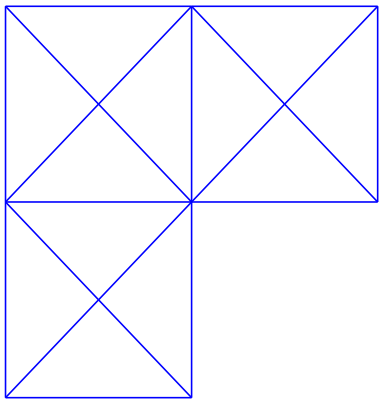

(a) mesh 1

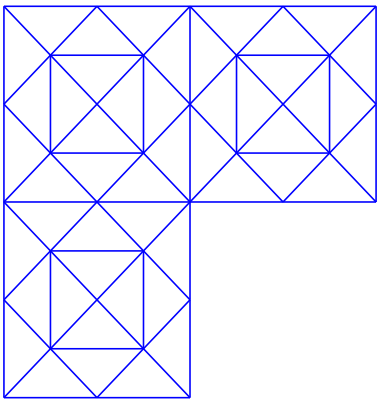

(b) mesh 2

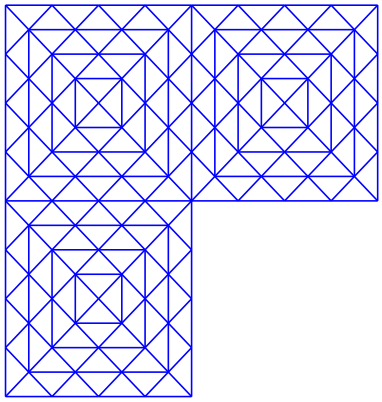

(c) mesh 3

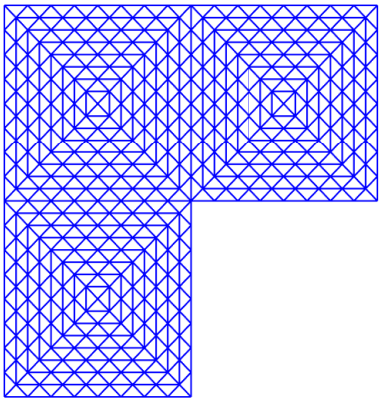

(d) mesh 4

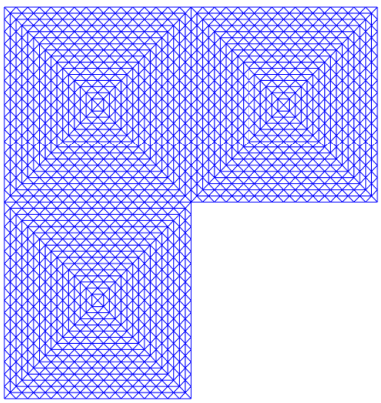

(e) mesh 5

Figure 3.21: Family of Simplicial-II meshes in L-shaped domain

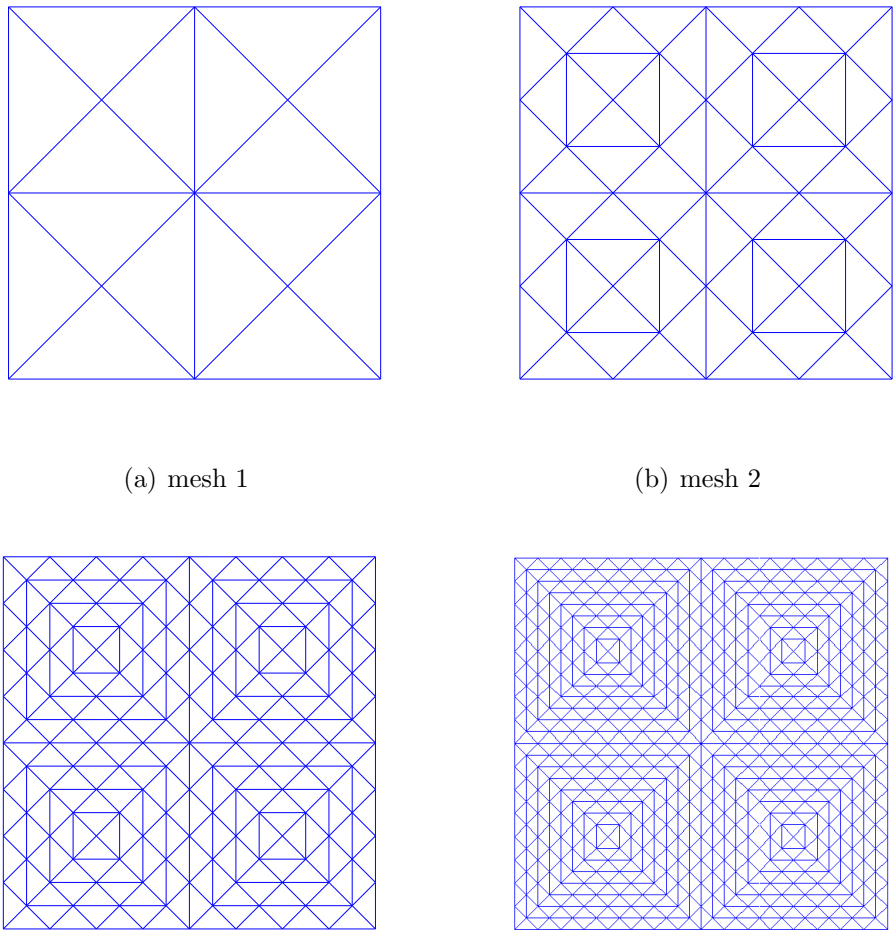

(a) mesh 1 (b) mesh 2

(c) mesh 3 (d) mesh 4

Figure 3.22: Family of Simplicial-III meshes in Square domain

Conclusions

In this paper, we have developed a complete a priori error analysis for a class of elliptic nonlinear problems, applying the HHO method. It is well known that there are previous works for nonlinear problems in the context of HHO methods, as Leray - Lions equations [64, 65], nonlinear elasticity [27], nonlinear Signorini boundary conditions [45], quasi-Newtonian Stokes problem [148], and nonlinear poroelasticity [29, 28]. However, the contibution of this work relies on Theorems 3.6.2, and 3.6.3, which establish the convergence of the L^2-projection of the potential error ($||\pi_h^k u - u_h||_\Omega$) and the super-convergence of the reconstructive potential error ($||p_h^{k+1}\underline{\mathbf{u}}_h -$

$u||_\Omega$), respectively. Up to author's knowledge, these errors estimates have not been proved before. It is important to remark that according to what has been discussed in [64, Section 4.1] for nonlinear problems, we need to consider a variant of the gradient reconstruction operator G_T^k. Otherwise, the rates of convergence will not be the expected. We provide a brief discussion on this in the Appendix 3.9, which includes a numerical comparison.

We have presented seven computational examples, considering three different nonlinear coefficients that verify the Hypotheses ***(H.1)***-***(H.4)***, and several admissible families of polytopal meshes, with or without hanging nodes (see Table 3.1). Numerical examples, provided in this paper, confirm our theoretical results, even for other boundary conditions not covered by us in the present work. In particular, Example 3.8.5, whose solution is nonsmooth, gives us the motivation to develop an a posteriori error analysis for nonlinear elliptic problems. This could be the subject of future work.

3.9 Appendix

Here, we compare the effect of using the standard Gradient reconstruction operator given in [75] and the variant of the Gradient reconstruction operator (with extended codomain, from $\nabla\mathbb{P}_d^{k+1}(T)$ to $[\mathbb{P}_d^k(T)]^d$) introduced in [64], when solving nonlinear elliptic problems with the HHO method. To clarify the difference, we solve the nonlinear HHO scheme associated to the Example 3.8.1, with a family of Trapezoidal meshes (cf. Figure 3.17), considering both kind of Gradient reconstruction operators. In Figures 3.23, 3.24 and 3.25, we display the rates of convergence of the potential, flux and reconstructive potential errors, with respect to the meshsize. The boxes on the left hand side corresponds to the results obtained when using the Standard gradient reconstruction operator, while the ones on the right hand side are the respective to the Extended gradient reconstruction operator. They are also reported in Tables 3.12 and 3.13. As expected, the numerical results associated to the Extended gradient reconstruction operator are in agreement with our theoretical results.

On the other hand, we notice that using the Standard gradient reconstruction operator, the rates of convergence of the potential and reconstructive potential errors, for $k = 0$ and $k = 1$, are the expected ones. For greater values of k, we observe a notorious loss in the rate of convergence. Respect to the flux error, we only recover the optimal rate of convergence for $k = 0$ when using the Standard gradient reconstruction operator. Indeed, for $k = 0$, both approaches have the same optimal approximation properties, thank to $\nabla\mathbb{P}^1(T) = [\mathbb{P}^0(T)]^d$.

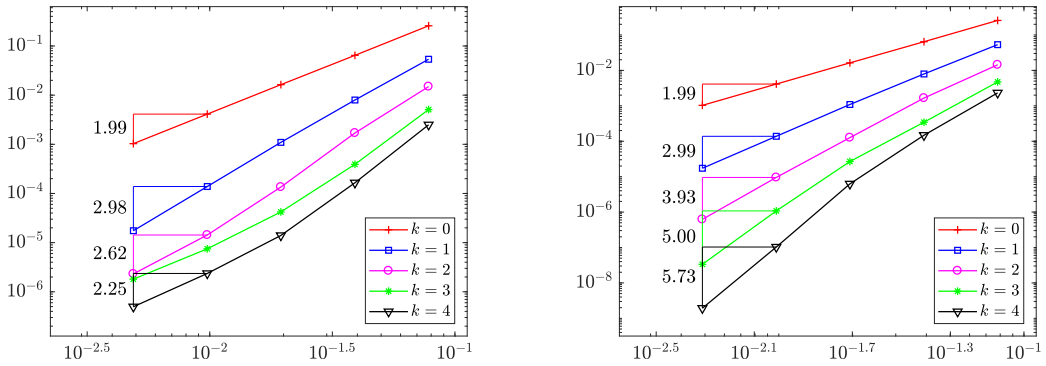

(a) Standard (b) Extended

Figure 3.23: Rates of the Potential error vs. h (appendix example)

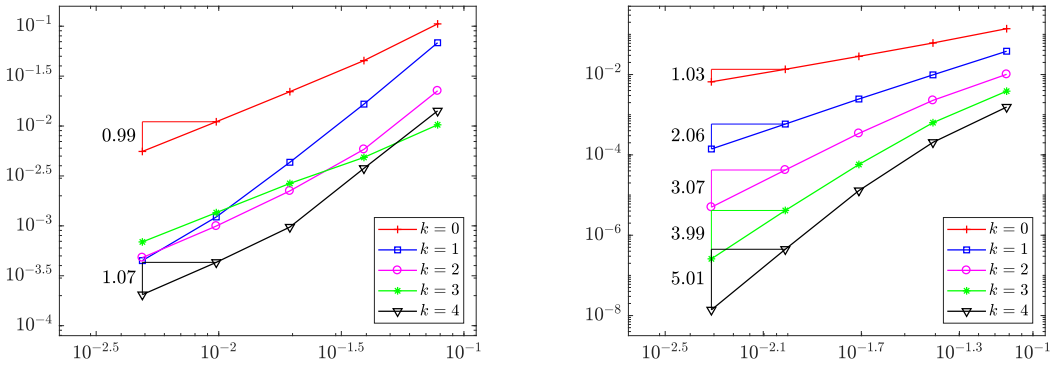

(a) Standard (b) Extended

Figure 3.24: Rates of the Flux error vs. h (appendix example)

Table 3.12: Histories of convergence of potential, flux, and reconstructive potential errors, considering $k \in \{0, 1, 2, 3, 4\}$, using Standard gradient reconstruction operator (appendix example)

Potential										
	$k=0$		$k=1$		$k=2$		$k=3$		$k=4$	
h	error	rate	error	rate	error	rate	error	rate	error	rate
7.81e-02	2.57e-01		5.37e-02		1.49e-02		5.09e-03		2.49e-03	
3.91e-02	6.44e-02	2.001	7.96e-03	2.759	1.70e-03	3.143	3.92e-04	3.706	1.65e-04	3.926
1.95e-02	1.63e-02	1.973	1.09e-03	2.851	1.35e-04	3.638	4.21e-05	3.206	1.40e-05	3.547
9.77e-03	4.11e-03	1.995	1.38e-04	2.992	1.43e-05	3.250	7.48e-06	2.499	2.36e-06	2.574
4.88e-03	1.03e-03	1.994	1.75e-05	2.982	2.31e-06	2.625	1.81e-06	2.048	4.96e-07	2.246
Flux										
	$k=0$		$k=1$		$k=2$		$k=3$		$k=4$	
h	error	rate	error	rate	error	rate	error	rate	error	rate
7.81e-02	1.05e-01		6.83e-02		2.25e-02		1.03e-02		1.42e-02	
3.91e-02	4.52e-02	1.223	1.66e-02	2.046	5.84e-03	1.951	4.85e-03	1.087	3.77e-03	1.916
1.95e-02	2.21e-02	1.031	4.33e-03	1.928	2.24e-03	1.378	2.66e-03	0.862	9.73e-04	1.947
9.77e-03	1.10e-02	1.004	1.23e-03	1.826	9.95e-04	1.173	1.36e-03	0.975	4.31e-04	1.178
4.88e-03	5.56e-03	0.986	4.49e-04	1.450	4.81e-04	1.049	6.90e-04	0.973	2.05e-04	1.073
Reconstructive potential										
	$k=0$		$k=1$		$k=2$		$k=3$		$k=4$	
h	error	rate	error	rate	error	rate	error	rate	error	rate
7.81e-02	2.74e-01		5.53e-02		1.50e-02		5.10e-03		2.50e-03	
3.91e-02	6.80e-02	2.013	8.12e-03	2.774	1.70e-03	3.146	3.96e-04	3.691	1.68e-04	3.906
1.95e-02	1.71e-02	1.980	1.11e-03	2.856	1.38e-04	3.613	4.49e-05	3.131	1.45e-05	3.523
9.77e-03	4.31e-03	1.998	1.41e-04	2.990	1.56e-05	3.152	8.48e-06	2.412	2.46e-06	2.565
4.88e-03	1.08e-03	1.996	1.79e-05	2.971	2.78e-06	2.485	2.07e-06	2.030	5.21e-07	2.235

Table 3.13: Histories of convergence of potential, flux, and reconstructive potential errors, considering $k \in \{0, 1, 2, 3, 4\}$, using Extended gradient reconstruction operator (appendix example)

Potential										
	$k=0$		$k=1$		$k=2$		$k=3$		$k=4$	
h	error	rate	error	rate	error	rate	error	rate	error	rate
7.81e-02	2.57e-01		5.33e-02		1.44e-02		4.73e-03		2.32e-03	
3.91e-02	6.44e-02	2.001	7.93e-03	2.754	1.66e-03	3.126	3.44e-04	3.788	1.48e-04	3.982
1.95e-02	1.63e-02	1.973	1.09e-03	2.852	1.26e-04	3.698	2.68e-05	3.670	6.25e-06	4.546
9.77e-03	4.11e-03	1.995	1.38e-04	2.991	9.50e-06	3.743	1.08e-06	4.645	1.03e-07	5.937
4.88e-03	1.03e-03	1.994	1.73e-05	2.993	6.22e-07	3.928	3.36e-08	5.000	1.93e-09	5.728
Flux										
	$k=0$		$k=1$		$k=2$		$k=3$		$k=4$	
h	error	rate	error	rate	error	rate	error	rate	error	rate
7.81e-02	1.38e-01		3.80e-02		1.01e-02		3.85e-03		1.55e-03	
3.91e-02	6.10e-02	1.184	9.81e-03	1.958	2.28e-03	2.156	6.33e-04	2.611	2.05e-04	2.923
1.95e-02	2.83e-02	1.103	2.46e-03	1.990	3.43e-04	2.723	5.76e-05	3.445	1.29e-05	3.976
9.77e-03	1.35e-02	1.073	5.85e-04	2.077	4.20e-05	3.036	4.13e-06	3.812	4.47e-07	4.866
4.88e-03	6.59e-03	1.032	1.40e-04	2.059	4.99e-06	3.069	2.58e-07	3.995	1.39e-08	5.005
Reconstructive potential										
	$k=0$		$k=1$		$k=2$		$k=3$		$k=4$	
h	error	rate	error	rate	error	rate	error	rate	error	rate
7.81e-02	2.74e-01		5.48e-02		1.45e-02		4.73e-03		2.32e-03	
3.91e-02	6.80e-02	2.013	8.07e-03	2.769	1.66e-03	3.130	3.44e-04	3.788	1.48e-04	3.982
1.95e-02	1.71e-02	1.980	1.11e-03	2.859	1.27e-04	3.698	2.68e-05	3.671	6.25e-06	4.546
9.77e-03	4.31e-03	1.998	1.40e-04	2.993	9.52e-06	3.745	1.08e-06	4.646	1.03e-07	5.937
4.88e-03	1.08e-03	1.996	1.75e-05	2.994	6.23e-07	3.928	3.36e-08	5.000	1.93e-09	5.728

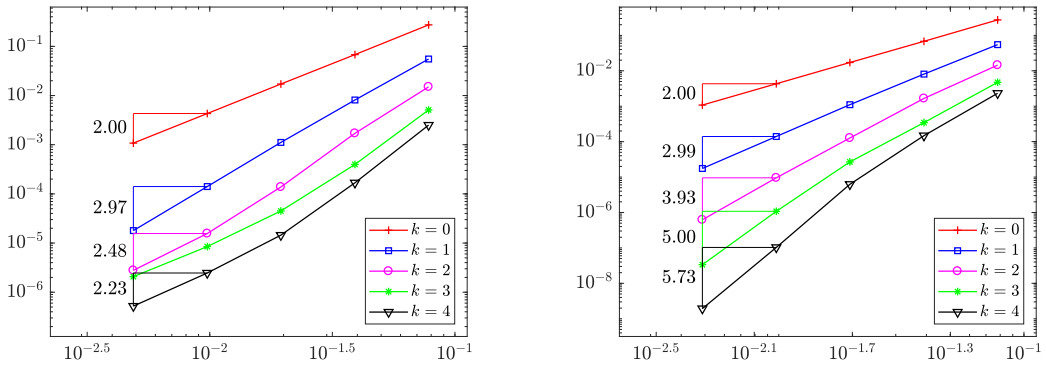

(a) Standard

(b) Extended

Figure 3.25: Rates of the Reconstructive potential error vs. h (appendix example)

Chapter 4

A mixed HHO formulation for a linear transmission elliptic problem

In this chapter, we analyse a linear transmission elliptic problem in a bounded domain, applying the already known Hybrid High Order (HHO) method. This approach gives approximation of unknowns in the interior volume of each element and on the faces of its boundary, in the following sense: obtaining approximations of exact solution on the space of polynomials of total degree at most k on the mesh elements and faces. Thus, we obtain a nonconforming discrete formulation, which is well posed, and after a condensation process, we can reduced it to another scheme defined on the skeleton induced by the mesh. This allows us to obtain a more compact system, and reduce significantly the number of unknowns. We point out that we need to introduce an auxiliary unknown in order to deal with the nonhomogeneous transmission conditions, that will act as a Lagrange multiplier. We prove that the method is optimally convergent in the energy norm, as well as in the L^2-norm for the potential, and a weighted L^2-norm for the Lagrange multiplier, for smooth enough solutions. Finally, we include some numerical experiments that validate our theoretical results, even in situations not covered by the current analysis.

4.1 Introduction

Transmission problems appear in many areas of engineering and science. They can involve multiple distinct materials or fluids with different densities, diffusions, conductivities, Youngs modulus, or Poisson ratio. For example, they appear in the calculation of magnetic fields of electromagnetic devices [117, 118], in problems of fluid mechanics and subsonic flow [90, 91, 32], in incompressible multiphase flows [123], in models of electroporation [114] and electrohydrodynamic [121], and many other fields.

There are two types of transmission problems, exterior and interior. The work developed here corresponds to an interior one. In turn, interior transmission problems fit into interface problems, which can be found in material properties [141], modeling solid mechanics problems [131, 32], in fluid dynamics [87, 25], and many other important phenomena in science and engineering.

On the other hand, the numerical solution of exterior problems usually combines the Finite Element (FE) method with the Boundary Element (BE) method (see, e.g. [15, 100, 34]). FE method was proposed, for interface problems, in [131, 30, 48]. Also, it is possible to combine local discontinuous Galerkin (LDG) method with BE method, which does not require any continuity condition across the interelement boundaries, it is robust with respect to discontinuous coefficients, and it allows the use of different polynomial degrees in each element (see [35, 36, 103, 37]).

Moreover, interface problems are divided into interface-fitted and unfitted mesh. The former is built on body fitted mesh that does not allow the interface to cut across any of the elements in the mesh, while the latter does not impose that restriction. There exists several methods, such as immersed interface method [126, 107], fitted FE method [30], unfitted FE method [115], embedded FE method [79], multiscale finite element methods [49], extended finite element (XFE) method [130, 131], fitted HDG method [114], unfitted HDG method [146, 80], for example. Also, there are works considering a curve as interface. We can refer to the classical

FE methods [12, 16], and HDG method [122, 145].

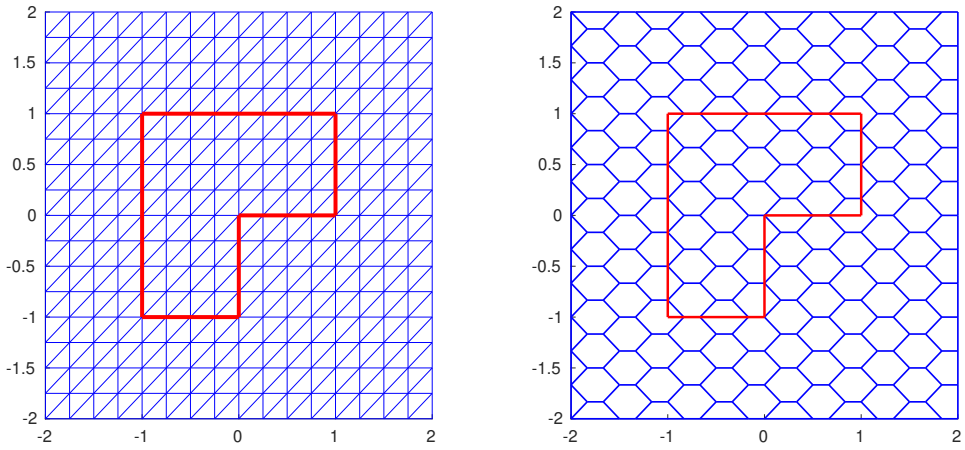

Figure 4.1: An interface-fitted mesh (left), and an unfitted mesh (right).

Interface-fitted mesh is also known as body-fitted or interface conforming, i.e. the meshes are tailored to fit the interface, (cf. left plot in Figure 4.1). Besides, the jump conditions across the interface can be easily incorporated into a standard FE formulation [30, 48]. There are sophisticated use of approximate interface-fitted meshes [149] and the use of Virtual element methods on an interface-fitted mesh [47].

However, interface-unfitted mesh is more used in time dependent problems, where the interface moves with time or during iteration (free-boundary), and when the boundary or the internal interface is curved. This is caused since generating a body fitted mesh of relatively high quality is challenging and computationally costly, especially when complex and/or moving interfaces are involved. In this sense, it may be advantageous to use the same mesh on the domain for different, nearby, locations of the interface.

A well-known disadvantage for unfitted mesh approach, is the difficulty to capture the complex geometry of the interface and to enforce jump conditions across the interface accurately. The resulting linear system may not be always symmetric and its conditioning has a strong dependence on how the interface cuts the mesh cells.

Furthermore, a rigorous error analysis is difficult to perform.

In this work, we consider an interface-fitted mesh, since we handle with a polygonal interface. In transmission problems, in general, it is identified/recognized an internal domain, a transmission or internal boundary, and an external (annular) domain. In the existing bibliography only Dirichlet and mixed conditions on the external boundary are addressed. In this paper we consider pure nonhomogeneous Neumann condition on the exterior boundary. This work is not addressed to nonmathching transmision mesh, although it is possible to extend our study, following the analysis in [116].

Now, we focus on the well known Hybrid High Order (HHO) method, introduced in [75, 72], which has been applied to a great variety of problems, thanks to its ability to handle physical parameters. We can mention, for example, linear diffusion problems [75, 72], quasi-incompressible linear elasticity [70], nonlinear elasticity problems in the small deformation regime [27], nonlinear Leray–Lions problems [64, 65], Stokes problem [3], incompressible Navier-Stokes equations [26], and finite deformations of hyperelastic materials [1], among other problems.

Its design relies on discrete unknowns that are broken polynomials on the mesh and on its skeleton, from which two key ingredients are devised:

(i) Local reconstructions, that are performed by solving small, parallel problems inside each element, and conceived so that their composition with the natural interpolator of sufficiently smooth functions yields a projector on local polynomial spaces (see Lemma 4.3.3).

(ii) Stabilisation terms that penalise residuals, and are defined at the element level, so they ensure stability while preserving the approximation properties of the reconstruction.

These ingredients are combined to formulate local contributions, which are then assembled as in standard Finite Element methods. We mention several advantageous

features. Management of polytopal meshes (with possibly hanging nodes), which is an actual topic that is considered to deal with cracks and other kinds of discontinuities induced by material defects [131]. Support arbitrary approximation orders in any space dimension, and exhibits a reduced computational cost, thanks to the compact stencil, along with the possibility to locally eliminate a large portion of the unknowns (see Section 5 in [39]), is achieved. Then, we deal with a (linear) system defined on the skeleton of the mesh.

In lowest-order version ($k = 0$), HHO method can be linked with the unified framework Hybrid Mixed Mimetic (HMM) method [67]. In high-order, there is a link of HHO approach with HDG method [59], a connection with High-Order mimetic (HOM) [127], and with the nonconforming version of the Virtual Element (VE) method [11]. In addition, we find a description of the relation between HHO and VE methods in [125], with an analysis that differs from the standard VE method described in [20].

We point out that a transmission problem with curved interface, has been studied in [31], applying an unfitted finite element method (introduced in [115]), with the philosophy of HHO method. However, we point-wise that this paper does not include numerical experiments. In this work, we applied the standard HHO method for a linear transmission problem with nonhomogeneous transmission conditions, extending the application of the HHO approach described in [75]. We remark that the analysis here is quite different to the presented in [31], since we introduce an auxiliary unknown living on the transmission interface, that acts as a Lagrange multiplier. As result, we derive a discrete mixed HHO formulation.

The rest of this paper is organized as follows. In Section 4.2, we introduce the model problem and discuss its well-posedness, at continuous level. In Section 4.3, we describe the main analysis tools, the Degrees of Freedom (DOFs) in the context of HHO method, and the potential reconstruction operator, with its key properties. In Section 4.4, we introduce the discrete problem and study its stability. In Section 4.5, we perform the a priori error analysis, first in the energy-norm, and then in the L^2-norm under additional elliptic regularity assumptions. In Section 4.6, we discuss

the aspects of the computational implementation. Finally, in Section 4.7, we present some numerical experiments, which are in agreement with our theoretical results.

4.2 Continuous settings

In the present chapter, we will work with two disjoint domains. Let Ω_1 be a bounded and simply connected domain in $\mathbb{R}^d$, $d \in \{2, 3\}$, with Lipschitz-continuous boundary $\Gamma_1 := \partial\Omega_1$. Let Ω_2 be the annular region bounded by Γ_1 and a second Lipschitz-continuous curve Γ_2, that is strictly contained in $\mathbb{R}^2 - \overline{\Omega}_1$ (see Figure 4.2). For any connected subset $X \subset \overline{\Omega}$ with nonzero Lebesgue measure, the inner product and norm of the Lebesgue space $L^2(X)$ are denoted by $(\cdot, \cdot)_X$ and $||\cdot||_{0,X}$, respectively.

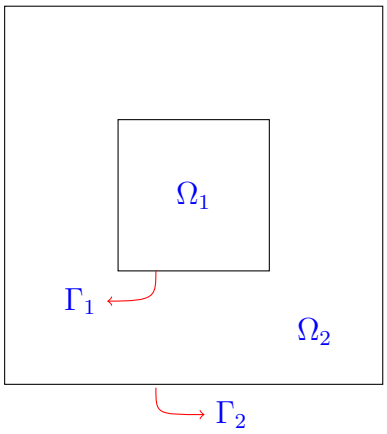

Figure 4.2: Geometry of the problem

Next, we consider the following transmission interior model problem: Find $u_1 : \Omega_1 \to \mathbb{R}$ and $u_2 : \Omega_2 \to \mathbb{R}$ such that

$$-\Delta u_1 = f_1 \text{ in } \Omega_1\,, \tag{4.1a}$$

$$-\Delta u_2 = f_2 \text{ in } \Omega_2\,, \tag{4.1b}$$

$$u_1 - u_2 = g \text{ on } \Gamma_1\,, \tag{4.1c}$$

$$\nabla u_1 \cdot \boldsymbol{n}_1 + \nabla u_2 \cdot \boldsymbol{n}_2 = g_1 \text{ on } \Gamma_1\,, \tag{4.1d}$$

$$\nabla u_2 \cdot \boldsymbol{n}_2 = g_2 \text{ on } \Gamma_2\,, \tag{4.1e}$$

$$\int_{\Omega_1} u_1 + \int_{\Omega_2} u_2 = 0\,, \tag{4.1f}$$

where $f_1 \in L^2(\Omega_1)$ and $f_2 \in L^2(\Omega_2)$ are the forcing terms, $g \in H^{1/2}(\Gamma_1)$ is the jump of traces of solutions on Γ_1, $g_1 \in H^{-1/2}(\Gamma_1)$ and $g_2 \in H^{-1/2}(\Gamma_2)$ are the jump of normal component of fluxes on Γ_1, and the normal component of u_2 on Γ_2, respectively. Here, $\boldsymbol{n}_1$ represents the unit outward normal to the boundary of Ω_1, while $\boldsymbol{n}_2$ denotes the unit outward normal to the boundary of Ω_2 given by $\partial\Omega_2 := \Gamma_1 \cup \Gamma_2$. Also we impose the following compatibility condition

$$\int_{\Omega_1} f_1 + \int_{\Omega_2} f_2 + \langle g_1, 1\rangle_{\Gamma_1} + \langle g_2, 1\rangle_{\Gamma_2} = 0\,, \tag{4.2}$$

for the well-posedness of problem (4.1).

The starting point of the HHO method relies on finding a primal-mixed variational formulation of (4.1). We consider the equations $-\Delta u_i = f_i$ in Ω_i, $i \in \{1,2\}$, and after integrating by parts, we deduce that

$$(\nabla u_1, \nabla v_1)_{\Omega_1} - \langle \nabla u_1 \cdot \boldsymbol{n}_1, \gamma_0^-(v_1)\rangle_{\Gamma_1} = (f_1, v_1)_{\Omega_1}\,, \tag{4.3}$$

$$(\nabla u_2, \nabla v_2)_{\Omega_2} - \langle \nabla u_2 \cdot \boldsymbol{n}_2, \gamma_0^+(v_2)\rangle_{\Gamma_1} - \langle \nabla u_2 \cdot \boldsymbol{n}_2, \gamma_0^+(v_2)\rangle_{\Gamma_2} = (f_2, v_2)_{\Omega_2}\,, \tag{4.4}$$

for all $(v_1, v_2) \in H^1(\Omega_1) \times H^1(\Omega_2)$, where $\langle\cdot,\cdot\rangle_{\Gamma_1}$ denotes the duality pairing of $H^{-1/2}(\Gamma_1)$ and $H^{1/2}(\Gamma_1)$ with respect to the $L^2(\Gamma_1)$-inner product, and analogously for $\langle\cdot,\cdot\rangle_{\Gamma_2}$. In addition, $\gamma_0^- : H^1(\Omega_1) \to H^{1/2}(\partial\Omega_1)$ and $\gamma_0^+ : H^1(\Omega_2) \to H^{1/2}(\partial\Omega_2)$ correspond to the trace operators on each subdomain. Then, using (4.1d), introducing the auxiliary unknown $\xi := \nabla u_1 \cdot \boldsymbol{n}_1 \in H^{-1/2}(\Gamma_1)$, and taking into account (4.1e), (4.3), and (4.4), we obtain

$$\sum_{i=1}^{2}(\nabla u_i, \nabla v_i)_{\Omega_i} - \langle g_1, \gamma_0^+(v_2)\rangle_{\Gamma_1} - \langle g_2, \gamma_0^+(v_2)\rangle_{\Gamma_2} - \langle \xi, \gamma_0^-(v_1) - \gamma_0^+(v_2)\rangle_{\Gamma_1} = \sum_{i=1}^{2}(f_i, v_i)_{\Omega_i}\,. \tag{4.5}$$

Further, we can formulate the jump of the traces of u_1 and u_2 on Γ_1, as

$$\langle \lambda, \gamma_0^-(u_1) - \gamma_0^+(u_2)\rangle_{\Gamma_1} = \langle \lambda, g\rangle_{\Gamma_1} \quad \forall\, \lambda \in H^{-1/2}(\Gamma_1)\,. \tag{4.6}$$

We now introduce the Hilbert space

$$\mathbf{U} := \left\{(v_1, v_2) \in H^1(\Omega_1) \times H^1(\Omega_2) \,:\, (v_1, 1)_{\Omega_1} + (v_2, 1)_{\Omega_2} = 0\right\}\,, \tag{4.7}$$

provided with the norm $||(v_1, v_2)||^2_{\mathbf{U}} := ||v_1||^2_{1,\Omega_1} + ||v_2||^2_{1,\Omega_2}$ and $Q := H^{-1/2}(\Gamma_1)$, with its usual norm $||\cdot||_{-1/2,\Gamma_1}$. Then, the variational formulation reads as: Find $((u_1, u_2), \xi) \in \mathbf{U} \times Q$ such that

$$a((u_1, u_2), (v_1, v_2)) + b((v_1, v_2), \xi) = F(v_1, v_2) \quad \forall (v_1, v_2) \in \mathbf{U}, \tag{4.8a}$$

$$-b((u_1, u_2), \lambda) = G(\lambda) \qquad \forall \lambda \in Q. \tag{4.8b}$$

where $a : \mathbf{U} \times \mathbf{U} \to \mathbb{R}$ and $b : \mathbf{U} \times Q \to \mathbb{R}$ are bilinear forms defined as

$$a((w_1, w_2), (v_1, v_2)) := (\nabla w_1, \nabla v_1)_{\Omega_1} + (\nabla w_2, \nabla v_2)_{\Omega_2} \quad \forall\, (w_1, w_2)\,,\, (v_1, v_2) \in \mathbf{U} \times \mathbf{U}\,,$$

$$b((v_1, v_2), \lambda) := \langle \lambda, \gamma_0^+(v_2) - \gamma_0^-(v_1)\rangle_{\Gamma_1} \quad \forall\, ((v_1, v_2), \lambda) \in \mathbf{U} \times Q\,,$$

while the linear functionals $F : \mathbf{U} \to \mathbb{R}$ and $G : Q \to \mathbb{R}$, are given by

$$F(v_1, v_2) := (f_1, v_1)_{\Omega_1} + (f_2, v_2)_{\Omega_2} + \langle g_1, \gamma_0^+(v_2)\rangle_{\Gamma_1} + \langle g_2, \gamma_0^+(v_2)\rangle_{\Gamma_2} \quad \forall\,,\,(v_1, v_2) \in \mathbf{U}\,,$$

$$G(\lambda) := \langle \lambda, g\rangle_{\Gamma_1} \quad \forall\, \lambda \in Q\,.$$

Lemma 4.2.1 *b is bounded.*

Proof. First, we fix $((v_1, v_2), \lambda) \in \mathbf{U} \times Q$. Then, we have

$$\begin{aligned} b((v_1, v_2), \lambda) &\leq ||\lambda||_{-1/2,\Gamma_1} \left(||\gamma_0^+(v_2)||_{1/2,\Gamma_1} + ||\gamma_0^-(v_1)||_{1/2,\Gamma_1}\right) \\ &\leq ||\lambda||_{-1/2,\Gamma_1} ||(v_1, v_2)||_{\mathbf{U}}\,, \end{aligned}$$

and we conclude the statement. □

Remark 4.2.1 *Thanks to the boundedness of bilinear form b, we can define a bounded linear operator $\boldsymbol{B} : \mathbf{U} \to Q'$, induced by the bilinear form b, such that*

$$[\boldsymbol{B}(v_1, v_2), \lambda] := b((v_1, v_2), \lambda) \quad \forall\, (v_1, v_2) \in \mathbf{U}\,, \forall\, \lambda \in Q\,,$$

where $[\cdot, \cdot]$ stands for the duality pairing induced by the operator and functional used in this case. It is not difficult to deduce that $\boldsymbol{B}((v_1, v_2)) := \mathcal{R}^*(\gamma_0^+(v_2) - \gamma_0^-(v_1)) \quad \forall\, (v_1, v_2) \in \mathbf{U}$, where $\mathcal{R} : H^{-1/2}(\Gamma_1) \to H^{1/2}(\Gamma_1)$ represents the canonical Riesz operator between $H^{-1/2}(\Gamma_1)$ and $H^{1/2}(\Gamma_1)$, while $\mathcal{R}^* : H^{1/2}(\Gamma_1) \to H^{-1/2}(\Gamma_1)$ corresponds to the adjoint (Hilbert) Riesz operator of $\mathcal{R}$. Hereafter, $\langle \cdot, \cdot \rangle_{r,\Gamma_1}$ denotes the inner product on $H^r(\Gamma_1)$, $r \in \{-1/2, 1/2\}$. Finally, $\mathrm{Ker}(\boldsymbol{B})$ is characterized by

$$\mathbf{V} := \mathrm{Ker}(\boldsymbol{B}) := \{(v_1, v_2) \in \mathbf{U} : \gamma_0^-(v_1) = \gamma_0^+(v_2) \text{ on } \Gamma_1\}\,. \tag{4.9}$$

Lemma 4.2.2 *a is bounded in* $\mathbf{U}\times\mathbf{U}$*, and* $\mathbf{V}$*-elliptic.*

Proof. The continuity of bilinear form a follows from the Cauchy-Schwarz inequality. To prove the coerciveness of a on $\mathbf{V}$, we first set $\Omega := \Omega_1 \cup \Gamma_1 \cup \Omega_2$. Next, given $(v_1, v_2) \in \mathbf{V}$, we define the following measurable function

$$v := \begin{cases} v_1 & , \quad \text{a.e. } \in \Omega_1 \\ v_2 & , \quad \text{a.e. } \in \Omega_2. \end{cases} \tag{4.10}$$

Since $v_1 \in H^1(\Omega_1)$, $v_2 \in H^1(\Omega_2)$, and $\gamma_0^-(v_1) = \gamma_0^+(v_2)$ on Γ_1, we infer that $v \in H^1(\Omega)$, with $\int_\Omega v = 0$. Then, thanks to the Poincaré-Wintinger inequality, the seminorm $|\cdot|_{1,\Omega}$ is equivalent to $||\cdot||_{1,\Omega}$ in $H^1(\Omega)\cap L^2_0(\Omega)$, we deduce

$$\begin{aligned} a((u_1,u_2),(v_1,v_2)) &= \|\nabla v_1\|^2_{0,\Omega_1} + \|\nabla v_2\|^2_{0,\Omega_2} = \|\nabla v\|^2_{0,\Omega} \\ &\geq (1+C_p^2)^{-1}\|v\|^2_{1,\Omega} \\ &= (1+C_p^2)^{-1}\|(v_1,v_2)\|^2_{\mathbf{U}}, \end{aligned} \tag{4.11}$$

where $C_p > 0$ is the constant of Poincaré. □

Lemma 4.2.3 $\mathbf{B}$ *is surjective.*

Proof. Given $\lambda \in H^{-1/2}(\Gamma_1)$, there exists $z := -\left(\tilde{\gamma}_0^-\right)^{-1}\left(\mathcal{R}^*\right)^{-1}\lambda \in [H^1_0(\Omega_1)]^\perp \subset H^1(\Omega_1)$, such that $\lambda = \mathcal{R}^*(\gamma_0^-(z))$, where $\tilde{\gamma}_0 := \gamma_0|_{[H^1_0(\Omega_1)]^\perp}$. For more details, we refer to [97] (pages 196-198). Now, by setting $c := -\dfrac{1}{|\Omega_1|+|\Omega_2|}\displaystyle\int_{\Omega_1} z$, we introduce $(v_1,v_2) \in H^1(\Omega_1)\times H^1(\Omega_2)$ such that $v_1 := z + c$ and $v_2 := c$, which in addition verifies that $(v_1,1)_{\Omega_1} + (v_2,1)_{\Omega_2} = 0$, letting us to conclude that $(v_1,v_2) \in \mathbf{U}$. Then, since $\gamma_0^+(v_2) - \gamma_0^-(v_1) = \gamma_0^-(-z)$ on Γ_1, we infer that

$$\mathbf{B}(v_1,v_2) = \mathcal{R}^*(\gamma_0^+(v_2) - \gamma_0^-(v_1)) = \mathcal{R}^*(\gamma_0^-(-z)) = \lambda\,.$$

□

We now establish the unique solvability of the variational problem.

Theorem 4.2.1 (Well-posedness) *The continuous problem* (4.8) *is well-posed.*

Proof. Taking into account Lemmas 4.2.1, 4.2.2 and 4.2.3, we invoke well known Babuška-Brezzi's theory, to conclude that the variational problem (4.8) is well-posed. □

Remark 4.2.2 *For $\lambda \in H^{1/2}(\Gamma_1)$ given, and $(v_1, v_2) \in \mathbf{U}$ defined as in the proof of Lemma 4.2.3, there holds*

$$\begin{aligned} b((v_1,v_2),\lambda) &= \langle \lambda\,,\, \gamma_0^+(v_2) - \gamma_0^-(v_1)\rangle_{\Gamma_1} \;=\; \langle \lambda\,,\, \gamma_0^-(-z)\rangle_{\Gamma_1} \\ &= \langle \lambda\,,\, \left(\mathcal{R}^*\right)^{-1}\lambda\rangle_{\Gamma_1} \;=\; ||\lambda||^2_{-1/2,\Gamma_1}\,. \end{aligned}$$

In addition, there exists $C_{\texttt{INF}} = C_{\texttt{INF}}(|\Omega_1|, |\Omega_2|) > 0$ such that

$$||(v_1,v_2)||^2_{\mathbf{U}} \;\leq\; C_{\texttt{INF}}\, ||z||^2_{1,\Omega_1}\,.$$

As result, we can establish the so called inf-sup condition for b:

$$\sup_{(w_1,w_2)\in\mathbf{U}\setminus\{0\}} \frac{b((w_1,w_2),\lambda)}{||(w_1,w_2)||_{\mathbf{U}}} \geq \frac{b((v_1,v_2),\lambda)}{||(v_1,v_2)||_{\mathbf{U}}} \geq C_{\texttt{INF}}^{-1/2}\, \frac{||\lambda||^2_{-1/2,\Gamma_1}}{||z||_{1,\Omega_1}} = C_{\texttt{INF}}^{-1/2}\, ||\lambda||_{-1/2,\Gamma_1}\,. \tag{4.12}$$

4.3 Discrete settings

We begin this section giving a general description of the discrete spaces, operators that we need to introduce for the discretization of the transmission problem, including some approximation properties. For simplicity, we let Ω be a domain with polyhedral boundary. Then, we introduce $\mathcal{H} \subset \mathbb{R}^+$ as a countable set of meshsizes having 0 as its unique accumulation point and $\{\mathcal{T}_h\}_{h\in\mathcal{H}}$ be an h-refined admissible mesh sequence of $\overline{\Omega}$ (see Section 1.4 in [69]). Each mesh $\mathcal{T}_h$ is a finite collection $\{T\}$ of nonempty, disjoint, open, polytopal elements such that $\overline{\Omega} = \bigcup_{T\in\mathcal{T}_h} \overline{T}$. In addition, there is a matching simplicial submesh of $\mathcal{T}_h$ with locally equivalent meshsize and which is shape-regular in the usual sense. We also assume (for simplicity) that for each $T \in \mathcal{T}_h$, either $T \subset \overline{\Omega}_1$ or $T \subset \overline{\Omega}_2$, and that there are no hanging nodes on the transmission boundary Γ_1. We call a face, any hyperplanar closed connected subset F of $\overline{\Omega}$ with positive $(d-1)$-dimensional measure, such that (i) either there exist T_1, $T_2 \in \mathcal{T}_h$ with $F \subset \partial T_1 \cap \partial T_2$ (and F is called an interface) or (ii) there exists $T \in \mathcal{T}_h$ such that $F \subset \partial T \cap \partial\Omega$ (and F is called a boundary face). Interfaces are collected in the set $\mathcal{F}_h^{\texttt{int}}$, boundary faces in $\mathcal{F}_h^{\texttt{b}}$, and we set the list of faces on skeletal induced by $\mathcal{T}_h$ as $\mathcal{F}_h := \mathcal{F}_h^{\texttt{int}} \cup \mathcal{F}_h^{\texttt{b}}$.

On the other hand, given $T \in \mathcal{T}_h$, $\mathcal{F}_T := \{F \in \mathcal{F}_h \,|\, F \subset \partial T\}$ denotes the set of faces lying on the boundary of T and, for each $F \in \mathcal{F}_T$, $\boldsymbol{n}_{TF}$ is the unit normal to

F pointing out of T. In an admissible mesh sequence, the diameters of the elements (h_T) and the diameters of the faces (h_F), linked to each element, are uniformly comparable, card($\mathcal{F}_T$) is uniformly bounded, the usual discrete and multiplicative trace inequalities hold on element faces, and the L^2-orthogonal projector onto polynomial spaces enjoys optimal approximation properties on each mesh element. In what follows, $A \lesssim B$ denotes the inequality $A \leq CB$ with positive constant C independent of the polynomial degree k, and the meshsize h of $\mathcal{T}_h$, which is set as $h := \max_{T\in\mathcal{T}_h} h_T$.

Lemma 4.3.1 (Approximation property of Orthogonal projector) *Given an integer $l \geq 0$, there exists a real positive number C_a, depending on the mesh regularity parameter and l, such that, for all $h \in \mathcal{H}$, and all $T \in \mathcal{T}_h$, denoting by π_T^l the L^2-orthogonal projector on $\mathbb{P}_d^l(T)$, and for all $s, t \in \mathbb{R}$ such that $0 \leq s \leq t \leq l+1$, there holds*

$$|v - \pi_T^l v|_{s,T} \leq C_a h_T^{t-s} |v|_{t,T}, \quad \forall\, v \in H^t(T)\,. \tag{4.13}$$

Moreover, there exists $\tilde{C}_a > 0$, such that, for all $1/2 < t \leq l+1$, there holds

$$\|v - \pi_T^l v\|_{0,\partial T} \leq \tilde{C}_a h_T^{t-1/2} |v|_{t,T}, \quad \forall\, v \in H^t(T), \tag{4.14}$$

where, given $r \geq 0$, $|\cdot|_{r,T}$ denotes the usual seminorm on Sobolev spaces $H^r(T)$.

Proof. We refer to the proofs of Theorems 3.2 and 3.3 in [102]. □

4.3.1 Degrees of freedom

Let a polynomial degree $k \geq 0$ be fixed. For each $T \in \mathcal{T}_h$, we define the local space of DOFs as $\underline{\mathbf{U}}_T^k := \mathbb{P}_d^k(T) \times \big(\prod_{F\in\mathcal{F}_T} \mathbb{P}_{d-1}^k(F)\big)$, where $\mathbb{P}_d^k(T)$ (resp., $\mathbb{P}_{d-1}^k(F)$) is spanned by the restrictions to T (resp., F) of d-variate (resp., $(d-1)$-variate) polynomials of total degree $\leq k$. The global space of DOFs on the domain Ω is then defined as,

$$\underline{\mathbf{U}}_{\mathcal{T}_h}^k := \left(\prod_{T\in\mathcal{T}_h} \mathbb{P}_d^k(T)\right) \times \left(\prod_{F\in\mathcal{F}_h} \mathbb{P}_{d-1}^k(F)\right).$$

Given $\underline{\mathbf{v}}_h := \Big((v_T)_{T\in\mathcal{T}_h}, (v_F)_{F\in\mathcal{F}_h}\Big) \in \underline{\mathbf{U}}_{\mathcal{T}_h}^k$, we introduce its restriction to the element $T \in \mathcal{T}_h$ as $\underline{\mathbf{v}}_T := \Big(v_T, (v_F)_{F\in\mathcal{F}_T}\Big) \in \underline{\mathbf{U}}_T^k$. In addition, by v_h we denote the function

belonging to $\mathbb{P}_d^k(\mathcal{T}_h)$, such that $v_h|_T = v_T \quad \forall T \in \mathcal{T}_h$. These notations allow us to introduce the usual seminorm on $\underline{\mathbf{U}}_{\mathcal{T}_h}^k$ (see Lemma 4 in [75])

$$\|\underline{\mathbf{v}}_h\|_{1,\mathcal{T}_h}^2 := \sum_{T\in\mathcal{T}_h} \|\underline{\mathbf{v}}_T\|_{1,T}^2 \quad , \quad \|\underline{\mathbf{v}}_T\|_{1,T}^2 := \|\nabla v_T\|_{0,T}^2 + |\underline{\mathbf{v}}_T|_{1,\partial T}^2 \,, \tag{4.15}$$

for all $\underline{\mathbf{v}}_h \in \underline{\mathbf{U}}_{\mathcal{T}_h}^k$ and all $\underline{\mathbf{v}}_T \in \underline{\mathbf{U}}_T^k$, where

$$|\underline{\mathbf{v}}_T|_{1,\partial T}^2 := \sum_{F\in\mathcal{F}_T} h_F^{-1} \|v_F - v_T\|_{0,F}^2 \,.$$

Now, for each $T \in \mathcal{T}_h$, we define the local reduction operator $\underline{\mathbf{I}}_T^k : H^1(T) \to \underline{\mathbf{U}}_T^k$ such that, for each $v \in H^1(T)$,

$$\underline{\mathbf{I}}_T^k v := (\pi_T^k v, (\pi_F^k v)_{F\in\mathcal{F}_T}), \tag{4.16}$$

where π_T^k and π_F^k are the L^2-orthogonal projectors onto $\mathbb{P}_d^k(T)$ and $\mathbb{P}_{d-1}^k(F)$, respectively. The corresponding global reduction operator $\underline{\mathbf{I}}_{\mathcal{T}_h}^k : H^1(\Omega) \to \underline{\mathbf{U}}_{\mathcal{T}_h}^k$ is defined by

$$\underline{\mathbf{I}}_{\mathcal{T}_h}^k v := ((\pi_T^k v)_{T\in\mathcal{T}_h}, (\pi_F^k v)_{F\in\mathcal{F}_h}) \quad \forall\, v \in H^1(\Omega) \,. \tag{4.17}$$

4.3.2 Local Gradient reconstruction

For all $T \in \mathcal{T}_h$, we define the local gradient reconstruction operator $G_T^k : \underline{\mathbf{U}}_T^k \to \nabla\mathbb{P}_d^{k+1}(T)$ such that, for all $\underline{\mathbf{v}}_T := (v_T, (v_F)_{F\in\mathcal{F}_T}) \in \underline{\mathbf{U}}_T^k$ and all $w \in \mathbb{P}_d^{k+1}(T)$,

$$(G_T^k \underline{\mathbf{v}}_T, \nabla w)_T = (\nabla v_T, \nabla w)_T + \sum_{F\in\mathcal{F}_T} (v_F - v_T, \nabla w \cdot \boldsymbol{n}_{TF})_F, \tag{4.18}$$

where $\boldsymbol{n}_{TF}$ is the unit normal to face F pointing out of element T. We define the potential reconstruction operator $p_T^{k+1} : \underline{\mathbf{U}}_T^k \to \mathbb{P}_d^{k+1}(T)$ such that, for all $\underline{\mathbf{v}}_T \in \underline{\mathbf{U}}_T^k$,

$$\nabla p_T^{k+1} \underline{\mathbf{v}}_T = G_T^k \underline{\mathbf{v}}_T \qquad \int_T p_T^{k+1} \underline{\mathbf{v}}_T = \int_T v_T \,. \tag{4.19}$$

Lemma 4.3.2 (Characterization of $p_T^{k+1}\underline{\mathbf{I}}_T^k$ and polynomial consistency) *The following property holds for all $v \in H^1(T)$:*

$$(\nabla(v - p_T^{k+1}\underline{\mathbf{I}}_T^k v), \nabla w)_T = 0 \quad \forall\, w \in \mathbb{P}_d^{k+1}(T). \tag{4.20}$$

Consequently, for all $v \in \mathbb{P}_d^{k+1}(T)$, we have

$$p_T^{k+1}\underline{\mathbf{I}}_T^k v = v. \tag{4.21}$$

Proof. We refer to the proof of Lemma 3.1 in [76]. □

Lemma 4.3.3 (Approximation properties for $p_T^{k+1}\underline{\mathbf{I}}_T^k$) *Let a polynomial degree $k \geq 0$, an integer $q \in \{0, \cdots, k\}$, and $\delta \in (1/2, 1]$ be given. There exists a real number $C > 0$, depending on the mesh regularity parameter, possibly on d, k, q, and δ, but independent of h_T, such that, for all $h \in \mathcal{H}$, for all $T \in \mathcal{T}_h$, and all $v \in H^{q+1+\delta}(T)$, there holds:*

$$\begin{aligned}&\left\|v - p_T^{k+1}\underline{\mathbf{I}}_T^k v\right\|_{0,T} + h_T^{1/2}\left\|v - p_T^{k+1}\underline{\mathbf{I}}_T^k v\right\|_{0,\partial T}\\ &+ h_T\left\|\nabla(v - p_T^{k+1}\underline{\mathbf{I}}_T^k v)\right\|_{0,T} + h_T^{3/2}\left\|\nabla(v - p_T^{k+1}\underline{\mathbf{I}}_T^k v)\right\|_{0,\partial T} \leq C h_T^{q+1+\delta}\left\|v\right\|_{q+1+\delta,T}.\end{aligned} \tag{4.22}$$

Proof. We adapt the proof of Lemma 3 in [75]. First, we fix $v \in H^{q+1+\delta}(T)$, with $q \in \{0, ..., k\}$, and notice from the orthogonality property (4.20), that

$$\begin{aligned}\|\nabla(v - p_T^{k+1}\underline{\mathbf{I}}_T^k v)\|_{0,T} &= \sup_{z \in \mathbb{P}_d^{k+1}(T)} \|\nabla v - \nabla z\|_{0,T}\\ &\leq \|\nabla(v - \pi_T^{k+1} v)\|_{0,T} \lesssim h_T^{q+\delta}\|v\|_{q+1+\delta,T},\end{aligned} \tag{4.23}$$

where we have used the approximation property (4.13) of π_T^{k+1} (with $t = q + 1 + \delta$ and $s = 1$).

Now, from the definition of p_T^{k+1} and $\underline{\mathbf{I}}_T^k$, we observe that $v - p_T^{k+1}\underline{\mathbf{I}}_T^k v \in L_0^2(T)$. Then, applying the very well known inequality $||z||_{0,T} \lesssim h_T|z|_{1,T}$, $\forall\, z \in H^1(T) \cap L_0^2(T)$, togehter with (4.23), we infer that

$$\|v - p_T^{k+1}\underline{\mathbf{I}}_T^k v\|_{0,T} \lesssim h_T\|\nabla(v - p_T^{k+1}\underline{\mathbf{I}}_T^k v)\|_{0,T} \lesssim h_T^{q+1+\delta}\|v\|_{q+1+\delta,T}. \tag{4.24}$$

The consecutive use of a continuous trace inequality, (4.23) and (4.24), yields

$$h_T\|v - p_T^{k+1}\underline{\mathbf{I}}_T^k v\|_{0,\partial T}^2 \lesssim \|v - p_T^{k+1}\underline{\mathbf{I}}_T^k v\|_{0,T}^2 + h_T^2\|\nabla(v - p_T^{k+1}\underline{\mathbf{I}}_T^k v)\|_{0,T}^2 \lesssim h_T^{2(q+1+\delta)}\|v\|_{q+1+\delta,T}^2. \tag{4.25}$$

Finally, for to bound $h_T^{3/2}\|\nabla(v - p_T^{k+1}\underline{\mathbf{I}}_T^k v)\|_{0,\partial T}$, we introduce $\pm\pi_T^k\nabla v$ inside the norm, obtaining

$$h_T^{3/2}\left\|\nabla(v - p_T^{k+1}\underline{\mathbf{I}}_T^k v)\right\|_{0,\partial T} \leq h_T^{3/2}\left\|\nabla v - \pi_T^k\nabla v\right\|_{0,\partial T} + h_T^{3/2}\left\|\pi_T^k\nabla v - \nabla p_T^{k+1}\underline{\mathbf{I}}_T^k v\right\|_{0,\partial T}.$$

Using the approximation property (4.14) of π_T^k (applied componentwise to ∇v with $t = q+\delta$ and $s = 0$), we infer that

$$h_T \left\| \nabla v - \pi_T^k \nabla v \right\|_{0,\partial T}^2 \lesssim h_T^{2(q+\delta)} \|v\|_{q+1+\delta,T}^2 . \tag{4.26}$$

Now, we apply the discrete trace inequality, using the fact that $\mathrm{card}(\mathcal{F}_T)$ is uniformly bounded, and that $\nabla p_T^{k+1} \underline{\mathbf{I}}_T^k v \in \left[\mathbb{P}_d^k(T)\right]^d$, to infer

$$\|\pi_T^k \nabla v - \nabla p_T^{k+1} \underline{\mathbf{I}}_T^k v\|_{0,\partial T} \lesssim h_T^{-1/2} \|\nabla (v - p_T^{k+1} \underline{\mathbf{I}}_T^k v)\|_{0,T} \lesssim h_T^{q+\delta-1/2} \|v\|_{q+1+\delta,T} . \tag{4.27}$$

Finally, the proof is concluded from (4.26) and (4.27). □

4.4 HHO formulation

From here on, we consider $g_1 \in L^2(\Gamma_1)$, $g_2 \in L^2(\Omega_2)$, $\Omega := \Omega_1 \cup \Gamma_1 \cup \Omega_2$, and let $\mathcal{T}_h$ be a triangulation of $\overline{\Omega}$, satisfying the geometric assumptions given in Section 4.3. Next, we introduce the triangulations induced by $\mathcal{T}_h$, of each subdomain $\overline{\Omega}_i$, $i \in \{1,2\}$, that is

$$\mathcal{T}_{i,h} := \{T \in \mathcal{T}_h \,:\, T \subset \Omega_i\},$$

with $\mathcal{F}_{i,h}$ being the list of faces on skeleton, induced by $\mathcal{T}_{i,h}$, $i \in \{1,2\}$. Moreover, by $\Gamma_{1,h}$ and $\Gamma_{2,h}$, we denote the partitions of Γ_1 and Γ_2, respectively, induced by $\mathcal{T}_{2,h}$. At this point we require also that the partition of transmission boundary Γ_1 inherited by $\mathcal{T}_h$, $\Gamma_{1,h}$, is quasi-uniform in the sense: considering $h_{\Gamma_1} := \max_{F \in \mathcal{F}_{1,h}} h_F$, there exists $C_{\mathtt{qu}} > 0$, independent of the meshsize, such that

$$C_{\mathtt{qu}}\, h_{\Gamma_1} \le h_F \quad \forall\, F \in \Gamma_{1,h} . \tag{4.28}$$

These notations allow us to introduce the discrete spaces

$$\underline{\mathbf{U}}_{\mathcal{T}_{i,h}}^k := \left(\prod_{T \in \mathcal{T}_{i,h}} \mathbb{P}_d^k(T) \right) \times \left(\prod_{F \in \mathcal{F}_{i,h}} \mathbb{P}_{d-1}^k(F) \right) , \quad i \in \{1,2\} .$$

Then, each element $\underline{\mathbf{v}}_{i,h} \in \underline{\mathbf{U}}_{\mathcal{T}_{i,h}}^k$ is characterized by $\underline{\mathbf{v}}_{i,h} := \left((v_{i,T})_{T \in \mathcal{T}_{i,h}}, (v_{i,F})_{F \in \mathcal{F}_{i,h}} \right)$, $i \in \{1,2\}$. Now, we set our discrete approximation space, as $\underline{\mathbf{U}}_{\mathcal{T}_h}^{k,0} \times Q_h^k$, where

$$\underline{\mathbf{U}}_{\mathcal{T}_h}^{k,0} := \left\{ \underline{\mathbf{v}}_h := (\underline{\mathbf{v}}_{1,h}, \underline{\mathbf{v}}_{2,h}) \in \underline{\mathbf{U}}_{\mathcal{T}_{1,h}}^k \times \underline{\mathbf{U}}_{\mathcal{T}_{2,h}}^k \,:\, \sum_{i=1}^{2} \sum_{T \in \mathcal{T}_{i,h}} (v_{i,T}, 1)_T = 0 \right\} ,$$

and $Q_h^k := \mathbb{P}_{d-1}^k(\Gamma_{1,h})$. From here on, we adopt the following notation. Given $\lambda_h \in Q_h^k$, we set $\lambda_F := \lambda_h|_F$, for all $F \in \Gamma_{1,h}$. Then, we introduce the characterization $\lambda_h := (\lambda_F)_{F\in\Gamma_{1,h}}$. The space Q_h^k is provided with the weighted L^2-norm

$$\|\lambda_h\|^2_{\Gamma_{1,h}} := \sum_{F\in\Gamma_{1,h}} h_F\|\lambda_F\|^2_{0,F}\,, \quad \forall\, \lambda_h := (\lambda_F)_{F\in\Gamma_{1,h}} \in Q_h^k\,. \tag{4.29}$$

We introduce the seminorm $|||\cdot|||_h : \underline{\mathbf{U}}^k_{\mathcal{T}_{1,h}} \times \underline{\mathbf{U}}^k_{\mathcal{T}_{2,h}} \to \mathbb{R}$, which is given, for each $(\underline{\mathbf{v}}_{1,h}, \underline{\mathbf{v}}_{2,h}) \in \underline{\mathbf{U}}^k_{\mathcal{T}_{1,h}} \times \underline{\mathbf{U}}^k_{\mathcal{T}_{2,h}}$, by

$$|||(\underline{\mathbf{v}}_{1,h}, \underline{\mathbf{v}}_{2,h})|||_h^2 := \|\underline{\mathbf{v}}_{1,h}\|^2_{1,\mathcal{T}_{1,h}} + \|\underline{\mathbf{v}}_{2,h}\|^2_{1,\mathcal{T}_{2,h}} + \sum_{F\in\Gamma_{1,h}} h_F^{-1}\|v_{1,F} - v_{2,F}\|^2_{0,F}. \tag{4.30}$$

Proposition 4.4.1 *The map $|||\cdot|||_h$ defines a norm on $\underline{\mathbf{U}}^{k,0}_{\mathcal{T}_h}$.*

Proof. It is enough to check that, for all $(\underline{\mathbf{v}}_{1,h}, \underline{\mathbf{v}}_{2,h}) \in \underline{\mathbf{U}}^{k,0}_{\mathcal{T}_h}$: $|||(\underline{\mathbf{v}}_{1,h}, \underline{\mathbf{v}}_{2,h})|||_h = 0 \Rightarrow (\underline{\mathbf{v}}_{1,h}, \underline{\mathbf{v}}_{2,h}) = (\underline{\mathbf{0}}, \underline{\mathbf{0}})$. Let $(\underline{\mathbf{v}}_{1,h}, \underline{\mathbf{v}}_{2,h}) \in \underline{\mathbf{U}}^{k,0}_{\mathcal{T}_h}$ be such that $|||(\underline{\mathbf{v}}_{1,h}, \underline{\mathbf{v}}_{2,h})|||_h = 0$. By definition of $|||\cdot|||_h$, this implies

$$\forall T \in \mathcal{T}_{1,h} \quad \nabla v_{1,T} \equiv 0 \quad , \quad \forall F \in \mathcal{F}_T \quad v_{1,T}|_F = v_{1,F} \tag{4.31a}$$

$$\forall S \in \mathcal{T}_{2,h} \quad \nabla v_{2,S} \equiv 0 \quad , \quad \forall F \in \mathcal{F}_S \quad v_{2,S}|_F = v_{2,F} \tag{4.31b}$$

$$\forall F \in \Gamma_{1,h} \quad v_{1,F} = v_{2,F}. \tag{4.31c}$$

We have from (4.31a), that $v_{1,T}$ is constant on each $T \in \mathcal{T}_{1,h}$, and that on each interior face $F \in \mathcal{F}_{1,h}$, there exist $T_1, T_2 \in \mathcal{T}_{1,h}$ with $F \subset \partial T_1 \cap \partial T_2$, such that $v_{1,T_1}|_F = v_{1,F} = v_{1,T_2}|_F$. Then, we infer that, there exists a constant $C_1 > 0$ such that $v_{1,F} = C_1\ \forall\, F \in \mathcal{F}_{1,h}$. In a similar way, we can deduce from (4.31b), that there exists $C_2 > 0$ such that $v_{2,F} = C_2\ \forall\, F \in \mathcal{F}_{2,h}$. Now by (4.31c), we have that on each transmission face $F \in \Gamma_{1,h}$, there exist $T \in \mathcal{T}_{1,h}$ and $S \in \mathcal{T}_{2,h}$ with $F \subset \partial T \cap \partial S$ such that,

$$C_1 = v_{1,T}|_F = v_{1,F} = v_{2,F} = v_{2,S}|_F = C_2\,,$$

which allows us to state that $v_{1,T} = v_{2,S} \equiv C_1 \quad \forall\,(T,S) \in \mathcal{T}_{1,h} \times \mathcal{T}_{2,h}$. Finally, due to the condition $\sum_{T\in\mathcal{T}_{1,h}}(v_{1,T},1)_T + \sum_{S\in\mathcal{T}_{2,h}}(v_{2,S},1)_S = 0$, we deduce that $C_1 = C_2 = 0$, and we conclude the proof. □

Now, for each $T \in \mathcal{T}_h$, we introduce $a_T : \underline{\mathbf{U}}^k_T \times \underline{\mathbf{U}}^k_T \to \mathbb{R}$ given by

$$a_T(\underline{\mathbf{u}}_T, \underline{\mathbf{v}}_T) := \left(G_T^k\underline{\mathbf{u}}_T, G_T^k\underline{\mathbf{v}}_T\right)_T + j_T(\underline{\mathbf{u}}_T, \underline{\mathbf{v}}_T)\,, \tag{4.32}$$

where

$$j_T(\underline{\mathbf{u}}_T, \underline{\mathbf{v}}_T) := \sum_{F \in \mathcal{F}_T} h_F^{-1} (\pi_F^k (u_F - R_T^{k+1} \underline{\mathbf{u}}_T), \pi_F^k (v_F - R_T^{k+1} \underline{\mathbf{v}}_T))_F \,,$$

with

$$R_T^{k+1} \underline{\mathbf{v}}_T := v_T + (p_T^{k+1} \underline{\mathbf{v}}_T - \pi_T^k p_T^{k+1} \underline{\mathbf{v}}_T) \,.$$

Then, we set the bilinear form $a_h : \underline{\mathbf{U}}_{\mathcal{T}_h}^{k,0} \times \underline{\mathbf{U}}_{\mathcal{T}_h}^{k,0} \to \mathbb{R}$, as

$$a_h((\underline{\mathbf{u}}_{1,h}, \underline{\mathbf{u}}_{2,h}), (\underline{\mathbf{v}}_{1,h}, \underline{\mathbf{v}}_{2,h})) \;=\; \sum_{T \in \mathcal{T}_{1,h}} a_T(\underline{\mathbf{u}}_{1,T}, \underline{\mathbf{v}}_{1,T}) + \sum_{S \in \mathcal{T}_{2,h}} a_S(\underline{\mathbf{u}}_{2,S}, \underline{\mathbf{v}}_{2,S}), \tag{4.33}$$

which can also be written as

$$a_h((\underline{\mathbf{u}}_{1,h}, \underline{\mathbf{u}}_{2,h}), (\underline{\mathbf{v}}_{1,h}, \underline{\mathbf{v}}_{2,h})) \;=\; A_h((\underline{\mathbf{u}}_{1,h}, \underline{\mathbf{u}}_{2,h}), (\underline{\mathbf{v}}_{1,h}, \underline{\mathbf{v}}_{2,h})) + j_h((\underline{\mathbf{u}}_{1,h}, \underline{\mathbf{u}}_{2,h}), (\underline{\mathbf{v}}_{1,h}, \underline{\mathbf{v}}_{2,h})) \,, \tag{4.34}$$

where the consistency contribution $A_h : \underline{\mathbf{U}}_{\mathcal{T}_h}^{k,0} \times \underline{\mathbf{U}}_{\mathcal{T}_h}^{k,0} \to \mathbb{R}$ and the stability contribution $j_h : \underline{\mathbf{U}}_{\mathcal{T}_h}^{k,0} \times \underline{\mathbf{U}}_{\mathcal{T}_h}^{k,0} \to \mathbb{R}$ are, respectively, defined as

$$A_h((\underline{\mathbf{u}}_{1,h}, \underline{\mathbf{u}}_{2,h}), (\underline{\mathbf{v}}_{1,h}, \underline{\mathbf{v}}_{2,h})) := \sum_{T \in \mathcal{T}_h} \left(G_T^k \underline{\mathbf{u}}_T, G_T^k \underline{\mathbf{v}}_T \right)_T \tag{4.35}$$

and

$$j_h((\underline{\mathbf{u}}_{1,h}, \underline{\mathbf{u}}_{2,h}), (\underline{\mathbf{v}}_{1,h}, \underline{\mathbf{v}}_{2,h})) := \sum_{T \in \mathcal{T}_h} j_T(\underline{\mathbf{u}}_T, \underline{\mathbf{v}}_T) \,. \tag{4.36}$$

We also introduce the bilinear form $b_h : \underline{\mathbf{U}}_{\mathcal{T}_h}^{k,0} \times Q_h^k \to \mathbb{R}$, which is defined as

$$b_h((\underline{\mathbf{v}}_{1,h}, \underline{\mathbf{v}}_{2,h}), \lambda_h) := \sum_{F \in \Gamma_{1,h}} (\lambda_F, v_{2,F} - v_{1,F})_F \quad \forall \, (\underline{\mathbf{v}}_{1,h}, \underline{\mathbf{v}}_{2,h}) \in \underline{\mathbf{U}}_{\mathcal{T}_h}^{k,0},$$
$$\lambda_h := (\lambda_F)_{F \in \Gamma_{1,h}} \in Q_h^k \,. \tag{4.37}$$

Then, the discrete scheme associated to (4.8) reads as follows: Find $((\underline{\mathbf{u}}_{1,h}, \underline{\mathbf{u}}_{2,h}), \xi_h) \in \underline{\mathbf{U}}_{\mathcal{T}_h}^{k,0} \times Q_h^k$ such that

$$a_h((\underline{\mathbf{u}}_{1,h}, \underline{\mathbf{u}}_{2,h}), (\underline{\mathbf{v}}_{1,h}, \underline{\mathbf{v}}_{2,h})) + b_h((\underline{\mathbf{v}}_{1,h}, \underline{\mathbf{v}}_{2,h}), \xi_h) = F_h((\underline{\mathbf{v}}_{1,h}, \underline{\mathbf{v}}_{2,h})) \;\forall (\underline{\mathbf{v}}_{1,h}, \underline{\mathbf{v}}_{2,h}) \in \underline{\mathbf{U}}_{\mathcal{T}_h}^{k,0} \,, \tag{4.38a}$$

$$-b_h((\underline{\mathbf{u}}_{1,h}, \underline{\mathbf{u}}_{2,h}), \lambda_h) = G_h(\lambda_h) \;\forall \lambda_h \in Q_h^k \,, \tag{4.38b}$$

where, for each $(\underline{\mathbf{v}}_{1,h}, \underline{\mathbf{v}}_{2,h}) \in \underline{\mathbf{U}}_{\mathcal{T}_h}^k$ and $\lambda_h \in Q_h^k$, we define the discrete linear functionals as:

$$F_h(\underline{\mathbf{v}}_{1,h}, \underline{\mathbf{v}}_{2,h}) := \sum_{T\in\mathcal{T}_{1,h}} (f_1, v_{1,T})_T + \sum_{S\in\mathcal{T}_{2,h}} (f_2, v_{2,S})_S + \sum_{F\in\Gamma_{1,h}} (g_1, v_{2,F})_F + \sum_{F\in\Gamma_{2,h}} (g_2, v_{2,F})_F, \tag{4.39}$$

and $G_h(\lambda_h) := (\lambda_h, g)_{\Gamma_{1,h}}$. In what follows, we recall the well known relationships between $||\cdot||_{0,\Gamma_1}$ and $||\cdot||_{-1/2,\Gamma_1}$.

Lemma 4.4.1 *There holds*

$$||\tilde{g}||_{-1/2,\Gamma_1} \lesssim ||\tilde{g}||_{0,\Gamma_1} \quad \forall\, \tilde{g} \in L^2(\Gamma_1)\,, \tag{4.40}$$

$$||\lambda_h||_{0,\Gamma_1} \lesssim h_{\Gamma_1}^{-1/2}\, ||\lambda_h||_{-1/2,\Gamma_1} \quad \forall\, \lambda_h \in Q_h^k\,. \tag{4.41}$$

Proof. A proof of (4.40) is available in [140] (page 115), while (4.41) can be proved in the same spirit of the proof of Lemma 4.6 in [96]. □

From here on, given $\underline{\mathbf{v}}_h \in \underline{\mathbf{U}}_{\mathcal{T}_h}^k$, we denote by v_h the $L^2(\Omega)$ function such that $v_h|_T = v_T$, for all $T \in \mathcal{T}_h$. Next result, which can be seen as the corresponding to Lemma 8.3 in [66] for Neumann boundary condition, will be useful for proving the continuity of linear functional F_h.

Lemma 4.4.2 *There holds*

$$||v_h||_{0,\Omega} \lesssim |\!|\!|\underline{\mathbf{v}}_h|\!|\!|_h \quad \forall\, \underline{\mathbf{v}}_h \in \underline{\mathbf{U}}_{\mathcal{T}_h}^{k,0}\,. \tag{4.42}$$

Proof. The proof for general domain Ω is provided in the appendix of this chapter. However, when Ω is convex, the proof of (4.42) can be done usign a different argument, more constructive, which is described next.

Let $\underline{\mathbf{v}}_h \in \underline{\mathbf{U}}_{\mathcal{T}_h}^{k,0}$. Since $v_h \in L_0^2(\Omega)$, there exists a unique weak solution $z \in H^1(\Omega)$ of

$$-\Delta z = v_h \quad \text{in} \quad \Omega\,, \quad \frac{\partial z}{\partial \boldsymbol{\nu}} = 0 \quad \text{on} \quad \partial\Omega\,. \tag{4.43}$$

Since Ω is convex, we can ensure that $z \in H^2(\Omega)$ and $||z||_{2,\Omega} \lesssim ||v_h||_{0,\Omega}$ (cf. [110]). This allows us to introduce $\boldsymbol{\tau}_v := -\nabla z \in [H^1(\Omega)]^2$, which satisfies:

$$\mathrm{div}(\boldsymbol{\tau}_v) = v_h \quad \text{in} \quad \Omega\,, \quad \boldsymbol{\tau}_v \cdot \boldsymbol{\nu} = 0 \quad \text{on} \quad \partial\Omega\,, \quad \text{and} \quad ||\boldsymbol{\tau}_v||_{1,\Omega} \lesssim ||v_h||_{0,\Omega}\,. \tag{4.44}$$

Then, taking into account the fact that $\boldsymbol{\tau}_v \in H(\mathrm{div};\Omega)$, and the first two statements in (4.44), we have

$$
\begin{aligned}
||v_h||^2_{0,\Omega} &= (v_h, \mathrm{div}(\boldsymbol{\tau}_v))_\Omega \;=\; (v_h, \mathrm{div}(\boldsymbol{\tau}_v))_{\Omega_1} \;+\; (v_h, \mathrm{div}(\boldsymbol{\tau}_v))_{\Omega_2} \\
&= \sum_{T\in\mathcal{T}_{1,h}} \left\{ -(\nabla v_{1,T}, \boldsymbol{\tau}_v)_T \;+\; \sum_{F\in\mathcal{F}_T} (\boldsymbol{\tau}_v\cdot\boldsymbol{n}_{TF}, v_{1,T})_F \right\} \\
&\quad + \sum_{T\in\mathcal{T}_{2,h}} \left\{ -(\nabla v_{2,T}, \boldsymbol{\tau}_v)_T \;+\; \sum_{F\in\mathcal{F}_T} (\boldsymbol{\tau}_v\cdot\boldsymbol{n}_{TF}, v_{2,T})_F \right\} \\
&= \sum_{T\in\mathcal{T}_{1,h}} \left\{ -(\nabla v_{1,T}, \boldsymbol{\tau}_v)_T \;+\; \sum_{F\in\mathcal{F}_T} (\boldsymbol{\tau}_v\cdot\boldsymbol{n}_{TF}, v_{1,T}-v_{1,F})_F \right\} \\
&\quad + \sum_{T\in\mathcal{T}_{2,h}} \left\{ -(\nabla v_{2,T}, \boldsymbol{\tau}_v)_T \;+\; \sum_{F\in\mathcal{F}_T} (\boldsymbol{\tau}_v\cdot\boldsymbol{n}_{TF}, v_{2,T}-v_{2,F})_F \right\} \\
&\quad + \sum_{F\in\Gamma_{1,h}} (\boldsymbol{\tau}_v\cdot\boldsymbol{n}_1, v_{1,F}-v_{2,F})_F \,. \qquad (4.45)
\end{aligned}
$$

Now, applying Cauchy-Schwarz, Minkowski and continuous local trace inequalities, we notice

$$
\begin{aligned}
&\sum_{T\in\mathcal{T}_{1,h}} \left\{ -(\nabla v_{1,T}, \boldsymbol{\tau}_v)_T \;+\; \sum_{F\in\mathcal{F}_T} (\boldsymbol{\tau}_v\cdot\boldsymbol{n}_{TF}, v_{1,T}-v_{1,F})_F \right\} \\
&\leq \sum_{T\in\mathcal{T}_{1,h}} \left(||\nabla v_{1,T}||_{0,T}||\boldsymbol{\tau}_v||_{0,T} \;+\; \sum_{F\in\mathcal{F}_T} \left(h_F^{-1/2}||v_{1,T}-v_{1,F}||_{0,F}\right)\left(h_F^{1/2}||\boldsymbol{\tau}_v||_{0,F}\right)\right) \\
&\leq ||\underline{v}_{1,h}||_{1,\mathcal{T}_{1,h}} \left\{ \sum_{T\in\mathcal{T}_{1.h}} \left(||\boldsymbol{\tau}_v||^2_{0,T} \;+\; h_T||\boldsymbol{\tau}_v||^2_{0,\partial T}\right)\right\}^{1/2} \\
&\lesssim ||\underline{v}_{1,h}||_{1,\mathcal{T}_{1,h}} \left\{ \sum_{T\in\mathcal{T}_{1.h}} \left(||\boldsymbol{\tau}_v||^2_{0,T} \;+\; ||\boldsymbol{\tau}_v||^2_{0,T} + h_T^2|\boldsymbol{\tau}_v|^2_{1,T}\right)\right\}^{1/2} \\
&\lesssim ||\underline{v}_{1,h}||_{1,\mathcal{T}_{1,h}}\, ||\boldsymbol{\tau}_v||_{1,\Omega_1}\,.
\end{aligned}
$$

Proceeding in analogous way, we deduce that

$$
\sum_{T\in\mathcal{T}_{2,h}} \left\{ -(\nabla v_{2,T}, \boldsymbol{\tau}_v)_T \;+\; \sum_{F\in\mathcal{F}_T} (\boldsymbol{\tau}_v\cdot\boldsymbol{n}_{TF}, v_{2,T}-v_{2,F})_F \right\} \lesssim ||\underline{v}_{2,h}||_{1,\mathcal{T}_{2,h}}\, ||\boldsymbol{\tau}_v||_{1,\Omega_2}\,,
$$

and

$$
\sum_{F\in\Gamma_{1,h}} (\boldsymbol{\tau}_v\cdot\boldsymbol{n}_1, v_{1,F}-v_{2,F})_F \lesssim \left(\sum_{F\in\Gamma_{1,h}} h_F^{-1}||v_{1,F}-v_{2,F}||^2_{0,F}\right)^{1/2} ||\boldsymbol{\tau}_v||_{1,\Omega_1}\,.
$$

Considering these relationships, and applying Minkowski inequality one more time and the regularity property in (4.44), (4.45) yields to

$$||v_h||^2_{0,\Omega} \lesssim |||\underline{v}_h|||_h \, ||v_h||_{0,\Omega} \, ,$$

and we conclude the proof. □

Lemma 4.4.3 *Bilinear forms a_h and b_h, as well as linear functionals F_h and G_h, are continuous.*

Proof. Let us establish the continuity of the discrete bilinear forms a_h and b_h. Thanks to the continuity of a_T (see [75]), and applying Cauchy-Schwarz and Minkowski inequalities, we have

$$\begin{aligned} |a_h((\underline{\mathbf{u}}_{1,h}, \underline{\mathbf{u}}_{2,h}), (\underline{\mathbf{v}}_{1,h}, \underline{\mathbf{v}}_{2,h}))| &\lesssim \|\underline{\mathbf{u}}_{1,h}\|_{1,\mathcal{T}_{1,h}} \cdot \|\underline{\mathbf{v}}_{1,h}\|_{1,\mathcal{T}_{1,h}} + \|\underline{\mathbf{u}}_{2,h}\|_{1,\mathcal{T}_{2,h}} \cdot \|\underline{\mathbf{v}}_{2,h}\|_{1,\mathcal{T}_{2,h}} \\ &\leq \left(\|\underline{\mathbf{u}}_{1,h}\|^2_{1,\mathcal{T}_{1,h}} + \|\underline{\mathbf{u}}_{2,h}\|^2_{1,\mathcal{T}_{2,h}} \right)^{1/2} \left(\|\underline{\mathbf{v}}_{1,h}\|^2_{1,\mathcal{T}_{1,h}} + \|\underline{\mathbf{v}}_{2,h}\|^2_{1,\mathcal{T}_{1,h}} \right)^{1/2} \\ &\leq |||(\underline{\mathbf{u}}_{1,h}, \underline{\mathbf{u}}_{2,h})|||_h \, |||(\underline{\mathbf{v}}_{1,h}, \underline{\mathbf{v}}_{2,h})|||_h \, . \end{aligned}$$

Now, for b_h, after applying Cauchy-Schwarz and Minkowski inequalities, and Lemma 4.4.1, we obtain

$$\begin{aligned} |b_h((\underline{\mathbf{u}}_{1,h}, \underline{\mathbf{u}}_{2,h}), \lambda_h)| &\leq \left(\sum_{F \in \Gamma_{1,h}} h_F^{-1} \|u_{1,F} - u_{2,F}\|^2_{0,F} \right)^{1/2} \left(\sum_{F \in \Gamma_{1,h}} h_F \|\lambda_F\|^2_{0,F} \right)^{1/2} \\ &\leq |||(\underline{\mathbf{u}}_{1,h}, \underline{\mathbf{u}}_{2,h})|||_h \, \|\lambda_h\|_{\Gamma_{1,h}} \, . \end{aligned} \tag{4.46}$$

Next, we prove the continuity of the discrete linear functional F_h. First, we notice that

$$\sum_{F \in \mathcal{F}_{1,h}} (g_1, v_{2,F})_F = \sum_{F \in \mathcal{F}_{1,h}} (g_1, v_{2,F} - c_2)_F + c_2 \langle g_1, 1 \rangle_{\Gamma_1} \tag{4.47}$$

$$\sum_{F \in \mathcal{F}_{2,h}} (g_2, v_{2,F})_F = \sum_{F \in \mathcal{F}_{2,h}} (g_2, v_{2,F} - c_2)_F + c_2 \langle g_2, 1 \rangle_{\Gamma_2} \, , \tag{4.48}$$

where $c_2 := \dfrac{1}{|\Omega_2|} \displaystyle\int_{\Omega_2} v_{2,h}$.

Applying Cauchy-Schwarz inequality appropriately, we have

$$
\begin{aligned}
|F_h(\underline{\mathbf{v}}_{1,h},\underline{\mathbf{v}}_{2,h})| \leq \|f_1\|_{0,\Omega_1}\left(\sum_{T\in\mathcal{T}_{1,h}}\|v_{1,T}\|^2_{0,T}\right)^{1/2} + \|f_2\|_{0,\Omega_2}\left(\sum_{S\in\mathcal{T}_{2,h}}\|v_{2,S}\|^2_{0,S}\right)^{1/2} \\
+ ||g_1||_{0,\Gamma_1}\left(\sum_{F\in\Gamma_{1,h}}\|v_{2,F}-c_2\|^2_{0,F}\right)^{1/2} + |c_2|\,|\Omega_2|^{1/2}\,||g_1||_{-1/2,\Gamma_1} \\
+ ||g_2||_{0,\Gamma_2}\left(\sum_{F\in\Gamma_{2,h}}\|v_{2,F}-c_2\|^2_{0,F}\right)^{1/2} + |c_2|\,|\Omega_2|^{1/2}\,||g_2||_{-1/2,\Gamma_2}\,.
\end{aligned}
\tag{4.49}
$$

Thanks to Minkowski inequality, (4.47), and the fact that $|c_2| \leq |\Omega_2|^{-1/2}\,||v_{2,h}||_{0,\Omega_2}$, we obtain

$$
|F_h(\underline{\mathbf{v}}_{1,h},\underline{\mathbf{v}}_{2,h})| \leq C\left(||v_{1,h}||^2_{0,\Omega_1} + ||v_{2,h}||^2_{0,\Omega_2} + \sum_{F\in\Gamma_{1,h}\cup\Gamma_{2,h}}\|v_{2,F}-c_2\|^2_{0,F}\right)^{1/2},
\tag{4.50}
$$

where

$$
C := \left(\|f_1\|^2_{0,\Omega_1} + \|f_2\|^2_{0,\Omega_2} + ||g_1||^2_{-1/2,\Gamma_1} + ||g_2||^2_{-1/2,\Gamma_2} + ||g_1||^2_{0,\Gamma_1} + ||g_2||^2_{0,\Gamma_2}\right)^{1/2}.
$$

Now, we bound the right hand side of (4.50). First, since $\underline{\mathbf{v}}_h \in \underline{\mathbf{U}}^{k,0}_{\mathcal{T}_h}$, we apply Lemma 4.4.2, and get

$$
||v_{1,h}||^2_{0,\Omega_1} + ||v_{2,h}||^2_{0,\Omega_2} = ||v_h||^2_{0,\Omega} \lesssim |||\underline{\mathbf{v}}_h|||^2_h\,.
\tag{4.51}
$$

On the other hand, considering $\underline{\mathbf{z}}_h := \left((v_{2,T}-c_2)_{T\in\mathcal{T}_{2,h}},(v_{2,F}-c_2)_{F\in\mathcal{F}_{2,h}}\right) \in \underline{\mathbf{U}}^{k,0}_{\mathcal{T}_{2,h}}$, and denoting by $\gamma_h(\underline{\mathbf{z}}_h)$ the discrete trace of $\underline{\mathbf{z}}_h$, such that $\gamma_h(\underline{\mathbf{z}}_h)|_F = v_{2,F}-c_2$, on each $F\in\mathcal{F}_{2,h}$, we apply Theorem 6.7 in [66], and deduce

$$
\sum_{F\in\Gamma_{1,h}\cup\Gamma_{2,h}}||v_{2,F}-c_2||^2_{0,F} = ||\gamma_h(\underline{\mathbf{z}}_h)||^2_{0,\partial\Omega_2} \lesssim ||\underline{\mathbf{z}}_h||^2_{1,\mathcal{T}_{2,h}} = ||\underline{\mathbf{v}}_{2,h}||^2_{1,\mathcal{T}_{2,h}}\,.
\tag{4.52}
$$

Finally, taking into account (4.51) and (4.52), we conclude from (4.50)

$$
|F_h(\underline{\mathbf{v}}_{1,h},\underline{\mathbf{v}}_{2,h})| \lesssim |||(\underline{\mathbf{v}}_{1,h},\underline{\mathbf{v}}_{2,h})|||_h\,,
\tag{4.53}
$$

which ensures the continuity of F_h.

Now, for the continuity of the discrete linear functional G_h, we recall that $g \in H^{1/2}(\Gamma_1) \subset L^2(\Gamma_1)$. Then, we have

$$|G_h(\lambda_h)| \;=\; \sum_{F\in\Gamma_{1,h}} (h_F^{1/2}\lambda_T\,,\, h_F^{-1/2} g)_F \;\leq\; ||\alpha^{1/2}\, g||_{0,\Gamma_1}\, ||\lambda_h||_{\Gamma_{1,h}}\,, \tag{4.54}$$

where α is a parameter defined on $\Gamma_{1,h}$ such that $\alpha|_F := h_F^{-1}$ for each $F \in \Gamma_{1,h}$. □

Remark 4.4.1 *The linear operator* $\mathbf{B}_h : \underline{\mathbf{U}}^{k,0}_{\mathcal{T}_h} \to Q_h^k$*, induced by* b_h*, is characterized by*

$$\mathbf{B}_h(\underline{\mathbf{v}}_{1,h}, \underline{\mathbf{v}}_{2,h}) \;:=\; (v_{2,F} - v_{1,F})_{F\in\Gamma_{1,h}} \quad \forall\, (\underline{\mathbf{v}}_{1,h}, \underline{\mathbf{v}}_{2,h}) \in \underline{\mathbf{U}}^{k,0}_{\mathcal{T}_h}\,. \tag{4.55}$$

It is important to notice that bilinear form a_h induces another seminorm on $\underline{\mathbf{U}}^k_{\mathcal{T}_{1,h}} \times \underline{\mathbf{U}}^k_{\mathcal{T}_{2,h}}$, that is given by

$$\|(\underline{\mathbf{v}}_{1,h}, \underline{\mathbf{v}}_{2,h})\|^2_{a,h} := a_h((\underline{\mathbf{v}}_{1,h}, \underline{\mathbf{v}}_{2,h}), (\underline{\mathbf{v}}_{1,h}, \underline{\mathbf{v}}_{2,h})) \quad \forall\, (\underline{\mathbf{v}}_{1,h}, \underline{\mathbf{v}}_{2,h}) \in \underline{\mathbf{U}}^k_{\mathcal{T}_{1,h}} \times \underline{\mathbf{U}}^k_{\mathcal{T}_{2,h}}. \tag{4.56}$$

Introducing $\mathbf{V}_h := \mathrm{Ker}(\mathbf{B}_h)$, we establish the following result.

Lemma 4.4.4 (Ellipticity) *a_h is $\mathbf{V}_h$-elliptic.*

Proof. From (4.37), we characterize the kernel of $\mathbf{B}_h$, as

$$\mathbf{V}_h := \{(\underline{\mathbf{v}}_{1,h}, \underline{\mathbf{v}}_{2,h}) \in \underline{\mathbf{U}}^{k,0}_{\mathcal{T}_h} \;:\; v_{1,F} = v_{2,F} \quad \forall F \in \Gamma_{1,h}\}\,.$$

Now, taking $(\underline{\mathbf{v}}_{1,h}, \underline{\mathbf{v}}_{2,h}) \in \mathbf{V}_h$ and considering the fact that $||\cdot||_{1,\mathcal{T}_{i,h}}$ is equivalent to $||\cdot||_{a,\mathcal{T}_{i,h}}$ (cf. Lemma 4 in [75]), we have

$$\begin{aligned} a_h((\underline{\mathbf{v}}_{1,h}, \underline{\mathbf{v}}_{2,h}), (\underline{\mathbf{v}}_{1,h}, \underline{\mathbf{v}}_{2,h})) \;&=\; \|\underline{\mathbf{v}}_{1,h}\|^2_{a,\mathcal{T}_{1,h}} + \|\underline{\mathbf{v}}_{2,h}\|^2_{a,\mathcal{T}_{2,h}} \\ &\gtrsim\; \|\underline{\mathbf{v}}_{1,h}\|^2_{1,\mathcal{T}_{1,h}} + \|\underline{\mathbf{v}}_{2,h}\|^2_{1,\mathcal{T}_{2,h}} \\ &=\; |\!|\!|(\underline{\mathbf{v}}_{1,h}, \underline{\mathbf{v}}_{2,h})|\!|\!|^2_h\,. \end{aligned} \tag{4.57}$$

□

Lemma 4.4.5 $\mathbf{B}_h$ *is a surjective operator.*

Proof. Given $\lambda_h \in Q_h^k$, we can define $(\underline{\mathbf{v}}_{1,h}, \underline{\mathbf{v}}_{2,h}) \in \underline{\mathbf{U}}_{\mathcal{T}_h}^{k,0}$, such that $v_{1,T} \equiv 0, \forall T \in \mathcal{T}_{1,h}$, $v_{1,F} = \begin{cases} -\lambda_F & , \quad F \in \Gamma_{1,h} \\ 0 & , \quad F \in \mathcal{F}_{1,h} \backslash \Gamma_{1,h} \end{cases}$, and $\underline{\mathbf{v}}_{2,h} = \underline{0}_{2,h}$. Then, the operator $\mathbf{B}_h$ is surjective. □

As in the continuous case, here we can establish also the so called discrete inf-sup condition, which will help us later to obtain an a priori error estimate corresponding to λ_h.

Lemma 4.4.6 *There exists $C > 0$, independent of the meshsize, such that*

$$\sup_{\underline{\mathbf{v}}_h \in \underline{\mathbf{U}}_{\mathcal{T}_h}^{k,0} \backslash \{0\}} \frac{b_h(\underline{\mathbf{v}}_h, \lambda_h)}{|||\underline{\mathbf{v}}_h|||_h} \geq C \, ||\lambda_h||_{\Gamma_{1,h}} \quad \forall \, \lambda_h \in Q_h^k \, . \tag{4.58}$$

Proof. Let $\lambda_h := (\lambda_F)_{F \in \Gamma_{1,h}} \in Q_h^k \backslash \{0\}$. Then, we construct $\underline{\mathbf{w}}_h := (\underline{\mathbf{w}}_{1,h}, \underline{\mathbf{w}}_{2,h}) \in \underline{\mathbf{U}}_{\mathcal{T}_h}^{k,0} \backslash \{0\}$ as in the proof of Lemma 4.4.5, and we notice that

$$|||\underline{\mathbf{w}}_h|||_h^2 = 2 \sum_{F \in \Gamma_{1,h}} h_F^{-1} ||\lambda_F||_{0,F}^2 \lesssim h_{\Gamma_1}^{-1} ||\lambda_h||_{0,\Gamma_1}^2 \, . \tag{4.59}$$

Then, taking into account (4.59) and the fact that $h_{\Gamma_1} \lesssim h_F$, for all $F \in \Gamma_{1,h}$, we have

$$\sup_{\underline{\mathbf{v}}_h \in \underline{\mathbf{U}}_{\mathcal{T}_h}^{k,0} \backslash \{0\}} \frac{b_h(\underline{\mathbf{v}}_h, \lambda_h)}{|||\underline{\mathbf{v}}_h|||_h} \geq \frac{b_h(\underline{\mathbf{w}}_h, \lambda_h)}{|||\underline{\mathbf{w}}_h|||_h} \gtrsim h_{\Gamma_1}^{1/2} \frac{||\lambda_h||_{0,\Gamma_1}^2}{||\lambda_h||_{0,\Gamma_1}} \gtrsim ||\lambda_h||_{\Gamma_{1,h}} \, . \tag{4.60}$$

This allows us to conclude the result. □

Proposition 4.4.2 (Well-posedness) *The discrete problem (4.38) is well-posed.*

Proof. It is a straightforward consequence of Lemmas 4.4.3, 4.4.4 and 4.4.5. We omit further details. □

Next result could be useful in the rest of this work.

Corollary 4.4.1 *There exists $\eta > 1$, independent of the meshsize, such that*

$$\eta^{-1} |||(\underline{\mathbf{v}}_{1,h}, \underline{\mathbf{v}}_{2,h})|||_h \leq ||(\underline{\mathbf{v}}_{1,h}, \underline{\mathbf{v}}_{2,h})||_{a,h} \quad \forall \, (\underline{\mathbf{v}}_{1,h}, \underline{\mathbf{v}}_{2,h}) \in \mathbf{V}_h \, , \tag{4.61}$$

$$||(\underline{\mathbf{v}}_{1,h}, \underline{\mathbf{v}}_{2,h})||_{a,h} \leq \eta |||(\underline{\mathbf{v}}_{1,h}, \underline{\mathbf{v}}_{2,h})|||_h \quad \forall \, (\underline{\mathbf{v}}_{1,h}, \underline{\mathbf{v}}_{2,h}) \in \underline{\mathbf{U}}_{\mathcal{T}_h}^{k,0} \, . \tag{4.62}$$

Proof. (4.61) follows straightforwardly from the $\mathbf{V}_h$-ellipticity of a_h (4.57), while (4.62) has been established in the proof of Lemma 4.4.3. We omit further details. □

4.5 A priori error analysis

From here on, we assume that exact solution $u_i \in H^{1+\delta_i}(\Omega_i)$, and $\delta_i \in (1/2, 1]$, and $\Delta u_i \in L^2(\Omega)$ for $i \in \{1,2\}$. These assumptions allow us to see ξ belonging to $L^2(\Gamma_1)$, and consider g_1 and g_2 as elements in $L^2(\Gamma_1)$ and $L^2(\Gamma_2)$, respectively. In addition, we introduce $\widehat{\underline{\mathbf{u}}}_{1,h} := \underline{\mathbf{I}}^k_{\mathcal{T}_{1,h}} u_1 \in \underline{\mathbf{U}}^k_{\mathcal{T}_{1,h}}$, $\widehat{\underline{\mathbf{u}}}_{2,h} := \underline{\mathbf{I}}^k_{\mathcal{T}_{2,h}} u_2 \in \underline{\mathbf{U}}^k_{\mathcal{T}_{2,h}}$, where $\underline{\mathbf{I}}^k_{\mathcal{T}_{i,h}}$, for $i \in \{1,2\}$, denotes the global interpolation operator that is defined in the same spirit as in (4.17), and $\widehat{\xi}_h \in Q^k_h$ is such that $\widehat{\xi}_h|_F := \pi^k_F(\xi)$, for each $F \in \Gamma_{1,h}$. It is not difficult to check that $(\widehat{\underline{\mathbf{u}}}_{1,h}, \widehat{\underline{\mathbf{u}}}_{2,h}) \in \underline{\mathbf{U}}^{k,0}_{\mathcal{T}_h}$. We recall again that, given $i \in \{1,2\}$, $\underline{\mathbf{v}}_{i,h} := \Big((v_{i,T})_{T\in\mathcal{T}_{i,h}}, (v_{i,F})_{F\in\mathcal{F}_{i,h}}\Big) \in \underline{\mathbf{U}}^k_{\mathcal{T}_{i,h}}$, and we set $v_{i,h} \in \mathbb{P}^k_d(\mathcal{T}_{i,h})$ such that $v_{i,h}|_T = v_{i,T} \quad \forall\, T \in \mathcal{T}_{i,h}$.

Now, we introduce the product space $\mathbf{X}_h := \underline{\mathbf{U}}^{k,0}_{\mathcal{T}_h} \times Q^k_h$, provided with the norm

$$||((\underline{\mathbf{v}}_{1,h}, \underline{\mathbf{v}}_{2,h}), \lambda_h)||_{\mathbf{X}_h} := \Big(|||(\underline{\mathbf{v}}_{1,h}, \underline{\mathbf{v}}_{2,h})|||^2_h + ||\lambda_h||^2_{\Gamma_{1,h}}\Big)^{1/2} \quad \forall\, ((\underline{\mathbf{v}}_{1,h}, \underline{\mathbf{v}}_{2,h}), \lambda_h) \in \mathbf{X}_h\,,$$

and the *consistency error* as the linear functional $\mathcal{E}_h(((u_1,u_2),\xi);\cdot) : \mathbf{X}_h \to \mathbb{R}$ such that, for each $((\underline{\mathbf{v}}_{1,h}, \underline{\mathbf{v}}_{2,h}), \lambda_h) \in \mathbf{X}_h$:

$$\begin{aligned}\mathcal{E}_h(((u_1,u_2),\xi);((\underline{\mathbf{v}}_{1,h}, \underline{\mathbf{v}}_{2,h}), \lambda_h)) :=& a_h((\widehat{\underline{\mathbf{u}}}_{1,h}, \widehat{\underline{\mathbf{u}}}_{2,h}), (\underline{\mathbf{v}}_{1,h}, \underline{\mathbf{v}}_{2,h})) + b_h((\underline{\mathbf{v}}_{1,h}, \underline{\mathbf{v}}_{2,h})), \widehat{\xi}_h) \\ &- b_h((\widehat{\underline{\mathbf{u}}}_{1,h}, \widehat{\underline{\mathbf{u}}}_{2,h}), \lambda_h) + G_h(\lambda_h) - F_h(\underline{\mathbf{v}}_{1,h}, \underline{\mathbf{v}}_{2,h})\,.\end{aligned}$$

In our case, we notice that, $\forall\, \lambda_h \in Q^k_h$:

$$\begin{aligned} b_h((\widehat{\underline{\mathbf{u}}}_{1,h}, \widehat{\underline{\mathbf{u}}}_{2,h}), \lambda_h) &= \sum_{F\in\Gamma_{1,h}} (\pi^k_F u_2 - \pi^k_F u_1, \lambda_F)_F \\ &= \sum_{F\in\Gamma_{1,h}} (\lambda_F, \gamma^+_0(u_2) - \gamma^-_0(u_1))_F = (\lambda_h, g)_{\Gamma_1} = G_h(\lambda_h)\end{aligned}$$

and thus, the consistency error reduces to

$$\begin{aligned}\mathcal{E}_h(((u_1,u_2),\xi);((\underline{\mathbf{v}}_{1,h}, \underline{\mathbf{v}}_{2,h}), \lambda_h)) =& a_h((\widehat{\underline{\mathbf{u}}}_{1,h}, \widehat{\underline{\mathbf{u}}}_{2,h}), (\underline{\mathbf{v}}_{1,h}, \underline{\mathbf{v}}_{2,h})) + b_h((\underline{\mathbf{v}}_{1,h}, \underline{\mathbf{v}}_{2,h})), \widehat{\xi}_h) \\ &- F_h(\underline{\mathbf{v}}_{1,h}, \underline{\mathbf{v}}_{2,h}) =: \widetilde{\mathcal{E}}_h(((u_1,u_2),\xi);(\underline{\mathbf{v}}_{1,h}, \underline{\mathbf{v}}_{2,h}))\,.\end{aligned} \tag{4.63}$$

The latter implies that

$$||\mathcal{E}_h(((u_1,u_2),\xi);\cdot)||_{\mathbf{X}^*_h} = ||\widetilde{\mathcal{E}}_h(((u_1,u_2),\xi);\cdot)||_{\underline{\mathbf{U}}^{k,0,*}_{\mathcal{T}_h}}\,, \tag{4.64}$$

with $\mathbf{X}^*_h$ and $\underline{\mathbf{U}}^{k,0,*}_{\mathcal{T}_h}$ denoting the dual space of $\mathbf{X}_h$ and $\underline{\mathbf{U}}^{k,0}_{\mathcal{T}_h}$, respectively. The following result will help us to bound (4.64).

Lemma 4.5.1 *There holds, for each* $(\underline{\mathbf{v}}_{1,h}, \underline{\mathbf{v}}_{2,h}) \in \underline{\mathbf{U}}_{\mathcal{T}_h}^{k,0}$:

$$F_h(\underline{\mathbf{v}}_{1,h}, \underline{\mathbf{v}}_{2,h}) - b_h((\underline{\mathbf{v}}_{1,h}, \underline{\mathbf{v}}_{2,h}), \widehat{\xi}_h) = \sum_{i=1}^{2} \sum_{T \in \mathcal{T}_{i,h}} (\nabla v_{i,T}, \nabla u_i)_T + \sum_{i=1}^{2} \sum_{T \in \mathcal{T}_{i,h}} \sum_{F \in \mathcal{F}_T} (\nabla u_i \cdot \boldsymbol{n}_{TF}, v_{i,F} - v_{i,T})_F. \tag{4.65}$$

Proof. Since $f_i = -\Delta u_i$ in Ω_i (weak sense), and after performing an element-wise integration by parts in $(f_i, v_{i,h})_{\Omega_i}$, with $i \in \{1,2\}$, we obtain that two first addends of F_h (cf. (4.39)) can be written as

$$(f_1, v_{1,h})_{\Omega_1} = \sum_{T \in \mathcal{T}_{1,h}} (\nabla u_1, \nabla v_{1,T})_T - \sum_{T \in \mathcal{T}_{1,h}} \sum_{F \in \mathcal{F}_T} (\nabla u_1 \cdot \boldsymbol{n}_{TF}, v_{1,T})_F, \tag{4.66}$$

$$(f_2, v_{2,h})_{\Omega_2} = \sum_{S \in \mathcal{T}_{2,h}} (\nabla u_2, \nabla v_{2,S})_S - \sum_{S \in \mathcal{T}_{2,h}} \sum_{F \in \mathcal{F}_S} (\nabla u_2 \cdot \boldsymbol{n}_{SF}, v_{2,S})_F. \tag{4.67}$$

Now, using the fact that $\nabla u_1 \cdot \boldsymbol{n}_1 + \nabla u_2 \cdot \boldsymbol{n}_2 = g_1$ a.e. on Γ_1, and $\nabla u_2 \cdot \boldsymbol{n}_2 = g_2$ a.e. on Γ_2, and that there exist $T \in \mathcal{T}_{1,h}$ and $S \in \mathcal{T}_{2,h}$, such that $\boldsymbol{n}_1 = \boldsymbol{n}_{TF}$ on $\partial\Omega_1$ and $\boldsymbol{n}_2 = \boldsymbol{n}_{SF}$ on $\partial\Omega_2$, we can write the last two addends of F_h as

$$\sum_{F \in \Gamma_{1,h}} (g_1, v_{2,F})_F = \sum_{F \in \Gamma_{1,h}} (\nabla u_1 \cdot \boldsymbol{n}_{TF}, v_{2,F})_F + \sum_{F \in \Gamma_{1,h}} (\nabla u_2 \cdot \boldsymbol{n}_{SF}, v_{2,F})_F, \tag{4.68}$$

$$\sum_{F \in \Gamma_{2,h}} (g_2, v_{2,F})_F = \sum_{F \in \Gamma_{2,h}} (\nabla u_2 \cdot \boldsymbol{n}_{SF}, v_{2,F})_F. \tag{4.69}$$

From the definition of $\widehat{\xi}_h$, property of π_F^k, the fact that $\xi = \nabla u_1 \cdot \boldsymbol{n}_1$ a.e. on Γ_1, and that there exist $T \in \mathcal{T}_{1,h}$ and $S \in \mathcal{T}_{2,h}$, such that $\boldsymbol{n}_1 = \boldsymbol{n}_{TF} = -\boldsymbol{n}_{SF}$ on Γ_1, we derive

$$b_h((\underline{\mathbf{v}}_{1,h}, \underline{\mathbf{v}}_{2,h}), \widehat{\xi}_h) = \sum_{F \in \Gamma_{1,h}} (\nabla u_1 \cdot \boldsymbol{n}_{TF}, v_{2,F})_F - \sum_{F \in \Gamma_{1,h}} (\nabla u_1 \cdot \boldsymbol{n}_{TF}, v_{1,F})_F. \tag{4.70}$$

Finally, from equations (4.66)-(4.70), knowing that $v_{i,F}$ is single-valued, and the normal component of ∇u_i is continuous on skeletal induced by $\mathcal{T}_{i,h}$, $i \in \{1,2\}$, we conclude the proof. □

Lemma 4.5.2 *Assuming that* $u_i \in H^{q+1+\delta_i}(\mathcal{T}_{i,h})$, $i \in \{1,2\}$, *and* $q \in \{0, ..., k\}$, *there exists* $C > 0$, *independent of the meshsize, such that*

$$||\mathcal{E}_h(((u_1,u_2),\xi);\cdot)||_{\mathbf{X}_h^*} \leq C \left(h_1^{2(q+\delta_1)} \|u_1\|^2_{q+1+\delta_1,\mathcal{T}_{1,h}} + h_2^{2(q+\delta_2)} \|u_2\|^2_{q+1+\delta_2,\mathcal{T}_{2,h}} \right)^{1/2}, \tag{4.71}$$

where $h_i := \max_{T \in \mathcal{T}_{i,h}} h_T$, $i = 1, 2$.

Proof. First, we take $(\underline{\mathbf{v}}_{1,h}, \underline{\mathbf{v}}_{2,h}) \in \underline{\mathbf{U}}^{k,0}_{\mathcal{T}_h}$. Then, after noticing that $G^k_T \underline{\mathbf{I}}^k_T(w) = \nabla p^{k+1}_T \underline{\mathbf{I}}^k_T(w)$, for any $w \in H^1(T)$, $T \in \mathcal{T}_h$, and introducing $\breve{u}_{1,T} := p^{k+1}_T \underline{\mathbf{I}}^k_T(u_1|_T)$, for each $T \in \mathcal{T}_{1,h}$ and $\breve{u}_{2,S} := p^{k+1}_S \underline{\mathbf{I}}^k_S(u_2|_S)$, for all $S \in \mathcal{T}_{2,h}$, we have

$$
\begin{aligned}
a_h((\widehat{\underline{\mathbf{u}}}_{1,h}, \widehat{\underline{\mathbf{u}}}_{2,h}), (\underline{\mathbf{v}}_{1,h}, \underline{\mathbf{v}}_{2,h})) &= \sum_{T\in\mathcal{T}_{1,h}} (G^k_T \widehat{\underline{\mathbf{u}}}_{1,T}, G^k_T \underline{\mathbf{v}}_{1,T})_T + \sum_{T\in\mathcal{T}_{1,h}} j_T(\widehat{\underline{\mathbf{u}}}_{1,T}, \underline{\mathbf{v}}_{1,T}) \\
&\quad + \sum_{S\in\mathcal{T}_{h,2}} (G^k_S \widehat{\underline{\mathbf{u}}}_{2,S}, G^k_S \underline{\mathbf{v}}_{2,S})_S + \sum_{S\in\mathcal{T}_{2,h}} j_S(\widehat{\underline{\mathbf{u}}}_{2,S}, \underline{\mathbf{v}}_{2,S}) \\
&= \sum_{T\in\mathcal{T}_{1,h}} (\nabla v_{1,T}, \nabla \breve{u}_{1,T})_T + \sum_{T\in\mathcal{T}_{1,h}} \sum_{F\in\mathcal{F}_T} (v_{1,F} - v_{1,T}, \nabla \breve{u}_{1,T} \cdot \boldsymbol{n}_{TF})_F \\
&\quad + \sum_{S\in\mathcal{T}_{2,h}} (\nabla v_{2,S}, \nabla \breve{u}_{2,S})_S + \sum_{S\in\mathcal{T}_{2,h}} \sum_{F\in\mathcal{F}_S} (v_{2,F} - v_{2,S}, \nabla \breve{u}_{2,S} \cdot \boldsymbol{n}_{SF})_F \\
&\quad + \sum_{T\in\mathcal{T}_{1,h}} j_T(\widehat{\underline{\mathbf{u}}}_{1,T}, \underline{\mathbf{v}}_{1,T}) + \sum_{S\in\mathcal{T}_{2,h}} j_S(\widehat{\underline{\mathbf{u}}}_{2,S}, \underline{\mathbf{v}}_{2,S}) \,. \qquad (4.72)
\end{aligned}
$$

At this point, from (4.72) and Lemma 4.5.1 , we can write the consistency error as

$$
\begin{aligned}
&\widetilde{\mathcal{E}}_h(((u_1, u_2), \xi); (\underline{\mathbf{v}}_{1,h}, \underline{\mathbf{v}}_{2,h})) \\
&= \underbrace{\sum_{T\in\mathcal{T}_{1,h}} (\nabla v_{1,T}, \nabla(\breve{u}_{1,T} - u_1))_T}_{\mathfrak{T}_1} + \underbrace{\sum_{T\in\mathcal{T}_{1,h}} \sum_{F\in\mathcal{F}_T} (v_{1,F} - v_{1,T}, \nabla(\breve{u}_{1,T} - u_1) \cdot \boldsymbol{n}_{TF})_F}_{\mathfrak{T}_2} \\
&\quad + \underbrace{\sum_{S\in\mathcal{T}_{2,h}} (\nabla v_{2,S}, \nabla(\breve{u}_{2,S} - u_2))_S}_{\mathfrak{T}_3} + \underbrace{\sum_{S\in\mathcal{T}_{2,h}} \sum_{F\in\mathcal{F}_S} (v_{2,F} - v_{2,S}, \nabla(\breve{u}_{2,S} - u_2) \cdot \boldsymbol{n}_{SF})_F}_{\mathfrak{T}_4} \\
&\quad + \underbrace{\sum_{T\in\mathcal{T}_{1,h}} j_T(\widehat{\underline{\mathbf{u}}}_{1,T}, \underline{\mathbf{v}}_{1,T})}_{\mathfrak{T}_5} + \underbrace{\sum_{S\in\mathcal{T}_{2,h}} j_S(\widehat{\underline{\mathbf{u}}}_{2,S}, \underline{\mathbf{v}}_{2,S})}_{\mathfrak{T}_6} \,. \qquad (4.73)
\end{aligned}
$$

Applying Cauchy-Schwarz inequality, followed by the approximation properties of $p^{k+1}_T \underline{\mathbf{I}}^k_T$ (cf. (4.22)), with T either in $\mathcal{T}_{1,h}$ or in $\mathcal{T}_{2,h}$, and the definition of the norm $||\cdot||_{1,\mathcal{T}_{i,h}}$, we can estimate $\mathfrak{T}_1$, $\mathfrak{T}_2$, $\mathfrak{T}_3$, and $\mathfrak{T}_4$ as

$$
|\mathfrak{T}_1| + |\mathfrak{T}_2| \lesssim ||\underline{\mathbf{v}}_{1,h}||_{1,\mathcal{T}_{1,h}} \cdot h_1^{q+\delta_1} |u_1|_{q+1+\delta_1,\mathcal{T}_{1,h}} \,, \qquad (4.74)
$$

$$
|\mathfrak{T}_3| + |\mathfrak{T}_4| \lesssim ||\underline{\mathbf{v}}_{2,h}||_{1,\mathcal{T}_{2,h}} \cdot h_2^{q+\delta_2} |u_2|_{q+1+\delta_2,\mathcal{T}_{2,h}} \,. \qquad (4.75)
$$

Invoking now Theorem 8 in [75], we deduce $h_F^{-1/2} ||\pi^k_F(\widehat{u}_{i,F} - R^{k+1}_T \widehat{\underline{\mathbf{u}}}_{i,T})||_F \lesssim h_i^{q+\delta_i} |u_i|_{q+1+\delta_i,T}$, $\forall\, F \in \mathcal{F}_T$, where $T \in \mathcal{T}_{i,h}$, $i \in \{1,2\}$. This allows us to estimate $\mathfrak{T}_5$

and $\mathfrak{T}_6$ as

$$|\mathfrak{T}_5| \lesssim ||\underline{\mathbf{v}}_{1,h}||_{1,\mathcal{T}_{1,h}} \cdot h_1^{q+\delta_1} |u_1|_{q+1+\delta_1,\mathcal{T}_{1,h}} , \tag{4.76}$$

$$|\mathfrak{T}_6| \lesssim ||\underline{\mathbf{v}}_{2,h}||_{1,\mathcal{T}_{2,h}} \cdot h_2^{q+\delta_2} |u_2|_{q+1+\delta_2,\mathcal{T}_{2,h}} . \tag{4.77}$$

Then, from (4.74)-(4.77), we deduce that for each $(\underline{\mathbf{v}}_{1,h}, \underline{\mathbf{v}}_{2,h}) \in \underline{\mathbf{U}}_{\mathcal{T}_h}^{k,0}$:

$$\begin{aligned} &\widetilde{\mathcal{E}}_h(((u_1,u_2),\xi);(\underline{\mathbf{v}}_{1,h},\underline{\mathbf{v}}_{2,h})) \\ &\lesssim |\!|\!|(\underline{\mathbf{v}}_{1,h},\underline{\mathbf{v}}_{2,h})|\!|\!|_h \left(h_1^{2(q+\delta_1)} |u_1|^2_{q+1+\delta_1,\mathcal{T}_{1,h}} + h_2^{2(q+\delta_2)} |u_2|^2_{q+1+\delta_2,\mathcal{T}_{2,h}} \right)^{1/2} . \end{aligned} \tag{4.78}$$

Finally, (4.78) yields to an upper bound for $||\widetilde{\mathcal{E}}_h(((u_1,u_2),\xi);\cdot)||_{\underline{\mathbf{U}}_{\mathcal{T}_h}^{k,0,*}}$, and thanks to (4.64), we conclude (4.71). □

Theorem 4.5.1 (Energy error estimate) *Assuming that $u_i \in H^{q+1+\delta_i}(\mathcal{T}_{i,h})$, $i \in \{1,2\}$, with $q \in \{0,...,k\}$, there exists $C > 0$, independent of the meshsize, such that:*

$$\begin{aligned} &\|((\widehat{\underline{\mathbf{u}}}_{1,h},\widehat{\underline{\mathbf{u}}}_{2,h}) - (\underline{\mathbf{u}}_{1,h},\underline{\mathbf{u}}_{2,h})), \widehat{\xi}_h - \xi_h)\|_{\mathbf{x}_h} \\ &\leq C \left(h_1^{2(q+\delta_1)} \|u_1\|^2_{q+1+\delta_1,\mathcal{T}_{1,h}} + h_2^{2(q+\delta_2)} \|u_2\|^2_{q+1+\delta_2,\mathcal{T}_{2,h}} \right)^{1/2} , \end{aligned} \tag{4.79}$$

where $h_i := \max_{T\in\mathcal{T}_{i,h}} h_T$, $i = 1,2$. Moreover, applying Lemma 4.3.3, there also holds

$$\begin{aligned} &\sum_{i=1}^{2} \sum_{T\in\mathcal{T}_{i,h}} ||\nabla u_i - \nabla p_T^{k+1} \underline{\mathbf{u}}_{i,T}||^2_{0,T} \\ &\leq C \left(h_1^{2(q+\delta_1)} \|u_1\|^2_{q+1+\delta_1,\mathcal{T}_{1,h}} + h_2^{2(q+\delta_2)} \|u_2\|^2_{q+1+\delta_2,\mathcal{T}_{2,h}} \right) . \end{aligned} \tag{4.80}$$

Proof. Since bilinear form a_h is coercive on $\mathbf{V}_h$ and b_h satisfies a discrete inf-sup condition, with corresponding constants that are independent of the meshsize, we can apply a variant of Lemma A.11 in the appendix in [66], which is valid according to Remark A.12 in this same appendix. As result, we can establish a global discrete inf-sup condition: For any $((\underline{\mathbf{w}}_{1,h},\underline{\mathbf{w}}_{2,h}),\zeta_h) \in \mathbf{X}_h$:

$$||((\underline{\mathbf{w}}_{1,h},\underline{\mathbf{w}}_{2,h}),\zeta_h)||_{\mathbf{x}_h} \lesssim \sup_{((\underline{\mathbf{v}}_{1,h},\underline{\mathbf{v}}_{2,h}),\lambda_h)\in\mathbf{X}_h\setminus\{0\}} \frac{\mathtt{A}_h(((\underline{\mathbf{w}}_{1,h},\underline{\mathbf{w}}_{2,h}),\zeta_h),((\underline{\mathbf{v}}_{1,h},\underline{\mathbf{v}}_{2,h}),\lambda_h))}{||((\underline{\mathbf{v}}_{1,h},\underline{\mathbf{v}}_{2,h}),\lambda_h)||_{\mathbf{x}_h}} , \tag{4.81}$$

where the bilinear form $\mathtt{A}_h : \mathbf{X}_h \times \mathbf{X}_h \to \mathbb{R}$ is given by

$$\begin{aligned} \mathtt{A}_h(((\underline{\mathbf{w}}_{1,h},\underline{\mathbf{w}}_{2,h}),\zeta_h),((\underline{\mathbf{v}}_{1,h},\underline{\mathbf{v}}_{2,h}),\lambda_h)) &:= a_h((\underline{\mathbf{w}}_{1,h},\underline{\mathbf{w}}_{2,h}),(\underline{\mathbf{v}}_{1,h},\underline{\mathbf{v}}_{2,h})) \\ &+ b_h((\underline{\mathbf{v}}_{1,h},\underline{\mathbf{v}}_{2,h}),\zeta_h) - b_h((\underline{\mathbf{w}}_{1,h},\underline{\mathbf{w}}_{2,h}),\lambda_h) . \end{aligned} \tag{4.82}$$

This allows us to apply Corollary A.13 in the appendix in [66], with $\mathtt{l}_h := F_h$ and $\mathtt{m}_h := G_h$, which yields us to

$$||((\widehat{\underline{\mathbf{u}}}_{1,h}, \widehat{\underline{\mathbf{u}}}_{2,h}) - (\underline{\mathbf{u}}_{1,h}, \underline{\mathbf{u}}_{2,h})), \widehat{\xi}_h - \xi_h)||_{\mathbf{x}_h} \lesssim ||\mathcal{E}_h(((u_1, u_2), \xi); \cdot)||_{\mathbf{x}_h^*} .$$

Then, (4.79) follows straightforwardly from Lemma 4.5.2.

Finally, in order to derive (4.80), we realize, after applying triangle inequality, that

$$||\nabla u_i - \nabla p_T^{k+1} \underline{\mathbf{u}}_{i,T}||_{0,T} \leq ||\nabla u_i - \nabla p_T^{k+1} \underline{\mathbf{I}}_T^k(u_i|_T)||_{0,T} + ||\nabla p_T^{k+1} \underline{\mathbf{I}}_T^k(u_i|_T) - \nabla p_T^{k+1} \underline{\mathbf{u}}_{i,T}||_{0,T} , \tag{4.83}$$

for each $T \in \mathcal{T}_{i,h}$, $i \in \{1, 2\}$. Thus, (4.80) is deduced from (4.83), after invoking (4.79) and Lemma 4.3.3. We omit further details. □

Remark 4.5.1 (L^2-error estimate of the projection of the trace error) *Concerning the L^2-norm of $\widehat{\xi}_h - \xi_h$, Theorem 4.5.1 establishes that, for $q \in \{0, ..., k\}$:*

$$||\widehat{\xi}_h - \xi_h||_{\Gamma_{1,h}} \lesssim h_1^{q+\delta_1} ||u_1||_{q+1+\delta_1, \mathcal{T}_{1,h}} + h_2^{q+\delta_2} ||u_1||_{q+1+\delta_2, \mathcal{T}_{2,h}} . \tag{4.84}$$

On the other hand, we know that

$$h_{\Gamma_1}^{1/2} ||\widehat{\xi}_h - \xi_h||_{0,\Gamma_1} \lesssim ||\widehat{\xi}_h - \xi_h||_{\Gamma_{1,h}} , \tag{4.85}$$

since we are assuming that the partition on Γ_1 is quasi-uniform (cf. (4.28)). Then, from (4.84) and (4.85), we deduce that

$$||\widehat{\xi}_h - \xi_h||_{0,\Gamma_1} \lesssim h_{\Gamma_1}^{-1/2} \left(h_1^{q+\delta_1} ||u_1||_{q+1+\delta_1, \mathcal{T}_{1,h}} + h_2^{q+\delta_2} ||u_1||_{q+1+\delta_2, \mathcal{T}_{2,h}} \right) . \tag{4.86}$$

Our next aim, is to provide an error estimate in the L^2-norm of the projection of the errors $e_{i,h} := \pi_{\mathcal{T}_{i,h}}^k u_i - u_{i,h}$ for each $i \in \{1, 2\}$, where given $\underline{\mathbf{u}}_{i,h} := \left((u_{i,T})_{T \in \mathcal{T}_{i,h}}, (u_{i,F})_{F \in \mathcal{F}_{i,h}} \right)$, we define $u_{i,h}$ as an element of $L^2(\Omega_i)$, such that

$$u_{i,h}|_T := u_{i,T} \quad \text{and} \quad \left(\pi_{\mathcal{T}_{i,h}}^k u_i \right)\Big|_T := \pi_T^k u_i \qquad \forall\, T \in \mathcal{T}_{i,h} , \, i \in \{1, 2\} . \tag{4.87}$$

To this end, we introduce the following auxiliar problem: *Given $(w_1, w_2) \in L^2(\Omega_1) \times L^2(\Omega_2)$ with $(w_1, 1)_{0,\Omega_1} + (w_2, 1)_{0,\Omega_2} = 0$, we look for $(z_1, z_2) \in \mathbf{U}$, such that, in weak*

sense, verifies

$$-\Delta z_1 = w_1 \text{ in } \Omega_1\,, \tag{4.88a}$$

$$-\Delta z_2 = w_2 \text{ in } \Omega_2\,, \tag{4.88b}$$

$$z_1 - z_2 = 0 \text{ on } \Gamma_1\,, \tag{4.88c}$$

$$\nabla z_1 \cdot \boldsymbol{n}_1 + \nabla z_2 \cdot \boldsymbol{n}_2 = 0 \text{ on } \Gamma_1\,, \tag{4.88d}$$

$$\nabla z_2 \cdot \boldsymbol{n}_2 = 0 \text{ on } \Gamma_2\,. \tag{4.88e}$$

Since the transmission conditions in (4.88) *are homogeneous, it is known that* (4.88) *is equivalent to: Find* $z \in H^1(\Omega) \cap L^2_0(\Omega)$ *such that:*

$$\begin{aligned} -\Delta z &= w \text{ in } \Omega := \Omega_1 \cup \Gamma_1 \cup \Omega_2\,, \\ \frac{\partial z}{\partial \boldsymbol{n}_2} &= 0 \text{ on } \Gamma_2 := \partial\Omega\,, \end{aligned} \tag{4.89}$$

with $w \in L^2_0(\Omega)$ *such that* $w|_{\Omega_1} = w_1$ *and* $w|_{\Omega_2} = w_2$*. In this case,* $z|_{\Omega_1} = z_1$ *and* $z|_{\Omega_2} = z_2$*. Then, we assume further regularity on* z*, the weak solution of* (4.89)*, so that* $z \in H^2(\Omega) \cap L^2_0(\Omega)$*, and there exists* $C > 0$*, independent of the meshsize, such that*

$$||z||^2_{2,\Omega} \leq C\, ||w||^2_{0,\Omega}\,,$$

or, equivalently

$$\|z_1\|^2_{2,\Omega_1} + \|z_2\|^2_{2,\Omega_2} \leq C \left(\|w_1\|^2_{0,\Omega_1} + \|w_2\|^2_{0,\Omega_2} \right)\,. \tag{4.90}$$

We remark that this assumption holds when, for example, the domain $\Omega := \Omega_1 \cup \Gamma_1 \cup \Omega_2$ *is convex. From here on, we introduce* $h := \max\{h_1, h_2\}$*.*

Theorem 4.5.2 (Error estimate of L^2-***projection of the potential)*** *Assuming that the exact solutions* $u_i \in H^{q+1+\delta_i}(\mathcal{T}_{i,h})$*,* $i \in \{1,2\}$*, with* $q \in \{0, ..., k\}$*, and there holds the elliptic regularity property* (4.90)*, we have, for* $k \geq 1$*:*

$$\begin{aligned} &\|\pi^k_{\mathcal{T}_{1,h}} u_1 - u_{1,h}\|_{0,\Omega_1} + \|\pi^k_{\mathcal{T}_{2,h}} u_2 - u_{2,h}\|_{0,\Omega_2} \\ &\lesssim h \left(h_1^{2(q+\delta_1)}\, ||u_1||^2_{q+1+\delta_1,\mathcal{T}_{1,h}} + h_2^{2(q+\delta_2)}\, ||u_2||^2_{q+1+\delta_2,\mathcal{T}_{2,h}} \right)^{1/2}\,. \end{aligned} \tag{4.91}$$

For $k=0$, assuming in addition that $f_i \in H^{\delta_i}(\mathcal{T}_{i,h})$, for $i \in \{1,2\}$, $g_1 \in \mathbb{P}_0(\Gamma_{1,h})$ and $g_2 \in \mathbb{P}_0(\Gamma_{2,h})$, there holds

$$\begin{aligned}
&\|\pi^0_{\mathcal{T}_{1,h}} u_1 - u_{1,h}\|_{0,\Omega_1} + \|\pi^0_{\mathcal{T}_{2,h}} u_2 - u_{2,h}\|_{0,\Omega_2} \\
&\lesssim h \left(h_1^{2(\delta_1)} \, ||u_1||^2_{1+\delta_1,\mathcal{T}_{1,h}} + h_2^{2(\delta_2)} \, ||u_2||^2_{1+\delta_2,\mathcal{T}_{2,h}} \right)^{1/2} \\
&\quad + \left(h_1^{2(1+\delta_1)} ||f_1||^2_{\delta_1,\mathcal{T}_{1,h}} + h_2^{2(1+\delta_2)} ||f_2||^2_{\delta_2,\mathcal{T}_{2,h}} \right)^{1/2} . \qquad (4.92)
\end{aligned}$$

Proof. *Let $((z_1,z_2),\eta) \in \mathbf{X} := \mathbf{U} \times H^{-1/2}(\Gamma_1)$ be the solution of the corresponding mixed variational formulation associated to (4.88), where $\eta := \nabla z_1 \cdot \boldsymbol{n}_1$ on Γ_1 is introduced as auxiliary unknown. This formulation can be seen as (4.8), with $F(v_1,v_2) := (w_1,v_1)_{\Omega_1} + (w_2,v_2)_{\Omega_2}$, and $G(\lambda) := 0$. Next, we denote by $((\underline{\mathbf{z}}_{1,h},\underline{\mathbf{z}}_{2,h}),\eta_h) \in \mathbf{X}_h$ the unique solution of the mixed HHO scheme corresponding to (4.88), that is*

$$\mathtt{A}_h(((\underline{\mathbf{z}}_{1,h},\underline{\mathbf{z}}_{2,h}),\eta_h),((\underline{\mathbf{v}}_{1,h},\underline{\mathbf{v}}_{2,h}),\lambda_h)) = (w_1,v_{1,h})_{\Omega_1} + (w_2,v_{2,h})_{\Omega_2} \qquad (4.93)$$

for all $((\underline{\mathbf{v}}_{1,h},\underline{\mathbf{v}}_{2,h}),\lambda_h) \in \mathbf{X}_h$.

We notice that there holds $\forall((\underline{\mathbf{v}}_{1,h},\underline{\mathbf{v}}_{2,h}),\lambda_h)\,,\,((\underline{\mathbf{w}}_{1,h},\underline{\mathbf{w}}_{2,h}),\zeta_h) \in \mathbf{X}_h$:

$$\mathtt{A}_h(((\underline{\mathbf{w}}_{1,h},\underline{\mathbf{w}}_{2,h}),\zeta_h),((\underline{\mathbf{v}}_{1,h},\underline{\mathbf{v}}_{2,h}),\lambda_h)) = \mathtt{A}_h(((\underline{\mathbf{v}}_{1,h},\underline{\mathbf{v}}_{2,h}),-\lambda_h),((\underline{\mathbf{w}}_{1,h},\underline{\mathbf{w}}_{2,h}),-\zeta_h)) . \qquad (4.94)$$

As a result, we notice that (4.93) can also be written as

$$\mathtt{A}_h(((\underline{\mathbf{v}}_{1,h},\underline{\mathbf{v}}_{2,h}),\lambda_h),((\underline{\mathbf{z}}_{1,h},\underline{\mathbf{z}}_{2,h}),-\eta_h)) = (w_1,v_{1,h})_{\Omega_1} + (w_2,v_{2,h})_{\Omega_2} \qquad (4.95)$$

for all $((\underline{\mathbf{v}}_{1,h},\underline{\mathbf{v}}_{2,h}),\lambda_h) \in \mathbf{X}_h$.

This lets us to state that the dual consistency error is given by

$$\begin{aligned}
\mathcal{E}^{\mathtt{d}}_h(((z_1,z_2),\eta),((\underline{\mathbf{v}}_{1,h},\underline{\mathbf{v}}_{2,h}),\lambda_h)) &:= \mathtt{A}_h(((\underline{\mathbf{v}}_{1,h},\underline{\mathbf{v}}_{2,h}),\lambda_h),((\widehat{\underline{\mathbf{z}}}_{1,h},\widehat{\underline{\mathbf{z}}}_{2,h}),-\widehat{\eta}_h))) \\
&\quad - (w_1,v_{1,h})_{\Omega_1} - (w_2,v_{2,h})_{\Omega_2} ,
\end{aligned}$$

where $\widehat{\underline{\mathbf{z}}}_{i,h} := \underline{\mathbf{I}}^k_{\mathcal{T}_{i,h}}(z_i) \in \underline{\mathbf{U}}^k_{\mathcal{T}_{i,h}}$, $i \in \{1,2\}$, and $\widehat{\eta}_h = \left(\pi^k_F(\eta|_F)\right)_{F\in\Gamma_{1,h}} \in Q^k_h$. Thanks to (4.94), it is not difficult to check that $\forall((\underline{\mathbf{v}}_{1,h},\underline{\mathbf{v}}_{2,h}),\lambda_h) \in \mathbf{X}_h$ there holds

$$\begin{aligned}
\mathcal{E}^{\mathtt{d}}_h(((z_1,z_2),\eta),((\underline{\mathbf{v}}_{1,h},\underline{\mathbf{v}}_{2,h}),-\lambda_h)) &= \mathtt{A}_h(((\widehat{\underline{\mathbf{z}}}_{1,h},\widehat{\underline{\mathbf{z}}}_{2,h}),\widehat{\eta}_h),((\underline{\mathbf{v}}_{1,h},\underline{\mathbf{v}}_{2,h}),\lambda_h)) \\
&\quad - (w_1,v_{1,h})_{\Omega_1} - (w_2,v_{2,h})_{\Omega_2} \\
&=: \mathcal{E}_h(((z_1,z_2),\eta),((\underline{\mathbf{v}}_{1,h},\underline{\mathbf{v}}_{2,h}),\lambda_h)) . \qquad (4.96)
\end{aligned}$$

Now, invoking Lemma A.14 in the appendix in [66] with $\mathtt{U} := \mathbf{U}$, $\mathtt{P} := H^{-1/2}(\Gamma_1)$, $\mathtt{U}_h := \underline{\mathbf{U}}^{k,0}_{\mathcal{T}_h}$, *provided with the* $|||\cdot|||_h-$*norm and interpolator* $\mathtt{I}_h := \underline{\mathbf{I}}^k_{\mathcal{T}_h}$ *(cf. (4.17)),* $\mathtt{P}_h := Q^k_h$, *equipped with* $||\cdot||_{\Gamma_{1,h}}-$*norm and interpolator* $\mathtt{J}_h := \pi^k_{\Gamma_{1,h}} := \left(\pi^k_F\right)_{F\in\Gamma_{1,h}}$, $\mathtt{a}_h := a_h$, *and* $\mathtt{b}_h := b_h$. *In addition, we introduce* $\mathtt{L} := L^2_0(\Omega)$, *with the reconstruction operator* $\mathtt{r}_h : \mathtt{U}_h \to \mathtt{L}$ *such that* $\mathtt{r}_h(\underline{\mathbf{v}}_h) := v_h$. *Then, the error estimate (A.30) in [66] reads as*

$$
\begin{aligned}
&||\pi^k_{\mathcal{T}_{1,h}}u_1 - u_{1,h}||_{0,\Omega_1} \,+\, ||\pi^k_{\mathcal{T}_{2,h}}u_2 - u_{2,h}||_{0,\Omega_2} \\
&\leq \underbrace{||((\underline{\mathbf{u}}_{1,h},\underline{\mathbf{u}}_{2,h}),\xi_h) - ((\widehat{\underline{\mathbf{u}}}_{1,h},\widehat{\underline{\mathbf{u}}}_{2,h}),\widehat{\xi}_h)||_{\mathbf{X}_h} \sup_{(w_1,w_2)\in L^2_0(\Omega)\,,\,||w||_\Omega=1} ||\mathcal{E}^{\mathtt{d}}_h(((z_1,z_2),\eta),\cdot)||_{\mathbf{X}^*_h}}_{\mathfrak{T}_1} \\
&\qquad + \underbrace{\sup_{(w_1,w_2)\in L^2_0(\Omega)\,,\,||w||_\Omega=1} \mathcal{E}_h(((u_1,u_2),\xi),((\widehat{\underline{\mathbf{z}}}_{1,h},\widehat{\underline{\mathbf{z}}}_{2,h}),\widehat{\eta}_h))}_{\mathfrak{T}_2}
\end{aligned}
\tag{4.97}
$$

Then (4.91) and (4.92) are obtained after bounding the terms on the right hand side of (4.97).

i) **Bounding** $\mathfrak{T}_1$**.** *From (4.79) in Theorem 4.5.1, we have*

$$
\begin{aligned}
&||((\underline{\mathbf{u}}_{1,h},\underline{\mathbf{u}}_{2,h}),\xi_h) - ((\widehat{\underline{\mathbf{u}}}_{1,h},\widehat{\underline{\mathbf{u}}}_{2,h}),\widehat{\xi}_h)||_{\mathbf{X}_h} \\
&\lesssim h_1^{q+\delta_1}||u_1||_{q+1+\delta_1,\mathcal{T}_{1,h}} \,+\, h_2^{q+\delta_2}||u_2||_{q+1+\delta_2,\mathcal{T}_{2,h}}\,.
\end{aligned}
\tag{4.98}
$$

From (4.96), we notice that

$$
||\mathcal{E}^{\mathtt{d}}_h(((z_1,z_2),\eta),\cdot)||_{\mathbf{X}^*_h} \,=\, ||\mathcal{E}_h(((z_1,z_2),\eta),\cdot)||_{\mathbf{X}^*_h}\,,
$$

which is estimated by applying Lemma 4.5.2 with $q = 0$ *and* $\delta_1 = \delta_2 = 1$, *yielding to*

$$
\begin{aligned}
||\mathcal{E}_h(((z_1,z_2),\eta),\cdot)||_{\mathbf{X}^*_h} &\lesssim (h_1\,||z_1||_{2,\Omega_1} \,+\, h_2\,||z_2||_{2,\Omega_2}) \\
&\lesssim h\,(||w_1||_{0,\Omega_1} \,+\, ||w_2||_{0,\Omega_2})\,,
\end{aligned}
\tag{4.99}
$$

where the last inequality has been obtained after applying the ellipticity property (4.90). Then, from (4.98) and (4.99), we deduce

$$
|\mathfrak{T}_1| \,\lesssim\, h\left(h_1^{q+\delta_1}||u_1||_{q+1+\delta_1,\mathcal{T}_{1,h}} \,+\, h_2^{q+\delta_2}||u_2||_{q+1+\delta_2,\mathcal{T}_{2,h}}\right)\,.
\tag{4.100}
$$

ii) **Bounding $\mathfrak{T}_2$.** *At this point, we need to consider two cases: $k \geq 1$ and $k = 0$.*

ii.A) The case $k \geq 1$. Taking into account (4.63) and the orthogonality property of p_T^{k+1} (4.20), we proceed as in the derivation of (4.73), and obtain

$$\begin{aligned}\widetilde{\mathcal{E}}_h(((u_1,u_2),\xi),((\widehat{\underline{\mathbf{z}}}_{1,h},\widehat{\underline{\mathbf{z}}}_{2,h}))) &= \underbrace{\sum_{T\in\mathcal{T}_{1,h}}\sum_{F\in\mathcal{F}_T}(\pi_F^k z_1 - \pi_T^k z_1, \nabla(\breve{u}_{1,T}-u_1)\cdot\boldsymbol{n}_{TF})_F}_{\mathfrak{E}_1}\\ &\quad+\underbrace{\sum_{S\in\mathcal{T}_{2,h}}\sum_{F\in\mathcal{F}_S}(\pi_F^k z_2 - \pi_S^k z_2, \nabla(\breve{u}_{2,S}-u_2)\cdot\boldsymbol{n}_{SF})_F}_{\mathfrak{E}_2}\\ &\quad+\underbrace{\sum_{T\in\mathcal{T}_{1,h}} j_T(\widehat{\underline{\mathbf{u}}}_{1,T},\widehat{\underline{\mathbf{z}}}_{1,T})}_{\mathfrak{E}_3}+\underbrace{\sum_{S\in\mathcal{T}_{2,h}} j_S(\widehat{\underline{\mathbf{u}}}_{2,S},\widehat{\underline{\mathbf{z}}}_{2,S})}_{\mathfrak{E}_4}\,.\end{aligned} \tag{4.101}$$

Now, taking into account (4.22) and (4.14) (with $l = q \geq 1$ and $t = 2$), we deduce

$$|\mathfrak{E}_1| \lesssim \sum_{T\in\mathcal{T}_{1,h}} h_T^{q+1+\delta_1}\,||u_1||_{q+1+\delta_1,T}\,||z_1||_{2,T}\,. \tag{4.102}$$

On the other hand, we notice that

$$\begin{aligned} j_T(\widehat{\underline{\mathbf{u}}}_{1,T},\widehat{\underline{\mathbf{z}}}_{1,T}) &\leq j_T(\widehat{\underline{\mathbf{u}}}_{1,T},\widehat{\underline{\mathbf{u}}}_{1,T})^{1/2} j_T(\widehat{\underline{\mathbf{z}}}_{1,T},\widehat{\underline{\mathbf{z}}}_{1,T})^{1/2}\\ &\lesssim (h_T^{q+\delta_1}\,|u_1|_{q+1+\delta_1})(h_T\,|z_1|_{2,T})\,,\end{aligned} \tag{4.103}$$

and then we derive

$$|\mathfrak{E}_3| \lesssim \sum_{T\in\mathcal{T}_{1,h}} h_T^{q+1+\delta_1}||u_1||_{q+1+\delta_1,T}\,||z_1||_{2,T}\,. \tag{4.104}$$

Proceeding in analogous way, we find that

$$|\mathfrak{E}_2| \lesssim \sum_{T\in\mathcal{T}_{2,h}} h_T^{q+1+\delta_2}\,||u_2||_{q+1+\delta_2,T}\,||z_2||_{2,T}\,, \tag{4.105}$$

$$|\mathfrak{E}_4| \lesssim \sum_{T\in\mathcal{T}_{2,h}} h_T^{q+1+\delta_2}||u_2||_{q+1+\delta_2,T}\,||z_2||_{2,T}\,. \tag{4.106}$$

Now, thanks to (4.102), (4.105), (4.104), (4.106), and the elliptic regularity property (4.90), we are able to bound

$\widetilde{\mathcal{E}}_h(((u_1,u_2),\xi),((\widehat{\underline{\mathbf{z}}}_{1,h},\widehat{\underline{\mathbf{z}}}_{2,h})))$ *(cf.* (4.101)*), and then* $\mathfrak{T}_2$*, arriving to*

$$|\mathfrak{T}_2| \lesssim \left(\sum_{T\in\mathcal{T}_{1,h}} h_T^{2(q+1+\delta_1)} \, ||u_1||^2_{q+1+\delta_1,T} + \sum_{T\in\mathcal{T}_{2,h}} h_T^{2(q+1+\delta_2)} \, ||u_2||^2_{q+1+\delta_2,T} \right)^{1/2} . \tag{4.107}$$

ii.B) The case $k=0$*. It is not difficult to establish*

$$(f_1,\pi_T^0 z_1)_T \;=\; (\pi_T^0 f_1, z_1)_T \;=\; (\pi_T^0 f_1 - f_1, z_1 - \pi_T^0 z_1)_T \;+\; (f_1,z_1)_T \quad \forall\, T\in\mathcal{T}_{1,h}\,, \tag{4.108}$$

$$(f_2,\pi_S^0 z_2)_S \;=\; (\pi_S^0 f_2, z_2)_S \;=\; (\pi_S^0 f_2 - f_2, z_2 - \pi_S^0 z_2)_S \;+\; (f_2,z_2)_S \quad \forall\, S\in\mathcal{T}_{2,h}\,, \tag{4.109}$$

$$(g_1,\pi_F^0 z_2)_F \;=\; (g_1,z_2)_F \quad \forall\, F\in\Gamma_{1,h}\,, \tag{4.110}$$

$$(g_2,\pi_F^0 z_2)_F \;=\; (g_2,z_2)_F \quad \forall\, F\in\Gamma_{2,h}\,. \tag{4.111}$$

Now, taking $(v_1,v_2) := (z_1,z_2)\in U$ *in* (4.8a)*, we have*

$$\begin{aligned} &(f_1,z_1)_{\Omega_1} \;+\; (f_2,z_2)_{\Omega_2} \;+\; \langle g_1,\gamma_0^+(z_2)\rangle_{\Gamma_1} \;+\; \langle g_2,\gamma_0^+(z_2)\rangle_{\Gamma_2} \\ &= (\nabla u_1,\nabla z_1)_{\Omega_1} \;+\; (\nabla u_2,\nabla z_2)_{\Omega_2} \;+\; \langle \xi, \underbrace{\gamma_0^+(z_2)-\gamma_0^-(z_1)}_{=0}\rangle_{\Gamma_1}\,, \end{aligned}$$

and from (4.108)*-*(4.111)*, we deduce that*

$$\begin{aligned} \sum_{T\in\mathcal{T}_{1,h}} (f_1,\pi_T^0 z_1)_T \;+\; \sum_{S\in\mathcal{T}_{2,h}} (f_2,\pi_S^0 z_2)_S \;+\; \sum_{F\in\Gamma_{1,h}} (g_1,\pi_F^0 z_2)_F \;+\; \sum_{F\in\Gamma_{2,h}} (g_2,\pi_F^0 z_2)_F \\ = \sum_{T\in\mathcal{T}_{1,h}} (\pi_T^0 f_1 - f_1, z_1 - \pi_T^0 z_1)_T \;+\; \sum_{S\in\mathcal{T}_{2,h}} (\pi_S^0 f_2 - f_2, z_2 - \pi_S^0 z_2)_S \\ + (\nabla u_1,\nabla z_1)_{\Omega_1} + (\nabla u_2,\nabla z_2)_{\Omega_2}\,. \end{aligned} \tag{4.112}$$

Then, taking into account (4.63) *and* (4.112)*, we have*

$$\begin{aligned}
&\mathcal{E}_h(((u_1,u_2),\xi),((\widehat{\underline{\mathbf{z}}}_{1,h},\widehat{\underline{\mathbf{z}}}_{2,h}),\widehat{\eta}_h))\\
&= \underbrace{\sum_{T\in\mathcal{T}_{1,h}}\left[(\nabla p_T^1\underline{\mathbf{I}}_T^0 u_1,\nabla p_T^1\underline{\mathbf{I}}_T^0 z_1)_T-(\nabla u_1,\nabla z_1)_T\right]}_{\mathfrak{E}_1}\\
&\quad+\underbrace{\sum_{S\in\mathcal{T}_{2,h}}\left[(\nabla p_S^1\underline{\mathbf{I}}_S^0 u_1,\nabla p_S^1\underline{\mathbf{I}}_S^0 z_1)_S-(\nabla u_2,\nabla z_2)_S\right]}_{\mathfrak{E}_2}\\
&\quad+\underbrace{\sum_{T\in\mathcal{T}_{1,h}} j_T(\widehat{\underline{\mathbf{u}}}_{1,T},\widehat{\underline{\mathbf{z}}}_{1,T})}_{\mathfrak{E}_3}+\underbrace{\sum_{S\in\mathcal{T}_{2,h}} j_S(\widehat{\underline{\mathbf{u}}}_{2,S},\widehat{\underline{\mathbf{z}}}_{2,S})}_{\mathfrak{E}_4}\\
&-\underbrace{\sum_{T\in\mathcal{T}_{1,h}}(\pi_T^0 f_1-f_1,z_1-\pi_T^0 z_1)_T}_{\mathfrak{E}_5}-\underbrace{\sum_{S\in\mathcal{T}_{2,h}}(\pi_S^0 f_2-f_2,z_2-\pi_S^0 z_2)_S}_{\mathfrak{E}_6}. \qquad (4.113)
\end{aligned}$$

In order to bound $\mathfrak{E}_1$*, we first notice that*

$$(\nabla u_1,\nabla z_1)_T-(\nabla p_T^1\underline{\mathbf{I}}_T^0 u_1,\nabla p_T^1\underline{\mathbf{I}}_T^0 z_1)_T=(\nabla u_1-\nabla p_T^1\underline{\mathbf{I}}_T^0 u_1,\nabla z_1-\nabla p_T^1\underline{\mathbf{I}}_T^0 z_1)_T,$$

and, after take into consideration (4.22)*, we deduce*

$$|\mathfrak{E}_1|\lesssim\left(\sum_{T\in\mathcal{T}_{1,h}} h_T^{2(1+\delta_1)}||u_1||^2_{1+\delta_1,T}\right)^{1/2}|z_1|_{2,\Omega_1}. \qquad (4.114)$$

Proceeding in similar way, we also derive

$$|\mathfrak{E}_2|\lesssim\left(\sum_{S\in\mathcal{T}_{2,h}} h_S^{2(1+\delta_2)}||u_2||^2_{1+\delta_2,S}\right)^{1/2}|z_2|_{2,\Omega_2}. \qquad (4.115)$$

Next, applying (4.103) *with* $k=0$*, we obtain*

$$|\mathfrak{E}_3|\lesssim\left(\sum_{T\in\mathcal{T}_{1,h}} h_T^{2(1+\delta_1)}||u_1||^2_{1+\delta_1,T}\right)^{1/2}|z_1|_{2,\Omega_1}, \qquad (4.116)$$

$$|\mathfrak{E}_4|\lesssim\left(\sum_{T\in\mathcal{T}_{2,h}} h_T^{2(1+\delta_2)}||u_2||^2_{1+\delta_2,T}\right)^{1/2}|z_2|_{2,\Omega_1}. \qquad (4.117)$$

For $\mathfrak{E}_5$*, we apply Cauchy-Schwarz inequality, and approximation theory, to*

have

$$|\mathfrak{E}_5| \leq \sum_{T\in\mathcal{T}_{1,h}} ||\pi_T^0 f_1 - f_1||_T ||z_1 - \pi_T^0 z_1||_T$$
$$\leq \sum_{T\in\mathcal{T}_{1,h}} \left(h_T^{\delta_1} ||f_1||_{\delta_1,T}\right) \left(h_T |z_1|_{1,T}\right)$$
$$\lesssim \left(\sum_{T\in\mathcal{T}_{1,h}} h_T^{2(1+\delta_1)} ||f_1||_{\delta_1,T}^2\right)^{1/2} |z_1|_{1,\Omega_1}\,. \tag{4.118}$$

Analogously, we derive

$$|\mathfrak{E}_6| \lesssim \left(\sum_{T\in\mathcal{T}_{2,h}} h_T^{2(1+\delta_1)} ||f_2||_{\delta_2,T}^2\right)^{1/2} |z_2|_{1,\Omega_2}\,. \tag{4.119}$$

Then, $\mathfrak{T}_2$ is bounded from (4.114)-(4.119). Finally, the conclusion is also achieved in this case, thanks to (4.100) (which also holds for $k = 0$). We omit further details.

□

Following the ideas given in the proof of Theorem 2.32 in [66] (see also the proof of Theorem 6.3 in [41]), and with the help of Theorem 4.5.2, we can establish a superconvergent estimate of the reconstructive potential error in the L^2-norm. To this end, we introduce $p_h^{k+1}\underline{\mathbf{u}}_{j,h} \in L^2(\Omega_j)$ such that $p_h^{k+1}\underline{\mathbf{u}}_{j,h}|_T := p_T^{k+1}\underline{\mathbf{u}}_{j,T}$, for all $T \in \mathcal{T}_{j,h}$, for all $j \in \{1,2\}$ (cf. (4.19)).

Theorem 4.5.3 (L^2-error estimate of the potential) *Under the assumptions that $u_i \in H^{q+1+\delta_i}(\mathcal{T}_{i,h})$, $i \in \{1,2\}$, and the elliptic regularity property (4.90), we have, for $k \geq 1$:*

$$\|p_h^{k+1}\underline{\mathbf{u}}_{1,h} - u_1\|_{0,\Omega_1} + \|p_h^{k+1}\underline{\mathbf{u}}_{2,h} - u_2\|_{0,\Omega_2}$$
$$\lesssim h \left(h_1^{2(q+\delta_1)} ||u_1||_{q+1+\delta_1,\mathcal{T}_{1,h}}^2 + h_2^{2(q+\delta_2)} ||u_2||_{q+1+\delta_2,\mathcal{T}_{2,h}}^2\right)^{1/2}, \tag{4.120}$$

For $k = 0$, assuming in addition that $f_i \in H^{\delta_i}(\mathcal{T}_{i,h})$, for $i \in \{1,2\}$, $g_1 \in \mathbb{P}_0(\Gamma_{1,h})$ and $g_2 \in \mathbb{P}_0(\Gamma_{2,h})$, there holds

$$\|p_h^1\underline{\mathbf{u}}_{1,h} - u_1\|_{0,\Omega_1} + \|p_h^1\underline{\mathbf{u}}_{2,h} - u_2\|_{0,\Omega_2}$$
$$\lesssim h \left(h_1^{2\delta_1} ||u_1||_{1+\delta_1,\mathcal{T}_{1,h}}^2 + h_2^{2\delta_2} ||u_2||_{1+\delta_2,\mathcal{T}_{2,h}}^2\right)^{1/2}$$
$$+ \left(h_1^{2(1+\delta_1)} ||f_1||_{\delta_1,\mathcal{T}_{1,h}}^2 + h_2^{2(1+\delta_2)} ||f_2||_{\delta_2,\mathcal{T}_{2,h}}^2\right)^{1/2}. \tag{4.121}$$

Proof. *We give a sketch of the proof, referring to [66, Theorem 2.32] for further insight. Let, for the sake of brevity* $\breve{u}_{i,h} := p_h^{k+1}\underline{\mathbf{I}}^k_{\mathcal{T}_{i,h}}(u_i|_T)$ *for* $i \in \{1,2\}$. *Then, by triangle inequality, we obtain*

$$\sum_{i=1}^{2} \|p_h^{k+1}\underline{\mathbf{u}}_{i,h} - u_i\|_{0,\Omega_i} \leq \underbrace{\sum_{i=1}^{2} \|u_i - \breve{u}_{i,h}\|_{0,\Omega_i}}_{\mathfrak{T}_1} + \underbrace{\sum_{i=1}^{2} \|p_h^{k+1}(\widehat{\underline{\mathbf{u}}}_{i,h} - \underline{\mathbf{u}}_{i,h})\|_{0,\Omega_i}}_{\mathfrak{T}_2} \tag{4.122}$$

Using inside each element $T \in \mathcal{T}_{i,h}$ *for* $i \in \{1,2\}$, *the approximation properties in Lemma 4.3.3 with* $q = k$, *it follows*

$$\mathfrak{T}_1 \lesssim \sum_{i=1}^{2} \sum_{T\in\mathcal{T}_{i,h}} h_T^{2(k+1+\delta_i)} ||u_i||^2_{k+1+\delta_i,T}. \tag{4.123}$$

Now, using the local PoincarWirtinger (1.24) and the fact $\left(p_T^{k+1}(\widehat{\underline{\mathbf{u}}}_{i,T} - \underline{\mathbf{u}}_{i,T}) - \pi_T^0(\widehat{u}_{i,T} - u_{i,T}), 1\right)_T = 0$ *for each* $i \in \{1,2\}$, *we have.*

$$\begin{aligned}
\mathfrak{T}_2^2 &\lesssim \sum_{i=1}^{2} \sum_{T\in\mathcal{T}_{i,h}} \|p_T^{k+1}(\widehat{\underline{\mathbf{u}}}_{i,T} - \underline{\mathbf{u}}_{i,T})\|^2_{0,T} \\
&\lesssim \underbrace{\sum_{i=1}^{2} \sum_{T\in\mathcal{T}_{i,h}} h_T^2 \|\nabla p_T^{k+1}(\widehat{\underline{\mathbf{u}}}_{i,T} - \underline{\mathbf{u}}_{i,T})\|^2_{0,T}}_{\mathfrak{E}_1} + \underbrace{\sum_{i=1}^{2} \sum_{T\in\mathcal{T}_{i,h}} \|\pi_T^0(\widehat{u}_{i,T} - u_{i,T})\|^2_{0,T}}_{\mathfrak{E}_2}.
\end{aligned} \tag{4.124}$$

Then, observing that, $\mathfrak{E}_1 \lesssim h^2\|(\widehat{\underline{\mathbf{u}}}_{1,h}, \widehat{\underline{\mathbf{u}}}_{2,h}) - (\underline{\mathbf{u}}_{1,h}, \underline{\mathbf{u}}_{2,h})\|^2_{a,h}$ *with* $G_T^k = \nabla p_T^{k+1}$, *(4.62) and (4.79), we obtain*

$$\mathfrak{E}_1 \lesssim h^2 \left(h_1^{2(k+\delta_1)} \|u_1\|^2_{k+1+\delta_1,\mathcal{T}_{1,h}} + h_2^{2(k+\delta_2)} \|u_2\|^2_{k+1+\delta_2,\mathcal{T}_{2,h}} \right). \tag{4.125}$$

And then, by L^2*-stability of* π_T^0

$$\mathfrak{E}_2 \lesssim \sum_{i=1}^{2} \|\pi^k_{\mathcal{T}_{i,h}} u_i - u_{i,h}\|^2_{0,\Omega_i}. \tag{4.126}$$

Finally, we conclude from (4.122)-(4.125), and using (4.126) with Theorem 4.5.2. □

4.6 Computational implementation aspects

We start remarking that the condition $(v_{1,h}, 1)_{\Omega_1} + (v_{2,h}, 1)_{\Omega_2} = 0$ *given in the definition of discrete space* $\underline{\mathbf{U}}_h^{k,0}$, *make it difficult to find a basis. Then, we impose*

this restriction in the HHO variational formulation with the help of a Lagrange multiplier. This procedure yields to the following equivalent discrete scheme: Find $(\underline{\mathbf{u}}_{1,h}, \underline{\mathbf{u}}_{2,h}, \alpha, \xi_h) \in \underline{\mathbf{U}}_{1,h}^k \times \underline{\mathbf{U}}_{2,h}^k \times \mathbb{R} \times Q_h^k$ *such that*

$$\begin{aligned}
&\sum_{T\in\mathcal{T}_{1,h}} a_T(\underline{\mathbf{u}}_{1,T}, \underline{\mathbf{v}}_{1,T}) + \alpha\left(\sum_{T\in\mathcal{T}_{1,h}} (v_{1,T},1)_T + \sum_{S\in\mathcal{T}_{2,h}} (v_{2,S},1)_S\right) + \sum_{F\in\Gamma_{1,h}} (v_{2,F}-v_{1,F},\xi_F)_F \\
&+ \sum_{S\in\mathcal{T}_{2,h}} a_S(\underline{\mathbf{u}}_{2,S}, \underline{\mathbf{v}}_{2,S}) + \beta\left(\sum_{T\in\mathcal{T}_{1,h}} (u_{1,T},1)_T + \sum_{S\in\mathcal{T}_{2,h}} (u_{2,S},1)_S\right) + \sum_{F\in\Gamma_{1,h}} (u_{2,F}-u_{1,F},\lambda_F)_F \\
&= F_h(\underline{\mathbf{v}}_{1,h}, \underline{\mathbf{v}}_{2,h}) - G_h(\lambda_h) \qquad \forall (\underline{\mathbf{v}}_{1,h}, \underline{\mathbf{v}}_{2,h}, \beta, \lambda_h) \in \underline{\mathbf{U}}_{1,h}^k \times \underline{\mathbf{U}}_{2,h}^k \times \mathbb{R} \times Q_h^k, \quad (4.127)
\end{aligned}$$

where we rewrite (4.39) as

$$\begin{aligned}
F_h((\underline{\mathbf{v}}_{1,h}, \underline{\mathbf{v}}_{2,h})) &= \sum_{T\in\mathcal{T}_{1,h}} \left\{ (f_1, v_{1,T})_T + \sum_{F\in\mathcal{F}_T\cap\Gamma_{1,h}} (g_1, v_{2,F})_F \right\} \\
&\quad + \sum_{S\in\mathcal{T}_{2,h}} \left\{ (f_2, v_{2,S})_S + \sum_{F\in\mathcal{F}_S\cap\Gamma_{2,h}} (g_2, v_{2,F})_F \right\}, \\
&= \sum_{T\in\mathcal{T}_{1,h}} F_T^1(\underline{\mathbf{v}}_{1,T}) + \sum_{S\in\mathcal{T}_{2,h}} F_S^2(\underline{\mathbf{v}}_{2,S}), \qquad (4.128)
\end{aligned}$$

and

$$G_h(\lambda_h) = \sum_{F\in\Gamma_{1,h}} (\lambda_F, g)_F. \qquad (4.129)$$

For integers $l \geq 0$ *and* $n \geq 0$*, we denote by* $N_n^l := \begin{pmatrix} l+n \\ l \end{pmatrix}$ *the dimension of the space polynomial in* $\mathbb{R}^n$*, of degree at most* l*.*

Now, given $\underline{\mathbf{v}}_{i,h}$ *in the global discrete space* $\underline{\mathbf{U}}_{i,h}^k$*, we collect its components with respect to the polynomial bases attached to the mesh cells and faces, in a global component vector denoted by* $V_{\mathcal{TF}}(i) \in \mathbb{R}^{N_{\mathcal{T}}^k(i)}$*, with*

$$N_{\mathcal{T}}^k(i) := \dim(\underline{\mathbf{U}}_{i,h}^k) = \mathrm{card}(\mathcal{T}_{i,h}) \times N_d^k + \mathrm{card}(\mathcal{F}_{i,h}) \times N_{d-1}^k \text{ for } i \in \{1,2\}. \quad (4.130)$$

Here, N_d^k *and* N_{d-1}^k *denote the dimension of the corresponding local cell and face bases (d represents the space dimension). We can decompose the global vector of coefficients as*

$$V_{\mathcal{TF}}(i) = \left[\begin{array}{c} V_{\mathcal{T}}(i) \\ \hdashline V_{\mathcal{F}}(i) \end{array}\right], \qquad (4.131)$$

where the vectors $V_{\mathcal{T}}(i)$ and $V_{\mathcal{F}}(i)$ collect the coefficients associated to element-based and face-based DOFS for each subdomain, respectively.

Also, the restriction of $V_{\mathcal{TF}}(i)$ over their components associated to T, ∂T and S, ∂S are denoted by the local component vectors $V_{T\mathcal{F}_T} \in \mathbb{R}^{N_T^k}$ and $V_{S\mathcal{F}_S} \in \mathbb{R}^{N_S^k}$, respectively. In similar way, we can split these local vectors as

$$V_{T\mathcal{F}_T} = \begin{bmatrix} V_T \\ \hdashline V_{\mathcal{F}_T} \end{bmatrix} \quad \text{and} \quad V_{S\mathcal{F}_S} = \begin{bmatrix} V_S \\ \hdashline V_{\mathcal{F}_S} \end{bmatrix}, \tag{4.132}$$

with V_T, $V_{\mathcal{F}_T}$, and V_S, $V_{\mathcal{F}_S}$, collecting the coefficients associated to the bases of the elements T, S, and their linked faces, respectively.

Expressing the functions in the discrete formulation (4.127) as a linear combination of its respective basis functions, we obtain the following problem: Find $(U_{\mathcal{TF}}(1), U_{\mathcal{TF}}(2), \alpha, \xi) \in \mathbb{R}^{N_{\mathcal{T}}^k(1)} \times \mathbb{R}^{N_{\mathcal{T}}^k(2)} \times \mathbb{R} \times \mathbb{R}^{N_{\mathcal{F}}^k}$ such that

$$\begin{aligned} &\sum_{T\in\mathcal{T}_{1,h}} V_{T\mathcal{F}_T}^t A(T) U_{T\mathcal{F}_T} + \alpha \left(\sum_{T\in\mathcal{T}_{1,h}} V_T^t M_T + \sum_{S\in\mathcal{T}_{2,h}} V_S^t M_S \right) + \sum_{F\in\Gamma_{1,h}} [V_F^2 - V_F^1]^t M_{FF} \xi_F \\ &+ \sum_{S\in\mathcal{T}_{2,h}} V_{S\mathcal{F}_S}^t A(S) U_{S\mathcal{F}_S} + \beta \left(\sum_{T\in\mathcal{T}_{1,h}} M_T^t U_T + \sum_{S\in\mathcal{T}_{2,h}} M_S^t U_S \right) + \sum_{F\in\Gamma_{1,h}} \lambda_F^t M_{FF} [U_F^2 - U_F^1] \\ &= \sum_{T\in\mathcal{T}_{1,h}} V_{T\mathcal{F}_T}^t F(T) + \sum_{S\in\mathcal{T}_{2,h}} V_{S\mathcal{F}_S}^t F(S) - \sum_{F\in\Gamma_{1,h}} \lambda_F^t G_F, \end{aligned} \tag{4.133}$$

for all $(V_{\mathcal{TF}}(1), V_{\mathcal{TF}}(2), \beta, \lambda) \in \mathbb{R}^{N_{\mathcal{T}}^k(1)} \times \mathbb{R}^{N_{\mathcal{T}}^k(2)} \times \mathbb{R} \times \mathbb{R}^{N_{\mathcal{F}}^k}$, where $N_{\mathcal{F}}^k := \text{card}(\Gamma_{1,h}) \times N_{d-1}^k$. Here, the local matrices $A(T)$, $A(S)$ represent the local bilinear forms a_T y a_S respectively. The local vector $F(T)$, $F(S)$ represent the linear functionals F_T^1 and F_S^2 in (4.128) respectively, and G_F represents the linear functional $(\lambda_F, g)_F$ in (4.129). The vector $M_T \in \mathbb{R}^{N_d^k}$ collects the average of the local base functions on T and for each $F \in \Gamma_{1,h}$, we define $M_{FF} := [(\psi_i, \psi_j)]_{1\le i,j\le N_{d-1}^k}$, where ψ_i represent the face polynomials on F.

In order to eliminate the element-based DOFS (by static condensation), we divide in blocks the following matrices

$$A(T) = \left[\begin{array}{c:c} A_{TT} & A_{T\mathcal{F}_T} \\ \hdashline A_{T\mathcal{F}_T}^t & A_{\mathcal{F}_T\mathcal{F}_T} \end{array}\right], \qquad F(T) = \begin{bmatrix} F_T \\ \hdashline F_{\mathcal{F}_T} \end{bmatrix}, \tag{4.134}$$

$$A(S) = \left[\begin{array}{c|c} A_{SS} & A_{S\mathcal{F}_S} \\ \hline A^t_{S\mathcal{F}_S} & A_{\mathcal{F}_S\mathcal{F}_S} \end{array}\right], \qquad F(S) = \left[\begin{array}{c} F_S \\ \hline F_{\mathcal{F}_S} \end{array}\right], \tag{4.135}$$

Arranging the equation (4.133) in a matrix form, where we collect/assemble the submatrices A_{TT}, $A_{T\mathcal{F}_T}$, $A_{\mathcal{F}_T\mathcal{F}_T}$, F_T, $F_{\mathcal{F}_T}$ *in* $A_{\mathcal{T}\mathcal{T}}(1)$, $A_{\mathcal{T}\mathcal{F}}(1)$, $A_{\mathcal{F}\mathcal{F}}(1)$, $F_{\mathcal{T}}(1)$, $F_{\mathcal{F}}(1)$, *and* A_{SS}, $A_{S\mathcal{F}_S}$, $A_{\mathcal{F}_S\mathcal{F}_S}$, F_S, $F_{\mathcal{F}_S}$ *in* $A_{\mathcal{T}\mathcal{T}}(2)$, $A_{\mathcal{T}\mathcal{F}}(2)$, $A_{\mathcal{F}\mathcal{F}}(2)$, $F_{\mathcal{T}}(2)$, $F_{\mathcal{F}}(2)$, *respectively, we obtain the linear global system corresponding to the discrete problem (4.127):*

$$\left[\begin{array}{cc|cc|cc} A_{\mathcal{T}\mathcal{T}}(1) & 0 & A_{\mathcal{T}\mathcal{F}}(1) & 0 & M_{\mathcal{T}}(1) & 0 \\ \hline 0 & A_{\mathcal{T}\mathcal{T}}(2) & 0 & A_{\mathcal{T}\mathcal{F}}(2) & M_{\mathcal{T}}(2) & 0 \\ \hline A^t_{\mathcal{T}\mathcal{F}}(1) & 0 & A_{\mathcal{F}\mathcal{F}}(1) & 0 & 0 & -M_{\Gamma\Gamma} \\ \hline 0 & A^t_{\mathcal{T}\mathcal{F}}(2) & 0 & A_{\mathcal{F}\mathcal{F}}(2) & 0 & M_{\Gamma\Gamma} \\ \hline M^t_{\mathcal{T}}(1) & M^t_{\mathcal{T}}(2) & 0 & 0 & 0 & 0 \\ \hline 0 & 0 & -M^t_{\Gamma\Gamma} & M^t_{\Gamma\Gamma} & 0 & 0 \end{array}\right] \left[\begin{array}{c} U_{\mathcal{T}}(1) \\ \hline U_{\mathcal{T}}(2) \\ \hline U_{\mathcal{F}}(1) \\ \hline U_{\mathcal{F}}(2) \\ \hline \alpha \\ \hline \xi_\Gamma \end{array}\right] = \left[\begin{array}{c} F_{\mathcal{T}}(1) \\ \hline F_{\mathcal{T}}(2) \\ \hline F_{\mathcal{F}}(1) \\ \hline F_{\mathcal{F}}(2) \\ \hline 0 \\ \hline -G_\Gamma \end{array}\right], \tag{4.136}$$

where $M_{\mathcal{T}}(1)$, $M_{\mathcal{T}}(2)$, G_Γ *and* $M_{\Gamma\Gamma}$ *collect the vectors* M_T, M_S, G_F *and the matrices* M_{FF}, *respectively.* $U_{\mathcal{T}}(1)$, $U_{\mathcal{T}}(2)$, $U_{\mathcal{F}}(1)$, $U_{\mathcal{F}}(2)$ *and* ξ_Γ *assemble the coefficients of the local unknowns* U_T, U_S, $U_{\mathcal{F}_T}$, $U_{\mathcal{F}_S}$ *and* ξ_F, *respectively. Now, we compact the system* (4.136), *as*

$$\left[\begin{array}{c|ccc} A_{\mathcal{T}\mathcal{T}} & A_{\mathcal{T}\mathcal{F}} & M_{\mathcal{T}} & 0 \\ \hline A^t_{\mathcal{T}\mathcal{F}} & A_{\mathcal{F}\mathcal{F}} & 0 & M_{\mathcal{F}\Gamma} \\ \hline M^t_{\mathcal{T}} & 0 & 0 & 0 \\ \hline 0 & M^t_{\mathcal{F}\Gamma} & 0 & 0 \end{array}\right] \left[\begin{array}{c} U_{\mathcal{T}} \\ \hline U_{\mathcal{F}} \\ \hline \alpha \\ \hline \xi_\Gamma \end{array}\right] = \left[\begin{array}{c} F_{\mathcal{T}} \\ \hline F_{\mathcal{F}} \\ \hline 0 \\ \hline -G_\Gamma \end{array}\right]. \tag{4.137}$$

Then, computing the Schur complement of the block $A_{\mathcal{T}\mathcal{T}}$ *of the system (4.137), we*

deduce another linear system, on the skeleton, as follows:

$$\left[\begin{array}{c|c|c} A_{\mathcal{F}\mathcal{F}} - A_{\mathcal{T}\mathcal{F}}^t A_{\mathcal{T}\mathcal{T}}^{-1} A_{\mathcal{T}\mathcal{F}} & -A_{\mathcal{T}\mathcal{F}}^t A_{\mathcal{T}\mathcal{T}}^{-1} M_{\mathcal{T}} & M_{\mathcal{F}\Gamma} \\ \hline -M_{\mathcal{T}}^t A_{\mathcal{T}\mathcal{T}}^{-1} A_{\mathcal{T}\mathcal{F}} & -M_{\mathcal{T}}^t A_{\mathcal{T}\mathcal{T}}^{-1} M_{\mathcal{T}} & 0 \\ \hline M_{\mathcal{F}\Gamma}^t & 0 & 0 \end{array}\right] \left[\begin{array}{c} U_{\mathcal{F}} \\ \hline \alpha \\ \hline \xi_\Gamma \end{array}\right] = \left[\begin{array}{c} F_{\mathcal{F}} - A_{\mathcal{T}\mathcal{F}}^t A_{\mathcal{T}\mathcal{T}}^{-1} F_{\mathcal{T}} \\ \hline -M_{\mathcal{T}}^t A_{\mathcal{T}\mathcal{T}}^{-1} F_{\mathcal{T}} \\ \hline -G_\Gamma \end{array}\right], \tag{4.138}$$

Instead of solving the global system (4.137), whose size is

$$\sum_{i=1}^{2} \left[\mathrm{card}(\mathcal{T}_{i,h}) \times N_d^k + \mathrm{card}(\mathcal{F}_{i,h}) \times N_{d-1}^k\right] + N_{\mathcal{F}}^k + 1, \tag{4.139}$$

we solve the reduced system (4.138), whose DOF corresponds to the skeleton of the mesh, then its size is

$$\mathrm{card}(\mathcal{F}_{1,h}) \times N_{d-1}^k + \mathrm{card}(\mathcal{F}_{2,h}) \times N_{d-1}^k + N_{\mathcal{F}}^k + 1, \tag{4.140}$$

Therefore, we obtain, $U_{\mathcal{F}}$, the vector of coefficients of variables polynomials faces and ξ_Γ, the vector of coefficients of the auxiliary variable transmission ξ. We remark that the faces on transmission boundary are counted three times, two times for the skeleton mesh of each subdomain, and one more for the transmission condition.

Denoting by $\underset{T\in\mathcal{T}_h}{\longleftarrow}$ the usual assembling procedure based on a global DOF map, we can assemble all matrix products appearing in (4.138) directly from their local counterparts for each T and S of their subdomains, as

$$F_{\mathcal{F}} - A_{\mathcal{T}\mathcal{F}}^t A_{\mathcal{T}\mathcal{T}}^{-1} F_{\mathcal{T}} \underset{T\in\mathcal{T}_h}{\longleftarrow} F_{\mathcal{F}_T} - A_{T\mathcal{F}_T}^t A_{TT}^{-1} F_T \quad , \quad A_{\mathcal{T}\mathcal{F}}^t A_{\mathcal{T}\mathcal{T}}^{-1} M_{\mathcal{T}} \underset{T\in\mathcal{T}_h}{\longleftarrow} A_{T\mathcal{F}_T}^t A_{TT}^{-1} M_T,$$
$$A_{\mathcal{F}\mathcal{F}} - A_{\mathcal{T}\mathcal{F}}^t A_{\mathcal{T}\mathcal{T}}^{-1} A_{\mathcal{T}\mathcal{F}} \underset{T\in\mathcal{T}_h}{\longleftarrow} A_{\mathcal{F}_T\mathcal{F}_T} - A_{T\mathcal{F}_T}^t A_{TT}^{-1} A_{T\mathcal{F}_T},$$

$$M_{\mathcal{T}}^t A_{\mathcal{T}\mathcal{T}}^{-1} M_{\mathcal{T}} = \sum_{T\in\mathcal{T}_{1,h}} M_T^t A_{TT}^{-1} M_T + \sum_{S\in\mathcal{T}_{2,h}} M_S^t A_{SS}^{-1} M_S,$$

$$\text{and} \quad M_{\mathcal{T}}^t A_{\mathcal{T}\mathcal{T}}^{-1} B_{\mathcal{T}} = \sum_{T\in\mathcal{T}_{1,h}} M_T^t A_{TT}^{-1} B_T + \sum_{S\in\mathcal{T}_{2,h}} M_S^t A_{SS}^{-1} B_S$$

Besides, from the static condensation (Schur complement), we can recover the global vector $U_{\mathcal{T}}$, obtaining

$$U_{\mathcal{T}} = A_{\mathcal{T}\mathcal{T}}^{-1}\left[F_{\mathcal{T}} - \widehat{A}_{\mathcal{T}\mathcal{F}}\widehat{U}_{\mathcal{F}}\right]. \tag{4.141}$$

Letting $\alpha = 0$ in $\widehat{U}_{\mathcal{F}}$, yields

$$U_{\mathcal{T}} = A_{\mathcal{T}\mathcal{T}}^{-1}\Big(F_{\mathcal{T}} - A_{\mathcal{T}\mathcal{F}}U_{\mathcal{F}}\Big), \tag{4.142}$$

After a post-processing procedure, we obtain the local vectors U_T and U_S in each subdomain, as follows

$$U_T = A_{TT}^{-1}\Big(F_T - A_{T\mathcal{F}_T}U_{\mathcal{F}_T}\Big)\,, \quad U_S = A_{SS}^{-1}\Big(F_S - A_{S\mathcal{F}_S}U_{\mathcal{F}_S}\Big). \tag{4.143}$$

4.7 Numerical results

In this section we present a comprehensive set of numerical tests to assess the theoretical results we have obtained. In all cases, we consider a family of uniform simplicial meshes, piecewise polynomials of degree at most k, with $k \in \{0,1,2,3,4\}$ to approximate the exact solution. The experimental order of convergence (r), is computed as

$$r = \log(e_{\mathcal{T}}/e_{\widetilde{\mathcal{T}}})/\log(h_{\mathcal{T}}/h_{\widetilde{\mathcal{T}}})\,,$$

where $e_{\mathcal{T}}$ and $e_{\widetilde{\mathcal{T}}}$ are the errors associated to the corresponding variable considering two consecutive meshes $\mathcal{T}$ and $\widetilde{\mathcal{T}}$, respectively.

The numerical tests have been run considering a modification of the code used in [39], which is based, in turn, on the one developed by Di Pietro in [70, 75]. The implementation of local gradient reconstruction operator (4.18), L^2-orthogonal projectors π_T^k and π_F^k, are based on the linear algebra facilities (robust Cholesky factorization) provided by the Eigen3 library [112]. The reduced system on the skeleton (4.138) is solved by using SuperLU [63] through the PETSc 3.4 interface [14].

From here on, given (u_1, u_2, ξ) and $(\underline{\mathbf{u}}_{1,h}, \underline{\mathbf{u}}_{2,h}, \xi_h)$ the unique solutions of (4.8) and (4.38), respectively, we introduce the potential error as

- *Energy norm of the potential error:* $||(\widehat{\underline{\mathbf{u}}}_{1,h}, \widehat{\underline{\mathbf{u}}}_{2,h}) - (\underline{\mathbf{u}}_{1,h}, \underline{\mathbf{u}}_{2,h})||_{a,h}$,
- *L^2-norm of the flux error:*

$$\Big(||\nabla u_1 - \nabla_h p_h^{k+1}\underline{\mathbf{u}}_{1,h}||_{0,\Omega_1}^2 \; + \; ||\nabla u_2 - \nabla_h p_h^{k+1}\underline{\mathbf{u}}_{2,h}||_{0,\Omega_2}^2\Big)^{1/2}\,,$$

- *Discrete norm of the projection of the trace error:* $||\widehat{\xi}_h - \xi_h||_{\Gamma_{1,h}}$,

- *L^2- norm of the projection of the trace error:* $||\widehat{\xi}_h - \xi_h||_{0,\Gamma_1}$,

- *L^2-norm of the potential error:*

$$\left(||u_{1,h} - \pi^k_{\mathcal{T}_{1,h}} u_1||^2_{0,\Omega_1} \; + \; ||u_{2,h} - \pi^k_{\mathcal{T}_{2,h}} u_2||^2_{0,\Omega_2}\right)^{1/2} \; ,$$

- *L^2-norm of the reconstructive potential error:*

$$\left(||u_1 - p_h^{k+1}\underline{\mathbf{u}}_{1,h}||^2_{0,\Omega_1} \; + \; ||u_2 - p_h^{k+1}\underline{\mathbf{u}}_{2,h}||^2_{0,\Omega_2}\right)^{1/2} \; ,$$

  where $\widehat{\underline{\mathbf{u}}}_{i,h} := \underline{\mathbf{I}}^k_{\mathcal{T}_{i,h}} u_i \in \underline{\mathbf{U}}^k_{\mathcal{T}_{i,h}}$, *for* $i \in \{1,2\}$.

4.7.1 Example 1: Regular test case

We solve a transmission problem with subdomains $\Omega_1 := (0,1)^2$ *and* $\Omega_2 := (-1,2)^2 \setminus \overline{\Omega}_1$ *(see Figure 4.6), such that the exact solution is given by*

$$u_1(x,y) = (\mathrm{e}^x - 1)(x-1)(\mathrm{e}^y - 1)(y-1) - \mathrm{e}^2 + 5\mathrm{e} - \frac{25}{4} \quad , \quad u_2(x,y) = \sin(\pi x)\sin(\pi y). \tag{4.144}$$

On the transmission boundary, we have nonhomogeneous jump of trace of their potentials, and also nonhomogeneous jump of normal trace of their fluxes. Table 4.1 shows the histories of convergence of the energy norm of the potential error and the flux error vs meshsize, noticing that they converge at the optimal orders $k+1$, *when the exact solution is approximated by piecewise polynomials of degree at most* $k \in \{0,...,4\}$. *On the other hand, in Table 4.2, we show the corresponding history of convergence of the auxiliary unknown* ξ, *considering the discrete trace (4.29) and the standard* L^2-*norms. We observe convergence in both two cases, for* $k \in \{0,...,4\}$, *with orders* $k+3/2$ *and* $k+1$, *respectively. In Table 4.3, we include the histories of convergence in* L^2-*norm of the potential and reconstructive potential errors, which behave as* $\mathcal{O}(h^{k+2})$. *We remark that all these results are in agreement with Theorems 4.5.1, 4.5.2, and 4.5.3, as well as Remark 4.5.1, considering* $\delta_1 = \delta_2 = 1$, *and they can also be observed in Figures 4.3, 4.4 and 4.5. In the case of* ξ, *we notice that rate of convergence in* $||\cdot||_{\Gamma_{1,h}}$ *is* $1/2$ *faster than the predicted by Theorem 4.5.1.*

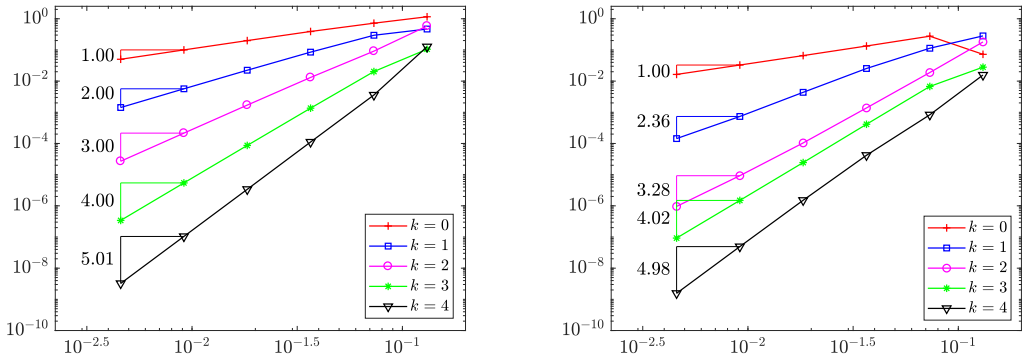

Figure 4.3: Rates of convergence of the (Left) energy norm of the potential error, and (Righ) flux error (Example 1)

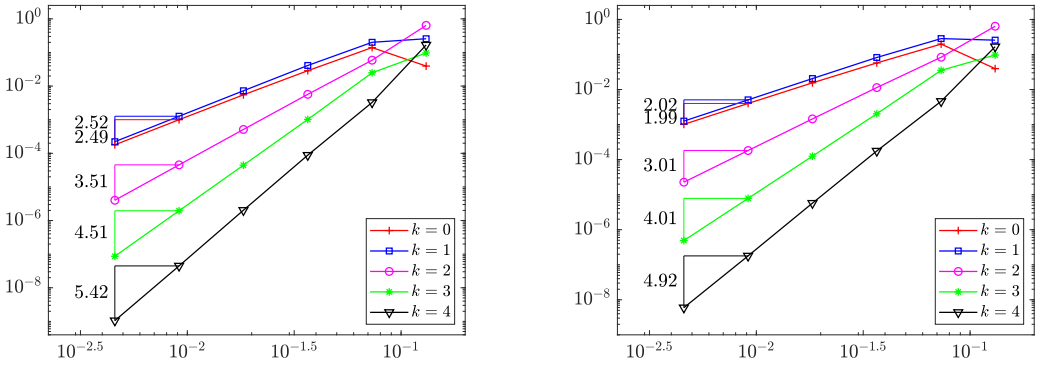

(a) $||\widehat{\xi}_h - \xi_h||_{\Gamma_{1,h}}$ vs. h (b) $||\widehat{\xi}_h - \xi_h||_{0,\Gamma_1}$ vs. h

Figure 4.4: Rates of convergence of the Lagrange multiplier considering the (a) Discrete trace norm $||\cdot||_{\Gamma_{1,h}}$, and (b) Standard L^2-norm (Example 1)

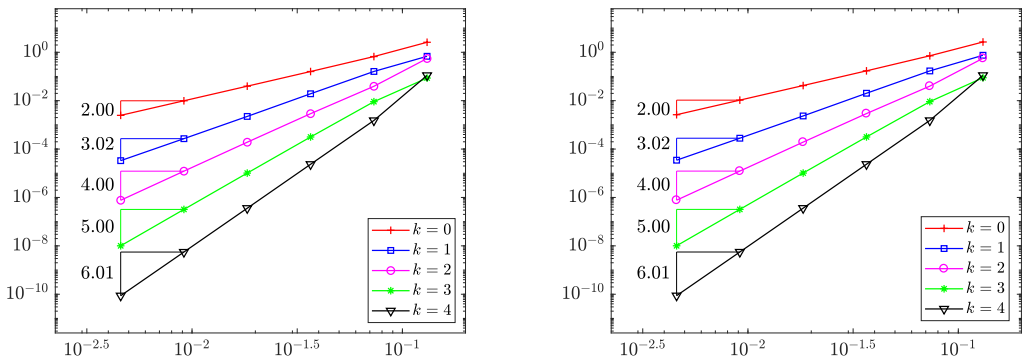

Figure 4.5: Rates of convergence of the L^2-norm of the (Left) potential error, and (Right) reconstructive potential error (Example 1).

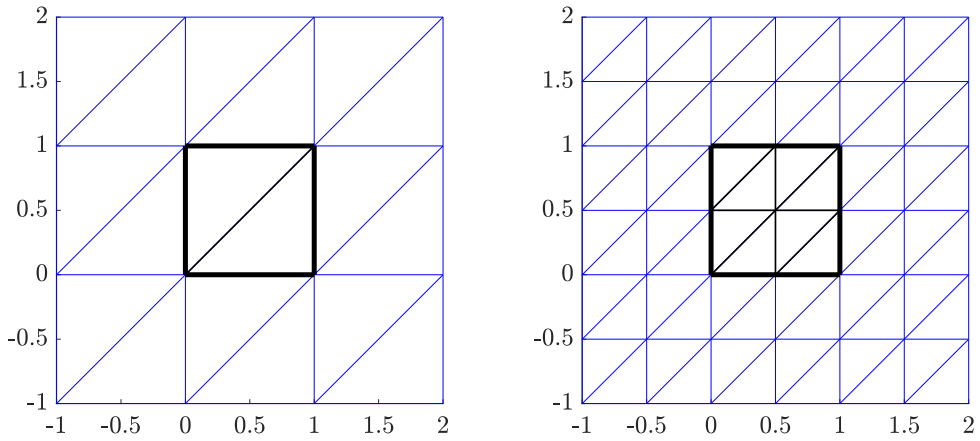

Figure 4.6: First two simplicial meshes for Example 1.

Table 4.1: Histories of convergence of the energy norm of the potential error and L^2-norm of the flux error, considering $k \in \{0, 1, 2, 3, 4\}$ (Example 1)

Energy norm of the potential error										
	$k=0$		$k=1$		$k=2$		$k=3$		$k=4$	
h	error	rate	error	rate	error	rate	error	rate	error	rate
1.31e-01	1.16e+00		4.68e-01		5.85e-01		1.05e-01		1.27e-01	
7.32e-02	7.21e-01	0.817	2.96e-01	0.790	9.15e-02	3.187	2.03e-02	2.835	3.59e-03	6.127
3.66e-02	3.91e-01	0.883	8.50e-02	1.798	1.31e-02	2.803	1.36e-03	3.903	1.11e-04	5.010
1.83e-02	2.00e-01	0.970	2.23e-02	1.928	1.70e-03	2.946	8.65e-05	3.970	3.38e-06	5.041
9.15e-03	1.00e-01	0.993	5.67e-03	1.978	2.15e-04	2.985	5.43e-06	3.993	1.04e-07	5.021
4.58e-03	5.02e-02	1.000	1.42e-03	1.997	2.69e-05	3.001	3.40e-07	4.005	3.24e-09	5.015
L^2-norm of the flux error										
	$k=0$		$k=1$		$k=2$		$k=3$		$k=4$	
h	error	rate	error	rate	error	rate	error	rate	error	rate
1.31e-01	7.23e-02		2.82e-01		1.81e-01		2.80e-02		1.57e-02	
7.32e-02	2.76e-01	-2.302	1.13e-01	1.567	1.89e-02	3.883	6.74e-03	2.448	8.31e-04	5.047
3.66e-02	1.34e-01	1.047	2.54e-02	2.158	1.38e-03	3.774	4.13e-04	4.030	4.18e-05	4.314
1.83e-02	6.59e-02	1.021	4.37e-03	2.540	1.04e-04	3.727	2.44e-05	4.080	1.51e-06	4.795
9.15e-03	3.28e-02	1.006	7.35e-04	2.572	9.25e-06	3.492	1.49e-06	4.034	4.92e-08	4.937
4.58e-03	1.64e-02	1.003	1.44e-04	2.360	9.57e-07	3.278	9.23e-08	4.019	1.56e-09	4.984

Table 4.2: Histories of convergence of the L^2-projection of $\xi - \xi_h$ in $||\cdot||_{\Gamma_{1,h}}$ and $||\cdot||_{0,\Gamma_1}$ norms, for $k \in \{0,1,2,3,4\}$ (Example 1)

$\|\widehat{\xi}_h - \xi_h\|_{\Gamma_{1,h}}$										
	$k=0$		$k=1$		$k=2$		$k=3$		$k=4$	
h	error	rate	error	rate	error	rate	error	rate	error	rate
1.31e-01	3.94e-02		2.56e-01		6.39e-01		9.66e-02		1.67e-01	
7.32e-02	1.40e-01	-2.174	2.01e-01	0.419	5.89e-02	4.096	2.49e-02	2.329	3.26e-03	6.760
3.66e-02	2.87e-02	2.285	4.10e-02	2.291	5.68e-03	3.376	1.02e-03	4.613	8.82e-05	5.210
1.83e-02	5.48e-03	2.388	7.26e-03	2.499	5.13e-04	3.470	4.43e-05	4.523	2.02e-06	5.445
9.15e-03	1.00e-03	2.454	1.27e-03	2.518	4.54e-05	3.497	1.96e-06	4.501	4.47e-08	5.501
4.58e-03	1.79e-04	2.487	2.22e-04	2.519	4.01e-06	3.507	8.65e-08	4.506	1.05e-09	5.417
$\|\widehat{\xi}_h - \xi_h\|_{0,\Gamma_1}$										
	$k=0$		$k=1$		$k=2$		$k=3$		$k=4$	
h	error	rate	error	rate	error	rate	error	rate	error	rate
1.31e-01	3.94e-02		2.56e-01		6.39e-01		9.66e-02		1.67e-01	
7.32e-02	1.98e-01	-2.769	2.84e-01	-0.177	8.34e-02	3.500	3.52e-02	1.734	4.62e-03	6.164
3.66e-02	5.74e-02	1.785	8.20e-02	1.791	1.14e-02	2.876	2.04e-03	4.113	1.76e-04	4.710
1.83e-02	1.55e-02	1.888	2.05e-02	1.999	1.45e-03	2.970	1.25e-04	4.023	5.73e-06	4.945
9.15e-03	4.00e-03	1.954	5.07e-03	2.018	1.82e-04	2.997	7.82e-06	4.001	1.79e-07	5.001
4.58e-03	1.01e-03	1.986	1.25e-03	2.019	2.27e-05	3.006	4.89e-07	4.005	5.95e-09	4.916

Table 4.3: Histories of convergence of L^2-norm of the potential and reconstructive potential errors, considering $k \in \{0, 1, 2, 3, 4\}$ (Example 1)

L^2-norm of the potential error										
	$k=0$		$k=1$		$k=2$		$k=3$		$k=4$	
h	error	rate	error	rate	error	rate	error	rate	error	rate
1.31e-01	2.59e+00		6.82e-01		5.52e-01		8.61e-02		1.11e-01	
7.32e-02	6.65e-01	2.338	1.61e-01	2.477	3.93e-02	4.542	9.08e-03	3.864	1.52e-03	7.369
3.66e-02	1.60e-01	2.053	1.93e-02	3.064	2.90e-03	3.759	3.16e-04	4.848	2.35e-05	6.016
1.83e-02	3.97e-02	2.013	2.23e-03	3.111	1.92e-04	3.918	1.02e-05	4.956	3.59e-07	6.032
9.15e-03	9.90e-03	2.003	2.69e-04	3.054	1.22e-05	3.976	3.20e-07	4.988	5.54e-09	6.017
4.58e-03	2.47e-03	2.004	3.32e-05	3.022	7.66e-07	3.999	1.00e-08	5.004	8.68e-11	6.005
L^2-norm of the reconstructive potential error										
	$k=0$		$k=1$		$k=2$		$k=3$		$k=4$	
h	error	rate	error	rate	error	rate	error	rate	error	rate
1.31e-01	2.66e+00		7.52e-01		5.64e-01		8.86e-02		1.11e-01	
7.32e-02	7.15e-01	2.259	1.70e-01	2.559	3.99e-02	4.551	9.12e-03	3.906	1.52e-03	7.369
3.66e-02	1.71e-01	2.067	2.03e-02	3.065	2.93e-03	3.768	3.17e-04	4.849	2.36e-05	6.015
1.83e-02	4.22e-02	2.017	2.34e-03	3.116	1.93e-04	3.920	1.02e-05	4.957	3.60e-07	6.031
9.15e-03	1.05e-02	2.004	2.81e-04	3.057	1.23e-05	3.977	3.21e-07	4.988	5.57e-09	6.016
4.58e-03	2.63e-03	2.004	3.47e-05	3.023	7.72e-07	4.000	1.01e-08	5.005	8.71e-11	6.006

4.7.2 Example 2: Another regular test case

We solve (4.1) *with subdomains* $\Omega_1 := (1,2)^2$ *and* $\Omega_2 := (0,3)^2 \setminus \overline{\Omega}_1$, *and the data are such that the exact solution is*

$$u_1(x,y) = \sin(\pi x)\sin(\pi y) - \frac{4}{\pi^2} \quad , \quad u_2(x,y) = \cos(\pi x)\cos(\pi y). \tag{4.145}$$

We notice that in this case, g_1 *and* g_2 *are nonhomogeneous on* Γ_1. *Table 4.4 shows the history of convergence of the energy norm of the potential error and the flux error, when approximating the exact solution with piecewise polynomials of degree at most* $k \in \{0, 1, 2, 3, 4\}$. *In both two cases, we observe that the rate of convergence is* $k+2$, *as predicted by Theorem 4.5.1, with* δ_1 *and* δ_2 *close to 1. Concerning the*

auxiliary transmission unknown ξ, in Table 4.6 we report the corresponding histories of convergence of the projection of $\xi - \xi_h$ in a weighted L^2- norm as well as the usual L^2-norm, for comparison. We notice that the rate of convergence of ξ in the weighted norm is close to $k+3/2$ (which is $1/2$ faster than the predicted by Theorem 4.5.1). Also, we observe an order of convergence $k+1$, for ξ in the usual L^2-norm, which is in agreement with Remark 4.5.1. The histories of convergence of L^2-norm of the potential and the reconstructive potential errors, are provided in Table 4.5. We notice that the rates of convergence for these errors are $k+2$, in agreement with Theorems 4.5.2 and 4.5.3. Figure 4.7 shows the first two initial meshes of the domain, considered in this numerical simulation, while Figures 4.9, 4.8 and 4.10 resume the information given in Tables 4.4,4.6 and 4.5, respectively.

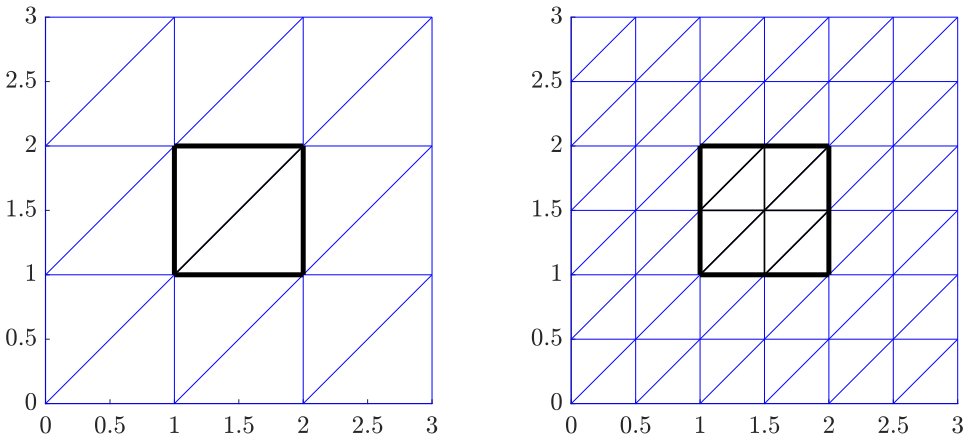

Figure 4.7: First two simplicial meshes for Example 2

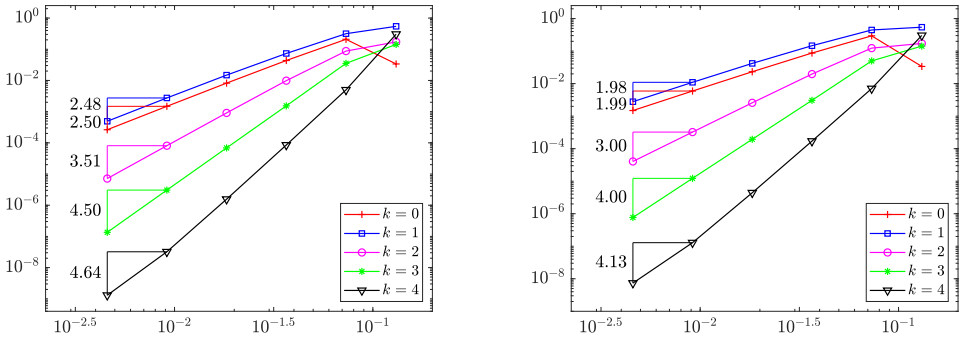

Figure 4.8: Rates of convergence of the Lagrange multiplier considering the (Left) Discrete trace norm $||\cdot||_{\Gamma_{1,h}}$, and (Right) Standard L^2-norm (Example 2)

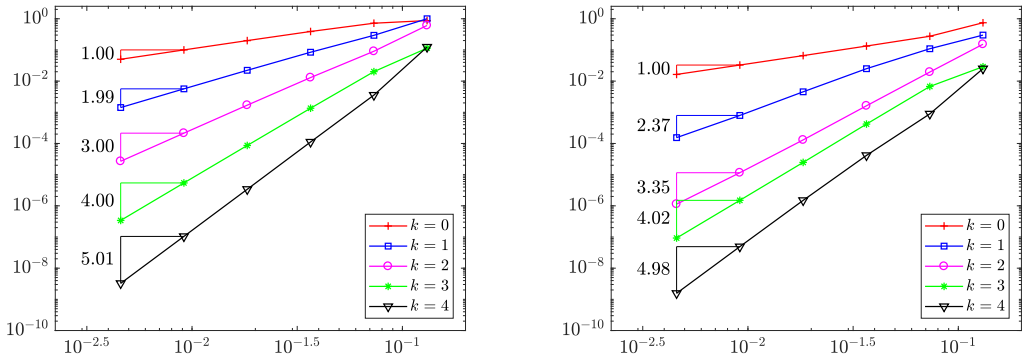

Figure 4.9: Rates of convergence of the (Left) energy norm of the potential error, and (Right) flux error (Example 2)

Table 4.4: Histories of convergence of the energy norm of the potential error and L^2-norm of the flux error, considering $k \in \{0, 1, 2, 3, 4\}$ (Example 2)

Energy norm of the potential error										
	$k = 0$		$k = 1$		$k = 2$		$k = 3$		$k = 4$	
h	error	rate	error	rate	error	rate	error	rate	error	rate
1.31e-01	8.74e-01		1.00e+00		6.11e-01		1.14e-01		1.24e-01	
7.32e-02	7.20e-01	0.334	2.94e-01	2.104	9.07e-02	3.276	2.01e-02	2.981	3.56e-03	6.102
3.66e-02	3.91e-01	0.882	8.44e-02	1.801	1.30e-02	2.803	1.35e-03	3.899	1.12e-04	4.996
1.83e-02	1.99e-01	0.970	2.22e-02	1.926	1.69e-03	2.941	8.63e-05	3.967	3.39e-06	5.039
9.15e-03	1.00e-01	0.993	5.65e-03	1.975	2.14e-04	2.982	5.43e-06	3.991	1.04e-07	5.023
4.58e-03	5.02e-02	1.000	1.42e-03	1.995	2.69e-05	2.999	3.40e-07	4.004	3.26e-09	5.010
L^2-norm of the flux error										
	$k = 0$		$k = 1$		$k = 2$		$k = 3$		$k = 4$	
h	error	rate	error	rate	error	rate	error	rate	error	rate
1.31e-01	7.45e-01		3.00e-01		1.53e-01		2.90e-02		2.51e-02	
7.32e-02	2.75e-01	1.716	1.09e-01	1.732	1.95e-02	3.532	6.73e-03	2.507	8.89e-04	5.738
3.66e-02	1.33e-01	1.042	2.50e-02	2.126	1.62e-03	3.594	4.19e-04	4.007	4.14e-05	4.424
1.83e-02	6.58e-02	1.019	4.54e-03	2.463	1.30e-04	3.637	2.47e-05	4.085	1.50e-06	4.792
9.15e-03	3.28e-02	1.006	7.92e-04	2.519	1.15e-05	3.496	1.50e-06	4.041	4.90e-08	4.931
4.58e-03	1.64e-02	1.003	1.54e-04	2.367	1.13e-06	3.354	9.26e-08	4.023	1.56e-09	4.979

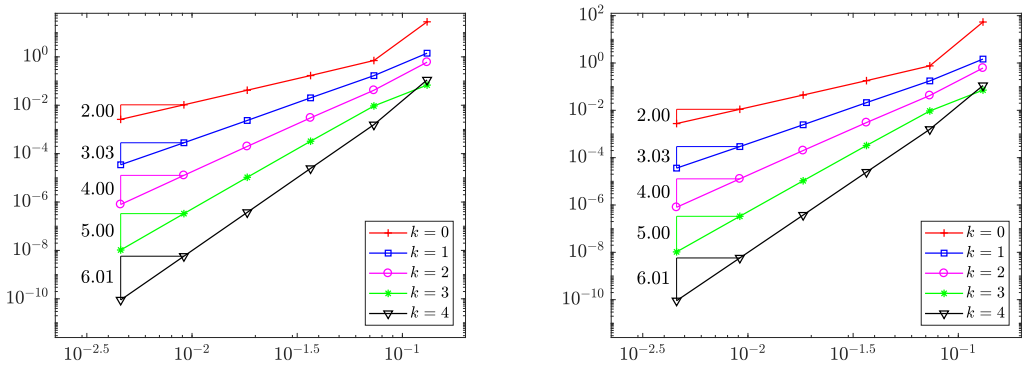

Figure 4.10: Rates of convergence of the L^2-norm of the (Left) potential error, and (Right) reconstructive potential error (Example 2)

Table 4.5: Histories of convergence of L^2-norm of the potential and reconstructive potential errors, considering $k \in \{0, 1, 2, 3, 4\}$ (Example 2)

L^2-norm of the potential error										
	$k = 0$		$k = 1$		$k = 2$		$k = 3$		$k = 4$	
h	error	rate	error	rate	error	rate	error	rate	error	rate
1.31e-01	2.81e+01		1.41e+00		6.02e-01		6.80e-02		1.11e-01	
7.32e-02	7.05e-01	6.331	1.67e-01	3.671	4.17e-02	4.589	9.33e-03	3.413	1.57e-03	7.321
3.66e-02	1.69e-01	2.062	2.02e-02	3.048	3.01e-03	3.792	3.25e-04	4.844	2.45e-05	6.007
1.83e-02	4.17e-02	2.015	2.35e-03	3.106	1.99e-04	3.921	1.05e-05	4.951	3.74e-07	6.033
9.15e-03	1.04e-02	2.004	2.82e-04	3.059	1.26e-05	3.975	3.32e-07	4.985	5.76e-09	6.018
4.58e-03	2.60e-03	2.004	3.46e-05	3.027	7.94e-07	3.998	1.04e-08	5.003	8.99e-11	6.012
L^2-norm of the reconstructive potential error										
	$k = 0$		$k = 1$		$k = 2$		$k = 3$		$k = 4$	
h	error	rate	error	rate	error	rate	error	rate	error	rate
1.31e-01	5.39e+01		1.46e+00		6.13e-01		7.14e-02		1.12e-01	
7.32e-02	7.57e-01	7.331	1.75e-01	3.646	4.23e-02	4.595	9.37e-03	3.490	1.58e-03	7.321
3.66e-02	1.80e-01	2.075	2.12e-02	3.050	3.04e-03	3.799	3.26e-04	4.845	2.45e-05	6.006
1.83e-02	4.43e-02	2.019	2.45e-03	3.109	2.00e-04	3.923	1.05e-05	4.952	3.75e-07	6.032
9.15e-03	1.10e-02	2.005	2.94e-04	3.061	1.27e-05	3.975	3.33e-07	4.985	5.79e-09	6.018
4.58e-03	2.76e-03	2.004	3.61e-05	3.029	8.00e-07	3.999	1.04e-08	5.003	9.03e-11	6.012

Table 4.6: Histories of convergence of the L^2-projection of $\xi - \xi_h$ in $||\cdot||_{\Gamma_{1,h}}$ and $||\cdot||_{0,\Gamma_1}$ norms, for $k \in \{0,1,2,3,4\}$ (Example 2)

$\|\widehat{\xi}_h - \xi_h\|_{\Gamma_{1,h}}$										
	$k=0$		$k=1$		$k=2$		$k=3$		$k=4$	
h	error	rate	error	rate	error	rate	error	rate	error	rate
1.31e-01	3.38e-02		5.43e-01		1.72e-01		1.43e-01		3.04e-01	
7.32e-02	2.08e-01	-3.127	3.16e-01	0.933	8.74e-02	1.164	3.53e-02	2.399	4.99e-03	7.061
3.66e-02	4.36e-02	2.258	7.33e-02	2.107	9.84e-03	3.151	1.53e-03	4.527	8.52e-05	5.870
1.83e-02	8.21e-03	2.408	1.48e-02	2.306	9.09e-04	3.435	6.87e-05	4.478	1.56e-06	5.772
9.15e-03	1.48e-03	2.471	2.75e-03	2.432	8.09e-05	3.490	3.06e-06	4.490	3.22e-08	5.600
4.58e-03	2.63e-04	2.496	4.92e-04	2.485	7.16e-06	3.505	1.35e-07	4.504	1.30e-09	4.636
$\|\widehat{\xi}_h - \xi_h\|_{0,\Gamma_1}$										
	$k=0$		$k=1$		$k=2$		$k=3$		$k=4$	
h	error	rate	error	rate	error	rate	error	rate	error	rate
1.31e-01	3.38e-02		5.43e-01		1.72e-01		1.43e-01		3.04e-01	
7.32e-02	2.95e-01	-3.722	4.46e-01	0.337	1.24e-01	0.569	4.99e-02	1.803	7.05e-03	6.466
3.66e-02	8.71e-02	1.758	1.47e-01	1.607	1.97e-02	2.651	3.06e-03	4.027	1.70e-04	5.370
1.83e-02	2.32e-02	1.908	4.19e-02	1.806	2.57e-03	2.935	1.94e-04	3.978	4.41e-06	5.272
9.15e-03	5.92e-03	1.971	1.10e-02	1.932	3.24e-04	2.990	1.22e-05	3.990	1.29e-07	5.100
4.58e-03	1.49e-03	1.995	2.78e-03	1.984	4.05e-05	3.004	7.66e-07	4.003	7.36e-09	4.135

4.7.3 Example 3: A numerical singularity

We solve transmission problem (4.1)*, considering* $\Omega_1 := (-1/2, 1/2)^2$ *and* $\Omega_2 := (-2,2)^2 \setminus \overline{\Omega}_1$*, with given data such that the exact solution is*

$$u_1(x,y) = \frac{xy}{(x-0.55)^2 + y^2}, \quad u_2(x,y) = \frac{x-y}{x^2+y^2}\,. \tag{4.146}$$

We pointwise that in this case, u_1 *presents a singularity at* $(0.55, 0)$*, which is close to* Γ_1*. For this example, we consider two families of simplicial meshes: one conforming mesh and the other nonconforming, with hanging nodes just on* Γ_1*. We emphasize that the latter is not covered by the current theory, so our aim is to check the robustness of our scheme in this situation.*

4.7.3.1 Results when solving using conforming meshes

From Tables 4.7, 4.9 and 4.8, we observe that the method converges at the optimal rates of convergence, in agreement with Theorems 4.5.1, 4.5.2 and 4.5.3, and Remark 4.5.1. Figure 4.11 shows the first two conforming meshes, considered in this situation, while in Figure 4.13 we display the rates of convergence of energy norm of the potential error and L^2-norm of the flux error. Moreover, the rates of convergence of $\widehat{\xi}_h - \xi_h$ in $||\cdot||_{\Gamma_{1,h}}$ and $||\cdot||_{0,\Gamma_1}$ norms, are shown in Figure 4.12. Information contained in Table 4.8 is reported in Figure 4.14.

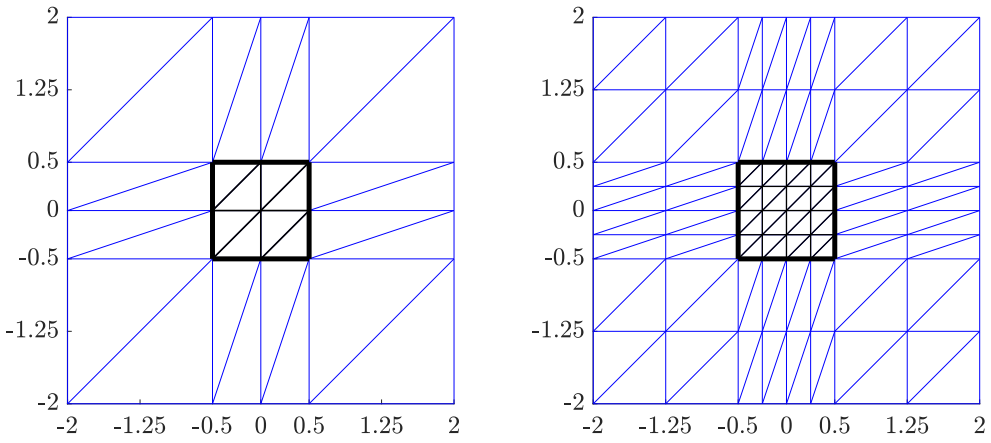

Figure 4.11: First two conforming meshes for Example 3.

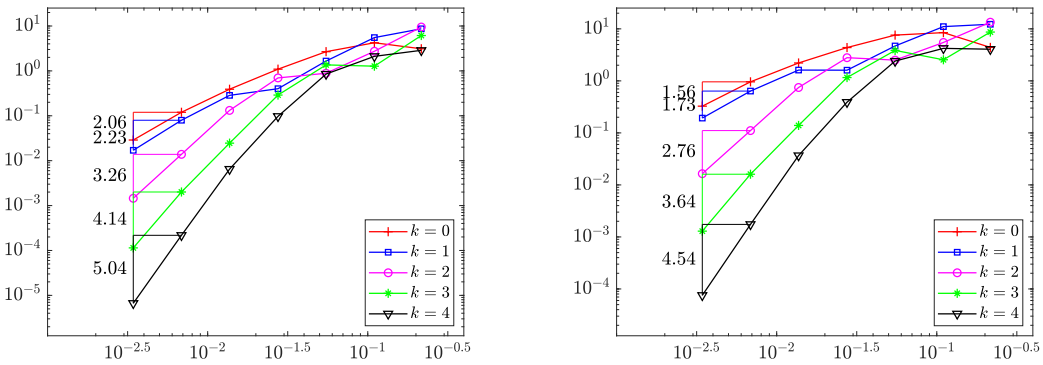

(a) $||\widehat{\xi}_h - \xi_h||_{\Gamma_{1,h}}$ vs. h (b) $||\widehat{\xi}_h - \xi_h||_{0,\Gamma_1}$ vs. h

Figure 4.12: Rates of convergence of the Lagrange multiplier considering the (a) Discrete trace norm $||\cdot||_{\Gamma_{1,h}}$, and (b) Standard L^2-norm (Example 3, conforming meshes)

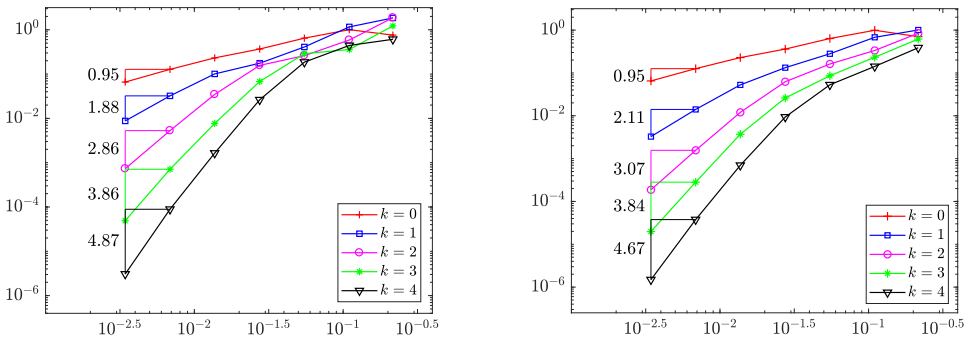

Figure 4.13: Rates of convergence of the (Left) energy norm of the potential error, and (Right) flux error (Example 3, conforming meshes)

Table 4.7: Histories of convergence of the energy norm of the potential error and L^2-norm of the flux error, considering $k \in \{0, 1, 2, 3, 4\}$ (Ex3, conforming meshes)

Energy norm of the potential error										
	$k=0$		$k=1$		$k=2$		$k=3$		$k=4$	
h	error	rate	error	rate	error	rate	error	rate	error	rate
2.16e-01	7.57e-01		1.85e+00		1.87e+00		1.22e+00		6.09e-01	
1.10e-01	1.01e+00	-0.419	1.16e+00	0.689	5.87e-01	1.718	3.59e-01	1.814	4.43e-01	0.472
5.49e-02	6.46e-01	0.635	4.09e-01	1.500	2.60e-01	1.170	2.89e-01	0.311	1.86e-01	1.249
2.75e-02	3.68e-01	0.816	1.76e-01	1.221	1.57e-01	0.730	6.79e-02	2.095	2.63e-02	2.828
1.37e-02	2.32e-01	0.662	1.01e-01	0.798	3.47e-02	2.166	7.69e-03	3.127	1.65e-03	3.978
6.86e-03	1.28e-01	0.861	3.22e-02	1.650	5.29e-03	2.721	7.10e-04	3.444	8.89e-05	4.220
3.43e-03	6.60e-02	0.952	8.77e-03	1.878	7.32e-04	2.854	4.91e-05	3.854	3.07e-06	4.856
L^2-norm of the flux error										
	$k=0$		$k=1$		$k=2$		$k=3$		$k=4$	
h	error	rate	error	rate	error	rate	error	rate	error	rate
2.16e-01	7.04e-01		1.01e+00		8.45e-01		6.18e-01		3.88e-01	
1.10e-01	9.90e-01	-0.505	6.79e-01	0.582	3.34e-01	1.375	2.33e-01	1.446	1.42e-01	1.490
5.49e-02	6.36e-01	0.637	2.80e-01	1.274	1.62e-01	1.046	8.60e-02	1.433	5.29e-02	1.419
2.75e-02	3.61e-01	0.821	1.33e-01	1.081	6.23e-02	1.378	2.60e-02	1.729	9.36e-03	2.505
1.37e-02	2.28e-01	0.656	5.26e-02	1.328	1.20e-02	2.364	3.71e-03	2.797	6.98e-04	3.725
6.86e-03	1.26e-01	0.859	1.41e-02	1.907	1.56e-03	2.949	2.82e-04	3.724	3.77e-05	4.221
3.43e-03	6.51e-02	0.951	3.27e-03	2.107	1.87e-04	3.062	1.98e-05	3.830	1.49e-06	4.659

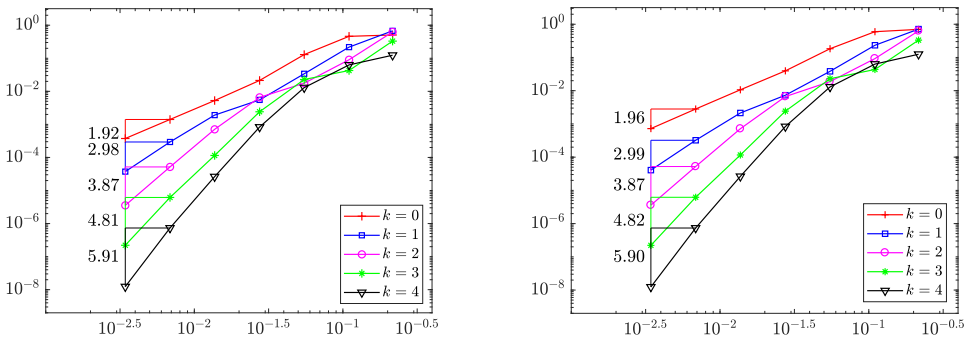

Figure 4.14: Rates of convergence of the L^2-norm of the (Left) potential error, and (Right) reconstructive potential error (Example 3, conforming meshes)

Table 4.8: Histories of convergence of L^2-norm of the potential and reconstructive potential errors, considering $k \in \{0, 1, 2, 3, 4\}$ (Example 3, conforming meshes)

L^2-norm of the potential error										
	$k = 0$		$k = 1$		$k = 2$		$k = 3$		$k = 4$	
h	error	rate	error	rate	error	rate	error	rate	error	rate
2.16e-01	5.06e-01		6.75e-01		6.25e-01		3.30e-01		1.24e-01	
1.10e-01	4.61e-01	0.138	2.17e-01	1.679	9.01e-02	2.870	4.26e-02	3.036	6.30e-02	1.001
5.49e-02	1.29e-01	1.830	3.40e-02	2.672	1.76e-02	2.348	2.28e-02	0.900	1.29e-02	2.276
2.75e-02	2.13e-02	2.605	5.51e-03	2.631	6.56e-03	1.430	2.41e-03	3.250	8.32e-04	3.970
1.37e-02	5.27e-03	2.008	1.91e-03	1.521	7.08e-04	3.195	1.15e-04	4.367	2.63e-05	4.959
6.86e-03	1.41e-03	1.907	2.94e-04	2.706	5.16e-05	3.786	6.16e-06	4.229	7.34e-07	5.172
3.43e-03	3.74e-04	1.912	3.73e-05	2.978	3.55e-06	3.861	2.21e-07	4.804	1.24e-08	5.893
L^2-norm of the reconstructive potential error										
	$k = 0$		$k = 1$		$k = 2$		$k = 3$		$k = 4$	
h	error	rate	error	rate	error	rate	error	rate	error	rate
2.16e-01	7.01e-01		7.13e-01		6.30e-01		3.32e-01		1.25e-01	
1.10e-01	5.96e-01	0.238	2.33e-01	1.659	9.24e-02	2.846	4.35e-02	3.013	6.31e-02	1.011
5.49e-02	1.83e-01	1.699	3.83e-02	2.598	1.88e-02	2.292	2.29e-02	0.924	1.30e-02	2.277
2.75e-02	3.96e-02	2.217	7.31e-03	2.394	6.65e-03	1.502	2.42e-03	3.248	8.35e-04	3.969
1.37e-02	1.06e-02	1.884	2.14e-03	1.766	7.16e-04	3.197	1.16e-04	4.359	2.64e-05	4.957
6.86e-03	2.81e-03	1.924	3.22e-04	2.735	5.22e-05	3.786	6.20e-06	4.237	7.37e-07	5.173
3.43e-03	7.23e-04	1.959	4.07e-05	2.985	3.59e-06	3.864	2.22e-07	4.805	1.24e-08	5.892

Table 4.9: Histories of convergence of the L^2-projection of $\xi - \xi_h$ in $||\cdot||_{\Gamma_{1,h}}$ and $||\cdot||_{0,\Gamma_1}$ norms, for $k \in \{0,1,2,3,4\}$ (Example 3, conforming meshes)

$\|\widehat{\xi}_h - \xi_h\|_{\Gamma_{1,h}}$										
	$k=0$		$k=1$		$k=2$		$k=3$		$k=4$	
h	error	rate	error	rate	error	rate	error	rate	error	rate
2.16e-01	3.11e+00		8.67e+00		9.49e+00		6.14e+00		2.87e+00	
1.10e-01	4.23e+00	-0.457	5.52e+00	0.668	2.74e+00	1.842	1.27e+00	2.330	2.11e+00	0.457
5.49e-02	2.68e+00	0.658	1.66e+00	1.732	8.86e-01	1.623	1.36e+00	-0.097	8.49e-01	1.309
2.75e-02	1.09e+00	1.299	4.01e-01	2.052	6.98e-01	0.346	2.90e-01	2.239	9.73e-02	3.134
1.37e-02	3.91e-01	1.476	2.85e-01	0.489	1.32e-01	2.391	2.46e-02	3.539	6.48e-03	3.888
6.86e-03	1.20e-01	1.708	7.96e-02	1.845	1.38e-02	3.258	2.01e-03	3.622	2.18e-04	4.906
3.43e-03	2.89e-02	2.054	1.70e-02	2.225	1.45e-03	3.253	1.14e-04	4.135	6.66e-06	5.030
$\|\widehat{\xi}_h - \xi_h\|_{0,\Gamma_1}$										
	$k=0$		$k=1$		$k=2$		$k=3$		$k=4$	
h	error	rate	error	rate	error	rate	error	rate	error	rate
2.16e-01	4.40e+00		1.23e+01		1.34e+01		8.68e+00		4.06e+00	
1.10e-01	8.47e+00	-0.970	1.10e+01	0.154	5.47e+00	1.328	2.55e+00	1.817	4.22e+00	-0.056
5.49e-02	7.58e+00	0.159	4.69e+00	1.234	2.51e+00	1.124	3.85e+00	-0.595	2.40e+00	0.810
2.75e-02	4.37e+00	0.797	1.60e+00	1.551	2.79e+00	-0.156	1.16e+00	1.738	3.89e-01	2.633
1.37e-02	2.21e+00	0.979	1.61e+00	-0.008	7.46e-01	1.894	1.39e-01	3.042	3.67e-02	3.391
6.86e-03	9.59e-01	1.207	6.37e-01	1.344	1.11e-01	2.757	1.61e-02	3.121	1.74e-03	4.405
3.43e-03	3.27e-01	1.554	1.93e-01	1.725	1.64e-02	2.753	1.29e-03	3.635	7.54e-05	4.530

4.7.3.2 Results when solving with meshes having hanging nodes only on Γ_1

The purpose here is to exhibit the robustness of the method when a family of meshes with hanging nodes only on Γ_1 is considered. We emphasize that this case is not covered by the current analysis. From Tables 4.10, 4.12 and 4.11, we observe that the different errors we have considered, go to zero at the optimal rates of convergence as indicated in Theorems 4.5.1, 4.5.2 and 4.5.3, as well as in Remark 4.5.1. Figure 4.7 shows the first two initial meshes (with hanging nodes on Γ_1) of the domain, to

perform this numerical simulation., In addition, Figures 4.17, 4.16 and 4.18, resume the information given in Tables 4.10, 4.12 and 4.11, respectively. This gives us numerical evidence that the approach can be extended to deal, at least, with hanging nodes on Γ_1. This could be the subject of future work.

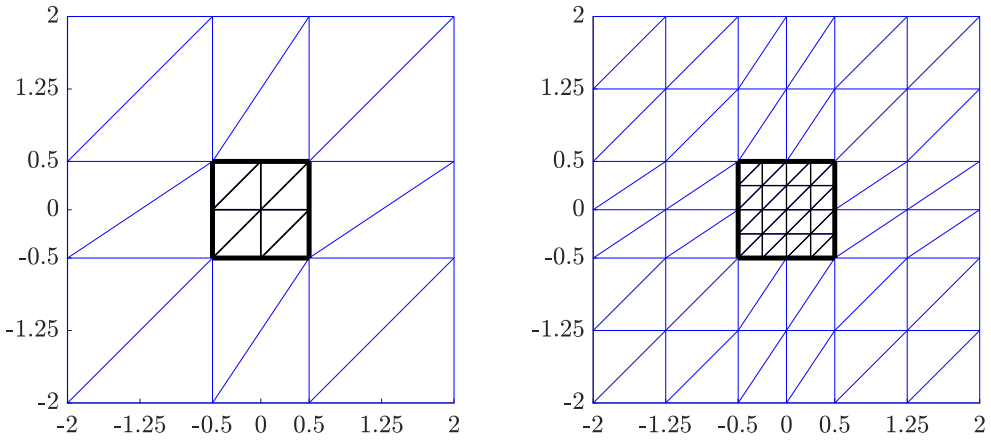

Figure 4.15: First two meshes with hanging nodes on Γ_1

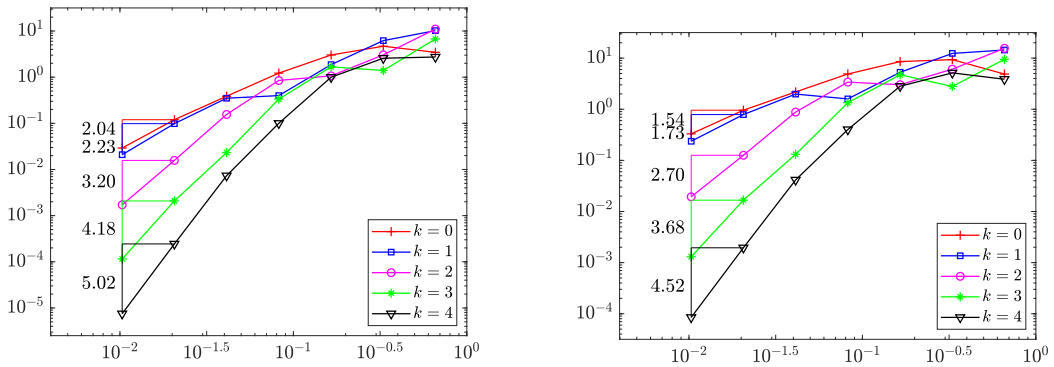

(a) $||\widehat{\xi}_h - \xi_h||_{\Gamma_{1,h}}$ vs. h (b) $||\widehat{\xi}_h - \xi_h||_{0,\Gamma_1}$ vs. h

Figure 4.16: Rates of convergence of the Lagrange multiplier considering the (a) Discrete trace norm $||\cdot||_{\Gamma_{1,h}}$, and (b) Standard L^2-norm (Example 3, nonconforming meshes)

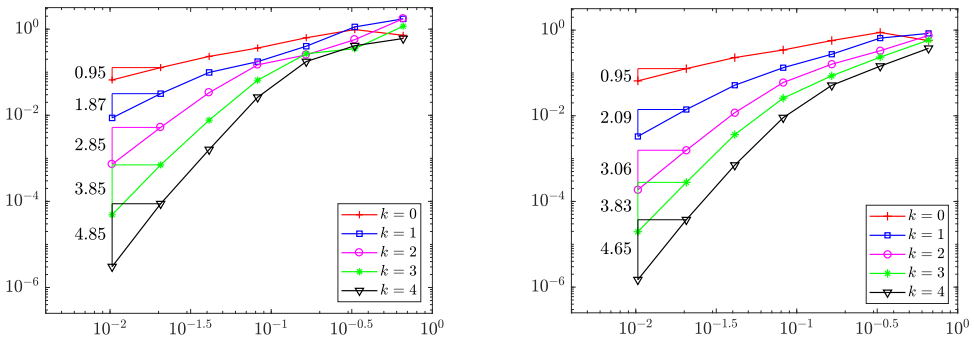

Figure 4.17: Rates of convergence of the (Left) energy norm of the potential error, and (Right) flux error (Example 3, nonconforming meshes)

Table 4.10: Histories of convergence of the energy norm of the potential error and L^2-norm of the flux error, using meshes with hanging nodes on Γ_1 (Example 3)

Energy norm of the potential error										
	$k=0$		$k=1$		$k=2$		$k=3$		$k=4$	
h	error	rate	error	rate	error	rate	error	rate	error	rate
2.16e-01	7.19e-01		1.73e+00		1.75e+00		1.17e+00		6.06e-01	
1.10e-01	9.78e-01	-0.456	1.13e+00	0.639	5.70e-01	1.661	3.52e-01	1.779	4.12e-01	0.574
5.49e-02	6.31e-01	0.630	4.01e-01	1.486	2.53e-01	1.172	2.69e-01	0.390	1.77e-01	1.217
2.75e-02	3.64e-01	0.795	1.76e-01	1.193	1.48e-01	0.771	6.52e-02	2.048	2.62e-02	2.762
1.37e-02	2.32e-01	0.646	9.87e-02	0.829	3.35e-02	2.133	7.70e-03	3.066	1.60e-03	4.013
6.86e-03	1.28e-01	0.862	3.17e-02	1.642	5.23e-03	2.687	7.04e-04	3.458	8.81e-05	4.189
3.43e-03	6.61e-02	0.952	8.69e-03	1.868	7.25e-04	2.849	4.89e-05	3.850	3.05e-06	4.853
L^2-norm of the flux error										
	$k=0$		$k=1$		$k=2$		$k=3$		$k=4$	
h	error	rate	error	rate	error	rate	error	rate	error	rate
6.59e-01	5.68e-01		8.38e-01		7.48e-01		5.84e-01		3.76e-01	
3.30e-01	8.82e-01	-0.637	6.51e-01	0.365	3.30e-01	1.183	2.34e-01	1.322	1.44e-01	1.386
1.65e-01	5.70e-01	0.630	2.73e-01	1.252	1.60e-01	1.044	8.57e-02	1.449	5.14e-02	1.487
8.24e-02	3.44e-01	0.728	1.33e-01	1.042	5.97e-02	1.420	2.58e-02	1.728	9.04e-03	2.502
4.12e-02	2.28e-01	0.591	5.16e-02	1.360	1.18e-02	2.340	3.63e-03	2.830	7.03e-04	3.684
2.06e-02	1.26e-01	0.857	1.40e-02	1.882	1.57e-03	2.912	2.79e-04	3.702	3.74e-05	4.233
1.03e-02	6.52e-02	0.951	3.29e-03	2.090	1.87e-04	3.064	1.96e-05	3.827	1.49e-06	4.652

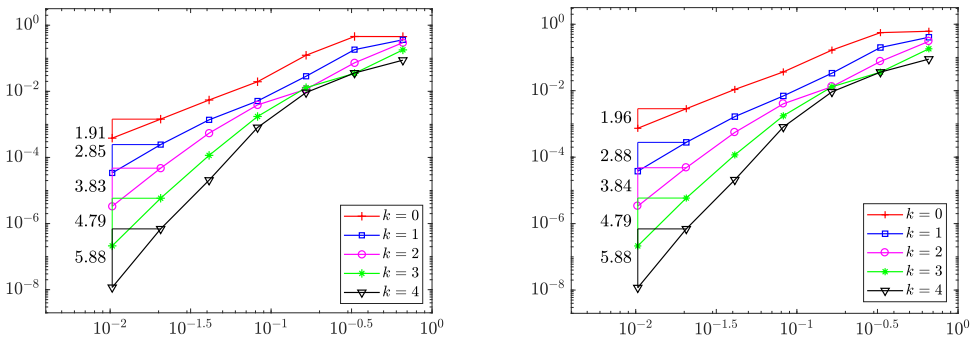

Figure 4.18: Rates of convergence of the L^2-norm of the (Left) potential error, and (Right) reconstructive potential error (Example 3, nonconforming meshes)

Table 4.11: Histories of convergence of L^2-norm of the potential and reconstructive potential errors, using meshes with hanging nodes (Example 3)

L^2-norm of the potential error										
	$k=0$		$k=1$		$k=2$		$k=3$		$k=4$	
h	error	rate	error	rate	error	rate	error	rate	error	rate
6.59e-01	4.53e-01		3.62e-01		2.97e-01		1.79e-01		8.76e-02	
3.30e-01	4.56e-01	-0.009	1.83e-01	0.990	7.28e-02	2.030	3.50e-02	2.362	3.59e-02	1.291
1.65e-01	1.23e-01	1.886	2.86e-02	2.676	1.16e-02	2.656	1.29e-02	1.439	9.20e-03	1.964
8.24e-02	1.95e-02	2.654	5.10e-03	2.483	3.88e-03	1.572	1.73e-03	2.891	8.05e-04	3.508
4.12e-02	5.46e-03	1.837	1.37e-03	1.890	5.43e-04	2.837	1.16e-04	3.907	2.06e-05	5.288
2.06e-02	1.44e-03	1.923	2.45e-04	2.490	4.74e-05	3.519	5.84e-06	4.308	6.90e-07	4.900
1.03e-02	3.83e-04	1.910	3.40e-05	2.848	3.32e-06	3.834	2.12e-07	4.785	1.17e-08	5.881
L^2-norm of the reconstructive potential error										
	$k=0$		$k=1$		$k=2$		$k=3$		$k=4$	
h	error	rate	error	rate	error	rate	error	rate	error	rate
2.16e-01	6.14e-01		4.05e-01		3.06e-01		1.82e-01		8.93e-02	
1.10e-01	5.59e-01	0.139	1.99e-01	1.051	7.58e-02	2.068	3.61e-02	2.397	3.62e-02	1.338
5.49e-02	1.66e-01	1.745	3.36e-02	2.561	1.32e-02	2.512	1.31e-02	1.461	9.23e-03	1.965
2.75e-02	3.67e-02	2.186	6.95e-03	2.282	4.03e-03	1.720	1.76e-03	2.907	8.07e-04	3.525
1.37e-02	1.09e-02	1.741	1.66e-03	2.056	5.54e-04	2.847	1.17e-04	3.888	2.08e-05	5.253
6.86e-03	2.87e-03	1.930	2.79e-04	2.579	4.81e-05	3.535	5.87e-06	4.323	6.93e-07	4.916
3.43e-03	7.38e-04	1.958	3.78e-05	2.882	3.36e-06	3.838	2.13e-07	4.787	1.18e-08	5.879

Table 4.12: Histories of convergence of the L^2-projection of $\xi - \xi_h$ in $||\cdot||_{\Gamma_{1,h}}$ and $||\cdot||_{0,\Gamma_1}$ norms, for $k \in \{0,1,2,3,4\}$ using meshes with hanging nodes (Example 3)

$\|\widehat{\xi}_h - \xi_h\|_{\Gamma_{1,h}}$										
	$k=0$		$k=1$		$k=2$		$k=3$		$k=4$	
h	error	rate	error	rate	error	rate	error	rate	error	rate
6.59e-01	3.45e+00		1.02e+01		1.10e+01		6.71e+00		2.73e+00	
3.30e-01	4.68e+00	-0.439	6.19e+00	0.722	3.04e+00	1.860	1.40e+00	2.271	2.57e+00	0.088
1.65e-01	3.03e+00	0.629	1.87e+00	1.728	1.07e+00	1.509	1.67e+00	-0.262	9.98e-01	1.366
8.24e-02	1.22e+00	1.304	3.99e-01	2.224	8.49e-01	0.331	3.36e-01	2.315	1.00e-01	3.310
4.12e-02	3.86e-01	1.664	3.50e-01	0.188	1.56e-01	2.448	2.32e-02	3.851	7.33e-03	3.774
2.06e-02	1.20e-01	1.688	9.84e-02	1.831	1.57e-02	3.306	2.08e-03	3.481	2.44e-04	4.909
1.03e-02	2.92e-02	2.037	2.09e-02	2.234	1.71e-03	3.199	1.15e-04	4.178	7.50e-06	5.023
$\|\widehat{\xi}_h - \xi_h\|_{0,\Gamma_1}$										
	$k=0$		$k=1$		$k=2$		$k=3$		$k=4$	
h	error	rate	error	rate	error	rate	error	rate	error	rate
6.59e-01	4.88e+00		1.44e+01		1.56e+01		9.49e+00		3.87e+00	
3.30e-01	9.36e+00	-0.940	1.24e+01	0.221	6.08e+00	1.359	2.79e+00	1.770	5.15e+00	-0.413
1.65e-01	8.56e+00	0.129	5.28e+00	1.228	3.02e+00	1.009	4.74e+00	-0.762	2.82e+00	0.866
8.24e-02	4.89e+00	0.805	1.59e+00	1.725	3.40e+00	-0.168	1.34e+00	1.816	4.01e-01	2.811
4.12e-02	2.18e+00	1.164	1.98e+00	-0.312	8.80e-01	1.948	1.31e-01	3.351	4.15e-02	3.274
2.06e-02	9.58e-01	1.188	7.87e-01	1.331	1.26e-01	2.806	1.67e-02	2.981	1.95e-03	4.409
1.03e-02	3.30e-01	1.537	2.37e-01	1.734	1.94e-02	2.699	1.30e-03	3.678	8.48e-05	4.523

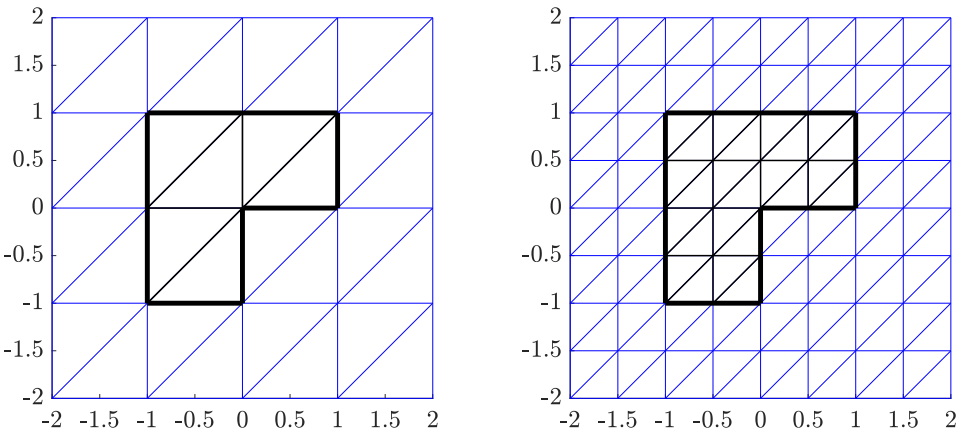

Figure 4.19: First two simplicial meshes for Example 4

4.7.4 Example 4: A nonregular exact solution

We solve transmission problem (4.1)*, considering* $\Omega_1 = (-1,1)^2 \setminus [0,1] \times [-1,0]$ *and* $\Omega_2 := (-2,2)^2 \setminus \overline{\Omega}_1$ *(see Figure 4.19), while the data are such that the exact solution is* (u_1, u_2)*, where*

$$u_1(r,\theta) = r^{2/3}\sin(2\theta/3) \; - \; c_1 \quad (\textit{in polar coordinates})\,,$$

$$u_2(x,y) = \sin(\pi x)\sin(\pi y) \; - \; c_2\,,$$

and c_1 *and* c_2 *are real constants such that* $u_j \in L^2_0(\Omega_j)$*,* $j \in \{1,2\}$*. We point out that* $u_1 \in H^{1+\frac{2}{3}-s}(\Omega_1)$*, for an arbitrary small number* $s > 0$*, and* u_2 *is a smooth function. Figure 4.19 shows the first two conforming meshes that we consider for our simulations, while Figure 4.21 exhibits the behavior of the energy norm of the potential error (left) and the flux error (right), with respect to the meshsize* h*. Their corresponding histories of convergence are given in Table 4.13, and do not contradict Theorem 4.5.1, since in this case the function* u_1 *is nonregular. Similar behavior is noticed in Table 4.15 for the error of* $\widehat{\xi}_h - \xi_h$ *in the weighted and usual* L^2-*norms, with rates of convergence* $2/3$ *and* $1/6$*, respectively. These are also displayed in Figure 4.20. In addition, Table 4.14 (see also Figure 4.15) reports the histories of convergence of the* L^2-*norm of the potential and the reconstructive potential errors, which are not the optimal ones, as prescribed by Theorems 4.5.2 and* (4.5.3)*, and by Remark 4.5.1, due to the lack of smoothness of function* u_1*.*

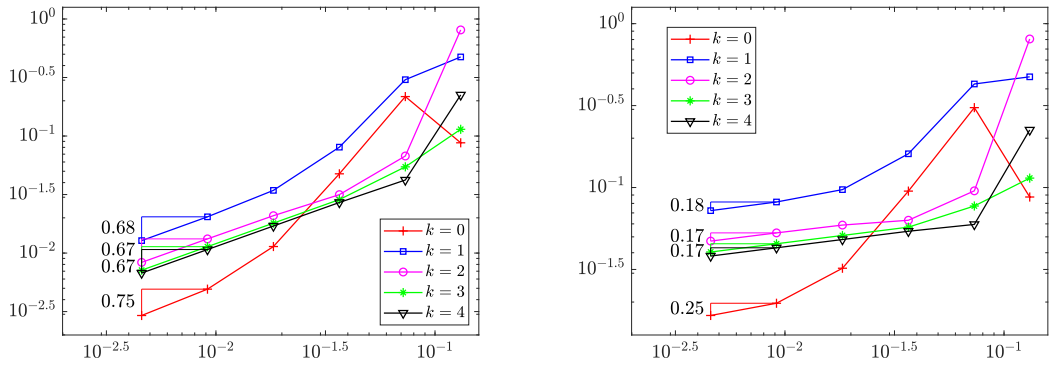

(a) $||\widehat{\xi}_h - \xi_h||_{\Gamma_{1,h}}$ vs. h (b) $||\widehat{\xi}_h - \xi_h||_{0,\Gamma_1}$ vs. h

Figure 4.20: Rates of convergence of the Lagrange multiplier considering the (a) Discrete trace norm $||\cdot||_{\Gamma_{1,h}}$, and (b) Standard L^2-norm (Example 4)

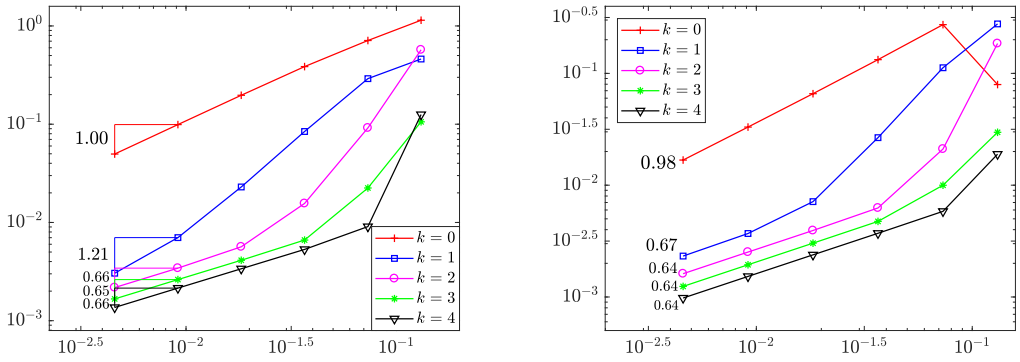

Figure 4.21: Rates of convergence of the (Left) energy norm of the potential error, and (Right) flux error (Example 4)

Table 4.13: Histories of convergence of the energy norm of the potential error and L^2-norm of the flux error, considering $k \in \{0, 1, 2, 3, 4\}$ (Example 4)

Energy norm of the potential error										
	$k=0$		$k=1$		$k=2$		$k=3$		$k=4$	
h	error	rate	error	rate	error	rate	error	rate	error	rate
1.31e-01	1.14e+00		4.61e-01		5.72e-01		1.06e-01		1.25e-01	
7.32e-02	7.11e-01	0.817	2.91e-01	0.790	9.17e-02	3.145	2.24e-02	2.664	9.08e-03	4.511
3.66e-02	3.86e-01	0.882	8.43e-02	1.787	1.56e-02	2.554	6.62e-03	1.760	5.31e-03	0.772
1.83e-02	1.97e-01	0.969	2.30e-02	1.875	5.65e-03	1.465	4.12e-03	0.683	3.38e-03	0.654
9.15e-03	9.91e-02	0.991	7.01e-03	1.712	3.43e-03	0.722	2.62e-03	0.654	2.15e-03	0.654
4.58e-03	4.97e-02	0.997	3.04e-03	1.206	2.17e-03	0.658	1.67e-03	0.655	1.36e-03	0.655
L^2-norm of the flux error										
	$k=0$		$k=1$		$k=2$		$k=3$		$k=4$	
h	error	rate	error	rate	error	rate	error	rate	error	rate
1.31e-01	7.94e-02		2.77e-01		1.85e-01		2.97e-02		1.89e-02	
7.32e-02	2.73e-01	–	1.12e-01	1.551	2.11e-02	3.734	9.99e-03	1.873	5.84e-03	2.023
3.66e-02	1.33e-01	1.040	2.66e-02	2.077	6.26e-03	1.751	4.74e-03	1.075	3.71e-03	0.652
1.83e-02	6.58e-02	1.012	7.13e-03	1.901	3.93e-03	0.670	3.03e-03	0.647	2.38e-03	0.640
9.15e-03	3.31e-02	0.992	3.70e-03	0.947	2.52e-03	0.641	1.94e-03	0.642	1.53e-03	0.641
4.58e-03	1.68e-02	0.981	2.32e-03	0.671	1.62e-03	0.643	1.24e-03	0.644	9.79e-04	0.643

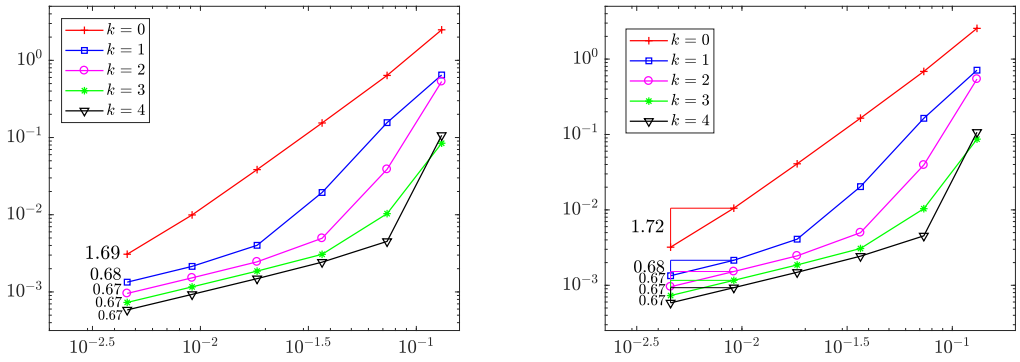

Figure 4.22: Rates of convergence of the L^2-norm of the (a) potential error, and (b) reconstructive potential error (Example 4)

Table 4.14: Histories of convergence of L^2-norm of the potential and reconstructive potential errors, considering $k \in \{0, 1, 2, 3, 4\}$ (Example 4)

L^2-norm of the potential error										
	$k = 0$		$k = 1$		$k = 2$		$k = 3$		$k = 4$	
h	error	rate	error	rate	error	rate	error	rate	error	rate
1.31e-01	2.48e+00		6.46e-01		5.31e-01		8.44e-02		1.07e-01	
7.32e-02	6.37e-01	2.338	1.56e-01	2.443	3.88e-02	4.498	1.03e-02	3.609	4.51e-03	5.435
3.66e-02	1.54e-01	2.046	1.94e-02	3.006	4.96e-03	2.967	3.07e-03	1.750	2.43e-03	0.893
1.83e-02	3.84e-02	2.007	4.02e-03	2.273	2.45e-03	1.014	1.86e-03	0.722	1.49e-03	0.709
9.15e-03	9.94e-03	1.950	2.14e-03	0.907	1.52e-03	0.689	1.16e-03	0.679	9.30e-04	0.678
4.58e-03	3.08e-03	1.693	1.34e-03	0.679	9.56e-04	0.672	7.31e-04	0.671	5.84e-04	0.670
L^2-norm of the reconstructive potential error										
	$k = 0$		$k = 1$		$k = 2$		$k = 3$		$k = 4$	
h	error	rate	error	rate	error	rate	error	rate	error	rate
1.31e-01	2.55e+00		7.12e-01		5.43e-01		8.67e-02		1.07e-01	
7.32e-02	6.86e-01	2.259	1.64e-01	2.525	3.94e-02	4.508	1.04e-02	3.649	4.52e-03	5.436
3.66e-02	1.65e-01	2.059	2.03e-02	3.010	4.99e-03	2.981	3.07e-03	1.754	2.43e-03	0.896
1.83e-02	4.09e-02	2.011	4.09e-03	2.315	2.46e-03	1.021	1.86e-03	0.723	1.49e-03	0.710
9.15e-03	1.05e-02	1.956	2.15e-03	0.929	1.52e-03	0.690	1.16e-03	0.680	9.30e-04	0.678
4.58e-03	3.20e-03	1.720	1.34e-03	0.682	9.56e-04	0.673	7.31e-04	0.671	5.84e-04	0.671

Table 4.15: Histories of convergence of the L^2- projection of $\xi - \xi_h$ in $||\cdot||_{\Gamma_{1,h}}$ and $||\cdot||_{0,\Gamma_1}$ norms, for $k \in \{0,1,2,3,4\}$ (Example 4)

$\|\widehat{\xi}_h - \xi_h\|_{\Gamma_{1,h}}$										
	$k=0$		$k=1$		$k=2$		$k=3$		$k=4$	
h	error	rate	error	rate	error	rate	error	rate	error	rate
1.31e-01	8.75e-02		4.74e-01		8.06e-01		1.14e-01		2.25e-01	
7.32e-02	2.17e-01	-1.562	3.03e-01	0.769	6.75e-02	4.262	5.45e-02	1.269	4.21e-02	2.877
3.66e-02	4.75e-02	2.192	8.03e-02	1.915	3.16e-02	1.096	2.86e-02	0.929	2.70e-02	0.638
1.83e-02	1.14e-02	2.064	3.43e-02	1.227	2.09e-02	0.597	1.80e-02	0.669	1.70e-02	0.668
9.15e-03	4.92e-03	1.210	2.04e-02	0.751	1.32e-02	0.659	1.13e-02	0.668	1.07e-02	0.668
4.58e-03	2.93e-03	0.749	1.28e-02	0.676	8.33e-03	0.668	7.14e-03	0.668	6.75e-03	0.668
$\|\widehat{\xi}_h - \xi_h\|_{0,\Gamma_1}$										
	$k=0$		$k=1$		$k=2$		$k=3$		$k=4$	
h	error	rate	error	rate	error	rate	error	rate	error	rate
1.31e-01	8.75e-02		4.74e-01		8.06e-01		1.14e-01		2.25e-01	
7.32e-02	3.07e-01	-2.158	4.28e-01	0.173	9.54e-02	3.667	7.71e-02	0.674	5.95e-02	2.281
3.66e-02	9.51e-02	1.692	1.61e-01	1.415	6.31e-02	0.596	5.73e-02	0.429	5.41e-02	0.138
1.83e-02	3.22e-02	1.564	9.71e-02	0.727	5.90e-02	0.097	5.10e-02	0.169	4.82e-02	0.168
9.15e-03	1.97e-02	0.710	8.16e-02	0.251	5.29e-02	0.158	4.54e-02	0.168	4.29e-02	0.168
4.58e-03	1.66e-02	0.248	7.23e-02	0.175	4.71e-02	0.167	4.04e-02	0.168	3.82e-02	0.167

4.7.5 Example 5: A nonsmooth enough exact solution

Here, we solve the linear transmission problem (4.1), considering the same domain as in Example 4, whose data are such that its exact solution is given by

$$u_1(x,y) = \cos\left(\frac{\pi}{2}y\right) + \chi(x)x^{3.5} \; - \; c_1\,,$$

where $\chi(x)$ is the characteristic function on $[0,1]$ with respect to x, and

$$u_2(x,y) = \sin(\pi x)\sin(\pi y) \; - \; c_2\,,$$

with c_1 and c_2 being real constants, such that u_1 and u_2 have zero mean value in Ω_1 and Ω_2, respectively. It is known that $u_1 \in H^4(\Omega_1)$, but does not belong to

$H^{4+\epsilon}(\Omega_1)$, *for an arbitrary small number* $\epsilon > 0$. *Table 4.16 reports the histories of convergence of the energy norm of the potential error and the flux error, considering* $k \in \{0, 1, 2, 3, 4\}$. *We observe that the rates of convergence are the expected optimal ones:* $k+1$, *when the solution is approximated by piecewise polynomials of degree at most* $k \in \{0, 1, 2, 3\}$. *These are in agreement with Theorems 4.5.1. For* $k = 4$, *we still notice convergence, but not at the optimal rate of convergence, since the exact solution is not smooth enough. We display these results also in Figure 4.24. On the other hand, in Figure 4.23, we show the behavior of the weighted and usual* L^2-*norms of* $\widehat{\xi}_h - \xi_h$, *with respect to the meshsize* h. *Their corresponding histories of convergence are displayed in Table 4.18, and they are the optimal ones, as predicted by Theorem 4.5.1 and Remark 4.5.1. In Table 4.17 we provide the histories of convergence in the* L^2-*norm of the potential and the reconstructive potential errors. The behavior of the rates of convergence, for* $k \in \{0, 1, 2, 3\}$ *are in agreement with the ones predicted by Theorems 4.5.2 and 4.5.3 for smooth functions, and are resumed in Figure 4.25. We notice again a lost in the order of convergence for* $k = 4$, *due to the small smoothness of* u_1.

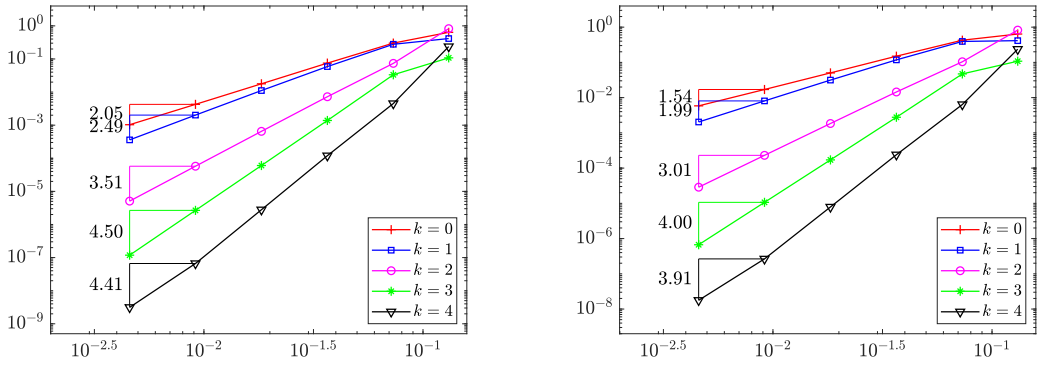

(a) $||\widehat{\xi}_h - \xi_h||_{\Gamma_{1,h}}$ vs. h (b) $||\widehat{\xi}_h - \xi_h||_{0,\Gamma_1}$ vs. h

Figure 4.23: Rates of convergence of the Lagrange multiplier considering the (a) Discrete trace norm $||\cdot||_{\Gamma_{1,h}}$, and (b) Standard L^2-norm (Example 5)

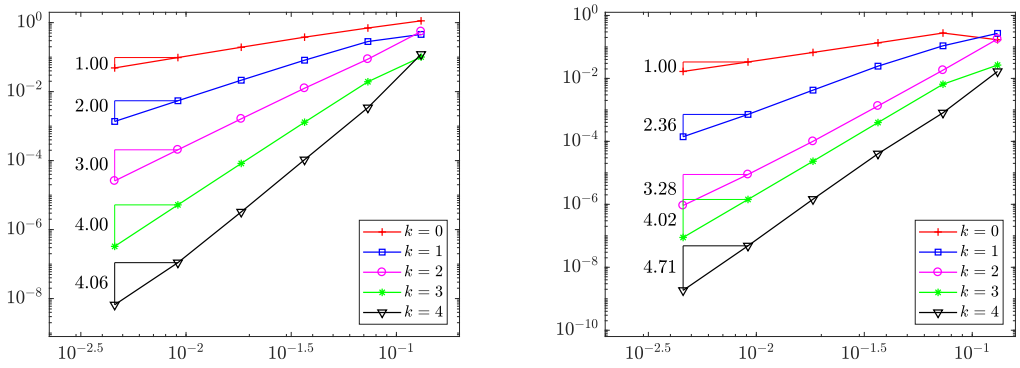

Figure 4.24: Rates of convergence of the (Left) energy norm of the potential error, and (Right) flux error (Example 5)

Table 4.16: Histories of convergence of the energy norm of the potential error and L^2-norm of the flux error, considering $k \in \{0, 1, 2, 3, 4\}$ (Example 5)

Energy norm of the potential error										
	$k = 0$		$k = 1$		$k = 2$		$k = 3$		$k = 4$	
h	error	rate	error	rate	error	rate	error	rate	error	rate
1.31e-01	1.13e+00		4.56e-01		5.54e-01		1.01e-01		1.21e-01	
7.32e-02	7.00e-01	0.820	2.83e-01	0.817	8.75e-02	3.171	1.93e-02	2.834	3.43e-03	6.124
3.66e-02	3.79e-01	0.884	8.15e-02	1.798	1.25e-02	2.802	1.30e-03	3.899	1.06e-04	5.010
1.83e-02	1.93e-01	0.970	2.14e-02	1.928	1.63e-03	2.946	8.28e-05	3.969	3.26e-06	5.030
9.15e-03	9.72e-02	0.993	5.44e-03	1.978	2.06e-04	2.985	5.21e-06	3.991	1.10e-07	4.887
4.58e-03	4.87e-02	1.000	1.37e-03	1.997	2.58e-05	3.001	3.27e-07	4.001	6.60e-09	4.065
L^2-norm of the flux error										
	$k = 0$		$k = 1$		$k = 2$		$k = 3$		$k = 4$	
h	error	rate	error	rate	error	rate	error	rate	error	rate
1.31e-01	1.69e-01		2.70e-01		1.79e-01		2.65e-02		1.66e-02	
7.32e-02	2.76e-01	–	1.09e-01	1.564	1.83e-02	3.921	6.53e-03	2.408	8.07e-04	5.198
3.66e-02	1.35e-01	1.035	2.45e-02	2.149	1.33e-03	3.775	3.96e-04	4.044	4.04e-05	4.320
1.83e-02	6.67e-02	1.016	4.24e-03	2.530	1.00e-04	3.733	2.34e-05	4.082	1.45e-06	4.799
9.15e-03	3.33e-02	1.004	7.18e-04	2.562	8.88e-06	3.498	1.43e-06	4.033	4.80e-08	4.918
4.58e-03	1.66e-02	1.003	1.40e-04	2.359	9.17e-07	3.281	8.85e-08	4.017	1.85e-09	4.706

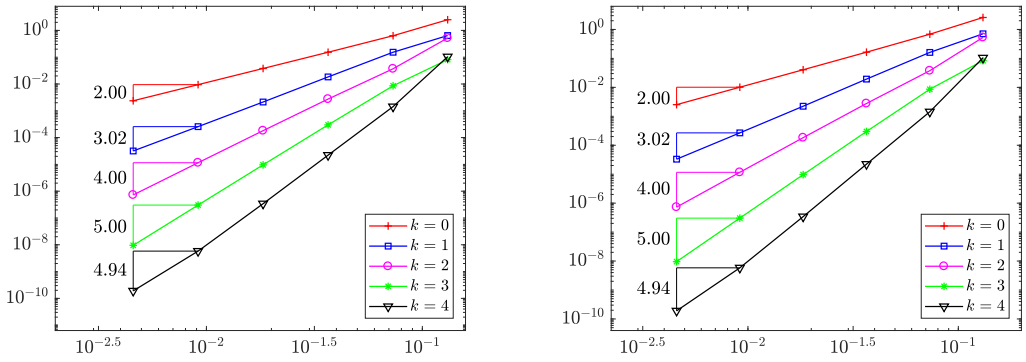

Figure 4.25: Rates of convergence of the L^2-norm of the (a) potential error, and (b) reconstructive potential error (Example 5)

Table 4.17: Histories of convergence of L^2-norm of the potential and reconstructive potential errors, considering $k \in \{0, 1, 2, 3, 4\}$ (Example 5)

L^2-norm of the potential error										
	$k = 0$		$k = 1$		$k = 2$		$k = 3$		$k = 4$	
h	error	rate	error	rate	error	rate	error	rate	error	rate
1.31e-01	2.50e+00		6.43e-01		5.20e-01		8.12e-02		1.04e-01	
7.32e-02	6.33e-01	2.362	1.53e-01	2.463	3.70e-02	4.538	8.57e-03	3.863	1.43e-03	7.367
3.66e-02	1.53e-01	2.049	1.84e-02	3.062	2.74e-03	3.756	2.98e-04	4.845	2.21e-05	6.015
1.83e-02	3.80e-02	2.012	2.13e-03	3.110	1.81e-04	3.917	9.61e-06	4.955	3.41e-07	6.021
9.15e-03	9.47e-03	2.003	2.56e-04	3.053	1.15e-05	3.976	3.03e-07	4.987	5.81e-09	5.876
4.58e-03	2.37e-03	2.004	3.17e-05	3.022	7.24e-07	3.999	9.52e-09	5.000	1.90e-10	4.940
L^2-norm of the reconstructive potential error										
	$k = 0$		$k = 1$		$k = 2$		$k = 3$		$k = 4$	
h	error	rate	error	rate	error	rate	error	rate	error	rate
1.31e-01	2.59e+00		7.07e-01		5.31e-01		8.35e-02		1.04e-01	
7.32e-02	6.84e-01	2.287	1.61e-01	2.542	3.76e-02	4.548	8.60e-03	3.905	1.44e-03	7.366
3.66e-02	1.64e-01	2.062	1.93e-02	3.063	2.77e-03	3.765	2.99e-04	4.846	2.22e-05	6.014
1.83e-02	4.05e-02	2.016	2.23e-03	3.114	1.83e-04	3.919	9.64e-06	4.956	3.42e-07	6.020
9.15e-03	1.01e-02	2.004	2.68e-04	3.056	1.16e-05	3.977	3.04e-07	4.987	5.83e-09	5.876
4.58e-03	2.52e-03	2.004	3.30e-05	3.023	7.29e-07	4.000	9.55e-09	5.000	1.90e-10	4.944

Table 4.18: Histories of convergence of the L^2-projection of $\xi - \xi_h$ in $||\cdot||_{\Gamma_{1,h}}$ and $||\cdot||_{0,\Gamma_1}$ norms, for $k \in \{0,1,2,3,4\}$ (Example 5)

$\|\widehat{\xi}_h - \xi_h\|_{\Gamma_{1,h}}$										
	$k=0$		$k=1$		$k=2$		$k=3$		$k=4$	
h	error	rate	error	rate	error	rate	error	rate	error	rate
1.31e-01	6.37e-01		4.14e-01		8.23e-01		1.08e-01		2.37e-01	
7.32e-02	3.01e-01	1.287	2.78e-01	0.685	7.36e-02	4.148	3.33e-02	2.023	4.50e-03	6.808
3.66e-02	7.49e-02	2.009	5.89e-02	2.237	7.23e-03	3.348	1.39e-03	4.586	1.20e-04	5.234
1.83e-02	1.78e-02	2.075	1.11e-02	2.406	6.51e-04	3.473	6.04e-05	4.520	2.79e-06	5.424
9.15e-03	4.25e-03	2.064	2.02e-03	2.463	5.75e-05	3.500	2.67e-06	4.501	6.63e-08	5.394
4.58e-03	1.03e-03	2.045	3.59e-04	2.491	5.08e-06	3.508	1.18e-07	4.504	3.14e-09	4.408
$\|\widehat{\xi}_h - \xi_h\|_{0,\Gamma_1}$										
	$k=0$		$k=1$		$k=2$		$k=3$		$k=4$	
h	error	rate	error	rate	error	rate	error	rate	error	rate
1.31e-01	6.37e-01		4.14e-01		8.23e-01		1.08e-01		2.37e-01	
7.32e-02	4.26e-01	0.692	3.93e-01	0.089	1.04e-01	3.553	4.71e-02	1.428	6.37e-03	6.212
3.66e-02	1.50e-01	1.509	1.18e-01	1.737	1.45e-02	2.848	2.77e-03	4.086	2.39e-04	4.734
1.83e-02	5.03e-02	1.575	3.14e-02	1.906	1.84e-03	2.973	1.71e-04	4.020	7.88e-06	4.924
9.15e-03	1.70e-02	1.564	8.06e-03	1.963	2.30e-04	3.000	1.07e-05	4.001	2.65e-07	4.894
4.58e-03	5.84e-03	1.544	2.03e-03	1.990	2.87e-05	3.007	6.69e-07	4.003	1.77e-08	3.907

The purpose of the next two examples, is to study the robustness of our implementation when the domain $\Omega := \Omega_1 \cup \Gamma_1 \cup \Omega_2$ *is nonconvex. We remark that in this situation, we can not ensure the validity of* (4.90)*, and then Theorems 4.5.2 and 4.5.3 do not hold, necessarily.*

4.7.6 Example 6: A regular solution in a nonconvex Ω

In this example, we approximate the solution of (4.1)*, with subdomains* $\Omega_1 = (-2,2)^2 \setminus [-1,2] \times [-2,1]$ *and* $\Omega_2 := (-3,3)^2 \setminus (\overline{\Omega}_1 \cup [0,3] \times [-3,0])$*, and the data*

are such that the exact solution is given by the smoothness functions

$$u_1(x,y) = \frac{xy}{x^2+y^2} - \frac{13\ln(2) - 5\ln(5)}{14} \quad , \quad u_2(x,y) = \cos(\pi x)\cos(\pi y)\,. \tag{4.147}$$

We consider a family of simplicial meshes, whose coarse/first mesh is displayed in Figure 4.26. In Tables 4.19 and 4.21 we report the rates of convergence of the method, when the solution is approximated by piecewise polynomials of degree at most $k \in \{0,1,2,3,4\}$. *We notice that the results are in agreement with Theorem 4.5.1 and Remark 4.5.1. On the other hand, from Table 4.20, we notice that the convergence of the potential and the reconstructive potential errors behave as* $\mathcal{O}(h^{k+2})$, *the optimal rate predicted by Theorems 4.5.2 and 4.5.3, despite the fact that this situation is not covered by the current theory. We can also see these behaviors in Figures 4.27, 4.29 and 4.28.*

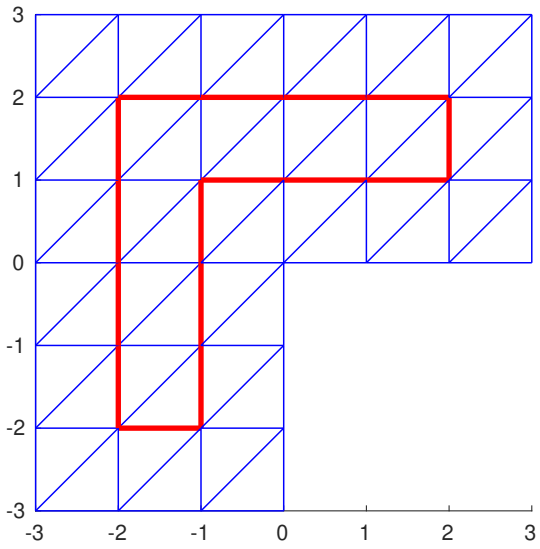

Figure 4.26: Initial mesh for Examples 6 and 7

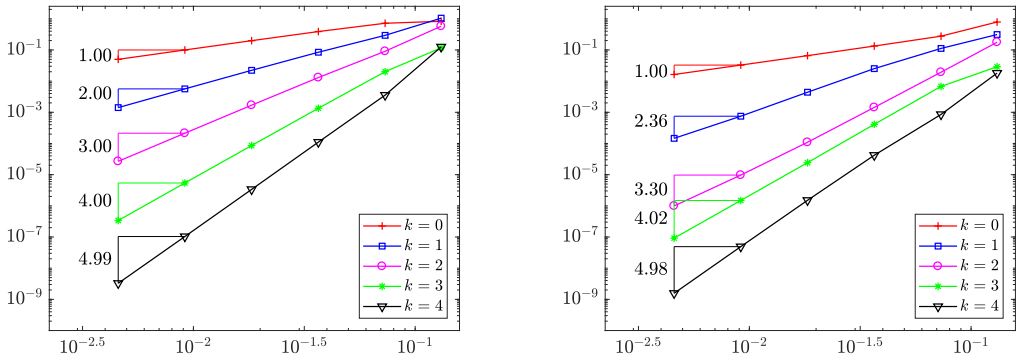

Figure 4.27: Rates of convergence of the (Left) energy norm of the potential error, and (Right) flux error (Example 6)

Table 4.19: Histories of convergence of energy norm of the potential error and L^2-norm of the flux error, considering $k \in \{0, 1, 2, 3, 4\}$ (Example 6)

Energy norm of the potential error										
	$k = 0$		$k = 1$		$k = 2$		$k = 3$		$k = 4$	
h	error	rate	error	rate	error	rate	error	rate	error	rate
1.31e-01	8.29e-01		1.05e+00		5.77e-01		1.17e-01		1.25e-01	
7.32e-02	7.18e-01	0.248	2.94e-01	2.182	9.07e-02	3.178	2.01e-02	3.032	3.55e-03	6.123
3.66e-02	3.89e-01	0.883	8.44e-02	1.800	1.30e-02	2.802	1.34e-03	3.899	1.10e-04	5.008
1.83e-02	1.99e-01	0.970	2.22e-02	1.928	1.69e-03	2.945	8.59e-05	3.968	3.36e-06	5.039
9.15e-03	9.98e-02	0.993	5.63e-03	1.977	2.13e-04	2.985	5.40e-06	3.992	1.04e-07	5.020
4.58e-03	4.99e-02	1.000	1.41e-03	1.996	2.68e-05	3.000	3.38e-07	4.004	3.27e-09	4.992
L^2-norm of the flux error										
	$k = 0$		$k = 1$		$k = 2$		$k = 3$		$k = 4$	
h	error	rate	error	rate	error	rate	error	rate	error	rate
1.31e-01	7.86e-01		3.12e-01		1.77e-01		2.90e-02		1.81e-02	
7.32e-02	2.76e-01	1.797	1.12e-01	1.763	1.93e-02	3.805	6.74e-03	2.505	8.53e-04	5.248
3.66e-02	1.33e-01	1.051	2.52e-02	2.150	1.43e-03	3.752	4.11e-04	4.036	4.19e-05	4.346
1.83e-02	6.56e-02	1.022	4.40e-03	2.517	1.09e-04	3.713	2.43e-05	4.081	1.50e-06	4.801
9.15e-03	3.27e-02	1.006	7.49e-04	2.555	9.68e-06	3.497	1.48e-06	4.034	4.90e-08	4.939
4.58e-03	1.63e-02	1.003	1.46e-04	2.362	9.89e-07	3.296	9.18e-08	4.019	1.57e-09	4.975

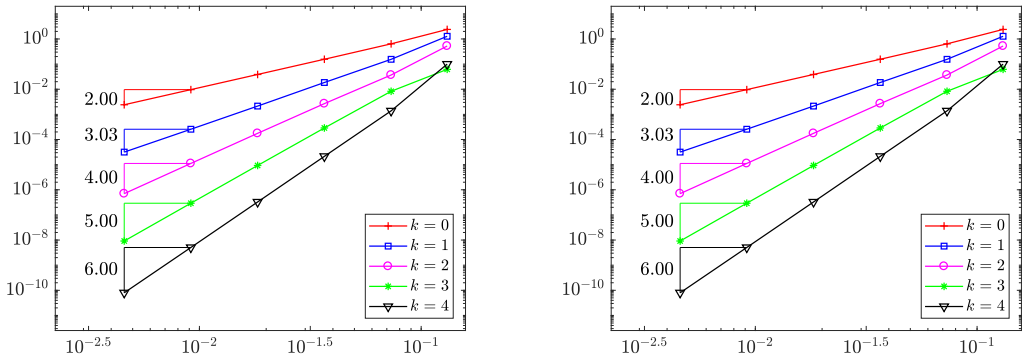

Figure 4.28: Rates of convergence of the L^2-norm of the (Left) potential error, and (Right) reconstructive potential error (Example 6)

Table 4.20: Histories of convergence of L^2-norm of the potential and reconstructive potential errors, considering $k \in \{0, 1, 2, 3, 4\}$ (Example 6)

L^2-norm of the potential error										
	$k = 0$		$k = 1$		$k = 2$		$k = 3$		$k = 4$	
h	error	rate	error	rate	error	rate	error	rate	error	rate
1.31e-01	3.25e-01		1.24e+00		5.13e-01		5.88e-02		9.96e-02	
7.32e-02	5.95e-01	-1.041	1.48e-01	3.650	3.63e-02	4.553	8.26e-03	3.374	1.38e-03	7.358
3.66e-02	1.46e-01	2.024	1.77e-02	3.064	2.65e-03	3.776	2.87e-04	4.848	2.13e-05	6.014
1.83e-02	3.64e-02	2.006	2.04e-03	3.113	1.75e-04	3.922	9.23e-06	4.957	3.26e-07	6.030
9.15e-03	9.10e-03	2.002	2.45e-04	3.057	1.11e-05	3.978	2.91e-07	4.988	5.03e-09	6.015
4.58e-03	2.27e-03	2.004	3.02e-05	3.025	6.96e-07	4.000	9.11e-09	5.005	7.94e-11	5.996
L^2-norm of the reconstructive potential error										
	$k = 0$		$k = 1$		$k = 2$		$k = 3$		$k = 4$	
h	error	rate	error	rate	error	rate	error	rate	error	rate
1.31e-01	2.40e+00		1.28e+00		5.24e-01		6.19e-02		9.99e-02	
7.32e-02	6.40e-01	2.269	1.55e-01	3.624	3.68e-02	4.563	8.29e-03	3.454	1.38e-03	7.358
3.66e-02	1.56e-01	2.038	1.85e-02	3.065	2.67e-03	3.784	2.88e-04	4.849	2.13e-05	6.013
1.83e-02	3.87e-02	2.010	2.14e-03	3.117	1.76e-04	3.924	9.26e-06	4.957	3.27e-07	6.029
9.15e-03	9.66e-03	2.003	2.56e-04	3.060	1.12e-05	3.978	2.92e-07	4.988	5.05e-09	6.015
4.58e-03	2.41e-03	2.004	3.16e-05	3.026	7.01e-07	4.000	9.14e-09	5.005	7.97e-11	5.996

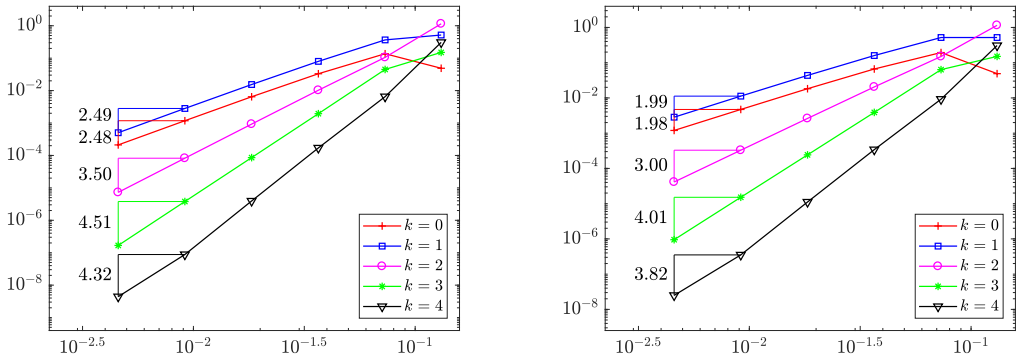

Figure 4.29: Rates of convergence of the Lagrange multiplier considering the (Left) Discrete trace norm $||\cdot||_{\Gamma_{1,h}}$, and (Right) Standard L^2-norm (Example 6)

Table 4.21: Histories of convergence of the L^2-projection of $\xi - \xi_h$ in $||\cdot||_{\Gamma_{1,h}}$ and $||\cdot||_{0,\Gamma_1}$ norms, for $k \in \{0,1,2,3,4\}$ (Example 6)

$\|\widehat{\xi}_h - \xi_h\|_{\Gamma_{1,h}}$										
	$k=0$		$k=1$		$k=2$		$k=3$		$k=4$	
h	error	rate	error	rate	error	rate	error	rate	error	rate
1.31e-01	4.88e-02		5.18e-01		1.15e+00		1.51e-01		3.07e-01	
7.32e-02	1.37e-01	-1.774	3.66e-01	0.595	1.06e-01	4.096	4.49e-02	2.080	6.51e-03	6.620
3.66e-02	3.31e-02	2.050	7.97e-02	2.199	1.03e-02	3.369	1.94e-03	4.531	1.70e-04	5.255
1.83e-02	6.45e-03	2.359	1.54e-02	2.372	9.26e-04	3.469	8.57e-05	4.503	3.94e-06	5.436
9.15e-03	1.18e-03	2.455	2.81e-03	2.453	8.22e-05	3.494	3.79e-06	4.498	8.79e-08	5.486
4.58e-03	2.11e-04	2.482	5.02e-04	2.488	7.27e-06	3.504	1.68e-07	4.506	4.41e-09	4.324
$\|\widehat{\xi}_h - \xi_h\|_{0,\Gamma_1}$										
	$k=0$		$k=1$		$k=2$		$k=3$		$k=4$	
h	error	rate	error	rate	error	rate	error	rate	error	rate
1.31e-01	4.88e-02		5.18e-01		1.15e+00		1.51e-01		3.07e-01	
7.32e-02	1.94e-01	-2.369	5.18e-01	-0.000	1.50e-01	3.501	6.35e-02	1.485	9.20e-03	6.025
3.66e-02	6.62e-02	1.550	1.59e-01	1.699	2.05e-02	2.869	3.88e-03	4.031	3.41e-04	4.755
1.83e-02	1.83e-02	1.859	4.35e-02	1.872	2.62e-03	2.969	2.42e-04	4.003	1.11e-05	4.936
9.15e-03	4.71e-03	1.955	1.12e-02	1.953	3.29e-04	2.994	1.52e-05	3.998	3.51e-07	4.986
4.58e-03	1.19e-03	1.981	2.84e-03	1.987	4.11e-05	3.004	9.48e-07	4.005	2.49e-08	3.823

4.7.7 Example 7: Nonsmooth solution in nonconvex Ω

Given $\Omega_1 = (-2,2)^2 \setminus [-1,2]\times[-2,1]$ *and* $\Omega_2 := (-3,3)^2 \setminus (\overline{\Omega}_1 \cup [0,3]\times[-3,0])$, *we solve* (4.38), *with* f_1, f_2, g_1, g_2 *and* g *given so that the exact solution is*

$$u_1(x,y) = \frac{xy}{x^2+y^2} - \frac{13\ln(2) - 5\ln(5)}{14} \quad , \quad u_2(r,\theta) = r^{2/3}\sin(2\theta/3) - c\,, \tag{4.148}$$

where u_2 *is given in polar coordinates, and* c *is a real constant such that* u_2 *has zero mean value in* Ω_2. *We pointwise that* $u_2 \in H^{1+2/3-\epsilon}(\Omega_2)$, *for an arbitrary small number* $\epsilon > 0$, *since its gradient has a singularity at origin. The family of simplicial meshes we consider here, is the same as in Example 4.7.6, and we approximate also the exact solution of* (4.1) *with polynomials of degree at most* $k \in \{0,1,2,3,4\}$. *The numerical results, obtained by the HHO method, can be seen in Tables 4.22, 4.24 and 4.23. They are also displayed in Figures 4.31, 4.30 and 4.32, respectively. We notice here that the nonsmoothness of* u_2 *affects the rates of convergence of the energy norm of the potential error, the flux error, the discrete norm of trace error, in the sense that they are not the optimal ones established in Theorem 4.5.1. On the other hand, we notice also that the potential and reconstructive potential errors decay to zero as* $\mathcal{O}(h^{2/3})$, *for any of the values of* k *we have considered in this simulation. This situation is not covered by our current analysis, and motivate us to obtain an a posteriori error estimator that could help us to improve the quality of the approximation. This could be the subject of future work.*

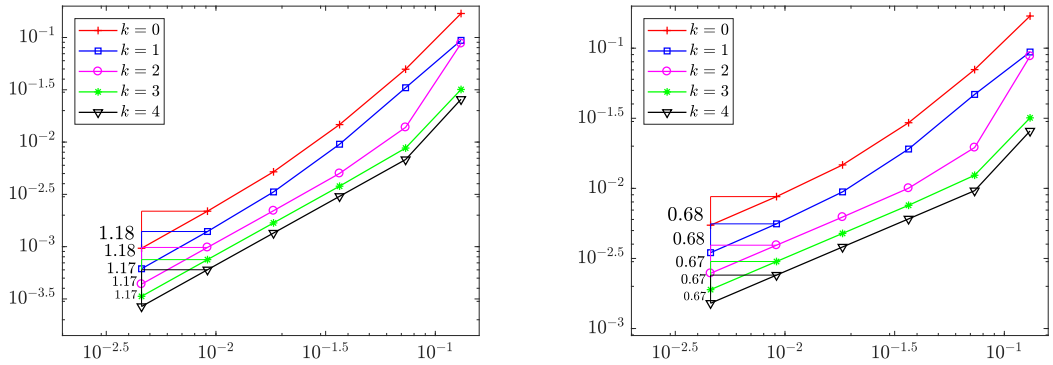

(a) $||\widehat{\xi}_h - \xi_h||_{\Gamma_{1,h}}$ vs. h (b) $||\widehat{\xi}_h - \xi_h||_{0,\Gamma_1}$ vs. h

Figure 4.30: Rates of convergence of the Lagrange multiplier considering the (a) Discrete trace norm $||\cdot||_{\Gamma_{1,h}}$, and (b) Standard L^2-norm (Example 7)

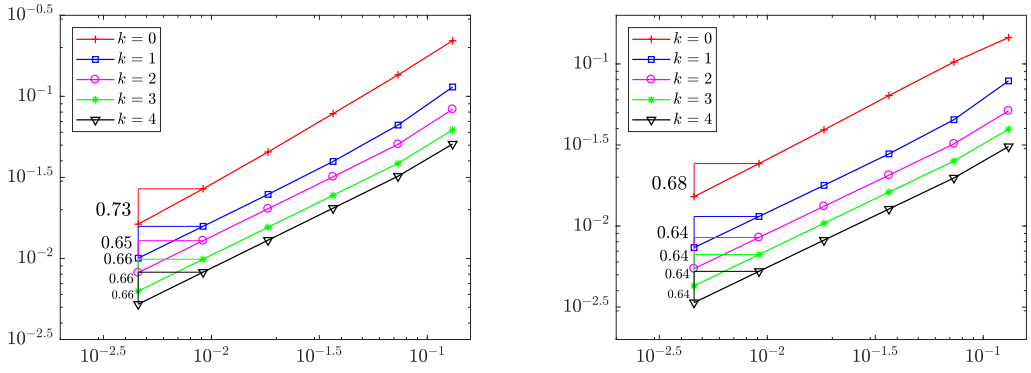

Figure 4.31: Rates of convergence of the (Left) energy norm of the potential error, and (Right) flux error (Example 7)

Table 4.22: Histories of convergence of the energy norm of the potential error and L^2-norm of the flux error, considering $k \in \{0, 1, 2, 3, 4\}$ (Example 7)

Energy norm of the potential error										
	$k = 0$		$k = 1$		$k = 2$		$k = 3$		$k = 4$	
h	error	rate	error	rate	error	rate	error	rate	error	rate
1.31e-01	2.21e-01		1.14e-01		8.32e-02		6.21e-02		5.08e-02	
7.32e-02	1.36e-01	0.836	6.65e-02	0.928	5.06e-02	0.855	3.86e-02	0.816	3.22e-02	0.786
3.66e-02	7.83e-02	0.793	3.97e-02	0.747	3.19e-02	0.665	2.45e-02	0.655	2.04e-02	0.655
1.83e-02	4.54e-02	0.786	2.49e-02	0.674	2.03e-02	0.655	1.56e-02	0.655	1.30e-02	0.655
9.15e-03	2.69e-02	0.755	1.58e-02	0.655	1.29e-02	0.655	9.89e-03	0.655	8.23e-03	0.656
4.58e-03	1.63e-02	0.726	1.00e-02	0.653	8.18e-03	0.656	6.28e-03	0.656	5.22e-03	0.657
L^2-norm of the flux error										
	$k = 0$		$k = 1$		$k = 2$		$k = 3$		$k = 4$	
h	error	rate	error	rate	error	rate	error	rate	error	rate
1.31e-01	1.45e-01		7.86e-02		5.14e-02		3.95e-02		3.09e-02	
7.32e-02	1.03e-01	0.597	4.53e-02	0.946	3.22e-02	0.805	2.52e-02	0.773	1.98e-02	0.766
3.66e-02	6.38e-02	0.687	2.79e-02	0.701	2.06e-02	0.642	1.62e-02	0.639	1.27e-02	0.637
1.83e-02	3.92e-02	0.703	1.78e-02	0.645	1.32e-02	0.638	1.04e-02	0.639	8.18e-03	0.638
9.15e-03	2.43e-02	0.691	1.15e-02	0.638	8.50e-03	0.639	6.67e-03	0.640	5.25e-03	0.639
4.58e-03	1.52e-02	0.678	7.36e-03	0.639	5.46e-03	0.641	4.28e-03	0.642	3.37e-03	0.641

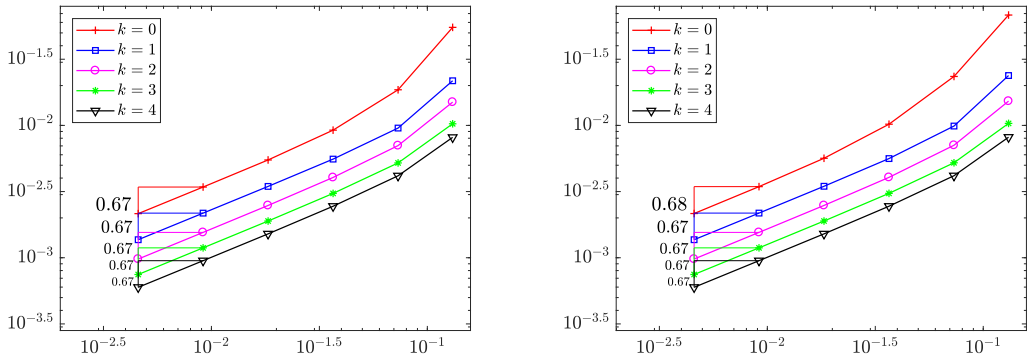

Figure 4.32: Rates of convergence of the L^2-norm of the (Left) potential error, and (Right) reconstructive potential error (Example 7)

Table 4.23: Histories of convergence of L^2-norm of the potential and reconstructive potential errors, considering $k \in \{0, 1, 2, 3, 4\}$ (Example 7)

L^2-norm of the potential error										
	$k = 0$		$k = 1$		$k = 2$		$k = 3$		$k = 4$	
h	error	rate	error	rate	error	rate	error	rate	error	rate
1.31e-01	5.51e-02		2.17e-02		1.50e-02		1.03e-02		8.12e-03	
7.32e-02	1.86e-02	1.866	9.55e-03	1.414	7.04e-03	1.300	5.20e-03	1.170	4.16e-03	1.149
3.66e-02	9.21e-03	1.014	5.56e-03	0.779	4.04e-03	0.800	3.06e-03	0.765	2.45e-03	0.764
1.83e-02	5.48e-03	0.748	3.46e-03	0.686	2.48e-03	0.703	1.89e-03	0.693	1.52e-03	0.693
9.15e-03	3.42e-03	0.680	2.17e-03	0.670	1.55e-03	0.676	1.19e-03	0.674	9.50e-04	0.673
4.58e-03	2.15e-03	0.669	1.37e-03	0.668	9.77e-04	0.670	7.47e-04	0.669	5.98e-04	0.669
L^2-norm of the reconstructive potential error										
	$k = 0$		$k = 1$		$k = 2$		$k = 3$		$k = 4$	
h	error	rate	error	rate	error	rate	error	rate	error	rate
1.31e-01	6.82e-02		2.38e-02		1.53e-02		1.04e-02		8.15e-03	
7.32e-02	2.34e-02	1.836	9.89e-03	1.510	7.08e-03	1.319	5.22e-03	1.177	4.17e-03	1.152
3.66e-02	1.02e-02	1.199	5.62e-03	0.816	4.05e-03	0.806	3.07e-03	0.768	2.45e-03	0.766
1.83e-02	5.64e-03	0.855	3.47e-03	0.696	2.48e-03	0.705	1.89e-03	0.694	1.52e-03	0.694
9.15e-03	3.45e-03	0.711	2.17e-03	0.673	1.55e-03	0.677	1.19e-03	0.674	9.50e-04	0.674
4.58e-03	2.16e-03	0.677	1.37e-03	0.669	9.77e-04	0.670	7.47e-04	0.669	5.98e-04	0.669

Table 4.24: Histories of convergence of the L^2-projection of $\xi - \xi_h$ in $||\cdot||_{\Gamma_{1,h}}$ and $||\cdot||_{0,\Gamma_1}$ norms, for $k \in \{0,1,2,3,4\}$ (Example 7)

$\|\widehat{\xi}_h - \xi_h\|_{\Gamma_{1,h}}$										
	$k=0$		$k=1$		$k=2$		$k=3$		$k=4$	
h	error	rate	error	rate	error	rate	error	rate	error	rate
1.31e-01	1.70e-01		9.39e-02		8.77e-02		3.18e-02		2.57e-02	
7.32e-02	4.97e-02	2.107	3.31e-02	1.792	1.38e-02	3.174	8.77e-03	2.216	6.80e-03	2.281
3.66e-02	1.47e-02	1.759	9.54e-03	1.795	5.01e-03	1.463	3.79e-03	1.212	3.03e-03	1.168
1.83e-02	5.20e-03	1.500	3.34e-03	1.515	2.21e-03	1.185	1.69e-03	1.166	1.35e-03	1.166
9.15e-03	2.18e-03	1.251	1.40e-03	1.257	9.83e-04	1.166	7.52e-04	1.166	6.01e-04	1.166
4.58e-03	9.65e-04	1.179	6.15e-04	1.185	4.38e-04	1.168	3.35e-04	1.168	2.68e-04	1.168
$\|\widehat{\xi}_h - \xi_h\|_{0,\Gamma_1}$										
	$k=0$		$k=1$		$k=2$		$k=3$		$k=4$	
h	error	rate	error	rate	error	rate	error	rate	error	rate
1.31e-01	1.70e-01		9.39e-02		8.77e-02		3.18e-02		2.57e-02	
7.32e-02	7.03e-02	1.512	4.68e-02	1.197	1.95e-02	2.578	1.24e-02	1.621	9.62e-03	1.685
3.66e-02	2.94e-02	1.259	1.91e-02	1.295	1.00e-02	0.963	7.57e-03	0.712	6.06e-03	0.668
1.83e-02	1.47e-02	1.000	9.44e-03	1.015	6.24e-03	0.685	4.77e-03	0.666	3.82e-03	0.666
9.15e-03	8.73e-03	0.751	5.58e-03	0.757	3.93e-03	0.666	3.01e-03	0.666	2.41e-03	0.666
4.58e-03	5.46e-03	0.678	3.48e-03	0.684	2.48e-03	0.667	1.89e-03	0.667	1.52e-03	0.668

Conclusions

In this chapter we have proposed a new mixed HHO formulation to approximate the solution of a transmission interior elliptic problem, with nonhomogeneous transmission boundary conditions. First, we derive the variational formulation, at continuous level, introducing the normal trace on the transmission boundary, of the solution living in inner subdomain, as an auxiliary unknown. In practice, this unknown acts as a Lagrange multiplier. Then, we propose a discrete variational scheme, applying the HHO approach. Although we have considered, for simplicity, a family of uniform simplicial meshes for the current analysis, it is possible to extend

it to deal with polytopal meshes, as in [39].

We have proved that our discrete mixed HHO scheme is well-posed and convergent in the energy-norm, as well as in the usual L^2-norm. Our a priori error estimates establish that when we approximate the solution with piecewise polynomial of degree at most $k \geq 0$, the flux and energy norm of the potential error go to zero with optimal order of convergence $k+\delta$, while the L^2-norm of potential and reconstructive potential errors' orders behave as $\mathcal{O}(h^{k+1+\delta})$, for some $\delta \in (1/2, 1]$ (cf. Theorems 4.5.1, 4.5.2 and 4.5.3). The L^2-projection of the error of Lagrange multiplier is measured in a suitable weighted L^2-norm (cf. (4.29)), and converges, at least, with order $k+\delta$ (cf. Theorem 4.5.1). We also have computed the classical L^2-norm of this projection, noticing a convergence that decays to 0 as $\mathcal{O}(h^{k+\delta-1/2})$, which is in agreement with Remark 4.5.1.

Numerical examples, provided in this work, are in agreement with our theoretical results. In particular, results from Examples 4.7.1, 4.7.2, and 4.7.3.1, show us that our theoretical rates of convergence are achieved. In Example 4.7.5, we consider as exact solution a function that lives in $H^4(\Omega_1)$ but not in $H^5(\Omega_1)$. According to Theorems 4.5.1, 4.5.2 and 4.5.3, we should expect optimal order of convergence for the energy norm of the potential error, the flux error in the L^2-norm, the weighted L^2- norm of the error of the Lagrange multiplier, the potential and the reconstructive potential errors in the L^2-norm, when the solution is approximated by piecewise polynomials of degree at most $k \leq 3$, which is what we observe in Tables 4.16, 4.18, and 4.17, whose results are also displayed in Figures 4.24, 4.23 and 4.25, respectively. On the other hand, since the exact solution in Example 4.7.4 is nonregular, we do not expect to obtain optimal rates of convergence. The results are displayed in Figures 4.21, 4.20 and 4.22, and reported in Tables 4.13, 4.15 and 4.14. Then, we just confirm that results from these tables are in agreement with Theorems 4.5.1, 4.5.2 and 4.5.3, for $q = 0$ and $k \in \{1, 2, 3, 4\}$. Surprisingly, we notice an unexpected (better) behavior of the errors for $k = 0$. As a consequence, this motivates us to develop, an a posteriori error analysis, in order to improve the quality of approximation and recover the optimal rate of convergence, if possible. This would be the subject of a future work.

We recall that in Example 4.7.3.2, we have performed our HHO approach, considering a family of simplicial meshes having hanging nodes only on the transmission boundary Γ_1. *We observe that the convergence of the method behaves similarly as when we solve the same problem considering a family of conforming meshes (see Example 4.7.3.1), despite the fact that our analysis, in its current form, does not covered the use of family of meshes with hanging nodes on* Γ_1. *This could also be the subject of future work, taking the analysis developed in [116] as reference.*

It is important to emphasize that the proofs of Theorems 4.5.2 and 4.5.3 rely on the well known elliptic regularity property (4.90), which can be established if we assume that $\Omega := \Omega_1 \cup \Gamma_1 \cup \Omega_2$ *is a convex domain. In this sense, and with the aim of testing the robustness of our computational implementation to deal with nonconvex domain* Ω *(cf. Figure 4.26), we consider Examples 4.7.6 and 4.7.7. We consider an smooth solution in Example 4.7.6, and the numerical results we obtain are surprisingly in agreement with Theorems 4.5.2 and 4.5.3 (and of course with Theorem 4.5.1, too), despite the our current theory does not support them. In Example 4.7.7, the solution is nonsmooth, and then, we do not expect optimal rates of convergence. The results have been reported in Tables 4.22, 4.24 and 4.23, and confirm our suspicious. As in Example 4.7.4, it would be desirable to find an a posteriori error estimator for this problem, that let us to improve our approximation and get the optimal convergence's behaviour.*

Finally, we point out that the analysis described in this paper, can be applied and/or extended to deal with linear transmission problems with variable diffusion, and / or with other type of boundary conditions on the external boundary of Ω_2. *In addition, taking into account [64] and [41], we are motivated to extend this approach to deal with certain class of nonlinear transmission problems.*

Appendix

In what follows, we write down the proof of Lemma 4.4.2, for a general $\Omega := \Omega_1 \cup \Gamma_1 \cup \Omega_2$ *(convex or nonconvex domain).*

To this aim, given $\underline{\mathbf{v}}_h := \left(\underline{\mathbf{v}}_{\mathcal{T}_{1,h}}, \underline{\mathbf{v}}_{\mathcal{T}_{2,h}}\right) \in \underline{\mathbf{U}}_{\mathcal{T}_h}^{k,0}$, *where we recall* $\mathcal{T}_h := \mathcal{T}_{1,h} \cup \mathcal{T}_{2,h}$, *we*

introduce $w_h \in \mathbb{P}_h^k(\mathcal{T}_h)$, *such that*

$$w_h\Big|_T := w_T := \begin{cases} v_{1,T}\ , & T \in \mathcal{T}_{1,h}\,, \\ v_{2,T}\ , & T \in \mathcal{T}_{2,h}\,. \end{cases}$$

We notice that $(w_h,1)_\Omega = (v_{1,h},1)_{\Omega_1} + (v_{2,h},1)_{\Omega_2} = 0$, *since* $\underline{\mathbf{U}}_h^{k,0}$. *Then, we define* $\underline{\mathbf{w}}_h := \Big((w_T)_{T\in\mathcal{T}_h},(w_F)_{F\in\mathcal{F}_h}\Big) \in \underline{\mathbf{W}}_h^{k,0} := \big\{\underline{\mathbf{z}}_h \in \underline{\mathbf{W}}_h^k \,|\, (z_h,1)_\Omega = 0\big\}$, *where* $\underline{\mathbf{W}}_h^k$ *collects the DOF's on* Ω, *such that*

$$w_F := \begin{cases} v_{F,1}\ , & F \in \mathcal{F}_{1,h}\backslash\Gamma_{1,h} \\ v_{F,2}\ , & F \in \mathcal{F}_{2,h} \end{cases}. \quad \textit{Then, applying Theorem 6.5 in [66], we infer that}$$

$$||v_{1,h}||_{0,\Omega_1}^2 + ||v_{2,h}||_{0,\Omega_2}^2 = ||w_h||_{0,\Omega}^2 \lesssim ||\underline{\mathbf{w}}_h||_{1,h}^2\,. \tag{4.149}$$

Using the definition of $\|\cdot\|_{1,h}$, *and that* $\sum_{T\in\mathcal{T}_h}\|\nabla w_T\|_{0,T}^2 = \sum_{T\in\mathcal{T}_{1,h}}\|\nabla v_{1,T}\|_{0,T}^2 + \sum_{T\in\mathcal{T}_{2,h}}\|\nabla v_{2,T}\|_{0,T}^2$, *we obtain*

$$\|\underline{\mathbf{w}}_h\|_{1,h}^2 = \sum_{T\in\mathcal{T}_{1,h}}\|\nabla v_{1,T}\|_{0,T}^2 + \sum_{T\in\mathcal{T}_{2,h}}\|\nabla v_{2,T}\|_{0,T}^2 + \sum_{T\in\mathcal{T}_h}\sum_{F\in\mathcal{F}_T} h_F^{-1}\|w_F - w_T\|_{0,F}^2, \tag{4.150}$$

Then, given $F \in \Gamma_{1,h}$ *(transmission face), there exist* $T \in \mathcal{T}_{1,h}$ *and* $S \in \mathcal{T}_{2,h}$, *such that* $F \subset \partial T \cap \partial S$, *and using definition of* $\underline{\mathbf{w}}_h$, *we obtain*

$$\|w_F - w_T\|_{0,F}^2 + \|w_F - w_S\|_{0,F}^2 = \|v_{2,F} - v_{1,T}\|_{0,F}^2 + \|v_{2,F} - v_{2,S}\|_{0,F}^2\,, \tag{4.151}$$

and by triangle inequality on the first term on the right hand side, we obtain

$$\|w_F - w_T\|_{0,F}^2 + \|w_F - w_S\|_{0,F}^2 \lesssim \|v_{2,F} - v_{1,F}\|_{0,F}^2 + \|v_{1,F} - v_{1,T}\|_{0,F}^2 + \|v_{2,F} - v_{2,S}\|_{0,F}^2\,. \tag{4.152}$$

Thus, we can write the third term on the right hand of (4.150), as

$$\begin{aligned}\sum_{T\in\mathcal{T}_h}\sum_{F\in\mathcal{F}_T} h_F^{-1}\|w_F - w_T\|_{0,F}^2 \lesssim \sum_{T\in\mathcal{T}_{1,h}}\sum_{F\in\mathcal{F}_T} h_F^{-1}\|v_{1,F} - v_{1,T}\|_{0,F}^2 + \\ + \sum_{S\in\mathcal{T}_{2,h}}\sum_{F\in\mathcal{F}_T} h_F^{-1}\|v_{2,F} - v_{2,S}\|_{0,F}^2 + \sum_{F\in\Gamma_{1,h}} h_F^{-1}\|v_{2,F} - v_{1,F}\|_{0,F}^2\,.\end{aligned} \tag{4.153}$$

Replacing (4.153) in (4.150), we have that

$$\|\underline{\boldsymbol{w}}_h\|_{1,h}^2 \lesssim \|\underline{\mathbf{v}}_{1,h}\|_{1,h}^2 + \|\underline{\mathbf{v}}_{2,h}\|_{1,h}^2 + \sum_{F\in\Gamma_{1,h}} h_F^{-1}\|v_{2,F} - v_{1,F}\|_{0,F}^2\,. \tag{4.154}$$

Finally, from (4.149) *and* (4.154), *we conclude the proof.*

Discussion and future works

In this thesis, we have developed primal and mixed schemes based on Hybrid High-Order (HHO) methods, which have been introduced by Di Pietro and Ern [75, 70]. We have established unique solvability of continuous and discrete problem, as well as their convergence, all illustrated by examples and numerical simulations. The main results/conclusions of this thesis are:

1. *In Chapter 2, a variable diffusion problem has been analyzed with pure Neumann boundary conditions, introducing a Lagrange multiplier for the null mean condition, to ensure uniqueness for problems with this kind of boundary conditions. It has been proved that the variational problem and its HHO formulation are well-posedness, and has been verified the a priori error estimate in an example with a sufficiently smooth exact solution. The scheme has been also tested with another example, whose exact solution this time is not smooth enough. This last example motivates us to carry out an a posteriori error analysis, to recover the optimal convergence rate found for smooth solutions. The content of this chapter have lead to the publication [39].*

2. *In Chapter 3, we have carried out an a priori error analysis of a class of nonlinear elliptic equations, applying the HHO method. In this case, the hypotheses on the nonlinear function are quite different of the works developed in [64, 65, 27]. In addition, we have demonstrated superconvergence for the potential, which has not been addressed for this problem in the literature, until now. The extension of this work to other boundary conditions should not be difficult. For a future work, we would like to address dual-dual HHO schemes for a class of elliptic nonlinear problems. This chapter is also contained in the*

pre-print [41].

3. *In Chapter 4, we propose a mixed scheme over two domains, where we deal with two different solutions that can represent the density of two different fluids. An additional unknown, that represents the flux from the interior to the exterior domain, has been introduced. This allows us to weakly imposed the jump of the solutions at the transmission boundary, in the mixed formulations. The existence and uniqueness of the mixed variational formulation and the corresponding mixed HHO scheme, have been proved invoking the Babuška-Brezzi theory. The analysis described in this chapter is contained in the pre-print [40]. We hope to extend our analysis to interior and exterior transmission problems with variable diffusion and/or including nonlinearities, as a future work.*

4. *We can say that the HHO method is more natural than other schemes discussed in the introduction of this thesis, since it involves local reconstructive operators, which have commutative properties with their respective differential operators. For example, the reconstructive gradient in (3.11) and the reconstructive divergent operator in [73, Lemma 2]. These operators are deduced from properties obtained by applying integration by parts to the differential operator. The stabilization term of this method helps us to preserve the high order of the approach. It let us to handle variable diffusive tensors, deformations in the field of elasticity, etc.*

5. *A relevant computational issue of HHO methods is the fact that we can solve a system on the skeleton of the mesh. This reduces the operational cost since smaller systems of equations would be being solved, showing to be a competitive scheme with the usual continuous Galerkin methods. In contrast to other methods that solve them on a reference element, HHO solves them on their respective physical element. This allows us to work with very general meshes, including with hanging nodes.*

6. *The use of hybridization technique has helped us to compare HHO method with other schemes, such as HDG, with the notorious difference that explicit*

numerical fluxes are not longer required by HHO approach. The deduction of equivalence between the discrete norm, in particular the one defined in Chapter 4 that includes the jump in the transmission boundary, as well as the induced "energy norm" of the schemes, has been very useful for bounding the error of consistency of HHO schemes. Another important contribution is the proof of superconvergence of the potential unknown, using duality tools.

7. *Finally, HHO schemes have been implemented in the C ++ programming language, and several numerical examples have been tested to verify the convergence error predicted in the a priori error analysis.*

Discusión y trabajos futuros

En esta tesis hemos desarrollado esquemas primales y mixtos basados en los métodos híbridos de alto orden (HHO), introducido por Di Pietro y Ern [75, 70]. Hemos demostrado solubilidad de los problemas continuo y discreto, así como su convergencia. Todo esto ha sido ilustrado mediante ejemplos y simulaciones numéricas. Los principales resultados y/o conclusiones de este trabajo son:

1. *En el Capítulo 2 se ha analizado el problema de difusión variable bajo condiciones de frontera Neumann puro, introduciendo un multiplicador de Lagrange para la condición de media nula. Esto último para asegurar la unicidad de solución para problemas con este tipo de condiciones de frontera. Se ha probado que el problema variacional y su formulación HHO están bien puestos. Además se ha comprobado la estimación de error a priori, con un ejemplo con solución exacta suficientemente suave. Se ha probado también el esquema con otro ejemplo, cuya solución esta vez no es suave. Este último ejemplo nos motiva a realizar un análisis de error a posteriori y recuperar la convergencia asintótica encontrada para soluciones suficientemente suaves. El contenido de este capítulo ha dado lugar a la publicación [39].*

2. *En el Capítulo 3 se ha desarrollado un análisis de error a priori para una clase de ecuaciones estacionarias elípticas no lineales, aplicando el método HHO. Las hipótesis sobre la función no lineal difieren de las consideradas en trabajos similares. Además, se ha probado un resultado de superconvergencia para el potencial, que no había sido deducido antes, según la literatura revisada hasta este momento. Creemos que la extensión de condiciones Dirichlet homogéneas a otras condiciones de frontera es natural. Para un trabajo futuro se desea*

abordar esquemas dual-dual para problemas no lineales elípticos. El contenido de este capítulo se encuentra en el pre-print [41].

3. *En el Capítulo 4, hemos obtenido un esquema mixto sobre dos subdominios, donde lidiamos con dos soluciones distintas que pueden representar la densidad de dos fluidos diferentes. Se ha introducido una incógnita adicional, que representa el flujo desde el dominio interior al exterior. Esto nos ha permitido imponer débilmente el salto de las soluciones en la frontera de transmisión, en la formulación mixta (continua) y en el equema mixto HHO también. La existencia y unicidad de la formulación variacional mixta y su esquema mixto HHO, ha sido asegurada gracias a la teoría de Babuška-Brezzi. Esperamos extender nuestro análisis a problemas de transmisión interior y exterior con difusión variable y/o incluyendo no linealidades. Este capítulo se ha plasmado en el pre-print [40].*

4. *Consideramos que el método HHO es más natural que otros esquemas discutidos en la introducción de esta tesis, debido a que involucra operadores reconstructivos locales, los cuales tienen propiedades conmutativas con sus operadores diferenciales de referencia. Es el caso del gradiente reconstructivo en (3.11) y del operador divergente reconstructivo en [73, Lemma 2]. Estos operadores se deducen de propiedades obtenidas al aplicar integración por partes al operador diferencial. El término de estabilización de este método ayuda a preservar el alto orden de aproximación del operador reconstructivo. Esto nos permite trabajar con tensores difusivos variables, deformaciones en el campo de la elasticidad, etc.*

5. *Un relevante aspecto computacional de los métodos HHO, es el hecho que permite resolver un sistema definido en el esqueleto del mallado. Esto reduce el costo operacional pues se estarían resolviendo sistemas de ecuaciones más pequeños, mostrando ser un esquema competitivo con los usuales métodos de Galerkin continuos. En constraste con otros mtodos que los resuelven en un elemento de referencia, el método HHO los puede resolver en su elemento físico respectivo. Esto nos permite trabajar con mallas muy generales, inclusive con*

nodos colgantes.

6. *El uso de la técnica de hibridización nos ha ayudado a comparar el método HHO con otros esquemas, como el HDG, con la notoria diferencia de no tener que definir explícitamente flujos numéricos en los esquemas HHO. La deducción de equivalencia entre la norma discreta, en particular la referida al Capítulo 4 que incluye el salto en la frontera de transmisión, y la "norma de energía" inducida de los esquemas, es muy útil a la hora de acotar el error de consistencia de los esquemas HHO. Otra importante contribución es la prueba de la superconvergencia de la incógnita potencial, aplicando herramientas de dualidad.*

7. *Por último, los esquemas HHO han sido implementados usando el lenguaje de programación C++, y se han testeado con varios ejemplos numéricos para verificar la velocidad de convergencia predicha en los análisis de error a priori.*

Bibliography

[1] Abbas, M., Ern, A., and Pignet, N. *Hybrid High-Order methods for finite deformations of hyperelastic materials.* Computational Mechanics 62*, 4 (2018), 909–928.*

[2] Abbas, M., Ern, A., and Pignet, N. *A Hybrid High-Order method for incremental associative plasticity with small deformations.* Computer Methods in Applied Mechanics and Engineering 346 *(2019), 891–912.*

[3] Aghili, J., Boyaval, S., and Di Pietro, D. A. *Hybridization of Mixed High-Order Methods on General Meshes and Application to the Stokes Equations.* Computational Methods in Applied Mathematics 15*, 2 (2015), 111–134.*

[4] Aghili, J., and Di Pietro, D. A. *An Advection-Robust Hybrid High-Order Method for the Oseen Problem.* Journal of Scientific Computing 77 *(2018), 1310–1338.*

[5] Ambrosio, L. *Optimal transport maps in Monge-Kantorovich problem. In* Proceedings of the International Congress of Mathematicians 2002 *(2002), T. Li and D. Li, Eds., vol. III, pp. 131–140.*

[6] Anderson, D., and Droniou, J. *An Arbitrary-Order Scheme on Generic Meshes for Miscible Displacements in Porous Media.* SIAM Journal on Scientific Computing 40*, 4 (2018), B1020–B1054.*

[7] Araya, R., Harder, C., Paredes, D., and Valentin, F. *Multiscale Hybrid-Mixed Method.* SIAM Journal on Numerical Analysis 51 *(2013), 3505–3531.*

[8] Arnold, D., Brezzi, F., Cockburn, B., and Marini, D. *Unified Analysis of Discontinuous Galerkin Methods for Elliptic Problems.* SIAM Journal on Numerical Analysis 39*, 5 (2002), 1749–1779.*

[9] Arnold, D. N. *An Interior Penalty Finite Element Method with Discontinuous Elements.* SIAM Journal on Numerical Analysis 19*, 4 (1982), 742–760.*

[10] Arnold, D. N., Brezzi, F., Cockburn, B., and Marini, D. *Discontinuous Galerkin methods for elliptic problems. In* Discontinuous Galerkin Methods: Theory, Computation and Applications*, B. Cockburn, G. E. Karniadakis, and C.-W. Shu, Eds., vol. 11 of* Lecture Notes in Computational Science and Engineering*. Springer, Berlin, Heidelberg, 2000, pp. 89–101.*

[11] Ayuso de Dios, B., Lipnikov, K., and Manzini, G. *The nonconforming virtual element method.* ESAIM: Mathematical Modelling and Numerical Analysis 50*, 3 (2016), 879–904.*

[12] Babuška, I. *The finite element method for elliptic equations with discontinuous coefficients.* Computing 5*, 3 (1970), 207–213.*

[13] Baker, G. A. *Finite element methods for elliptic equations using nonconforming elements.* Mathematics of Computation 31*, 137 (1977), 45–59.*

[14] Balay, S., Brown, J., Buschelman, K., Gropp, W. D., Kaushik, D., Knepley, M. G., Curfman McInnes, L., Smith, B. F., and Zhang, H. *PETSc.* http://www.mcs.anl.gov/petsc*, 2011.*

[15] Barrenechea, G., Gatica, G. N., and Thomas, J.-M. *Primal mixed formulations for the coupling of FEM and BEM. Part I: Linear problems.* Numerical Functional Analysis and Optimization 19 *(1998), 7–32.*

[16] Barrett, J., and Elliot, C. *Fitted and Unfitted Finite-Element Methods for Elliptic Equations with Smooth Interfaces.* IMA Journal of Numerical Analysis 7 *(1987), 283–300.*

[17] Barrett, J., and Liu, J. G. *Finite Element Approximation of the p−Laplacian.* Mathematics of Computation 61 *(1993), 523–537.*

[18] Bassi, F., and Rebay, S. *A High-Order Accurate Discontinuous Finite Element Method for the Numerical Solution of the Compressible NavierStokes Equations.* Journal of Computational Physics 131*, 2 (1997), 267 – 279.*

[19] Bebendorf, M. *A Note on the Poincaré Inequality for Convex Domains.* Zeitschrift Fur Analysis Und Ihre Anwendungen 22 *(2003), 751–756.*

[20] Beirão da Veiga, L., Brezzi, F., Cangiani, A., Manzini, G., Marini, L. D., and Russo, A. *Basic principles of Virtual Element Methods.* Mathematical Models and Methods in Applied Sciences 23*, 1 (2013), 199–214.*

[21] Beirão da Veiga, L., Droniou, J., and Manzini, G. *A unified approach to handle convection terms in Finite Volumes and Mimetic Discretization Methods for elliptic problems.* IMA Journal of Numerical Analysis 31*, 4 (2011), 1357–1401.*

[22] Beirão da Veiga, L., Lipnikov, K., and Manzini, G. The Mimetic Finite Difference Method for Elliptic Problems*, vol. 11 of* Modeling, Simulation and Applications*. Springer International Publishing, 2014.*

[23] Beirão da Veiga, L., Lovadina, C., and Mora, D. *A Virtual Element Method for elastic and inelastic problems on polytope meshes.* Computer Methods in Applied Mechanics and Engineering 295 *(2015), 327–346.*

[24] Bi, C., and Lin, Y. *Discontinuous Galerkin method for monotone nonlinear elliptic problems.* International Journal of Numerical Analysis and Modeling 9*, 4 (2012), 999–1024.*

[25] Bos, F., and Gravemeier, V. *Numerical simulation of premixed combustion using an enriched finite element method.* Journal of Computational Physics 228 *(2009), 3605–3624.*

[26] Botti, L., Di Pietro, D. A., and Droniou, J. *A Hybrid High-Order method for the incompressible Navier-Stokes equations based on Temam's device.* Journal of Computational Physics 376 *(2019), 786 – 816.*

[27] Botti, M., Di Pietro, D. A., and Sochala, P. *A Hybrid High-Order Method for Nonlinear Elasticity.* SIAM Journal on Numerical Analysis 55*, 6 (2017), 2687–2717.*

[28] Botti, M., Di Pietro, D. A., and Sochala, P. *A Nonconforming High-Order Method for Nonlinear Poroelasticity. In* Finite Volumes for Complex Applications VIII - Hyperbolic, Elliptic and Parabolic Problems. FVCA*, C. Cancès and P. Omnes, Eds. Springer, Cham, 05 2017, pp. 537–545.*

[29] Botti, M., Di Pietro, D. A., and Sochala, P. *A Hybrid High-Order Discretization Method for Nonlinear Poroelasticity.* Computational Methods in Applied Mathematics 20*, 2 (2020), 227–249.*

[30] Bramble, J. H., and King, J. T. *A finite element method for interface problems in domains with smooth boundaries and interfaces.* Advances in Computational Mathematics 6*, 1 (1996), 109–138.*

[31] Burman, E., and Ern, A. *An Unfitted Hybrid High-Order Method for Elliptic Interface Problems.* SIAM Journal on Numerical Analysis 56*, 3 (2017), 1525–1546.*

[32] Burman, E., and Fernández, M. *An unfitted Nitsche method for incompressible fluid-structure interaction using overlapping meshes.* Computer Methods in Applied Mechanics and Engineering 279 *(2014), 497–514.*

[33] Bustinza, R. *A unified analysis of the local discontinuous Galerkin method for a class of nonlinear problems.* Applied Numerical Mathematics 56 *(2006), 1293–1306.*

[34] Bustinza, R., García, G., and Gatica, G. N. *A mixed finite element method with Lagrange multipliers for nonlinear exterior transmission problems.* Numerische Mathematik 96 *(2004), 481–523.*

[35] Bustinza, R., and Gatica, G. N. *A Local Discontinuous Galerkin Method for Nonlinear Diffusion Problems with Mixed Boundary Conditions.* SIAM Journal Scientific Computing 26 *(2004), 152–177.*

[36] Bustinza, R., Gatica, G. N., and Sayas, F.-J. *A LDG-BEM Coupling for a Class of Nonlinear Exterior Transmission Problems. In* Proceedings of ENUMATH 2005 *(2006), A. Bermúdez de Castro, D. Gómez, P. Quintela, and P. Salgado, Eds., Springer, Berlin, Heidelberg, pp. 1129–1136.*

[37] Bustinza, R., Gatica, G. N., and Sayas, F.-J. *On the coupling of local discontinuous Galerkin and boundary element methods for non-linear exterior transmission problems.* IMA Journal of Numerical Analysis 28 *(2007), 225–244.*

[38] Bustinza, R., and Munguia, J. *Revisión del método Híbrido de Alto Orden para un problema de difusión variable.* REVCIUNI 21*, 1 (2018), 6–14.*

[39] Bustinza, R., and Munguia-La-Cotera, J. *A hybrid high-order formulation for a Neumann problem on polytopal meshes.* Numerical Methods for Partial Differential Equations 36*, 3 (2020), 524–551.*

[40] Bustinza, R., and Munguia-La-Cotera, J. *A mixed Hybrid High-Order formulation for linear interior transmission elliptic problems.* Centro de Investigación en Ingeniería Matemática, Universidad de Concepción, Chile *(2020). Pre-print 2020-10.*

[41] Bustinza, R., and Munguia-La-Cotera, J. *An a priori error analysis for a class of nonlinear elliptic problems with the hybrid high-order method.* Centro de Investigación en Ingeniería Matemática, Universidad de Concepción, Chile *(2020). Pre-print 2020-08.*

[42] Calo, V., Cicuttin, M., Deng, Q., and Ern, A. *Spectral approximation of elliptic operators by the Hybrid High-Order method.* Mathematics of Computation 88*, 318 (2019), 1559–1586.*

[43] Cangiani, A., Manzini, G., and Sutton, O. *Conforming and nonconforming virtual element methods for elliptic problems.* IMA Journal of Numerical Analysis 37*, 3 (2017), 1317–1354.*

[44] Cascavita, K. L., Bleyer, J., Chateau, X., and Ern, A. *Hybrid Discretization Methods with Adaptive Yield Surface Detection for Bingham Pipe Flows.* Journal of Scientific Computing 77 *(2018), 1424–1443.*

[45] Cascavita, K. L., Chouly, F., and Ern, A. *Hybrid high-order discretizations combined with Nitsches method for Dirichlet and Signorini boundary conditions.* IMA Journal of Numerical Analysis 40 *(2020), 2189–2226.*

[46] Castillo, P., Cockburn, B., and Dominik, I. *An A Priori Error Analysis Of The Local Discontinuous Galerkin Method For Elliptic Problems.* SIAM Journal on Numerical Analysis 38*, 5 (2000), 1676–1706.*

[47] Chen, L., Wei, H., and Wen, M. *An interface-fitted mesh generator and virtual element methods for elliptic interface problems.* Journal of Computational Physics 334 *(2017), 327–348.*

[48] Chen, Z., and Zou, J. *Finite element methods and their convergence for elliptic and parabolic interface problems.* Numerische Mathematik 79 *(1998), 175–202.*

[49] Chu, C.-C., Graham, I., and Hou, T.-Y. *A new multiscale finite element method for high-contrast elliptic interface problems.* Mathematics of Computation 79*, 272 (2010), 1915–1955.*

[50] Cicuttin, M., Di Pietro, D. A., and Ern, A. *Implementation of Discontinuous Skeletal methods on arbitrary-dimensional, polytopal meshes using generic programming.* Journal of Computational and Applied Mathematics 86*, 307 (2017), 852–874.*

[51] Cicuttin, M., Ern, A., and Gudi, T. *Hybrid High-Order Methods for the Elliptic Obstacle Problem.* Journal of Scientific Computing 83 *(2020), Art. 8.*

[52] Cicuttin, M., Ern, A., and Lemaire, S. *On the Implementation of a Multiscale Hybrid High-Order Method. In* Numerical Mathematics and Advanced Applications ENUMATH 2017*, F. Radu, K. Kumar, I. Berre, J. Nordbotten, and I. Pop, Eds., vol. 126. Springer, Cham, 2017, pp. 509–517. Lecture Notes in Computational Science and Engineering.*

[53] Cicuttin, M., Ern, A., and Lemaire, S. *A Hybrid High-Order Method for Highly Oscillatory Elliptic Problems.* Computational Methods in Applied Mathematics 19*, 4 (2019), 723–748.*

[54] Clough, R. *Early history of the finite element method from the view point of a pioneer.* International Journal for Numerical Methods in Engineering 60 *(2004), 283 – 287.*

[55] Clough, R. W. *Areas of application of the finite element method.* Computers & Structures 4*, 1 (1974), 17 – 40.*

[56] Cockburn, B. *Devising discontinuous Galerkin methods for non-linear hyperbolic conservation laws.* Journal of Computational and Applied Mathematics 128*, 1 (2001), 187–204. Numerical Analysis 2000. Vol. VII: Partial Differential Equations.*

[57] Cockburn, B., Di Pietro, D. A., and Ern, A. *Bridging the Hybrid High-Order and Hybridizable Discontinuous Galerkin Methods.* ESAIM: Mathematical Modelling and Numerical Analysis 50 *(2016), 635–650.*

[58] Cockburn, B., Dong, B., and Guzmn, J. *A superconvergent LDG-hybridizable Galerkin method for second-order elliptic problems.* Mathematics of Computation 77*, 264 (2008), 1887–1916.*

[59] Cockburn, B., Gopalakrishnan, J., and Lazarov, R. *Unified Hybridization of Discontinuous Galerkin, Mixed, and Continuous Galerkin Methods for Second Order Elliptic Problems.* SIAM Journal on Numerical Analysis 47 *(2009), 1319–1365.*

[60] Cockburn, B., Kanschat, G., Perugia, I., and Schötzau, D. *Superconvergence of the Local Discontinuous Galerkin Method for Elliptic Problems on Cartesian Grids.* SIAM Journal on Numerical Analysis 39*, 1 (2001), 264–285.*

[61] Cockburn, B., and Shu, C.-W. *The Runge-Kutta local projection P^1-discontinuous-Galerkin finite element method for scalar conservation laws.* ESAIM: Mathematical Modelling and Numerical Analysis - Modélisation Mathématique et Analyse Numérique 25*, 3 (1991), 337–361.*

[62] Cockburn, B., and Shu, C.-W. *The Local Discontinuous Galerkin Method for Time-Dependent Convection-Diffusion Systems.* SIAM Journal on Numerical Analysis 35*, 6 (1998), 2440–2463.*

[63] Demmel, J. W., Eisenstat, S. C., Gilbert, J. R., Li, X. S., and Liu, J. W. H. *A Supernodal Approach to Sparse Partial Pivoting.* SIAM Journal of Matrix Analysis and Applications 20*, 3 (1999), 720–755.*

[64] Di Pietro, D. A., and Droniou, J. *A Hybrid High-Order method for Leray–Lions elliptic equations on general meshes.* Mathematics of Computation 86*, 307 (2017), 2159–2191.*

[65] Di Pietro, D. A., and Droniou, J. *$W^{s,p}$-approximation properties of elliptic projectors on polynomial spaces, with application to the error analysis of a Hybrid High-Order discretisation of Leray-Lions problems.* Mathematical Models and Methods in Applied Sciences 27*, 5 (2017), 879–908.*

[66] Di Pietro, D. A., and Droniou, J. The Hybrid High-Order Method for Polytopal Meshes: Design, Analysis, and Applications.*, vol. 19 of* Modeling, Simulation and Applications series*. Springer International Publishing, 2020. 528 pages.*

[67] Di Pietro, D. A., Droniou, J., and Ern, A. *A Discontinuous-Skeletal Method for Advection-Diffusion-Reaction on General Meshes.* SIAM Journal on Numerical Analysis 53 *(2015), 2135 – 2157.*

[68] Di Pietro, D. A., Droniou, J., and Manzini, G. *Discontinuous Skeletal Gradient Discretisation Methods on polytopal meshes.* Journal of Computational Physics 355 *(2018), 397–425.*

[69] Di Pietro, D. A., and Ern, A. Mathematical Aspects of Discontinuous Galerkin Methods*, vol. 69 of* Mathématiques et Applications*. Springer-Verlag, Berlin, 2012.*

[70] Di Pietro, D. A., and Ern, A. *A hybrid high-order locking-free method for linear elasticity on general meshes.* Computer Methods in Applied Mechanics and Engineering 283 *(2014), 1–21.*

[71] Di Pietro, D. A., and Ern, A. *Equilibrated tractions for the Hybrid High-Order method.* Comptes Rendus Mathematique 353*, 3 (2015), 279 – 282.*

[72] Di Pietro, D. A., and Ern, A. *Hybrid High-Order methods for variable diffusion problems on general meshes.* Comptes Rendus Mathematique 353*, 1 (2015), 31–34.*

[73] Di Pietro, D. A., and Ern, A. *Arbitrary-order mixed methods for heterogeneous anisotropic diffusion on general meshes.* IMA Journal of Numerical Analysis 37*, 1 (2017), 40–63.*

[74] Di Pietro, D. A., ern, a., and Formaggia, L. Numerical Methods for PDEs: State of the Art Techniques*, first ed., vol. 15 of* SEMA-SIMAI*. Springer International Publishing, 2018.*

[75] Di Pietro, D. A., Ern, A., and Lemaire, S. *An Arbitrary-Order and Compact-Stencil Discretization of Diffusion on General Meshes Based on Local Reconstruction Operators.* Computational Methods in Applied Mathematics 14*, 4 (2014), 461–472.*

[76] Di Pietro, D. A., Ern, A., and Lemaire, S. *A Review of Hybrid High-Order Methods: Formulations, Computational Aspects, Comparison with Other Methods. In* Building Bridges: Connections and Challenges in Modern

Approaches to Numerical Partial Differential Equations*, G. R. Barrenechea, F. Brezzi, A. Cangiani, and E. H. Georgoulis, Eds., vol. 114. Springer International Publishing, Cham, 2016, ch. 7, pp. 205–236. Lecture Notes in Computational Science and Engineering.*

[77] Di Pietro, D. A., Kapidani, B., Specogna, R., and Trevisan, F. *An Arbitrary-Order Discontinuous Skeletal Method for Solving Electrostatics on General Polyhedral Meshes.* IEEE Transactions on Magnetics 53*, 6 (2017), 1–4.*

[78] Diaz, J. I., and Thelin, F. *On a Nonlinear Parabolic Problem Arising in Some Models Related to Turbulent Flows.* SIAM Journal on Mathematical Analysis 25*, 4 (1994), 1085–1111.*

[79] Dolbow, J., and Harari, I. *Erratum: An efficient finite element method for embedded interface problems.* International Journal for Numerical Methods in Engineering 78 *(2009), 229–252.*

[80] Dong, H., Wang, B., Xie, Z., and Wang, L.-L. *An unfitted hybridizable discontinuous Galerkin method for the Poisson interface problem and its error analysis.* IMA Journal of Numerical Analysis 37*, 1 (2016), 444–476.*

[81] Droniou, J. *Finite volume schemes for fully non-linear elliptic equations in divergence form.* ESAIM: Mathematical Modelling and Numerical Analysis 40*, 6 (2006), 1069–1100.*

[82] Droniou, J., and Eymard, R. *A mixed finite volume scheme for anisotropic diffusion problems on any grid.* Numerische Mathematik 105*, 1 (2006), 35–71.*

[83] Droniou, J., Eymard, R., Gallouët, T., and Herbin, R. *A unified approach to mimetic finite difference, hybrid finite volume and mixed finite volume methods.* Mathematical Models and Methods in Applied Sciences 20*, 2 (2010), 265 – 295.*

[84] Du, S., and Sayas, F.-J. An Invitation to the Theory of the Hybridizable Discontinuous Galerkin Method: Projections, Estimates, Tools*, first ed. SpringerBriefs in Mathematics. Springer International Publishing, 2019.*

[85] Efendiev, Y., Lazarov, R., and Shi, K. *A Multiscale HDG Method for Second Order Elliptic Equations. Part I. Polynomial and Homogenization-Based Multiscale Spaces.* SIAM Journal on Numerical Analysis 53*, 1 (2013), 342–369.*

[86] Ern, A., and Guermond, J.-L. Theory and Practice of Finite Elements*. Applied Mathematical Sciences. Appl. Math. Sci. 159, Springer-Verlag, New York, 2004.*

[87] Esser, P., Grande, J., and Reusken, A. *An extended finite element method applied to levitated droplet problems.* International Journal for Numerical Methods in Engineering 84 *(2010), 757–773.*

[88] Eymard, R., Gallouët, T., and Herbin, R. *Discretization of heterogeneous and anisotropic diffusion problems on general nonconforming meshes SUSHI: a scheme using stabilization and hybrid interfaces.* IMA Journal of Numerical Analysis 30*, 4 (2010), 1009–1043.*

[89] Eymard, R., Gallout, T., and Herbin, R. *Finite volume methods. In* Solution of Equation in ℝn (Part 3), Techniques of Scientific Computing (Part 3)*, vol. 7 of* Handbook of Numerical Analysis*. Elsevier, 2000, pp. 713 – 1018.*

[90] Feistauer, M. *Mathematical and numerical study of nonlinear problems in fluid mechanics. In* Proceedings of the International Conference on Differential Equations and their Applications (Equadiff 6) *(1986), vol. 1192, Springer-Verlag Berlin Heidelberg, pp. 3–16.*

[91] Feistauer, M. *On the Finite Element Approximation of a Cascade Flow Problem.* Numerische Mathematik 50 *(1987), 655–684.*

[92] Feistauer, M., and Ženíšek, A. *Finite element solution of nonlinear elliptic problems.* Numerische Mathematik 50 *(1986), 451–475.*

[93] Figalli, A. The Monge-Ampère Equation and Its Applications, *vol. 22 of* Zurich Lectures in Advanced Mathematics. *European Mathematical Society, 2017.*

[94] Fortin, M. *An analysis of the convergence of mixed nite element methods.* RAIRO. Analyse numrique 11 *(1977), 341–354.*

[95] Friedman, A. *The Stefan Problem in Several Space Variables.* Transactions of The American Mathematical Society 133, *1 (1968), 51–87.*

[96] Gatica, G. N. A simple introduction to the mixed finite element method. Theory and applications. *SpringerBriefs in Mathematics. Springer, Cham, 2014.*

[97] Gatica, G. N. Introducción al Análisis Funcional. Teoría y Aplicaciones. *Editorial Reverté S.A., 2014.*

[98] Gatica, G. N., Heuer, N., and Meddahi, S. *On the numerical analysis of nonlinear twofold saddle point problems.* IMA Journal of Numerical Analysis 23, *2 (2003), 301–330.*

[99] Gatica, G. N., Marquez, A., and Rudolph, W. *A priori and a posteriori error analyses of augmented twofold saddle point formulations for nonlinear elasticity problems.* Computer Methods in Applied Mechanics and Engineering 264 *(2013), 23–48.*

[100] Gatica, G. N., and Meddahi, S. *A dual-dual mixed formulation for nonlinear exterior transmission problems.* Mathematics of Computation 70 *(2001), 1461–1480.*

[101] Gatica, G. N., and Meddahi, S. *A dual-dual mixed formulation for nonlinear exterior transmission problems.* Mathematics of Computation 70, *236 (2001), 1461–1480.*

[102] Gatica, G. N., and Sayas, F.-J. *A note on the local approximation properties of piecewise polynomials with applications to LDG methods.* Complex Variables 51 *(2006), 109–117.*

[103] Gatica, G. N., and Sayas, F.-J. *An a priori error analysis for the coupling of local discontinuous Galerkin and boundary element methods.* Mathematics of Computation 75 *(2006), 1675–1696.*

[104] Gatica, G. N., and Stephan, E. *A mixed-FEM formulation for nonlinear incompressible elasticity in the plane.* Numerical Methods for Partial Differential Equations 18*, 1 (2002), 105–128.*

[105] Glowinski, R. Numerical Methods for Nonlinear Variational Problems. *Springer Series in Computational Physics. Springer-Verlag, New York, 1984.*

[106] Glowinski, R., and Rappaz, J. *Approximation of a nonlinear elliptic problem arising in a non-Newtonian fluid flow model in glaciology.* ESAIM: Mathematical Modelling and Numerical Analysis 37*, 1 (2003), 175–186.*

[107] Gong, Y., Li, B., and Li, Z. *Immersed interface finite element methods for elliptic interface problems with nonhomogeneous jump conditions.* SIAM Journal on Numerical Analysis 46*, 1 (2008), 472–495.*

[108] Grisvard, P. *Problèmes aux limites dans les polygones mode d'emploi, EDF Bulletin de la direction des études et recherches, Serie C, Mathématiques Informatique, 1986.*

[109] Grisvard, P. Singularities in boundary value problems*, vol. 22 of* Recherches en mathématiques appliquées. *Masson; Berlin : Springer, 1992.*

[110] Grisvard, P. Elliptic problems in nonsmooth domains. *Classics in Applied Mathematics. SIAM, USA, 2011. Reprint of the 1983 edition.*

[111] Grünbaum, B., Kaibel, V., Klee, V., and Ziegler, G. M. Convex polytopes. *Springer, New York, 2003.*

[112] Guennebaud, G., and Jacob, B. *Eigen v3.* http://eigen.tuxfamily.org*, 2010.*

[113] Gupta, K. K., and Meek, J. L. *A Brief History of the Beginning of the Finite Element Method.* International Journal for Numerical Methods in Engineering 39*, 22 (1996), 3761–3774.*

[114] Guyomarc'h, G., Lee, C.-O., and Jeon, K. *A discontinuous Galerkin method for elliptic interface problems with application to electroporation.* Communications in Numerical Methods in Engineering 25*, 10 (2009), 991 – 1008.*

[115] Hansbo, A., and Hansbo, P. *An unfitted finite element method based on Nitsche's method for elliptic interface problems.* Computer Methods in Applied Mechanics and Engineering 191 *(2002), 5537–5552.*

[116] Hansbo, P., Lovadina, C., Perugia, I., and Sangalli, G. *A Lagrange multiplier method for the finite element solution of elliptic interface problems using non-matching meshes.* Numerische Mathematik 100*, 1 (2005), 91–115.*

[117] Heise, B. *Nonlinear Field Calculations with Multigrid-Newton Methods.* IMPACT of Computing in Science and Engineering 5*, 2 (1993), 75 – 110.*

[118] Heise, B. *Analysis of a Fully Discrete Finite Element Method for a Nonlinear Magnetic Field Problem.* SIAM Journal on Numerical Analysis 31*, 3 (1994), 745–759.*

[119] Herbin, R., and Hubert, F. *Benchmark on Discretization Schemes for Anisotropic Diffusion Problems on General Grids. In* Finite Volumes for Complex Applications V*, R. Eymard and J.-M. Hérard, Eds. John Wiley & Sons, 2008, pp. 659–692.*

[120] Hou, T., Wu, X.-H., and Cai, Z. *Convergence of multi-scale finite element method for elliptic problems with rapidly oscillating coefficients.* Mathematics of Computation 68 *(1999), 913–943.*

[121] Hu, W.-F., Lai, M.-C., and Young, Y.-N. *A hybrid immersed boundary and immersed interface method for electrohydrodynamic simulations.* Journal of Computational Physics 282 *(2015), 47–61.*

[122] Huynh, L., Nguyen, N., Peraire, J., and Khoo, B. *A high-order hybridizable discontinuous Galerkin method for elliptic interface problems.* International Journal for Numerical Methods in Engineering 93 *(2013), 183–200.*

[123] Kummer, F., and Oberlack, M. *An Extension of the Discontinuous Galerkin Method for the Singular Poisson Equation.* SIAM Journal on Scientific Computing 35*, 2 (2013), A603–A622.*

[124] La Saint, P., and Raviart, P. A. *On a Finite Element Method for Solving the Neutron Transport Equation. In* Mathematical Aspects of Finite Elements in Partial Differential Equations: Proceedings of a Symposium Conducted by the Mathematics Research Center, the University of Wisconsin–Madison*, C. de Boor, Ed. Elsevier, 1974, pp. 89–123.*

[125] Lemaire, S. *Bridging the hybrid high-order and virtual element methods.* IMA Journal of Numerical Analysis 41*, 1 (2021), 549–593.*

[126] LeVeque, R. J., and Li, Z. *The immersed interface method for elliptic equations with discontinuous coefficients and singular sources.* SIAM Journal on Numerical Analysis 31*, 4 (1994), 1019–1044.*

[127] Lipnikov, K., and Manzini, G. *A high-order mimetic method on unstructured polyhedral meshes for the diffusion equation.* Journal of Computational Physics 272 *(2014), 360–385.*

[128] Mantilla, I., and Munguia, J. *Construcción de mapas de ruido con elementos finitos y Newmark.* TECNIA 22*, 2 (2012), 35–44.*

[129] Medjo, T. *Mixed formulation of the two-layer quasi-geostrophic equations of the ocean.* Numerical Methods for Partial Differential Equations 15 *(1999), 489–502.*

[130] Melenk, J. M., and Babuška, I. *The partition of unity finite element method: basic theory and applications.* Computer methods in applied mechanics and engineering 139*, 1 (1996), 289–314.*

[131] Moës, N., Dolbow, J., and Belytschko, T. *A Finite Element Method for Crack Growth without Remeshing.* International Journal for Numerical Methods in Engineering 46*, 1 (1999), 131–150.*

[132] Moukalled, F., Mangani, L., and Darwish, M. The finite volume method in computational fluid dynamics : an advanced introduction with OpenFOAM and Matlab*, vol. 113 of* Fluid Mechanics and Its Applications*. Cham : Springer, 10 2016.*

[133] Nečas, J. Introduction to the theory of nonlinear elliptic equations. *A Wiley-Interscience Publication. John Wiley & Sons, Ltd., Chichester, 1986. Reprint of the 1983 edition.*

[134] Nguyen, N. C., Peraire, J., and Cockburn, B. *Hybridizable Discontinuous Galerkin Methods. In* Spectral and High Order Methods for Partial Differential Equations*, J. Hesthaven and E. Rønquist, Eds., vol. 76. Springer, Berlin, Heidelberg, 2011, pp. 63 – 84. Lecture Notes in Computational Science and Engineering.*

[135] Ortner, C., and Süli, E. *Discontinuous Galerkin Finite Element Approximation of Nonlinear Second-Order Elliptic and Hyperbolic Systems.* SIAM Journal on Numerical Analysis 45*, 4 (2007), 1370–1397.*

[136] Petyt, M. *Finite Element Techniques for Acoustics. In* Theoretical Acoustics and Numerical Techniques*, P. Filippi, Ed., vol. 277. Springer, Vienna, 1983, pp. 51 – 103.*

[137] Potier, C. L. *A finite volume method for the approximation of highly anisotropic diffusion operators on unstructured meshes. In* Finite Volumes for Complex Applications IV: Problems and Perspectives *(2005), F. Benkhaldoun, D. Ouazar, and S. Raghay, Eds., ISTE LTD, pp. 401–412.*

[138] Reed, W. H., and Hill, T. R. *Triangular mesh methods for the neutron transport equation. Tech. Rep. LA-UR–73-479, Los Alamos Scientific Laboratory, Los Alamos, NM, 1973.*

[139] Rueschendorf, L. *Monge-Kantorovich transportation problem and optimal couplings.* Jahresbericht der Deutschen Mathematiker-Vereinigung (DMV) 109 *(2007).*

[140] Sayas, F.-J., Brown, T. S., and Hassel, M. E. Variational techniques for elliptic partial differential equations. Theoretical tools and advanced applications. *CRC Press. TAYLOR & Francis Group, LCC, 2019.*

[141] Sethian, J. A. Level Set Methods and Fast Marching Methods Evolving Interfaces in Computational Geometry, Fluid Mechanics, Computer Vision, and Materials Science. *Cambridge University Press, 1999.*

[142] Stein, E. *History of the Finite Element Method Mathematics Meets Mechanics Part I: Engineering Developments. In* The History of Theoretical, Material and Computational Mechanics - Mathematics Meets Mechanics and Engineering*, E. Stein, Ed., vol. 1 of* Lecture Notes in Applied Mathematics and Mechanics. *Springer, Berlin, Heidelberg, 2014, pp. 399–442.*

[143] Turner, M. J., Clough, R. W., Martin, H. C., and Topp, L. J. *Stiffness and deflection analysis of complex structures.* Journal of Aeronautical Sciences 23*, 9 (1956), 805–823.*

[144] Ženíšek, A. Nonlinear elliptic and evolution problems and their finite element approximations. *Computational Mathematics and Applications. Academic Press, Inc. [Harcourt Brace Jovanovich, Publishers], London, 1990. With a foreword by P.-A. Raviart.*

[145] Wang, B., and Khoo, B. *Hybridizable discontinuous Galerkin method (HDG) for Stokes interface flow.* Journal of Computational Physics 247 *(2013), 262 – 278.*

[146] Wang, Q., and Chen, J. *An unfitted discontinuous Galerkin method for elliptic interface problems.* Journal of Applied Mathematics *(2014), Art. ID 241890.*

[147] Wheeler, M. *An Elliptic Collocation-Finite Element Method with Interior Penalties.* SIAM Journal on Numerical Analysis 15*, 1 (1978), 152–161.*

[148] Zhang, Y., and Mei, L. *A hybrid high-order method for a class of quasi-Newtonian Stokes equations on general meshes.* Applied Mathematics and Computation 366 *(2020), Art. ID 124741.*

[149] Zheng, X., and Lowengrub, J. *An interface-fitted adaptive mesh method for elliptic problems and its application in free interface problems with surface tension.* Advances in Computational Mathematics 42*, 5 (2016), 1225–1257.*

[150] Zienkiewicz, O. *The birth of the finite element method and of computational mechanics.* International Journal for Numerical Methods in Engineering 60 *(2004), 3 – 10.*

[151] Zienkiewicz, O. C., and Cheung, Y. K. The Finite Element Method in Structural and Continuum Mechanics*, 1 ed. McGraw-Hill, 1967.*